



UNIVERSITAT DE
BARCELONA

Role of the atypical CDK activator RINGO beyond meiosis

Laura González Pérez

ADVERTIMENT. La consulta d'aquesta tesi queda condicionada a l'acceptació de les següents condicions d'ús: La difusió d'aquesta tesi per mitjà del servei TDX (www.tdx.cat) i a través del Dipòsit Digital de la UB (diposit.ub.edu) ha estat autoritzada pels titulars dels drets de propietat intel·lectual únicament per a usos privats emmarcats en activitats d'investigació i docència. No s'autoritza la seva reproducció amb finalitats de lucre ni la seva difusió i posada a disposició des d'un lloc aliè al servei TDX ni al Dipòsit Digital de la UB. No s'autoritza la presentació del seu contingut en una finestra o marc aliè a TDX o al Dipòsit Digital de la UB (framing). Aquesta reserva de drets afecta tant al resum de presentació de la tesi com als seus continguts. En la utilització o cita de parts de la tesi és obligat indicar el nom de la persona autora.

ADVERTENCIA. La consulta de esta tesis queda condicionada a la aceptación de las siguientes condiciones de uso: La difusión de esta tesis por medio del servicio TDR (www.tdx.cat) y a través del Repositorio Digital de la UB (diposit.ub.edu) ha sido autorizada por los titulares de los derechos de propiedad intelectual únicamente para usos privados enmarcados en actividades de investigación y docencia. No se autoriza su reproducción con finalidades de lucro ni su difusión y puesta a disposición desde un sitio ajeno al servicio TDR o al Repositorio Digital de la UB. No se autoriza la presentación de su contenido en una ventana o marco ajeno a TDR o al Repositorio Digital de la UB (framing). Esta reserva de derechos afecta tanto al resumen de presentación de la tesis como a sus contenidos. En la utilización o cita de partes de la tesis es obligado indicar el nombre de la persona autora.

WARNING. On having consulted this thesis you're accepting the following use conditions: Spreading this thesis by the TDX (www.tdx.cat) service and by the UB Digital Repository (diposit.ub.edu) has been authorized by the titular of the intellectual property rights only for private uses placed in investigation and teaching activities. Reproduction with lucrative aims is not authorized nor its spreading and availability from a site foreign to the TDX service or to the UB Digital Repository. Introducing its content in a window or frame foreign to the TDX service or to the UB Digital Repository is not authorized (framing). Those rights affect to the presentation summary of the thesis as well as to its contents. In the using or citation of parts of the thesis it's obliged to indicate the name of the author.



UNIVERSITAT DE BARCELONA

Facultat de Farmàcia i Ciències de l'Alimentació

Programa de doctorat en Biomedicina

Role of the atypical CDK activator RINGO beyond meiosis

Memòria presentada per Laura González Pérez per optar al títol de doctor per la
Universitat de Barcelona

Aquesta tesi s'ha realitzat a l'Institut de Recerca Biomèdica de Barcelona
(IRB Barcelona)

DIRECTOR

Ángel Rodríguez Nebreda, PhD

DOCTORANDA

Laura González Pérez

TUTORA

Neus Agell Jané, PhD

Barcelona 2019

Al Jaume i a la Joana,

Acknowledgments

Gairebé sense creure-m'ho, aquest treball està a punt d'arribar al final. Amb alegria i una certa melangia, ara em passen pel cap moltíssimes coses. Ha estat una etapa molt intensa i enriquidora, tant a nivell científic com a nivell personal i, per això, agraeixo a totes les persones que m'han acompanyat en aquest viatge la seva ajuda i suport. Totes elles han fet aportacions imprescindibles per tal de finalitzar aquest treball. Han celebrat amb mi els moments més feliços i també m'han alleugerit en d'altres que no ho eren tant, resultant finalment així en un recorregut molt satisfactori.

Este viaje empezó gracias a Ángel, que depositó su confianza en mí. Quiero agradecerle, por un lado, el haberme dado esta gran oportunidad para formarme como científica, y por otro lado, por haberme ofrecido su ayuda durante todo este tiempo. Además, diferentes personas han contribuido con su conocimiento y experiencia a ayudarme a entender la ciencia en diferentes aspectos y a desarrollar mi pensamiento crítico: I would like to acknowledge the members of my thesis advisor committee, Travis Stracker, my tutor Neus Agell and Jens Lüders. Thank you for following the steps of my research and providing helpful advice when I needed it. Gracias a mi tribunal de tesis: Isabel Fariñas, Josep Clotet, Marcos Malumbres, Raúl Méndez y Gabriel Gil, por vuestro tiempo y por aceptar formar parte de esta última y tan importante parte de mi doctorado.

He tenido la suerte de que esta aventura se desarrollase en el IRB de Barcelona, donde he podido conocer a personas fantásticas y a la vez forjar grandes amistades. A todas ellas me gustaría agradecer su presencia:

Quisiera agradecer a todos los miembros del Nebreda's lab que, de una forma u otra, han dejado su huella en mí. El RINGO team: Petra and Michi for their help in the initial steps dealing with this unpredictable protein and all the fun and funny moments we had. Marc, has sigut essencial per desencallar aquesta història; gràcies pel teu entusiasme i sentit de

Acknowledgments

l'humor; per fer-me costat en l'alegria i, en ocasions en la desesperació; i no menys important és haver estat l'autor de la RINGO story BSO! Gràcies a l'Elisabet per la seva ajuda i optimisme. Gracias, Mónica, por ser la mejor lab manager del mundo; gràcies Lorena per els farts de riure, Bego i Raquel per els vostres consells i gràcies a la Clara d'ou, Nevenka i Dan per la vostra alegria i entusiasme. También gracias a Mariana y Marga, por estar a mi lado en esta recta final! Gracias a todos aquellos que, aunque ya hace tiempo que no compartimos *bench*, habéis sido también parte del camino; como mis queridos Eli y Sebas, a Kostya, Nati, Ivan... Gràcies Jessi, por ser un amor. Unes gràcies infinites a la meva estimada Nuri; recordo quantes matades fent experiments fins les tantes, quants debats científics i no científics, i quin fart de riure! Què en farem d'aquest garrí? Gràcies per fer aquest camí molt més interessant i assequible.

Dins l'IRB moltíssimes persones han contribuït a aquest treball, sempre disposades a ajudar-me. Entre tots voldria agrair el suport d' en Toni, guiant-me pels camins de la neuro. Thanks to the "Stracker team", next door, not only Travis, who has been very supportive with helpful advice and nice ideas, but also Ilaria, Marina, Sandra, Berta... always willing to help. També voldria donar les gràcies a les persones de les facilities de l'IRB; gràcies a la Sònia i el Jaume per ajudar amb el que calgui, i més! A la Neus i facility d'histologia per el suport amb el fenotipatge de ratolins; gràcies també als components de la mouse mutant facility, microscòpia... gràcies a tots els qui m'heu ajudat en tot el que he necessitat per al meu treball.

Aquest doctorat m'ha permès crear vincles amb grans persones que han aportat ritme a la història, protagonistes de mil aventures, i això és el millor que m'emporto. Gràcies Helena pepinet. Amb tu, mai es fa fosc. Gemma tomàquet, fa molt que ens coneixem i ha sigut molt guai seguir juntes aquesta etapa. Cris, gràcies per ser tan bona persona i també, no ho oblidis, una gran companya de sac! Ricardinho ¡Ya casi llegamos a la cima, contigo ha sido más fácil! Gràcies Ernest, company de descansos i xerrameques, gràcies Craig, Adrián, Helena R., Suñer, Salva, Martí, Jürgen, Jordi... Celia, tu entusiasmo reivindicativo se contagia; gracias a todas las congostillas! En definitiva, moltíssimes gràcies a aquestes persones i a moltes més que he conegut al Parc Científic, pels mil moments viscuts i pels que vindran!

Gràcies també a tots els qui des de fora l'IRB m'heu fet costat en aquest camí: les eternes riudecolenques i reusencs, gràcies també a l'Alexia, al Ferran i a l'Álvaro per ser-hi sempre;

gràcies a l'Alberto per haver-me acompanyat en els meus primers passos pel món de la ciència; vull agrair a la Maite els seus càlids consells i també a la Sandra i l'Edu pel seu constant suport en el dia a dia...

Finalment, vull expressar un agraïment especial als més propers, sense vosaltres no hagués arribat fins aquí. Marc, tu has fet que tot resulti més fàcil, gràcies per fer que tot hagi estat més lleuger i assequible. En aquest treball hi ha molt de tu. Gràcies per les aventures viscudes i totes les que vindran! Gràcies a la meva meravellosa família, tinc moltíssima sort de tenir-vos, sou el meu gran pilar. Gràcies a les meves germanes Núria i Carme per ser amigues i mami; Núria, gràcies per acompanyar-me des del primer pas en el món de la biologia. Gràcies també als meus germans Xavi i Jordi per ser-hi sempre, sense oblidar els meus cunyats i cunyades, nebotets i nebotetes enanos, i no tan enanos, per omplir-ho tot d'alegria. Per últim un gràcies gegant als meus pares als quals dedico aquesta tesi: els vostres valors m'obren el camí guiant-me a cada pas, sou presents en tot el que faig.

Contents

Summary	17
Resum	19
List of abbreviations	21
Introduction	25
Overview of the mitotic cell cycle.....	27
Molecular regulation of the cell cycle.....	29
<i>Cyclins and Cyclin-Dependent Kinases</i>	29
<i>Regulation of cell cycle progression and cellular checkpoints</i>	31
G1/S transition and progression through S phase.....	32
G2/M transition and M progression.....	35
DNA damage and repair.....	37
<i>Nuclear architecture</i>	39
<i>Cohesins</i>	41
The role of cell cycle related CDKs and cyclins <i>in vivo</i>	44
<i>Functional redundancy and complementation in the mammalian cell cycle</i>	44
<i>Meiotic cell cycle and gametogenesis</i>	46
<i>Role of Cdk2 in vivo</i>	49
<i>Neurogenesis and the cell cycle</i>	49
<i>Cancer and cell cycle regulators</i>	52
Atypical CDK activators: the RINGO proteins.....	55
<i>RingoA structure and CDK activation</i>	56
RINGO activates CDK1 and CDK2 independently of Thr-160 phosphorylation.....	57
<i>Proposed functions of RINGO in cell cycle regulation in vitro</i>	59
Regulation of RINGO proteins during the cell cycle.....	59
RingoA interacts with p27 ^{kip1}	59
RingoA and DNA damage.....	60
<i>Physiological roles of RINGO proteins</i>	60
RingoA in meiosis.....	60
RingoA in tumorigenesis.....	61
Objectives	65
Materials & Methods	69
General buffers and solutions.....	71
Commercial reagents and kits.....	72

Contents

Mouse work.....	75
<i>Mouse housing</i>	75
<i>Generation of mouse models</i>	75
<i>Animal treatments</i>	76
<i>Mouse genotyping</i>	77
<i>Tumor growth analysis in mice</i>	78
<i>Immunohistochemistry</i>	78
<i>Visualization of Katushka-Luciferase reporter</i>	79
<i>Maintenance and subculture of adherent cells</i>	80
<i>Freezing and thawing of cells</i>	81
<i>Mycoplasma detection</i>	81
<i>Generation, maintenance and differentiation of adult brain-derived neurospheres</i>	81
<i>Generation of epithelial cell lines from PyMT tumors</i>	83
<i>Cre recombinase induction with 4-hydroxytamoxifen (4-OHT)</i>	83
<i>Cell transfection</i>	84
<i>Retroviral and lentiviral infection</i>	85
Cellular and molecular biology.....	86
<i>Colony assay</i>	86
<i>Time-lapse imaging</i>	86
<i>Flow cytometry</i>	86
<i>Metaphase spreads</i>	88
<i>Protein detection by immunofluorescence</i>	88
<i>Protein extraction and quantification</i>	89
<i>Protein detection by western blotting</i>	89
<i>Protein co-immunoprecipitation</i>	90
<i>BioID screening</i>	91
<i>Gene expression analysis by RT-qPCR</i>	92
<i>Statistical analysis</i>	93
Results	95
SECTION 1- Elucidating the molecular function of RingoA in human cells.....	97
<i>RingoA knock-down reduces cell proliferation and increases cell death</i>	97
<i>Unbiased proteomic approach for the identification of potential RingoA interactors</i>	100
Setting up the RingoA BioID screening: BirA* <i>RingoA</i> expression and location.....	101
BioID analysis suggests three different clusters of potential RingoA interactors involved in cell cycle regulation and RNA processing.....	103
Validation of RingoA potential interactors.....	105
<i>RingoA interacts with the cohesin complex</i>	106
<i>RingoA localizes to discrete nuclear sites in human cells and its expression depends on the cell cycle</i>	108
<i>RingoA location in human cells</i>	110
RingoA partially localizes to nuclear speckles and accumulates upon transcription inhibition.....	110

SECTION 2 - Characterization of RingoA and RingoB KO mouse models	113
<i>Expression of RingoA and RingoB mRNAs</i>	113
<i>Histological characterization of RingoA KO, RingoB KO and RingoA/RingoB double KO mice</i>	114
Effects of RingoB or RingoA/RingoB depletion in gonads.....	114
Effects of RingoA, RingoB or RingoA/RingoB downregulation in somatic tissues.....	115
Histological characterization of RingoA and RingoB inducible KO: male testes but not female ovaries mimic phenotypes of constitutive RingoA KO.....	116
<i>Katushka-Luciferase reporter of RingoA promoter activity</i>	118
Analysis of RingoA promoter activity using the Katushka reporter.....	119
Analysis of RingoA promoter activity using the Luciferase reporter.....	120
SECTION 3 - The role of RINGO proteins in the brain	123
<i>RingoA mRNA is expressed in neural stem cells and proliferating progenitor cells</i>	123
<i>Analysis of neural stem cells and progenitor self-renewal capacity in RingoA/RingoB KO</i>	126
Impaired ability of RingoA/RingoB KO cells to form neurospheres	126
<i>Brains of RingoA/RingoB KO mice show normal histology and unaltered proliferation and mitotic index in the SVZ</i>	129
SECTION 4- The role of RINGO proteins in breast cancer	131
<i>RingoA is expressed in PyMT-induced mammary tumors</i>	131
<i>RingoA and RingoB are required for mammary tumor growth</i>	132
<i>Role of RingoA and RingoB in immortalized cancer cell lines derived from mammary tumors</i>	134
Effect of RingoA and RingoB downregulation in mammary cancer cells	136
Effect of 4-OHT treatment and Cre activation in mammary cancer cells	136
<i>Histological characterization of RingoA/RingoB deficient mammary tumors</i>	139
Discussion	143
Cell cycle regulation by RingoA in mammalian cell lines.....	145
Uncovering the RingoA interactome network.....	147
<i>Identification of new RingoA interactors</i>	147
<i>Molecular clues for the identification of RingoA sub-cellular location and dynamics</i>	150
Role of RingoA <i>in vivo</i>	153
<i>RingoA expression in mice</i>	153
<i>RingoA is essential for meiosis</i>	154
<i>RingoA is not essential for the homeostasis of somatic tissues</i>	154
<i>RingoA in the brain</i>	155
<i>RingoA in tumorigenesis</i>	159
Conclusions	165
Appendix	169
References	177

Table of figures

Introduction

Figure I1. Evolutionary relationships among CDKs.	30
Figure I2. Cell cycle phases and regulators.	32
Figure I3. Molecular regulation of G1/S progression and the G1/S DNA damage checkpoint.	34
Figure I4. Molecular regulation of the G2/M checkpoint.	36
Figure I5. Steps of the DDR.	37
Figure I6. Nuclear architecture and hierarchical organization of the 3D genome.	40
Figure I7. Cohesin dynamics during the cell cycle.	42
Figure I8. Functions of the cohesin complex during the cell cycle.	43
Figure I9. Summary of CDK and cyclin phenotypes in KO mice.	45
Figure I10. Representation of male and female gametogenesis and meiosis in mice.	48
Figure I11. NSCs in the embryonic and adult brain.	50
Figure I12. Representation of neural differentiation stages in NSCs produced at the SVZ.	51
Figure I13. Phylogenetic tree of mammalian RINGO proteins.	55
Figure I14. Comparison of CDK2-RingoA and CDK2-Cyclin A structures.	56
Figure I15. Model for CDK-RINGO substrate phosphorylation.	58

Results

Figure R1. Cell cycle changes and reduced DNA replication in RingoA KD cells.	98
Figure R2. Reduced number of mitoses and increased cell death in RingoA KD cells.	99
Figure R3. Setting-up the RingoA BioID screening.	102
Figure R4. Interacting networks of the candidate RingoA interactors identified in the BioID screening.	104
Figure R5. RingoA interacts with WAPL and ANKRD11.	106
Figure R6. RingoA co-immunoprecipitates with different subunits of the cohesin complex.	107
Figure R7. WAPL interacts with RingoA better than with CDK2, Cyclin E2 and Cyclin A2.	108
Figure R8. RingoA localizes to discrete nuclear sites during interphase and its expression is lost in mitosis.	109
Figure R9. RingoA co-localizes with nuclear speckles and accumulates upon transcription inhibition.	111
Figure R10. RingoA partially colocalizes with cohesins.	112
Figure R11. RingoA and RingoB mRNA expression in mouse.	113
Figure R12. Histological analysis of ovaries and testes.	115
Figure R13. Inducible RingoA/RingoB KO mimics the phenotype of the constitutive KO in testes but not in the ovaries.	117
Figure R14. Schematic representation of the Katushka-Luciferase (K/L) reporter.	119
Figure R15. Katushka expression under control of the RingoA promoter.	121
Figure R16. Luciferase expression under control of the RingoA promoter.	122
Figure R17. RingoA is expressed in actively dividing NSC.	124
Figure R18. RingoA mRNA is expressed in proliferating NSCs but not in differentiated cells.	125
Figure R19. Reduction of neurosphere number and size upon RingoA and RingoB deletion.	126
Figure R20. RingoA/RingoB KO neurospheres show no differences in proliferation, cell cycle states or cell death compared to WT.	127

Figure R21. RingoA/RingoB downregulation affects the expression of neural differentiation markers.	128
Figure R22. RingoA/RingoB KO brains have normal histology and cell proliferation in the SVZ.	130
Figure R23. RingoA gene promoter is expressed in mammary tumors.	132
Figure R24. Mammary tumor growth decreases upon RingoA/RingoB downregulation.	133
Figure R25. Generation of epithelial cell lines derived from PyMT mammary tumors.	134
Figure R26. RingoA/RingoB double KO cells show reduced proliferation.	135
Figure R27. Analysis of RingoA and RingoB downregulation in mammary cancer cells.	136
Figure R28. 100nM 4-OHT does not have an effect in mammary cancer cell proliferation.	137
Figure R29. Activation of Cre recombinase impairs cell proliferation and cell cycle progression.	137
Figure R30. Comparison of phenotypes induced by different 4-OHT concentrations.	138
Figure R31. Histological analysis of RingoA and RingoB KO mammary tumors.	140
Table R1. Histological analysis of somatic tissues.	116
Table R2. Histological analysis of the inducible RingoA/RingoB KO	118
Supplementary figure 1. Proteins identified in BioID screening.	171
Supplementary figure 2. Results of Reactome analysis of the Bio-ID derived data.	173
Supplementary figure 3. RingoA co-immunoprecipitates with CDK2 and Skp2.	174

Summary

The cell cycle is orchestrated by the periodic activation of Cyclin-dependent kinases (CDKs). The enzymatic activity of CDKs depends on their association with cyclins, however, in some cases these kinases can be activated by non-cyclin proteins. RINGO is an atypical CDK activator which regulates the meiotic maturation of *Xenopus* oocytes and has been recently described as essential for meiotic prophase in mouse. As an activator of CDKs, RINGO has a potential role in cell cycle regulation. CDK regulation by RINGO has been extensively studied *in vitro*. However, the implication of RINGO in particular cellular processes is poorly understood. Moreover, very little is known about RINGO functions *in vivo* beyond meiosis.

This thesis has addressed the functional relevance of mammalian RINGO proteins in somatic cells, both during homeostasis and in cancer. We have characterized the effects of RingoA knock-down in human cells and found changes in cell cycle progression as well as reduced cell viability. In an attempt to reveal the RingoA interactome, an unbiased proteomic approach was used, which allowed the identification of the cohesin complex and ANKRD11 as new RingoA interactors. Moreover, we describe the expression of endogenous RingoA during the cell cycle of human cells and show that it is present in nuclear speckles. The study of RingoA expression *in vivo* using a reporter system and gene expression analysis pointed to the brain as the somatic tissue where *RingoA* is most expressed. We have also analyzed genetically modified mice and found that RingoA and RingoB are not essential for somatic tissue homeostasis. Nevertheless, RingoA is expressed in the sub-ventricular zone of the adult mouse brain and is important for neural stem cell self-renewal *ex vivo*. Finally, using the Polyoma middle T mammary tumorigenesis model, we showed that RingoA and RingoB are required for tumor growth.

Resum

El cicle cel·lular és orquestrat per l'activació periòdica de les quinases dependents de ciclins (CDKs). L'activitat enzimàtica de les CDKs depèn de la seva associació amb ciclins, no obstant hi ha excepcions on aquestes quinases poden ser activades per proteïnes no englobades en la família de les ciclins. RINGO n'és un exemple; aquesta proteïna és un activador atípic de CDKs que regula la maduració meiòtica dels oòcits de *Xenopus*. A més, recentment també s'ha descrit com a essencial en la profase meiòtica i progrés meiòtic en ratolins. RINGO, com a activador de CDKs, té un rol potencial en la regulació del cicle cel·lular. La regulació d'aquestes quinases per RINGO s'ha estudiat en detall *in vitro* però poc se sap de la implicació de RINGO en processos cel·lulars. A més no se sap gairebé res de la funció de RINGO *in vivo* més enllà de la meiosi.

En aquesta tesi s'estudia la rellevància funcional de les proteïnes RINGO de mamífers en cèl·lules somàtiques, durant condicions homeostàtiques i càncer. S'han caracteritzat els efectes del *knock-down* de RingoA en cèl·lules humanes i trobat canvis en la viabilitat i cicle cel·lular d'aquestes. Amb l'objectiu de revelar l'interactoma de RINGO, s'ha utilitzat un cribratge de proteòmica que ha permès la identificació del complex de cohesines i la proteïna ANKRD11 com interactors de RingoA. A més, s'ha descrit l'expressió de RingoA durant el cicle cel·lular de cèl·lules humanes i descobert que està present en *nuclear speckles*. L'estudi de l'expressió de RingoA utilitzant un sistema reporter i l'anàlisi de l'expressió gènica ha permès la identificació del cervell com el teixit somàtic amb més expressió de RingoA. Mitjançant l'estudi de models de ratolí modificats genèticament s'ha demostrat que RingoA i RingoB no són essencials per la homeòstasi de teixits somàtics. No obstant, RingoA s'expressa en la zona sub-ventricular del cervell adult i és important per la renovació de cèl·lules mare *ex vivo*. Per últim, utilitzant el model tumoral *Polyoma middle T*, que permet la generació de tumors mamaris en ratolí, s'ha demostrat que RingoA i RingoB són importants en el creixement tumoral.

List of abbreviations

4-OHT	4-hydroxy tamoxifen
53BP1	p53 binding protein 1
A.U.	Arbitrary units
ACA	Anti-centromere antibody
ANKRD11	Ankyrin repeat domain 11
APC/C	Anaphase-promoting complex/ cylosome
ATM	Ataxia telangiectasia mutated
ATR	Ataxia telangiectasia and Rad3 related
AURKB	Aurora kinase B
BRCA1	Breast cancer 1
BrdU	5-bromo-2'-deoxyuridine
BSA	Bovine serum albumin
CAK	CDK-activating kinase
CBD	Cyclin box domain
CBF	Cyclin box fold
Cdc	Cell division cycle
CDK	Cyclin dependent kinase
CFSE	Carboxyfluorescein succinimidyl ester
CHK	Checkpoint kinase
CIN	Chromosomal instability
CKI	CDK inhibitor
Co-IP	Co-immunoprecipitation
CreERT2	Cre Recombinase estrogen receptor T2 mutant
DAB	3,3-diaminobenzidine
DAPI	4',6-diamidino-2-phenylindole
DCX	Neuronal migration protein doublecortin
ddH ₂ O	Double distilled H ₂ O
DDR	DNA damage response
DG	Dentate gyrus
dKO	Double knock-out
DMEM	Dulbecco's Modified Eagle Medium
DNA	Deoxyribonucleic acid
DPX	Distyrene, plasticizer, xylene
DSB	Double strand break
DTT	Dithiothreitol
EGF	Epidermal growth factor
EPCAM	Epithelial cell adhesion molecule
ER α	Estrogen receptor-alpha
FACS	Fluorescence-activated cell sorting
FBS	Fetal bovine serum
FDR	False discovery rate
FGF	Fibroblast growth factor
GAPDH	Glyceraldehyde 3-phosphate dehydrogenase
GFAP	Glial fibrillary acidic protein

List of abbreviations

GFP	Green fluorescent protein
γH2AX	Gamma (phosphorylated-S139) H2A histone family
GIN	Genomic instability
H&E	Hematoxinilin and Eosin
H3	Histone 3
HBSS	Hanks balanced salt solution
HPRT	Hypoxanthine-guanine phosphoribosyltransferase
HR	Homologous recombination
HRP	Horseradish peroxidase
IF	Immunofluorescence
IHC	Immunohistochemistry
IR	Ionizing radiation
IVIS	Spectrum in vivo imaging system
K/L	Katushka-Luciferase
KD	Knock-down
KI	Knock-in
KL	Katushka-Luciferase
KO	Knock-out
MCM	Mini-chromosome maintenance
MEF	Mouse embryonic fibroblast
MS	Mass spectrometry
min	Minutes
MMTV	Mouse mammary tumor virus
MTT	3-(4,5-Dimethylthiazol-2-yl)-2,5-diphenyltetrazolium bromide
NB	Neuroblast
NeuN	Neuronal nuclei
NHEJ	Non-homologous end joining
NIPBL	Nipped-B-like protein
NS	Nuclear speckles
NSC	Neural stem cell
NT	Non targeting
O/N	Overnight
OB	Olfactory bulb
OCT	Optimal cutting temperature
ORC	Origin recognition complex
PARP	PolyADP ribose polymerase
PBS	Phosphate buffer solution
PCNA	Proliferating cell nuclear antigen
PCR	Polymerase chain reaction
PDL	Poly-D-lysine
PE	Phycoerythrin
PEI	Polyethylenimine
PFA	Paraformaldehyde
PI	Propidium Iodide
PMSF	Phenylmethanesulfonyl fluoride
Pre-RC	Pre-replication complex
PyMT	Polyoma middle T
RAKL	RingoA Katushka Luciferase

List of abbreviations

Rb	Retinoblastoma
RINGO	Rapid inducer of G2/M progression in oocytes
RIPA	Radioimmunoprecipitation assay
RNA	Ribonucleic acid
Rnase	Ribonuclease
RPA	Replication protein A
RPL	Ribosomal protein large subunit
RT	Room temperature
RT-qPCR	Quantitative reverse transcription PCR
RTU	Ready to use
SA	Stromal antigen
SAC	Spindle assembly checkpoint
SAINT	Significance analysis of Interactome
SCC	Sister chromatid cohesion protein
SDS	Sodium dodecyl sulfate
Sec	Seconds
SEM	Standard error of the mean
SGZ	Subgranular zone
SMC	Structural maintenance of chromosome
SSB	Single strand breaks
SVZ	Subventricular zone
TAD	Topologically associating domains
TAP	Transit amplifying progenitor
TUNEL	Terminal deoxynucleotidyl transferase dUTP nick-end labeling
UV	Ultraviolet
WAPL	Wings apart-like protein homolog

Introduction

Overview of the mitotic cell cycle

Cell cycle is the ordered set of events that mediate the process of division of one cell into two daughter cells. Over the years, many of the molecular keys of the cell cycle and its complexity have been gradually revealed. In the 70s, major players of cell cycle regulation were discovered in yeast, namely the cell division cycle proteins (Cdc), including those known as cyclin-dependent kinases (CDKs) (Hartwell et al. 1970; Nurse et al. 1975). Soon thereafter, in the 80s, major CDK activators were discovered and named cyclins (Evans et al. 1983). Since then, many studies have revealed the biochemical and physiological functions of these complexes. The specialization of the cell cycle proteins over evolution and their functional diversification and redundancy results in substantial complexity that has been deciphered in recent years. It is now clear that *in vivo* studies are needed in order to understand their physiological functions of these proteins and also the consequences of their malfunction.

Cells have to complete four major steps during the cell cycle; they must grow, replicate their DNA, segregate their chromosomes in two identical sets, and divide. DNA duplication occurs during the *S* phase, while DNA segregation and cell division occurs in *M* phase (mitosis). These two phases are separated by two gap phases: *G1* phase between M and S phase, and *G2* phase between S phase and mitosis. Gap phases provide time for the cell to grow, to assess the external and internal environment, and to ensure that the conditions are suitable for the following phases. Cells in *G1* may enter a specialized resting state named *G0* in which they can remain for an undetermined amount of time. When the signals are favorable, cells in *G1/G0* phase might progress to a restriction point, from which they are committed to replicate DNA, even if the favorable signals cease (Alberts et al. 2007). In addition, the cell cycle has several mechanisms to ensure correct progression through the different phases and to avoid the accumulation and transference of mutations to the daughter cells. These mechanisms are known as *cell cycle checkpoints*.

Mitosis is the process in which the eukaryotic nucleus splits into two, followed by the division of the cell into daughter cells. This process can be sub-divided into different phases. During

Introduction

the first phase, named *prophase*, the replicated chromosomes condense in a process that is regulated by several DNA binding proteins, including condensins and cohesins. Condensins form rings that organize the chromosomes in a highly compacted form, while cohesins hold sister chromatids together. In prophase the mitotic spindle starts to develop, microtubules gradually assemble between the centrosomes, which have replicated and moved apart. In *prometaphase*, the nuclear envelope breaks down, allowing chromosomes to attach to the microtubule spindle via kinetochores. During *metaphase*, chromosomes align at the equator of the spindle and microtubules attach to the centromeric region of sister chromatids at opposite poles of the spindle. In *anaphase*, chromosome cohesion is lost and sister chromatids are pulled toward the opposite spindle poles. At *telophase*, the daughter chromatids reach the opposite poles of the spindle, chromosomes decondense, and the new nuclear envelope is formed. Finally, in cytokinesis, the cytoplasm of the two daughter cells is divided by a contractile ring. (Alberts et al. 2007; Mitchison and Salmon 2001).

Cell cycle control depends on cyclins and CDKs. The activity of the CDK family proteins oscillates during the cell cycle leading to changes in the phosphorylation of different substrates that will regulate the events that determine cell cycle progression.

Molecular regulation of the cell cycle

Cyclins and Cyclin-Dependent Kinases

Cyclins are a family of regulatory proteins that are fundamental for cell cycle control. They activate CDKs, which control cell cycle progression through phosphorylation. The name “cyclin” reflects the ability of the first discovered members of this family to be synthesized and degraded during the cell cycle in a cyclic manner. The sequences of the different members of the cyclin family are remarkably different but they share either one or two copies of the cyclin box domain (CBD), which is a sequence of about 100 amino acids arranged in five α -helices and is required for CDK binding and activation. Cyclins have been traditionally classified as cell cycle or canonical cyclins (A,B,D,E) and transcriptional cyclins (C,H,K,L,Q,T), the latter mainly involved in RNA polymerase regulation. More recently, other proteins containing a CBD have been identified, which are poorly characterized and have an unknown or atypical CDK partner. These proteins are known as orphan or atypical cyclins. All together, in humans, the cyclin family is composed of more than 30 cyclins. The cyclins that regulate cell cycle-related CDKs share the property of having oscillating protein levels, which is crucial for their cell cycle regulation properties. Conversely, cyclins that associate with transcription-related CDKs do not show significant protein level oscillation during the cell cycle (Quandt et al. 2019). Cyclin-CDK complexes can regulate progression through the different phases of the cell cycle by a variety of mechanisms, including cyclical synthesis and degradation, subcellular localization and post-translational modifications.

Cyclin-Dependent Kinases are a family of serine/threonine kinases that were first identified in genetic screens using mutants with defects in cellular division of budding yeast (Hartwell et al. 1970) and later of fission yeast (Nurse et al. 1975). Up to 20 CDK family members have been identified in humans. However, only some are believed to be directly involved in driving the cell cycle. From an evolutionary and functional point of view, human CDKs can be distinguished as cell cycle-related or transcription-related. Furthermore, CDKs can be evolutionarily subdivided into eight groups. CDK1, CDK4, CDK5 are considered the cell cycle-related groups and CDK7, CDK8, CDK9, CDK11, CDK20 the transcription-related groups (Figure I1).

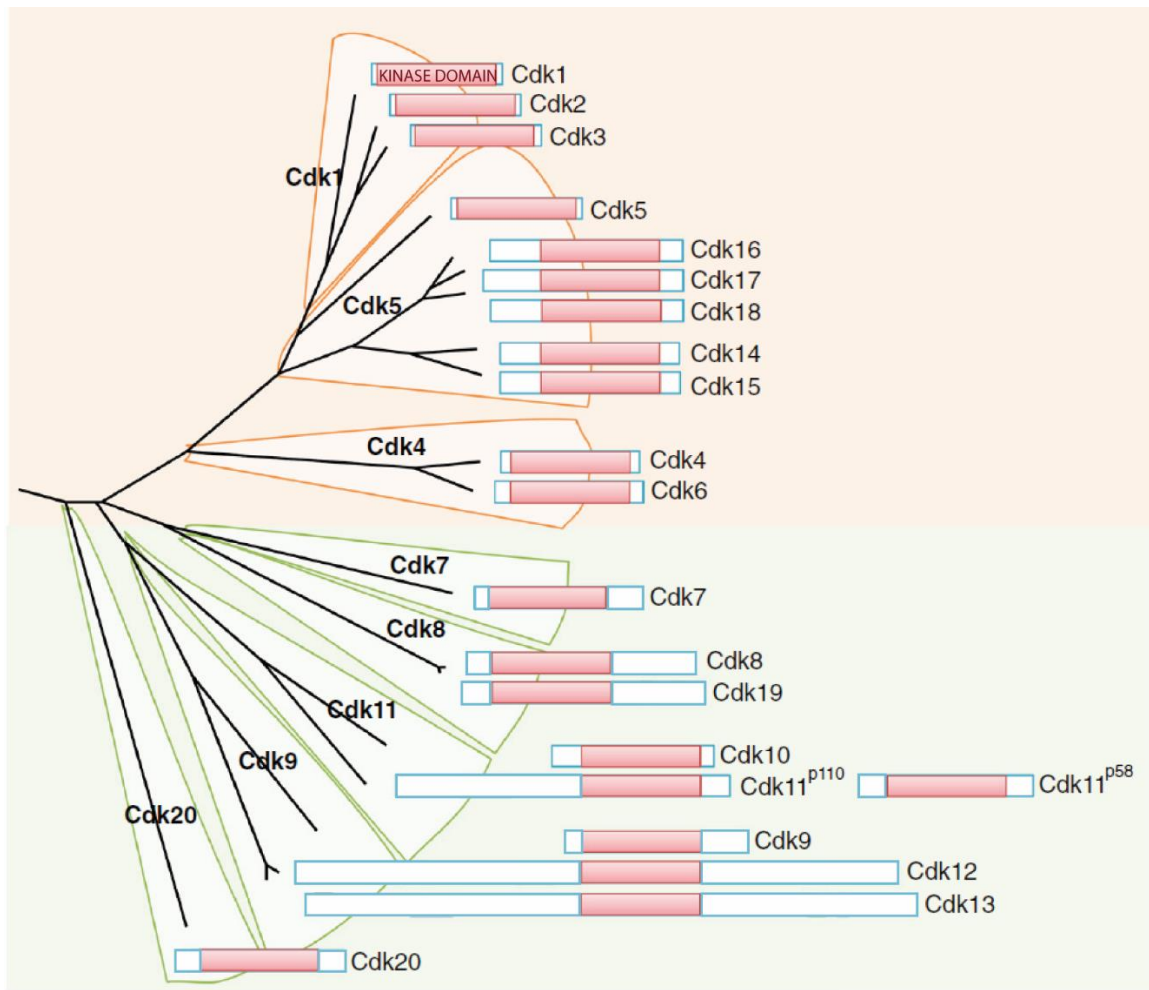


Figure I1. Evolutionary relationships among CDKs. Evolutionary relationships among members of the cell cycle-related subfamilies Cdk1, Cdk5, Cdk4 (orange background) and the transcription related subfamilies Cdk7, Cdk8, Cdk11, Cdk9 and Cdk20 (green background) are represented. (Modified from Malumbres 2014).

CDK regulation in the cell cycle: CDKs are two-lobed proline-directed serine/threonine-protein kinases. The N-lobe is predominantly formed by anti-parallel β -sheets and contains a glycine-rich loop and a single major helix (α C helix), which contains the conserved PSTAIRE sequence, important for cyclin binding. The C-lobe is composed of mainly α -helices and contains the activation loop (T-loop) with the phosphorylation sensitive residue (Thr 160 in CDK2). The ATP binding site is located between the two lobes. The function of CDK is

controlled by cyclin binding, phosphorylation and binding of protein inhibitors. Monomeric CDKs are inactive, the catalytic cleft is closed by the T-loop and the activation segment is partially disordered. The association of cyclins with the C helix induces conformational changes. The loop moves away from the active site resulting in partial activation of the enzyme and allowing the threonine to be accessible for activating phosphorylation by CDK-activating kinases (CAKs). This phosphorylation leads to further conformational changes that result in the full activation of the CDK. The mechanism of CDK2 activation is also conserved in CDK1 (De Bondt et al. 1993; Wood and Endicott 2018).

CDK-cyclin active complexes can be inactivated by dephosphorylation of the T loop threonine and also by cyclin degradation. Additionally, they can be inhibited by phosphorylation at Thr14 and Tyr15 (in CDK2) (Gu et al. 1992). In humans, the kinase Wee1 phosphorylates Tyr15 while Myt1 phosphorylates both Thr14 and Tyr15. These phosphorylations should be removed for CDK activation, which is catalyzed by the dual-specificity Cdc25 phosphatases (Dunphy and Kumagai 1991; Liu et al. 1997; Mueller et al. 1995; Sebastian et al. 1993). For further regulation, the CDK-cyclin activated complexes can be inactivated by the direct binding of CDK inhibitor (CKI) proteins. CDK4 and CDK6 are affected by the INK4 family of inhibitors: p16^{INK4a}, p15^{INK4b}, p18^{INK4c} and p19^{INK4d}. Conversely, Cip/Kip family members p21^{Cip1}, p27^{Kip1} and p57^{Kip2} can inhibit CDK1 and CDK2 as well as CDK4 and CDK6 (Sherr and Roberts 1999).

Regulation of cell cycle progression and cellular checkpoints

Despite the existence of many cyclin and CDK family members, only some are directly involved in driving the cell cycle: the interphasic CDK2, CDK4 and CDK6, and the mitotic CDK1. In parallel, cyclins A, B, D, and E are those believed to have a direct role in cell cycle control (Malumbres and Barbacid 2009) (**Figure I2**).

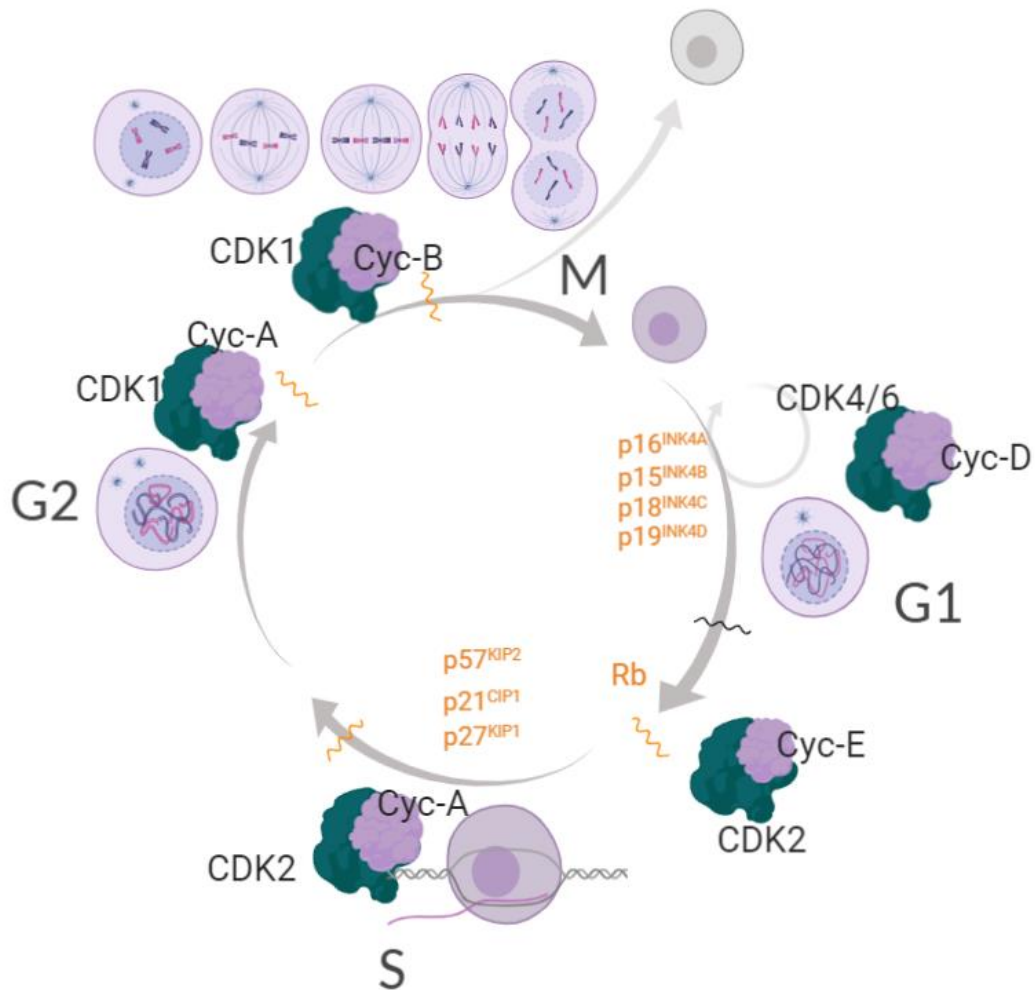


Figure I2. Cell cycle phases and regulators. The different cell cycle phases are represented. Mitotic stages are illustrated in the upper part of the scheme: prophase/ prometaphase/ metaphase/ anaphase/ telophase and cytokinesis from left to the right. Cell restriction point is indicated as a grey wavy line. Cycle checkpoints are shown as orange lines. Classically described CDK and cyclin regulators and INK and CIP family inhibitors are represented. INK family members exclusively inhibit CDK4/6 whereas CIP/KIP family are able to inhibit the activity of all cell cycle CDKs. (Figure created with BioRender).

G1/S transition and progression through S phase

Growth factors are necessary to initiate and maintain the transition through G1 phase leading to S phase. In normal cells, removal of growth factors prevents entry into S phase. The point at G1 at which commitment occurs and the cell no longer requires growth factors to complete the cell cycle has been termed the *restriction point* (Blagosklonny and Pardee 2002). The transition from G1 to S phase is coordinated by CDK4, CDK6 and CDK2. The activation of signaling pathways by mitogenic stimuli such as growth factors leads to Cyclin D

accumulation and subsequent activation of CDK4 and CDK6. One of the main substrates of these interphasic kinases are the retinoblastoma (Rb) family proteins, which negatively regulate E2F transcription factors. The hyperphosphorylation of Rb by CDKs attenuates its repressive properties, leading to E2F transcriptional activation of genes that are crucial for the following phases of the cell cycle. This is the case of genes encoding Cyclin E, Cyclin A and important proteins for DNA replication, DNA damage repair, mitosis and cell cycle checkpoints (Bracken et al. 2004). Cyclin E accumulation and activation of CDK2 concludes the phosphorylation of Rb previously initiated by Cyclin D activated kinases (Bertoli et al. 2013). CDK2-Cyclin E phosphorylates the protein p27^{Kip1} among others (**Figure I3**). The phosphorylation of p27^{Kip1} at T187 results in its proteasome-dependent degradation and therefore upregulation of CDK2 activity, thereby allowing entry into S phase (Montagnoli et al. 1999).

The *G1/S checkpoint* is a mechanism to prevent the aberrant replication of damaged DNA in S phase and it is driven mainly by two effectors, p53 and Cdc25A. When there is DNA damage, the kinases ATM and Chk2 are activated. On the one hand, this activation, promotes Cdc25A phosphorylation and, subsequently, its proteasome-mediated degradation, thus preventing CDK2 activation. On the other hand, ATM, through the activation of Chk1/2, leads to the phosphorylation and stabilization of p53, by preventing its Mdm2-mediated degradation. Then, p53 activates the expression of its downstream target p21^{Cip1}, further promoting G1 arrest by inhibiting CDK2-Cyclin E/A (Lukas et al. 2004). (**Figure I3**).

DNA replication is initiated at defined loci known as replication origins and comprises two step processes: origin licensing and firing. The two-step mediated regulation of this process is essential to avoid re-replication of DNA in the same cell cycle. The first step occurs at late mitosis and early G1 phase. The replication origins are recognized and bound by the pre-replication complex (pre-RC), which is formed by origin recognition complex (ORC1-6), Cdc6 and mini-chromosome maintenance (MCM2-7) proteins. This is known as origin licensing. The second step occurs in S phase, when DNA synthesis is activated. This process is known as origin “firing” and involves the activation of MCM2-7 helicase component for DNA unwinding (Fragkos et al. 2015). After DNA duplex unwinding, single strand DNA is stabilized

Introduction

by RPA, and DNA polymerases and proliferating cell nuclear antigen (PCNA) are recruited and catalyze DNA replication elongation (Bell and Dutta 2002).

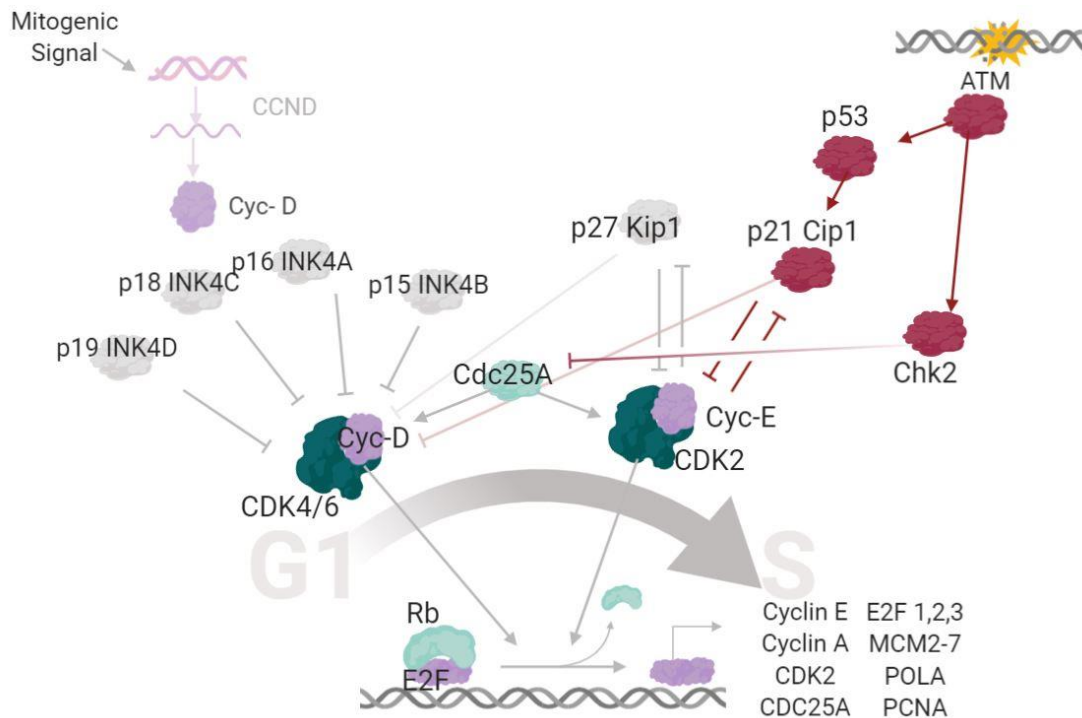


Figure I3. Molecular regulation of G1/S progression and the G1/S DNA damage checkpoint. Schematic representation of the main molecular events leading to progression to S phase. G1/S DNA damage checkpoint proteins are highlighted in red. (Figure created with BioRender).

CDK2-Cyclin E is involved in the initiation of DNA replication partly by facilitating the loading of MCM proteins to replication origins (Coverley et al. 2002). When cells have entered S phase, CDK2-Cyclin E phosphorylates Cyclin E, which becomes ubiquitinated and is degraded by the proteasome (Koepp et al. 2001). CDK2 then switches to Cyclin A binding. CDK2-Cyclin A control processes involved in S phase progression, especially those related to DNA replication maintenance, including the phosphorylation of components of the DNA replication machinery like Cdc6, which is important for restricting DNA replication to once per cell cycle. Moreover, CDK2-Cyclin A allow the accumulation of mitotic proteins such as Cyclin B (Lukas et al. 1999). At the end of S phase, Cyclin A will finally associate with CDK1 (Pagano et al. 1992).

DNA replication is considered one of the biggest challenges to maintain genomic integrity, since errors make DNA vulnerable to damage. Damage generated by errors during DNA replication are referred to as replication stress (Mazouzi et al. 2014). Genotoxic stresses

trigger a transient and reversible inhibition of DNA replication, which is known as *Intra S checkpoint*. This checkpoint inhibits firing of the replication origins that have not yet been initiated, and also protects the integrity of stalled replication forks, preventing the conversion of primary lesions into DNA breaks and facilitating recovery. This checkpoint is controlled by ATM/ATR and the downstream kinases Chk1/Chk2, which promote Cdc25A phosphorylation and degradation, inhibiting CDK2 activation. Another branch of the checkpoint depends on ATM-mediated phosphorylation of NBS1 and the cohesin complex proteins SMC1 and SMC3 (Kastan and Bartek 2004).

G2/M transition and M progression

An increase of Cyclin B protein levels through G2 phase leads to gradual accumulation of CDK1-Cyclin B complexes that are phosphorylated in the T loop activation residue by CAK. However, the complexes will not be active until the inhibitory phosphorylation is eliminated. This is catalyzed by the phosphatase Cdc25 and happens in parallel to the inhibition of Myt1 and Wee1 (Bulavin et al. 2003; Michael and Newport 1998; Theis-Febvre et al. 2003). Progression through mitosis also involves the ubiquitin ligase anaphase-promoting complex/cyclosome (APC/C), whose substrate specificity depends on the regulatory proteins Cdc20 and Cdh1. On the one hand, the activation mediated by Cdh1 is controlled by CDK phosphorylation during S, G2 and early M, which inhibit its association with the APC/C. On the other hand, the activation of APC/C by Cdc20 is controlled by the spindle assembly checkpoint (SAC), as explained below. At metaphase-anaphase, active APC/C-Cdc20 degrades Cyclin A and the degradation of Cyclin B begins. At anaphase, APC-Cdh1 is activated and subsequently, Cdc20 and Cyclin B will be degraded. The exit from M phase requires the inactivation of CDK1-Cyclin B complexes. This inactivation allows the different processes required for cytokinesis and M phase exit such as sister chromatid separation, chromosome condensation, disassembly of the mitotic spindle, and envelope reformation (Pérez de Castro et al. 2007).

The transition from G2 to M phase has a system to avoid the cell entering mitosis with unrepaired DNA damage, which is known as the *G2/M checkpoint*. The target of this checkpoint is CDK1-Cyclin B. This checkpoint is triggered by the activation of ATM/ATR and Chk1/Chk2, which induce the inhibition or degradation of Cdc25A and Cdc25C. Another layer

Introduction

of G2/M checkpoint control consists of the activation of p53, thereby allowing p21^{Cip1} accumulation (Kastan and Bartek 2004). (Figure I4).

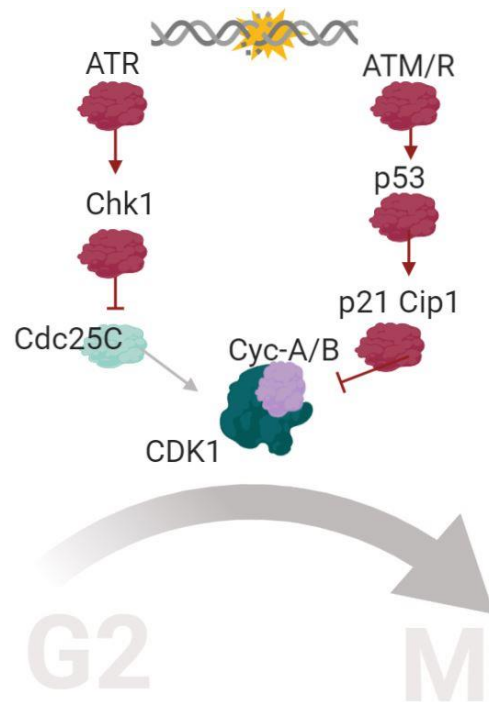


Figure I4. Molecular regulation of the G2/M checkpoint. (Figure created with BioRender).

The Spindle assembly checkpoint (SAC) is a molecular control to ensure the correct segregation of chromosomes during mitosis. It delays anaphase onset until the chromosomes are properly attached to the mitotic spindle, thus avoiding premature separation and chromosome copy number alterations. Unattached kinetochores recruit proteins such as Bub1, BubR1, Mad1, and Mad2. BubR1 and Mad2 sequester Cdc20 and inhibit APC/C. When microtubules are properly attached, Mad2 is released and APC/C is activated. This leads to the phosphorylation and degradation of securin and subsequent activation of separase, which cleaves the cohesins remaining at centromeres, thereby allowing chromatid separation. At the same time, Cyclin B is degraded and CDK1 inactivated, thus allowing mitotic exit (Pérez de Castro et al. 2007).

DNA damage and repair

DNA damage can be produced as a consequence of endogenous sources such as cellular metabolism and problems in DNA replication, or alternatively by environmental insults such as ionizing radiation, ultraviolet radiation or chemical agents. Single strand breaks (SSB) and double strand breaks (DSB) are the most harmful types of DNA damage. (Ciccia and Elledge 2010).

In order to maintain genomic integrity, DNA must be protected from damage. Therefore, in response to DNA damage, cells activate various mechanisms to minimize the effects on their genetic material. When damage is detected, as explained above, the cell cycle is stopped by the DNA damage checkpoints, and the DNA damage response (DDR) machinery is recruited to damage sites to initiate repair. If the damaging insult persists or damage cannot be repaired apoptotic pathways are activated (Ciccia and Elledge 2010).

The DDR includes the molecular processes spanning from the detection of DNA damage to DNA repair and reinitiation of the cell cycle or, alternatively, the induction of cell death. The molecular players of this signaling cascade can be classified as sensors (e.g. RPA, MRN complex), transducers (ATM, ATR, DNA-PK), mediators (e.g. 53BP1, BRCA1), amplification kinases (CHK1, CHK2) and effectors of cellular responses (e.g. p53, Cdc25, p21^{Cip1}) (D'Adda Di Fagagna 2008) (**Figure 15**).

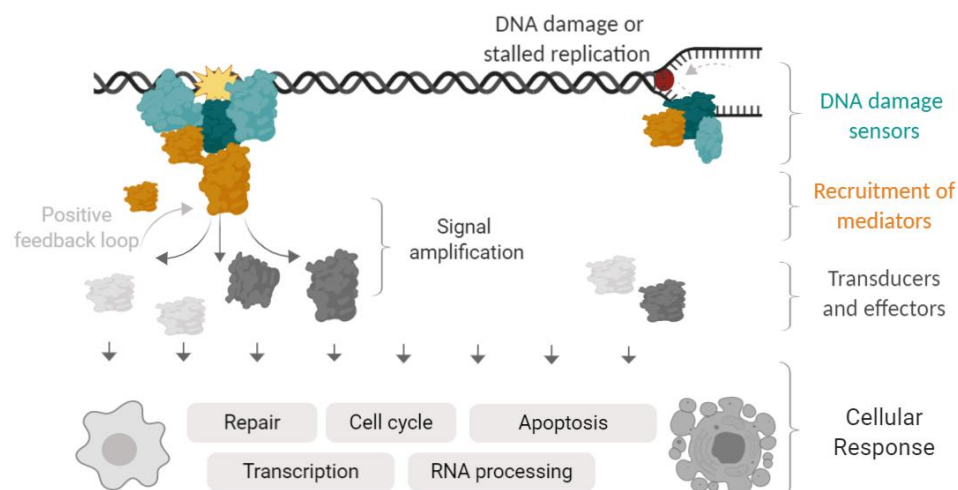


Figure 15. Steps of the DDR. Lesions in the DNA are recognized by sensor proteins, which also stabilize DNA and make scaffold functions for the recruitment of repair proteins. Sensors initiate signaling pathways that will lead to signal amplification and finally control a wide variety of cellular processes. (figure created with BioRender).

Introduction

During DNA replication, the slowing or stalling in replication fork progression can lead to replication fork collapse and DNA breaks. When improperly repaired, SSB originated in this process can become DSB upon convergence with the progressing replication forks. DSB can also be generated as a consequence of exogenous deleterious insults such as ionizing radiation and chemotherapeutic agents. Although this type of damage type is among the most toxic lesions and must be repaired to preserve genomic integrity, several physiologically important processes require programmed DSB. For example, they are required for V(D)J recombination for assembling immunoglobulin and T-cell receptor genes (Mehta and Haber 2014). Moreover, in meiosis, the generation of DSB by the enzyme Spo11 is essential for meiotic recombination (Cooper et al. 2014).

There are two main systems of DSB repair: homologous recombination (HR) and non-homologous end joining (NHEJ). In HR, DNA is repaired using homolog chromosome regions as a template. This mechanism is effective in preventing DNA errors and is only possible in S phase and G2/M phases of the cell cycle. NHEJ is more efficient. However, since it requires ligation of independent DSB ends, it is error prone and it promotes chromosomal aberrations (Helleday et al. 2008).

When DNA is damaged, sensors not only recognize lesions but also stabilize DNA ends and promote the recruitment of repair proteins. Upon DSB or SSB, ATM and ATR are recruited. The recruitment of these transducer kinases leads to the phosphorylation of the histone H2AX on S139 (γ H2AX), a key step in the DDR and a widely used marker of DNA damage (Fernandez-Capetillo et al. 2004). ATM activation at the DSB depends on the MRN complex. When activated, ATM phosphorylates a number of key substrates for DDR at several steps, from sensing to repair. A key ATM substrate is CHK2 (Blackford and Jackson 2017). ATR is activated by several types of DNA damage such as DSB or replication stress, but its main initiator is thought to be single strand DNA (ssDNA) coated with RPA, including ssDNA generated as a result of DSB repair, when DNA is resected. One of the main substrates of ATR is CHK1 (Nam and Cortez 2011). As mentioned before, ATM, ATR and their targets CHK1 and CHK2 phosphorylate p53, leading to its stabilization. P53 regulates the expression of various genes, such as *CDKN1A*, which encodes p21^{Cip1}, and *PUMA* (*p53 upregulated modulator of apoptosis*). The expression of p21^{Cip1} promotes cell cycle arrest, and the

expression of pro-apoptotic proteins such as PUMA induces cell death when damage is not repaired or the stimuli persist (Kasthuber and Lowe 2017).

Nuclear architecture

Advances in molecular genomics have allowed a good understanding of the three-dimensional organization of the eucariotic nucleus. Chromatin organization varies across different processes such as cell cycle progression and differentiation. Chromosomes undergo drastic structural changes every cell cycle, being highly compacted in mitotic cells and more decondensed in interphase. Moreover, there is heterogeneity among the regions of DNA replication, gene transcription and gene silencing (Nagano et al. 2017). Chromosomes largely occupy defined regions in the nucleus, known as chromosome territories, which harbor different levels of organization. Topologically associating domains (TADs) are functional domains of the genome that facilitate interaction within chromatin regions. They are formed by chromatin loops that connect chromatin regions such as promoters and enhancers. (**Figure I6**). Although different characteristics of 3D genome organization are being progressively described, the regulation of the genome distribution within the nucleus is still to be unraveled (Shah et al. 2018).

Proteins in the nucleus can be classified in a broad manner as “diffused” or “aggregated”. Transcription factors and chromatin remodelling factors are examples of proteins frequently distributed as diffused. The aggregated fraction can be composed mainly of proteins associated with DNA or RNA and have a cluster or speckle appearance. It comprises membrane-less structures such as the nucleolus, cajal bodies or nuclear speckles (**Figure I6**). These compartments are dynamic and have been proposed to be assembled through phase transition principles. Most of the proteins within them have disordered domains (Uversky 2017).

It has been shown that specific regions of the genome organize around nuclear bodies. One example is RNA polymerase transcribed rDNA genes, which localize around the nucleolus. Moreover, certain hubs of highly transcribed genomic regions organize around nuclear speckles, whereas gene-poor regions are more prone to localize around the nucleolus (Quinodoz et al. 2018).

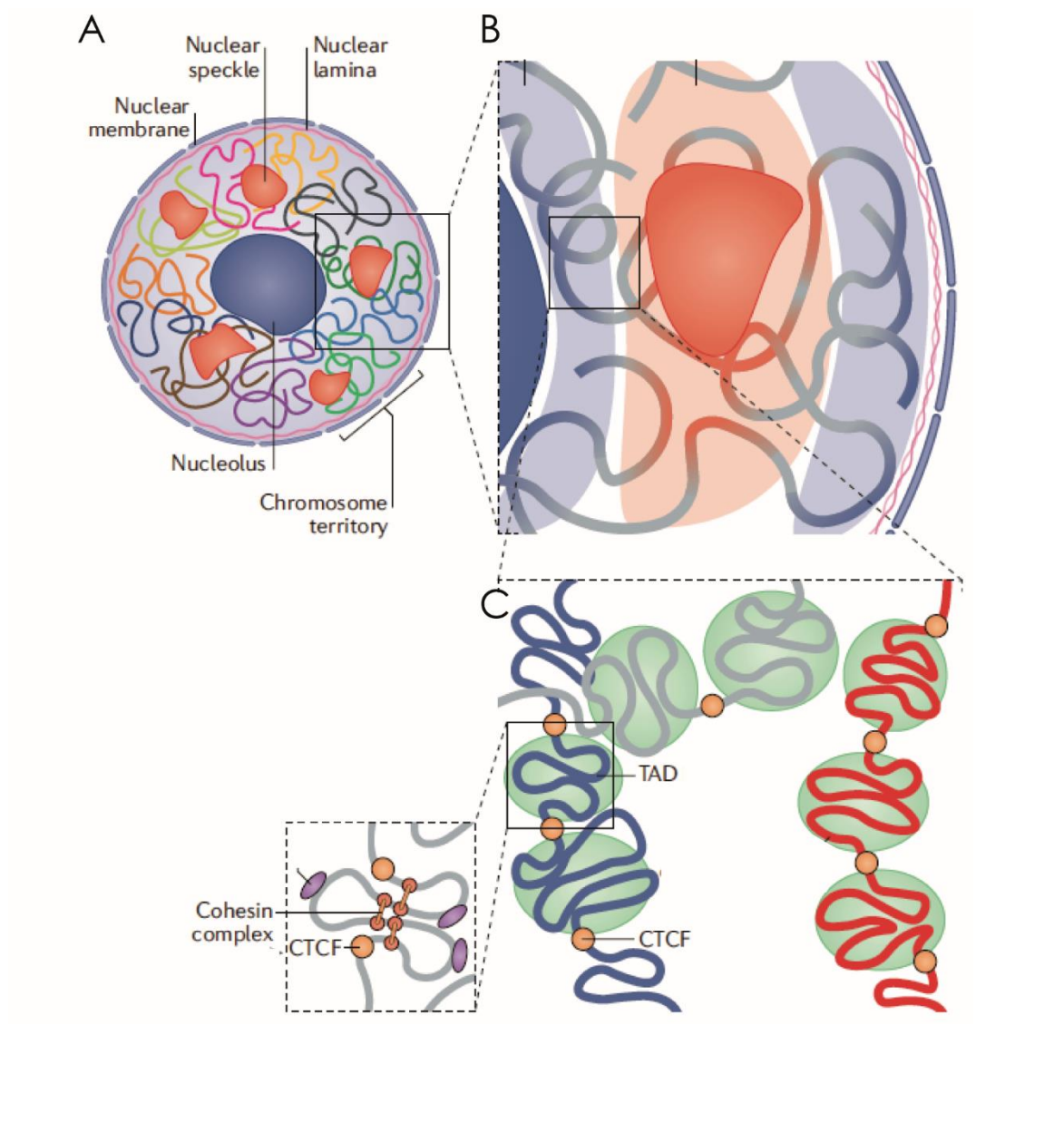


Figure 16. Nuclear architecture and hierarchical organization of the 3D genome. **A.** Representation of the eukaryotic nucleus with nuclear bodies (nuclear speckles and nucleolus). Chromosome territories are filled with different colors. **B.** Certain regions that are transcriptionally active preferentially distribute in the interior of the nuclear space and interact among active regions. These active regions from different chromosomes tend to distribute close to nuclear speckles (red). Inactive regions tend to associate with nuclear lamina and nucleolus (blue). **C.** Genomic domains associate in topologically associated domains (TADs). Inside TADs, cohesin-mediated loop formation facilitate chromatin folding. CTCF and cohesin are essential in regulation of loop dynamics. (Modified from Zheng and Xie 2019).

Cohesins

Cohesins were identified as key molecular regulators of sister chromatid cohesion during mitosis, which is essential for biorientation of chromosomes or the mitotic spindle (Peters and Nishiyama 2012). However, cohesins are also indispensable for several functions, including DNA repair, DNA looping and the regulation of meiosis. The cohesin complex is crucial for genomic stability in homeostasis, and there is growing evidence of its implication in cancer (Losada 2014).

In mammals, cohesin core complexes are composed of four subunits: structural maintenance of chromosomes (SMC) SMC1 and SMC3; Kleisin subunit RAD21 (also named Scc1) and stromal antigen (SA) SA1 or SA2. These proteins interact to form a ring-shaped structure that associates with chromatin. The association is thought to be through its ring-like shape, which encircles the chromatin instead of binding directly to DNA. Therefore, there is not a requirement for recognition of a specific DNA sequence. In addition, the cohesin complex has regulatory factors such as wings apart-like protein homolog (WAPL) and PDS5 proteins, which can associate with the core complex through SCC1 and SA1/2 (Peters et al. 2008).

Cohesin loading occurs in G1 and is assisted by the nipped-B-like protein (NIPBL)-MAU2 heterodimer. On the other hand, cohesin unloading is mediated mainly by WAPL association to PDS5A or PDS5B. Of note, WAPL is essential not only for chromosome arms separation in mitotic prophase but also in meiosis (Bri e o-Enr iquez et al. 2016). A third cohesin interactor, sororin, is thought to bind PDS5, thereby displacing WAPL from the cohesin core and preventing WAPL activity. Sororin phosphorylation generates a conformational change that allows the interaction of WAPL with the structural subunits and the opening of the cohesin ring (Losada 2014; Nishiyama et al. 2010).

During the progression of the cell cycle, there is a dynamic association of the cohesin complex with DNA. In G1, this complex is loaded surrounding single chromatids. In S phase, after DNA replication, cohesin rings encircle the sister chromatids to establish their cohesion. At prophase of mitosis, most cohesins are removed from the sister chromatids through WAPL-PDS5 regulation. This step is regulated by sororin phosphorylation mediated by CDK1 and Aurora kinase B (AURKB) (T. Nishiyama et al. 2010; T. Nishiyama et al. 2013).

Introduction

Cohesion of chromosomes remains only in the centromeric region, where sugoshin 1 keeps cohesin integrity preventing the premature separation of chromatids. Once APC/C is activated, securin is degraded allowing separase activation and cohesin cleavage, leading to chromatid separation. A schematic representation of cohesin regulation during the cell cycle stages is shown in **Figure 17**.

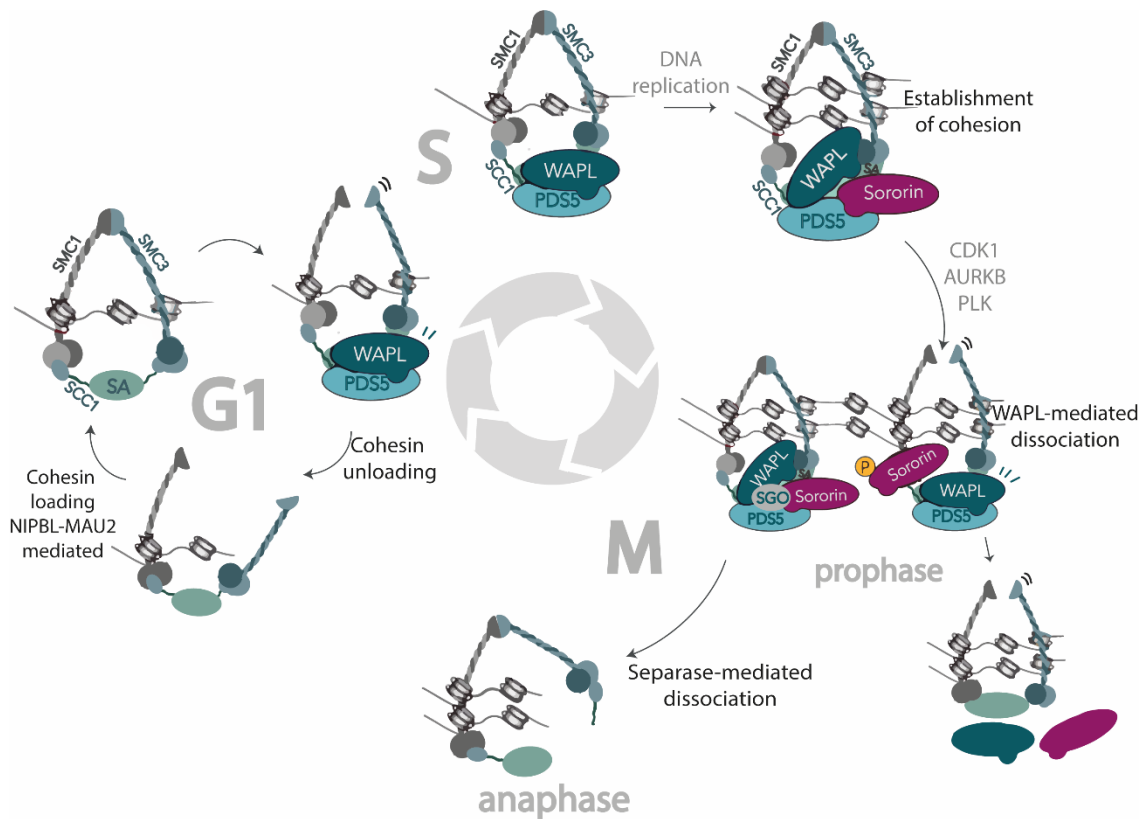


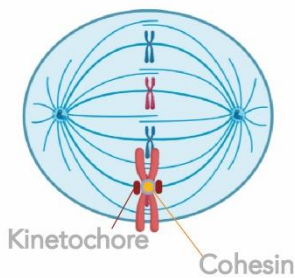
Figure 17. Cohesin dynamics during the cell cycle. (G1). Cohesin is loaded in G1 phase through NIPBL-MAU2 heterodimer mediation. Cohesin remains destabilized by WAPL. (S). When DNA is replicated at S phase, SMC3 is acetylated and this mediates the loading of sororin which displaces WAPL and antagonizes its unloading function; cohesion is established. (M, prophase). Sororin is phosphorylated by kinases such as CDK1 or AURKB, which allows sororin displacement and WAPL binding thereby leading to the opening of the cohesin ring. (M, anaphase). Cohesin remaining at centromeric regions, which is protected by sugoshin1 (SGO1), remains loaded until cleaved by separase, at metaphase-anaphase transition.

Cohesin complexes are crucial for chromatid cohesion-dependent and cohesion-independent functions (**Figure 18**). Among the functions related to chromatid cohesion, the cohesin complex is not only important for chromatid segregation in mitosis but also for DNA replication and DNA repair. For example, it facilitates the use of the sister chromatid as a template for DBS repair by homologous recombination (Losada 2014). Regarding cohesion-independent functions, the role of WAPL and cohesin in chromatin regulation during

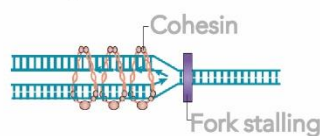
interphase is well established. The deficiency of WAPL causes chromatin compaction in interphase by stabilizing cohesin. Cohesin distribution in the interphasic DNA depends on transcription, CTCF and WAPL. WAPL and CTCF play an essential role in the regulation of TADs and chromatin loops in interphase, which are crucial for DNA replication, transcription and the regulation of gene expression (Busslinger et al. 2017; Haarhuis et al. 2017).

Cohesion dependent

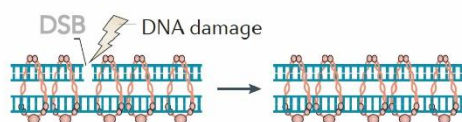
Chromosome orientation & cohesion



DNA replication

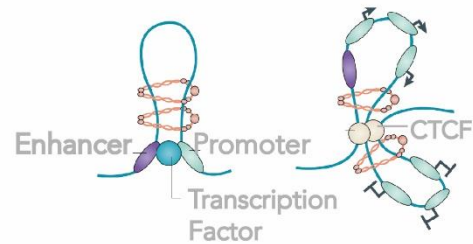


DNA repair. Homologous-recombination

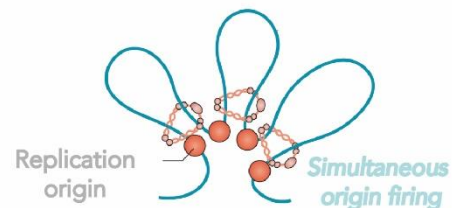


Cohesion independent

Transcription regulation



DNA replication



Genome compartmentalization

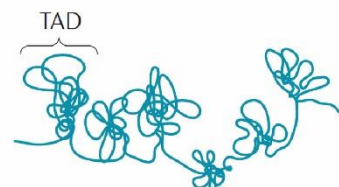


Figure 18. Functions of the cohesin complex during the cell cycle. The different functions are represented differentiating between cohesion-dependent and cohesion-independent. *Mitosis*: essential for preventing precocious chromatid separation and also for chromosome correct orientation. *DNA replication (cohesion dependent)*: cohesin mediates the stabilization of stalled forks, helping their re-start. *DNA repair*: cohesin facilitates the DNA repair using sister chromatid as a template. *Transcription regulation*: facilitates transcription by connecting promoters with enhancer regulatory regions. *DNA replication (cohesion independent)*: cohesin has been proposed to mediate the formation of chromatin loops, which allow simultaneous firing of the clustered origins. *Genome compartmentalization*: facilitates the distribution of TADs, genome partition units. (Modified from Losada 2014).

The role of cell cycle related CDKs and Cyclins *in vivo*

Functional redundancy and complementation in the mammalian cell cycle

Only a subset of the about 20 CDKs and more than 30 cyclins that have been identified are thought to be directly involved in cell cycle regulation. The roles of many of these proteins *in vitro* have been well-established by biochemical studies in yeast and mammalian cells. These studies depict a simplified view of the cell cycle where different CDK-cyclin complexes determine the progression of the distinct phases. However, animal models indicate that the scenario is much more complex. For instance, in contrast to *in vitro* studies, only CDK1 is essential for every cell division in mice (Santamaría et al. 2007), whereas CDK2, CDK4 and CDK6 are dispensable for the cell cycle of most cell types. Several studies have gradually revealed the phenotypes of the individual deletion of different CDKs and cyclins, which are thought to be essential for cell cycle phases. In this regard, Cyclin B1 and Cyclin A2, key CDK1 regulators *in vitro*, have been shown to be essential for the cell cycle of most cells *in vivo*, thereby supporting the notion that these proteins have a crucial role in CDK1 regulation in tissues. (Brandeis et al. 1998; Murphy et al. 1997). The results are summarized in **Figure I9**.

There is evidence for multiple non-consensus interactions between CDKs and cyclins, and also for compensatory roles. For instance, when the Cyclin D interaction partners CDK4 and CDK6 are absent, CDK2 can bind to D-type cyclins (Malumbres et al. 2004). Also, CDK1 can bind to Cyclin E when CDK2 is absent or alternatively to Cyclin D in the absence of CDK4 (Santamaría et al. 2007). Similarly, the CDK partners of Cyclin Y play overlapping roles: loss of function of Cyclin Y results in a Wnt-loss of function phenotype in *Xenopus* embryos, whereas the individual knock-down of Cyclin Y-interacting CDK partners did not show any phenotype (Davidson and Niehrs 2010).

GENE	PHENOTYPE IN SOMATIC TISSUES	PHENOTYPE IN GONADS
<i>CDK1</i>	Embryonic lethality in first cell divisions	
<i>CDK2</i>	Viable	Sterility - defective meiosis
<i>CDK4</i>	Viable. Diabetes and defective postnatal proliferation of endocrine cells	
<i>CDK6</i>	Viable. Defective proliferation of some hematopoietic cells	
<i>CCNA1</i>	Viable	Male sterility; arrest at diplotene. Required for Meiosis II phase entry. Females are fertile
<i>CCNA2</i>	Embryonic lethality E5.5	
<i>CCNB1</i>	Embryonic lethality. Arrest in G2 at 4-cell stage	
<i>CCNB2</i>	Viable	Fertile
<i>CCNB3</i>	Viable	Female sterility. Failure in Met. I to Anaphase I transition
<i>CCND1</i>	Viable. Defects in retina and mammary tissue.	Fertile
<i>CCND2</i>	Viable. Effects in certain neuronal populations of the cerebellum	Female sterility. Due to defects in granulosa cells; male hypoplastic testis
<i>CCND3</i>	Viable. Effects in T-lymphocyte development	Fertile
<i>CCNE1</i>	Viable	Fertile
<i>CCNE2</i>	Viable	Fertile; sub-fertile with smaller testes and reduced sperm count

Figure 19. Summary of CDK and cyclin phenotypes in KO mice. The main mitotic and meiotic phenotypes of the depletion of cell cycle CDKs and cyclins in mice are summarized based on the work reviewed in (Malumbres and Barbacid 2009) and (Chotiner et al. 2019).

This functional redundancy and complementation results in a lack of abnormal phenotypes in the KO models of several cell cycle proteins. Sometimes the combined KO of multiple family members is necessary in order to detect severe effects in mice. Of note, the absence of phenotypes in interphase CDKs is not simply a consequence of redundancy, as the combined deletion of multiple family members of these kinases unmasks phenotypes in some cell types, but they are not essential for proliferation of every cell in the body under homeostatic conditions. Some examples of the phenotypes arising from the combined KO of CDKs or cyclins are summarized below.

Cdk2 and Cdk4 double KO mice show defects in embryonic cardiomyocytes that cause embryonic lethality (Barrière et al. 2007; Berthet et al. 2006). Cdk4 and Cdk6 double KO mice show late embryonic lethality produced by the impaired proliferation of hematopoietic

Introduction

precursors with no other major phenotypes (Malumbres et al. 2004). The triple KO of the interphasic CDKs Cdk2, Cdk4 and Cdk6 causes embryonic lethality due to hematopoietic defects and decreased cardiomyocyte precursors (Santamaría et al. 2007).

Cyclin D1, Cyclin D2 and Cyclin D3 triple KO mice show embryonic lethality resulting from hematopoietic and myocardium development defects, very similar to the phenotype observed in CDK4 and CDK6 double KO mice. This observation suggests that these cyclins are fundamental in the regulation of these kinases also *in vivo*.

Of note, some KO combinations that show embryonic lethality also have meiotic effects when specifically deleted in gonads. For instance, conditional KO of Cyclin A2 in postnatal oocytes shows abnormalities in meiosis II spindle formation (Chotiner et al. 2019).

Meiotic cell cycle and gametogenesis

Meiosis is the process that allows the formation of gametes with a haploid set of chromosomes for sexual reproduction. This is achieved by two consecutive chromosome segregation events preceded by a single round of DNA replication. Although this process is not strictly speaking a cycle, many of the key regulators are common to the regulation of the mitotic cell cycle. The generation of gametes requires both specific meiotic proteins and general cell cycle regulators. During this process, specialized cell cycle proteins will ensure that there are two consecutive segregation events (Marston and Amon 2004).

After DNA replication, meiosis I starts with a particular prophase that is subdivided into four stages: leptotene, zygotene, pachytene and diplotene. During the meiosis I prophase, homologous chromosomes align and undergo recombination between non-sister chromatids. At the onset of prophase, in the leptotene stage, DSB are generated throughout the chromosomes by Spo11, and the breaks are repaired by HR. The chromosomes start to repair and synapse at zygotene where the axial core of homolog chromosomes is tightly linked forming the synaptonemal complex. Chromosomal synapses are then completed and chromosomes recombine to form crossovers. Finally, at diplotene stage, chromosomes de-synapse. After that, metaphase-I and anaphase-I are completed, thereby separating the duplicated homolog chromosomes. This is followed by meiotic division II, which produces haploid spermatids. Meiosis II occurs rapidly and closely resembles a mitotic division, but

without a step of DNA replication. Cohesin complexes play crucial roles in segregating the homologs during meiosis I, being major components of the axial core of each homolog. Some cohesin subunits and regulators that operate in meiosis are shared with the mitotic cell cycle and others are specific for meiosis. Sexual chromosomes in males only share homology in a small region. Outside this region, the sex chromosomes remain unsynapsed and are condensed to form a compact structure known as the sex body (Reig-Viader and Ruiz-Herrera 2016; Subramanian and Hochwagen 2014).

In the process of gametogenesis, primordial germ cells formed during embryonic development undergo mitotic division and eventually enter meiosis I. This process is carried out in different stages of development and adult life depending on the sex.

Spermatogenesis: in males, primordial germ cells go through several rounds of mitosis in the embryo and then enter G0 arrest. Proliferation is resumed after birth and the pool of spermatogonia stem cells is established. Spermatogenesis is maintained from puberty throughout life. Spermatogonia, which are diploid (2C), continuously generate tetraploid (4C) primary spermatocytes in a process that requires a switch from the mitotic cell cycle to meiosis. Spermatocytes then undergo two rounds of meiotic divisions to generate spermatids. Primary spermatocytes divide generating secondary spermatocytes (2C), whose division generates haploid spermatids (1C) (Sun et al. 2018) (**Figure I10, upper part**). In adult mice, several waves of spermatogenesis occur simultaneously, and the seminiferous tubule contains germ cells coordinated at different development stages (Phillips et al. 2010).

Oogenesis: in females, the meiotic process starts in embryonic stages, and cells are then arrested in diplotene of prophase I until the moment of ovulation in the adult organism. In the adult, in response to luteinizing hormone, oocyte maturation and meiotic progression is resumed and involves germinal vesicle breakdown and the finalization of meiosis I. Cells then remain arrested in metaphase of meiosis II until fertilization (**Figure I10, lower part**) (Li and Albertini 2013).

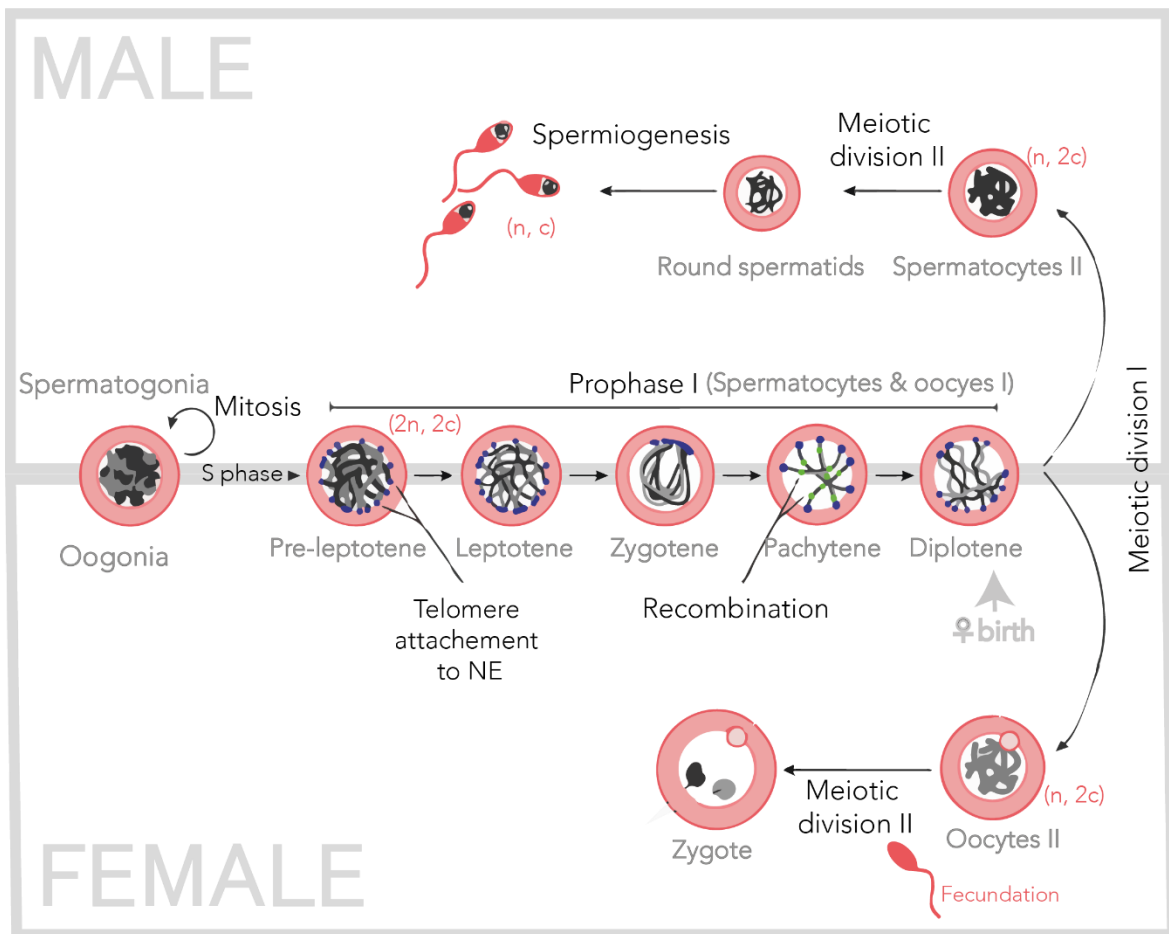


Figure I10. Representation of male and female gametogenesis and meiosis in mice. In males, after birth mitotic divisions of spermatogonia are resumed from puberty throughout the adult's life. In females, meiosis starts in embryonic stages. Cells remain arrested in diplotene until the moment of ovulation in the adult. Telomere and chromosome dynamics in meiotic prophase I are represented; telomeres attach to the nuclear envelope at pre-leptotene, synapsis starts at zygotene and concludes at pachytene, when meiotic recombination occurs. At diplotene, chromosomes desynapse. (Inspired by Reig-Viader and Ruiz-Herrera 2016).

Role of Cdk2 *in vivo*

CDK2 is classically considered an interphasic CDK regulator that is essential for G1/S transition and S phase progression in association with Cyclin E and Cyclin A, respectively. However, genetic models revealed that constitutive CDK2 KO mice develop normally and are viable, with no major defects in somatic tissues. Moreover, immortalized CDK2 KO mouse embryonic fibroblasts (MEFs) do not have significant defects in proliferation, although they were shown to enter the culture crisis stage earlier than immortalized WT MEFs (Ortega et al. 2003). In contrast, CDK2 has an indispensable role in meiosis, and testes of postnatal day 20 (P20) CDK2 KO mice are atrophic, with massive apoptosis. Furthermore, spermatocytes are arrested in pachytene-like stage of meiotic prophase. CDK2 has been reported to be crucial for meiotic telomere attachment to the nuclear envelope (Ortega et al. 2003; Viera et al. 2015).

Despite the KO of CDK2 does not have any phenotypes incompatible with life, a role of this kinase in particular cell populations of the brain has been proposed. Progenitors and neural stem cells (NSCs) from adult brains of CDK2 KO mice were reported to show reduced proliferation both cultured as neurospheres and in *in vivo* analysis (Jablonska et al. 2007).

Neurogenesis and the cell cycle

NSCs are capable of generating neurons and glial cells, including astrocytes and oligodendrocytes, both in the developing and adult brain. Neurogenesis starts from early development, and in the postnatal brain, few neurogenic zones are present. The main neurogenic regions in the adult are restricted to the sub-ventricular zone (SVZ), and the sub-granular zone (SGZ) of the dentate gyrus (DG) in the hippocampus (**Figure I11**). NSCs of the SVZ generate neurons and oligodendrocytes, while the SGZ produces neurons and astrocytes. Neurogenesis in the adult brain is more restricted than in embryos. One of its main features is that while embryonic NSCs have a high proliferative rate, adult NSCs, similarly to stem cells in other mature tissues, remain arrested at G0 phase for long periods (Götz and Huttner 2005; Urbán and Guillemot 2014).

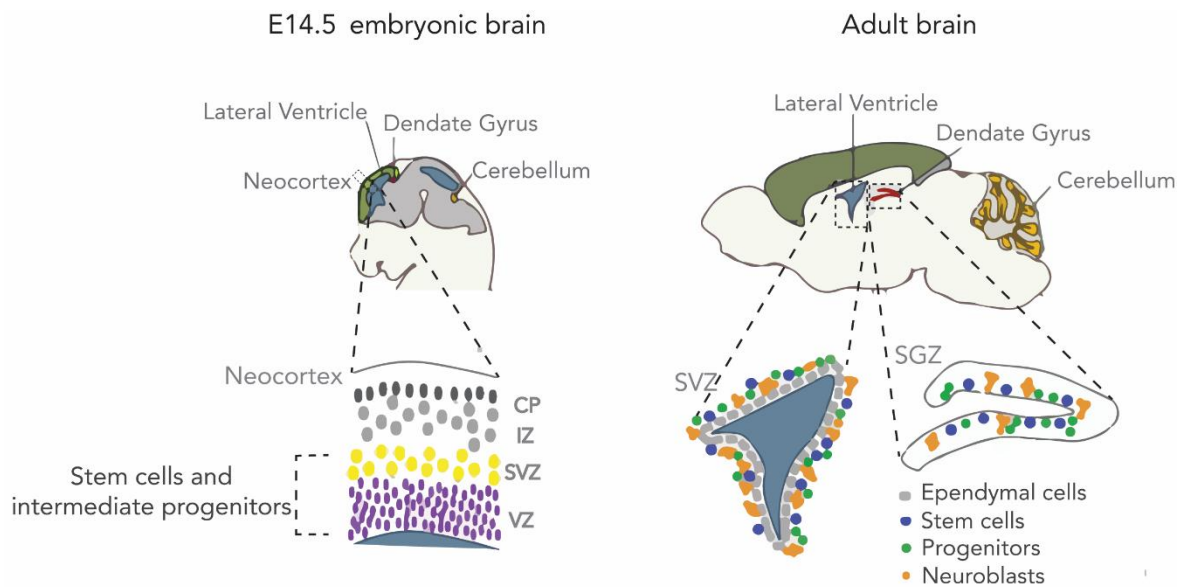


Figure I11. NSCs in the embryonic and adult brain. On the left, sagittal representation of the embryonic brain with expanded view of the neocortex at the bottom. The stem cells and progenitors are restricted to the ventricular zone (VZ) and subventricular zone (SVZ) of the neocortex, adjacent to the ventricle. The intermediate zone (IZ) contains migrating cells and the cortical plate (CP) is formed by post-mitotic neurons. The CP grows during development and originates the adult isocortex (green). On the right, the two main neurogenic regions are represented in a sagittal view of adult brain, the sub-ventricular zone (SVZ) and sub-granular zone (SGZ) of the Dentate Gyrus (dashed lines). (Inspired by Barazzuol et al. 2015).

The ventricle of the adult mammalian brain contains several thousand NSCs distributed along its walls. These NSCs generate transit amplifying progenitors (TAPs), which later produce neuroblasts that continuously migrate along the rostral migratory stream to the olfactory bulb, giving rise to granule and periglomerular neurons (Lim et al. 2016; Ponti et al. 2013) (**Figure I12**).

In both the embryo and adult brain, NSCs are considered a specialized kind of glia located in the neurogenic niches (Kriegstein and Alvarez-Buylla 2009). Interestingly, after brain injury, dormant NSCs in neurogenic niches can be activated and proliferation is boosted, which is believed to contribute to lesion repair (Llorens-Bobadilla et al. 2015).

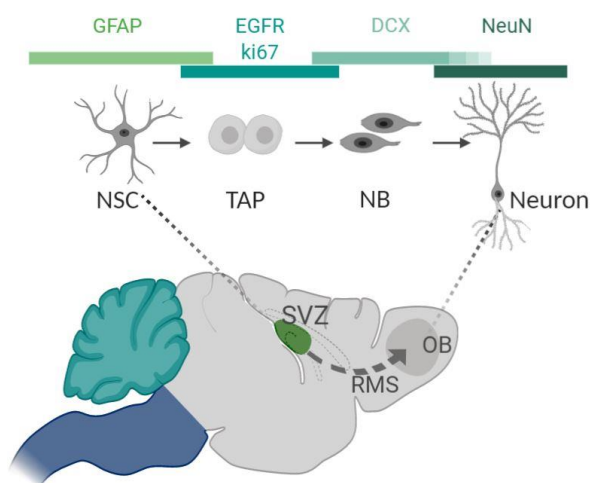


Figure I12. Representation of neural differentiation stages in NSCs produced at the SVZ. The ventricle of the SVZ contains NSCs distributed along its walls that produce transit amplifying progenitors (TAP), which then divide and produce neuroblasts (NB) that migrate through the rostral migratory stream (RMS) to the olfactory bulb (OB) and have restricted division capacity. Then cells will differentiate to interneurons. Some of the markers of the different differentiation stages are indicated. (Gusel'nikova and Korzhevskiy 2015; Ming and Song 2011; Walker et al. 2007) (figure created with BioRender).

Several studies have addressed the role of different CDKs and cell cycle proteins in regulating brain NSCs. Proliferation defects have been found in the SVZ upon CDK2 depletion *in vivo* and also in adult progenitors when cultured as neurospheres (Jablonska et al. 2007), a widely used system to study neural progenitors and NSCs *in vitro* (Pastrana et al. 2011). Conversely, no differences in embryonic stem cell proliferation were observed in the same study, which was explained by the complementation of CDK4, which is upregulated in CDK2 KO embryonic brains. Accordingly, a different study has shown that CDK2 and CDK4 double KO embryo brains have ablated intermediate zone and cortical plate, and NSCs proliferate but their cell cycle is altered and they are predisposed to differentiate into neurons (Lim and Kaldis 2012). Studies involving interphasic CDKs have shown a correlation between a longer G1 phase and an increased rate of differentiation. CDK6 has been shown to play a role in proliferation in the DG and SVZ of adult brains, with CDK6 KO showing a longer G1 phase and increased differentiation (Beukelaers et al. 2011). CDK2 and CDK4 double KO are also more prone to differentiate into neurons (Lim and Kaldis 2012). Conversely, shortening the cell cycle by CDK4-Cyclin D overexpression expands the progenitor cells, resulting in a thicker SVZ and larger surface area of the cortex (Lange et al. 2009).

Other cell cycle regulators are also involved in brain development and neurogenesis. Although the absence of Cyclin D2 seems to be compensated by Cyclin D1 in embryos, Cyclin D2 has been proposed to be important for adult proliferation and neurogenesis in the DG and SVZ (Kowalczyk et al. 2004). CDK5 and its non-cyclin regulators p35 and p39 are

Introduction

important in post-mitotic neurons and are involved in the migration of neuroblasts from the SVZ to the olfactory bulb and in the adult hippocampal neurogenesis (Hirasawa et al. 2004; Ko et al. 2001; Lagace et al. 2008; Ohshima et al. 1996).

In addition, CKIs also have important roles in the brain. P27^{Kip1} KO mice have increased TAPs and decreased neuroblasts, while the number of NSCs is not affected. The overall proliferation is increased in p27^{Kip1} KO in both basal and ischemia conditions (Doetsch et al. 2002; Qiu et al. 2009). P21^{Cip1} has been shown to be important for adult NSC expansion through the regulation of Sox2 expression (Marqués-Torrejón et al. 2013).

Cancer and cell cycle regulators

Tumors are complex tissues with uncontrolled cell proliferation potential. Their development is progressive and involves the accumulation of genetic abnormalities over time. Cancer is considered an evolutionary process in which cells gather mutations sequentially undergoing a sub-clonal selection. These mutations may arise from environmental factors or intrinsic processes such as replication errors, thereby providing distinctive capabilities related to cell growth, survival and dissemination, defined as the *hallmarks of cancer* (Hanahan and Weinberg 2011). Tumor cells can acquire the ability to maintain sustained proliferation through a number of mechanisms. For example, they can produce growth factor ligands that lead to autocrine proliferative signaling (Heldin 2012) or express constitutively active mutated forms of proteins such as the oncogene B-Raf, which stimulate mitogenic signaling without the requirement of growth factors (Fiskus and Mitsiades 2016). In addition to cancer cells, the *tumor microenvironment* includes immune cells, fibroblasts and endothelial cells. These tumor associated cells can provide growth factors, angiogenic factors or other signals required for the evasion of apoptosis (Gajewski et al. 2013; Pietras and Östman 2010). Moreover, cancer cells develop systems to actively evade recognition and elimination by immune cells (Chen and Mellman 2017).

Genetic alterations in oncogenes (overexpression, amplification and gain of function) or tumor suppressors (deletion, silencing and loss of function) are widely known to be crucial for cancer. However, tumor development also depends also on proteins and pathways that are not oncogenic per se. These pathways are frequently important for the cancer cell but

are not required to the same extent for normal cell fitness. This has been referred to as “non-oncogene addiction”. The idea is that tumor cells experience numerous stresses, such as DNA damage and replication or metabolic stress, which are less frequent in normal cells, thereby making tumor cells more dependent on stress support pathways (Luo et al. 2009).

Cell cycle checkpoint regulators and CDK inhibitors are frequently lost or overridden during the process of malignant transformation. This loss of checkpoints and the subsequent alterations in genome maintenance and repair mechanisms lead to chromosomal instability (CIN) and genomic instability (GIN). GIN is an established hallmark of cancer that is present in most of the tumors, it leads to the accumulation of mutations in cancer cells (Negrini et al. 2010). However, the loss of checkpoints can also make tumor cells more sensitive to cell death caused by genotoxic drugs, raising the possibility of eliminating cancer cells by exaggerating the checkpoint control losses that initially led to their uncontrolled proliferation (Dobbelstein and Sørensen 2015). As a result, inhibitors of DNA damage checkpoints or repair proteins are being studied as potential boosters of cancer cell vulnerabilities by deregulation of the balance between stress support pathways and stress (J. Luo et al. 2009). One example is the targeting of BRCA1 and BRCA2 mutated tumors with PARP inhibitors (Lord and Ashworth 2017). ATR inhibitors are also being explored for cancer treatment due to their ability to enhance replication stress and GIN (Lecona and Fernandez-Capetillo 2018).

CDKs and Cyclins in cancer: besides the studies clarifying the roles of interphasic CDKs in somatic cells, an important question remains. Do tumor cells retain the same cell cycle requirements as their cells of origin? A better understanding of the requirements for interphase CDKs in cancer cells should help to develop strategies to target specific tumors more efficiently (Asghar et al. 2015).

CDK4 and CDK6 and their activator Cyclin D have been found overexpressed or amplified in several tumors such as sarcoma, glioma or breast cancer. Conversely, CDK2 is not usually mutated; however, the regulators of this kinase are frequently altered. Cyclin E is often overexpressed in human tumors and p21^{Cip1} and p27^{Kip1} are frequently silenced. Another example is Skp2, a ubiquitin ligase that targets p27^{Kip1} and p21^{Cip1} for degradation, which has also been found overexpressed (Gstaiger et al. 2001; Hershko 2008 ; Chu et al. 2008; El-Deiry and Wafik 2016). These observations suggest that although CDK2 is not usually directly

Introduction

affected by mutations, its activity might be indirectly modified through its regulation system. In line with this idea, transgenic mice overexpressing Cyclin E1 in the mammary gland develop mammary tumors (Bortner and Rosenberg 1997).

In an attempt to modulate the function of CDKs in the cancer cell cycle, CDK inhibitors have been tested for cancer therapies. However, this has been historically challenging. The first rounds of inhibitors had low selectivity, affecting different CDKs. Therefore, the lack of therapeutic window was possibly a consequence of targeting critical proteins for the proliferation of normal cells such as CDK1. Moreover, in many cases, there was a poor understanding of the mechanisms of action. Interestingly, several clinical studies targeting CDK4 and CDK6 have shown promising clinical efficacy. However, some tumors seem to be resistant or acquire rapid resistance to these inhibitors. In these cases, other CDKs such as CDK2 are likely to compensate (Asghar et al. 2015; Malumbres and Barbacid 2009; Otto and Sicinski 2017).

In addition to their role as effectors of the DNA damage checkpoint pathways, CDKs also participate in regulation of DNA repair. For instance, the yeast CDK1 seems important in DNA resection for homologous recombination in DSB repair (Huertas et al. 2008). Moreover, human CDK1 and CDK2 phosphorylate BRCA2 to regulate its interaction with RAD51, which is important for the stimulation of the homologous recombination repair pathway in S and G2 phases (Esashi et al. 2005). CDK1 has also been proposed to phosphorylate RAP80, a protein that targets BRCA1 to DNA damage sites (Cho et al. 2013).

Atypical CDK activators: the RINGO proteins

Although cyclins are universal CDK activators, there are cases in which CDKs are activated by proteins not belonging to the cyclin family and independently of cyclin binding. The proteins p35 and p39 are examples of atypical CDK5 activators. These proteins have very little sequence similarity with cyclins, although they have been reported to adopt a similar three-dimensional structure to the so-called cyclin box fold (CBF). As mentioned above, activated CDK5 has been reported to have functions in post-mitotic cells of the brain (Tsai et al. 1994; Tang et al. 1995; Shupp et al. 2017).

RINGO proteins are another case of atypical CDK activators. The first RINGO protein was discovered in *Xenopus*, in two independent screenings. The first screening aimed to find proteins that, when overexpressed in G2-arrested *Xenopus* oocytes, were able to trigger meiotic maturation, and named it RINGO (**R**apid **I**nducer of **G**2/**M** progression in **O**ocytes) (Ferby et al. 1999). The other screening searched for *Xenopus* genes that were able to confer resistance to UV when overexpressed in a Rad1-deficient mutant of the yeast *Schizosaccharomyces pombe*, and named it Speedy (Lenormand et al. 1999). Co-immunoprecipitation (co-IP) studies revealed that RINGO/Speedy interact with CDK2. Moreover, RINGO was shown to be able to directly activate CDK2 kinase activity *in vitro* (Ferby et al. 1999; Lenormand 1999).

In mammals, there are several homologs of *Xenopus* RINGO/Speedy (XRINGO): RingoA, RingoC and RingoE in humans; RingoA, RingoB and RingoD in mouse. Of note, RINGO family proteins differ notably between human and mouse, with RingoA being the most conserved among species (**Figure I13**). In humans, RingoA (also referred to as Spy1) is expressed as two splicing variants, RingoA1 and RingoA2 (Nebreda 2006).

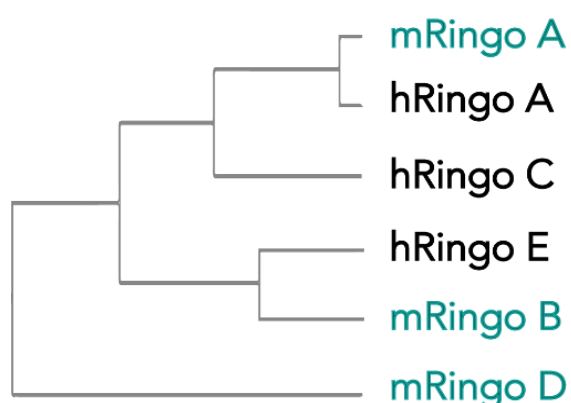


Figure I13. Phylogenetic tree of mammalian RINGO proteins. Human and mouse RingoA have 85% identity and are the most similar to XRINGO. The different mouse homologs are shown in blue and human homologs in black. Alternative names listed are as follows:
 RingoA/SpeedyA/Ringo3/Spy1
 RingoB/SpeedyB/Ringo4
 RingoC/SpeedyC/Ringo2
 RingoD/SpeedyD/Ringo5
 RingoE/SpeedyE/Ringo1
 (Adapted from Nebreda 2006).

RingoA structure and CDK activation

All members of the RINGO protein family have a central conserved region of approximately 140 residues referred to as the Ringo box (or S/R box), which is the region required for CDK binding. Mutational analysis has revealed that most polar and conserved residues within this region are required for RINGO-CDK interaction. At the same time, mutation of only two residues are required for RINGO-CDK interaction. At the same time, mutation of only two residues in the CDK2 PSTAIRE region abolishes XRINGO-CDK2 binding: Ile-49 and Arg-50, similar to those required for the interaction between CDK2 and Cyclin A. Overexpression studies in *Xenopus* oocytes have shown that the RINGO Box is necessary and sufficient for CDK activation by RINGO proteins. Although dispensable for XRINGO activity, the C terminal region may in some cases contribute to CDK activation. The N-terminal domain seems important for RingoA stability, as truncated N-terminal forms are more stable (Cheng et al. 2005; Dinarina et al. 2005; Nebreda 2006; Porter et al. 2002). RINGO proteins have very little similarity in amino acid sequence with cyclins; however, structural studies have shown that the RingoA box adopts a CBF that binds CDK2 in the same position as the N-terminal CBF of Cyclin A (**Figure I14**). Moreover, the secondary structural elements of the RINGO box at the CDK PSTAIRE interphase align with Cyclin A. The largest interface between RingoA and CDK2 is between PSTAIRE of CDK2 and the helices $\alpha 3$ and $\alpha 5$ of RingoA (McGrath et al. 2017).

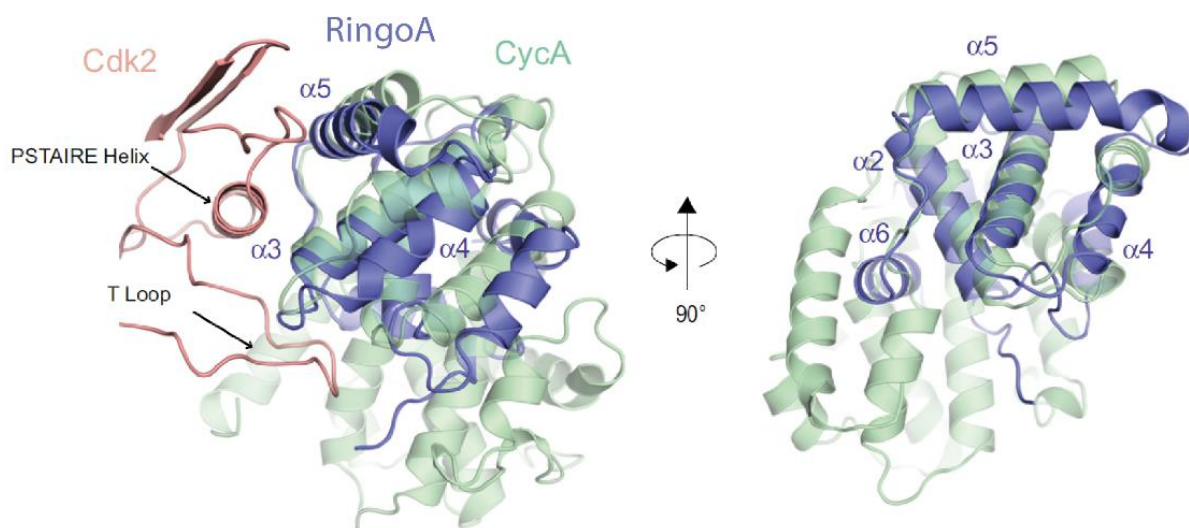


Figure I14. Comparison of CDK2-RingoA and CDK2-Cyclin A structures. The CDK2 kinase domain of both complexes are aligned. The helices of RingoA protein that contact the PSTAIRE domain of CDK2 have a similar conformation to those of Cyclin A. (McGrath et al. 2017).

RINGO activates CDK1 and CDK2 independently of Thr-160 phosphorylation

Not long after XRINGO was discovered, *in vitro* studies using purified recombinant proteins and *Xenopus* oocytes were done in order to evaluate CDK1 and CDK2 activation. As explained, CDK1-Cyclin B and CDK2-Cyclin A complexes are fully active only after CAK mediated phosphorylation of a residue located in the T-loop (Thr-161 for CDK1 and Thr-160 in CDK2). Surprisingly, XRINGO is able to activate CDK1 and CDK2 independently of the presence of CAK proteins or Thr phosphorylation (Karaïskou et al. 2001). In addition to XRINGO, mouse and human RingoA, RingoB, RingoC and RingoE have also been shown to bind to and directly activate CDK1 and CDK2. Moreover, RingoE overexpressed in *Xenopus* oocytes binds to CDK5 (Cheng et al. 2005; Dinarina et al. 2005; Porter et al. 2002).

The CDK2-RingoA crystal structure gave further insights into the differences between CDK activation by RingoA and Cyclin A. The structure of CDK2 bound to residues of the RINGO (S/R) box was found to be similar to the CDK2-Cyclin A structure (Jeffrey et al. 1995). Upon RingoA binding, the PSTAIRE region and the T-loop of CDK adopt a conformation associated with the active kinase. Importantly, the non-phosphorylated form of CDK2-RingoA adopts a conformation similar to the phosphorylated CDK2-Cyclin A complex. This observation further supports the notion that the binding of RingoA suffices to activate CDK2 regardless of the Thr160 phosphorylation state. Consistent with this, phosphorylated CDK2-Cyclin A shows a two-fold decrease in Michaelis-Menten constant (K_m) compared to non-phosphorylated CDK2-Cyclin A. In contrast, CDK2-RingoA has a very similar K_m independently of whether Thr-160 of CDK2 is phosphorylated or not. Mutational analysis have identified the residues D97 and E135 as critical for interaction with the T-loop of CDK2 and important for activation of the complex (McGrath et al. 2017).

Furthermore, Wee1 and Myt1 kinases are known to phosphorylate CDK Thr-14 and Tyr-15 inhibitory residues, and these phosphorylations must be removed for complete kinase activation. Interestingly, Myt1 is less efficient at inhibiting CDK-XRINGO complexes than CDK-cyclin complexes (Karaïskou et al. 2001).

The observation that RINGO can activate CDK2 regardless of its activating phosphorylation and that RINGO-CDK complexes are less inhibited by inhibitory phosphorylation suggests

Introduction

that RINGO proteins might be important in specific situations in which CDK-cyclin complexes are inhibited.

Regarding CDK-RINGO substrates, there is evidence of broader substrate specificity by RINGO activated complexes compared with CDK2-Cyclin A complexes. Studies using peptide libraries have shown a preference of Lys at +3 position of the phospho-acceptor site ((S/T)PX(K/R)) for CDK2-RingoA complexes (Cheng et al. 2005). During *Xenopus* oocyte G2/M phase transition, CDK-XRINGO phosphorylates three residues at the N-terminal regulatory domain of Myt1 thereby promoting its inhibition, and these residues are poorly phosphorylated by CDK-cyclin complexes (Ruiz et al. 2008). Therefore, CDK-RINGO complexes seem to differ in substrate specificity (**Figure I15**). It has also been shown that XRINGO binds to Myt1 in a different region than cyclins, which may account for the different sites phosphorylated by the two CDK2 complexes (Ruiz et al. 2008). Therefore, the properties of RingoA are intriguing: it can activate CDK regardless of T160 phosphorylation, it shows reduced susceptibility to inhibitors, and it can potentially direct CDKs to phosphorylate specific substrates.

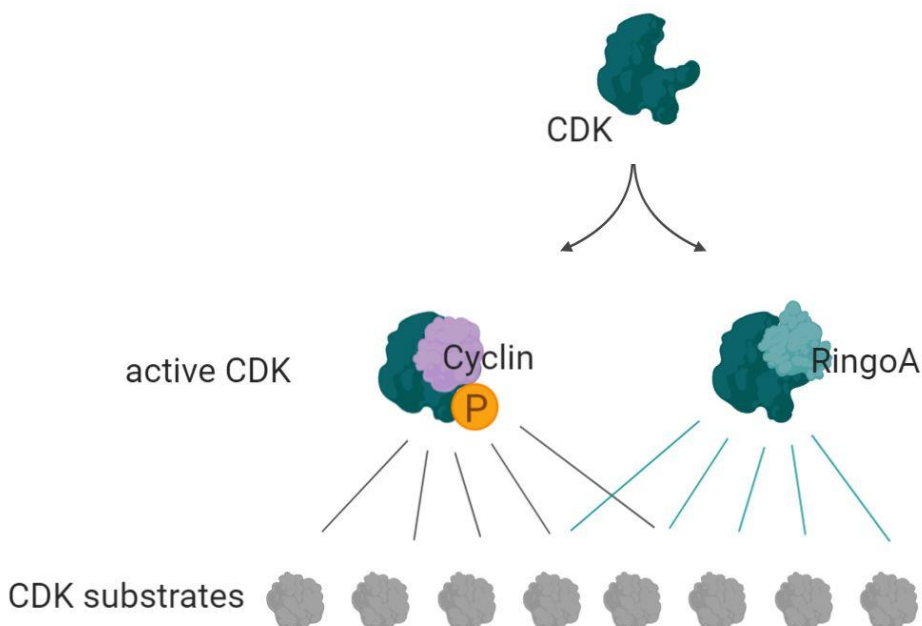


Figure I15. Model for CDK-RINGO substrate phosphorylation. CDK-RINGO may target different subsets of phosphorylation sites in the same or different proteins.

Proposed functions of RINGO in cell cycle regulation *in vitro*

Regulation of RINGO proteins during the cell cycle

Studies in U2OS cells showed that RingoA mRNA is expressed in all stages of the cell cycle, but that it peaks in M phase, very similar to Cyclin A2. Moreover, constitutively overexpressed myc-RingoA protein accumulates periodically, reaching the highest peak in the G1 phase. Interestingly, RingoA is phosphorylated in mitosis (Dinarina et al. 2009). Overexpressed RingoA protein was found to be highly unstable and degraded by the proteasome, as it accumulates upon treatment with the MG132 inhibitor. Interestingly, the expression of a non-degradable form of RingoA results in impaired cell cycle progression. The ubiquitin ligase Skp2 was identified as capable of binding RingoA and of inducing RingoA degradation (Dinarina et al. 2009). NEDD4 is another ubiquitin ligase proposed to induce RingoA degradation in human cell lines (Al Sorkhy et al. 2009).

RingoA interacts with p27^{Kip1}

RingoA was proposed to be important for G1/S transition in human cell lines. This was based on different observations: RingoA overexpression resulted in a reduction of G1 length and conversely, RingoA siRNA led to an increase in G1 and reduction in G2/M phases (Porter et al. 2002). As a potential explanation for the changes in G1, p27^{Kip1} was identified as an interactor of human RingoA/Spy1 (Porter et al. 2003), as well as of RingoC and RingoE (Dinarina et al. 2005).

RingoA overexpression was claimed to overcome p27^{Kip1} mediated arrest in G1 (Porter et al. 2003) by activating CDK2 for the phosphorylation of p27^{Kip1} at T187 both *in vitro* and in cells (McAndrew et al. 2007). To further understand the interplay between RINGO and p27^{Kip1} in cell cycle regulation, it should be noted that CDK2-RINGO complexes have reduced sensitivity to inhibitors such as p21^{Cip1} and p27^{Kip1}. These proteins bind to the cyclin CBF through the MRAIL region, which RINGO lacks, thereby explaining for the poor inhibition (Karaïskou et al. 2001; McGrath et al. 2017). Of note, despite the binding of p27^{Kip1} to the CDK2-RingoA complex is weak due to the lack of MRAIL, p27^{Kip1} still shows some inhibitory activity although weaker than on CDK2-Cyclin A (McGrath et al. 2017).

Introduction

RingoA and DNA damage

RingoA has been proposed to participate in the DDR. First, it was identified as being able to confer resistance to UV in Rad1-deficient *Schizosaccharomyces pombe* (Lenormand 1999). Moreover, in the U2OS human cell line, the overexpression of RingoA was proposed to increase cell survival in response to genotoxic drugs (Barnes et al. 2003). The RingoA-overexpressing U2OS cells show reduced levels of phospho-Chk1 and phospho-RPA, two proteins involved in the DDR (Gastwirt et al. 2006). Conversely, NSC34 cells overexpressing SOD1^{G93A} to induce DNA damage show increased cell death upon treatment with RingoA siRNA (Wang et al. 2019).

Taken together, the experiments using cell lines and overexpressed proteins have linked RingoA to cell cycle regulation and checkpoint signaling. However, they do not necessarily reveal the physiological role of endogenous RingoA in a tissue context. Therefore, the use of genetic models to generate KO mice should help to elucidate the physiological roles of RINGO proteins *in vivo*.

Physiological roles of RINGO proteins

RingoA in meiosis

Recent studies using mouse genetic models have shown that RingoA is essential for meiosis in both males and females, phenocopying the phenotypes of CDK2 KO mice (Mikolcevic et al. 2016). Together with the observation that RingoA can complex with CDK2 and activate this kinase, these findings suggest that RingoA is an essential activator of CDK2 during meiosis. These observations are supported by another study published later (Tu et al. 2017).

Both reports show that RingoA is localized to the telomeric regions of spermatocytes, overlapping with TRF1 from leptotene to pachytene. This location at telomeres is very similar to the location described for CDK2. In pre-leptotene, RingoA is detectable only in telomeres that are in contact with the nuclear envelope. RingoA co-localizes with CDK2 in telomeres from leptotene and its expression is then maintained during leptotene and zygotene. The signal disappears from telomeres as cells enter diplotene. Moreover, RingoA and CDK2 also co-localize along the asynapsed axial elements of sex chromosomes in 58% of their surface.

RingoA was shown to interact with CDK2 in testis by co-IP (Mikolcevic et al. 2016; Tu et al. 2017). RingoA protein expression in testis starts from postnatal day 12 (P12). Conversely, in female germ cells mRNA expression starts around 14.5 day post coitum (dpc14.5), when they enter meiosis, and decreases when they become arrested at dictyate (from dpc18.5). In adult ovaries, the expression is dramatically reduced (Tu et al. 2017).

In spermatocytes, RingoA is essential for the tethering of telomeres to the NE during meiotic prophase. RingoA KO spermatocytes show non-homologous pairing and telomere fusions, as well as impaired DSB repair, and they also lack the sex body. Spermatogenesis is arrested in mid-pachytene of meiosis I. Interestingly, CDK2 is absent in telomeres at pachytene-like stage in RingoA KO (Mikolcevic et al. 2016; Tu et al. 2017). Experiments overexpressing RingoA mutants in spermatocytes further support the notion that RingoA is essential for CDK2 location to telomeres, and also reveal the relevance of the N-terminus for telomere binding (Tu et al. 2017).

The telomeres of RingoA deficient spermatocytes lack Sun1, a protein that is essential for telomere tethering to the nuclear envelope. Moreover, CDK2-RingoA can phosphorylate Sun1 *in vitro*, thereby giving a possible explanation for many of the phenotypes observed. However, it is unlikely that this explains the telomere fusion phenotype observed (Mikolcevic et al. 2016).

Taken together, it is not surprising that the depletion of RingoA leads to infertility in both males and females. RingoA KO male mice show normal testes at P7 but from two months of age lack round and elongated spermatids and their testis are atrophied, hypoplastic and smaller. Histological analysis shows abnormal epithelium, narrower seminiferous tubules and lack of post-meiotic cells (Mikolcevic et al. 2016; Tu et al. 2017). In RingoA KO females, there is an almost total loss of oocytes and ovaries are also atrophic and mainly composed of interstitial and stromal cells.

RingoA in tumorigenesis

RingoA has been proposed to have a role in cancer. It has been reported to be overexpressed in human tumors such as glioblastoma and breast cancer (Lubanska et al. 2014; Al Sorkhy et al. 2012). In glioblastoma, the overexpression of RingoA was proposed to correlate with

Introduction

tumor grade. Moreover, shRNA-mediated knockdown of RingoA reduced the proliferation of glioblastoma cell lines, and RingoA was proposed to regulate the self-renewal capability of the stem cell population CD133+ (Lubanska et al. 2014). Regarding breast cancer, HC11 cells overexpressing RingoA were shown to have accelerated tumorigenesis when implanted into mammary fat pads of BALB/C mice (Golipour et al. 2008). Furthermore, breast tumor growth was partially inhibited when the implanted HC11 cells expressed a RingoA mutant with reduced ability to bind to p27^{Kip1} or CDK2 (Al Sorkhy et al. 2016). It has been also proposed that RingoA expression can be induced by ER α and that RingoA is able to upregulate ERK1/2 signaling in a CDK dependent manner promoting tamoxifen resistance. (Ferraiuolo et al. 2017).

In contrast to the RingoA function in meiosis, which has been clearly demonstrated *in vivo* by different groups, the experiments addressing the role of RingoA in cancer and cell cycle regulation have been done in cell lines and mostly overexpressing RingoA. To date, there are no reports using genetic mouse models to address the importance of RingoA during homeostasis and tumorigenesis, and very little is known about substrates and interactors of RingoA in mammals beyond p27^{Kip1}. Therefore, studies to understand the relevance of RingoA in cell regulation *in vivo* are much needed.

Objectives

The aim of this project is to investigate the role of the non-canonical CDK activator RINGO in mammalian somatic cells and tissues, both in homeostatic conditions and in cancer.

Specific objectives:

- Define the subcellular location of RingoA
- Identify new RingoA interacting proteins
- Analyze the consequences of the loss of function of RingoA in mammalian cells
- Study RingoA and RingoB expression in mouse tissues
- Characterize the role of RingoA and RingoB *in vivo* both in homeostasis and in tumor growth by using genetic mouse models

Materials & Methods

General buffers and solutions

Davidson's fixative

30% absolute ethanol
30% neutral buffered formalin (10%)
10% glacial acetic acid

HBS buffer 2X

50mM HEPES
280mM NaCl
1.5mM Na₂HPO₄
pH 7.12

IP buffer

50 mM Tris-HCl (pH 7.5)
150 mM NaCl
5 mM EGTA
5 mM EDTA
1% NP-40
1mM Na₃O₄V
1 mM PMSF
10 µg/ml pepstatin A
10 µg/ml aprotinin
10 µg/ml leupeptin
20 mM NaF
1 µM mycrocystin
2.5 mM benzamidine

Ponceau Red

0.1% Red Ponceau S powder
5% acetic acid

Protein Loading buffer 5X

250 mM Tris pH 6.8
50% glycerol
250 mM DTT
10% SDS
0.1% bromophenol blue

Lysis Buffer

50 mM Tris-HCl pH 7.5
150 mM NaCl
1 mM EDTA
1 mM EGTA
1% Triton X-100
0.1% SDS
Protease inhibitor cocktail
25u/ml Benzonase

NID buffer

10mM Tris pH 8.3
50mM KCl
2mM MgCl₂
0.1 mg/ml gelatin
0.45% NP40
0.45% Tween20

PBS 10X

1.37 M NaCl
27 mM KCl
100 mM Na₂HPO₄
17.5 mM KH₂PO₄
pH 7.4

Running Buffer 10X

0.25 M Tris base
2 M glycine
1% SDS
pH 8.3

Tail Buffer

100 mM NaCl
50mM Tris-HCl pH8
10mM EDTA pH8
1% SDS

Materials & Methods

RIPA buffer

50mM Tris-HCl
150mM NaCl
1% NP-40
5mM EDTA
0.25% Sodium deoxycholate
1mM DTT
1mM Na₃O₄V
1mM PMSF
10µg/ml pepstatin A
10µg/ml aprotinin
10µg/ml leupeptin
20mM NaF
1µM mycrocystin
2.5 mM benzamidine

Transfer Buffer 10X

0.2 M Tris base
1.5 M glycine

TBS 1X

0.1 M Trizma base
1.5 NaCl

Commercial reagents and kits

Commercial reagents

Reagent	Company	Reference
4-OH-Tamoxifen	Sigma	H6278
Acetic acid	Panreac	131008.1611
Ammonium bicarbonate	Sigma	09830
Aprotinin	Sigma	A6279
B27 supplement	Life Technologies	17504-044
Benzamidine	Sigma	B6506
Benzonase Nuclease	Sigma	E1014-5KU
bFGF	Stem Cell	2634
BioTaq	Ecogen	21060
Bromophenol blue	Sigma	B8026
Cell strainer 70µm nylon BD	Falcon	352350
CFSE	ThermoFisher	C34554
Colcemide	Sigma	10295892001
Collagenase A	Roche	10103586001
Corn oil	Sigma	C8267
Cresyl Violet	Sigma	10510-54-0
D(+) Glucose	G8270	Sigma
DAB	Dako	K3468
DAPI	Life Technologies	P36935
Dispase	Gibco	17105-045
DMEM	Sigma	5796
DMEM/F12	Invitrogen	313300-95
DMSO	Sigma	D5796
DPX	Leica Biosystems	08600E
DTT	GE Healthcare	17-1318-02

Dynabeads MyOne Streptavidin C1	ThermoFisher	65001
EDTA	Sigma	E4378
EGF	Peptotech	AF-100-15
EGTA	Sigma	E46758
Eosin	Panreac	251301-1611
Ethanol absolute	Panreac	131086.1214
FBS	ThermoFisher	E6541L
Fluorescence mounting media	Dako	s3023
Gelatine	Merck	4070
Giemsa stain	Merck	G5637
GlutaMAX	Life Technologies	35050-038
Glutamine	LabClinics	M11-004
Glycerol	Sigma	49782
Glycine	Sigma	G7126
HBSS	Gibco	14175-137
Hematoxylin	Panreac	254766-1611
Heparin	Sigma	H3393
HEPES	Gibco	15630-049
Hyaluronidase	Sigma	H3506
Laminin	Roche	11243217001
Leupeptin	Sigma	L2884
Magnesium chloride	Merck	1.05833
Methanol	Panreac	131091.1214
Mycocystin	Enzo LifeScience	ALX350012
Neural Basal Medium	Life Technologies	21103-049
Neutral buffered formalin (10%)	Sigma	HT501128
Nitrocellulose membrane 0.2µm	GE Healthcare	10600002
Non-treated multidishes	Nunc	150239
NP-40	AppliChem	A16960250
OCT compound	Fisher	23-730-571
Opti-MEM	ThermoFisher	11058021
Penicillin/Streptomycin	LabClinics	P11-010
Pepstatin A	Sigma	P4265
Peroxidase blocking buffer	Dako	S2023
PMSF	Sigma	P7626
Polybrene	Sigma	H9268
Poly-D-lysine	Sigma	P7280
Polyethylenimine	Polysciences	23966-1
Ponceau S	Sigma	P3504
Propidium Iodide	Sigma	P4864
Potassium chloride	Sigma	P9541
Potassium phosphate dibasic	Sigma	P3786
ProLong Gold antifade mountant with DAPI	Life Technologies	P36935
Protease inhibitor cocktail	Calbiochem	539134
Proteinase K	Roche	03115852001
Puromycin	Sigma	P9620
Random Primers	Invitrogen	48190-011
Rnase A	Roche	10109142001

Materials & Methods

RNAasin 2500U	Promega	N211
SDS	Sigma	71725
Sequencing grade modified trypsin	Promega	V5113
Sodium chloride	Sigma	433209
Sodium deoxycholate	Sigma	6504
Sodium Floride	Sigma	S7920
Sodium orthovanadate	Sigma	S6508
Sodium phosphate dibasic	Sigma	255793
StemPro Accutase Cell Dissociation Reagent	Thermo-fisher	A1110501
Superfrost glass slides	VWR	J1800AMNZ
Superfrost Plus Adhesion Microscope Slides	ThermoFisher	J7800AMNT
Triton X-100	Sigma	T9284
TRIZMA-base	Sigma	T6066
TRIZMA-HCl	Sigma	T3253
Trizol	ThermoFisher	15596026
Trypan Blue Solution 0.4%	Gibco	15250061
Trypsin-EDTA	Sigma	T3924
Tween 20	Sigma	P7949
VECTASHIELD Antifade Mounting Medium	NOVUS	H-1000-NB

Commercial Kits

In Situ Cell Death Detection Kit (TUNEL)	Roche	11684795910
Annexin V FITC Apoptosis Detection Kit	BD Biosciences	556547
FITC Mouse Anti- BrdU Set	BD Biosciences	556028
MycoAlert	Lonza	LT07-318
PureLink on column Dnase set	Invitrogen	121-85-010
QIAfilter plasmid maxi kit	Quiagen	12263
Random primers	Invitrogen	48190-011
RC DC protein assay kit II	BioRad	5000122
RNA PureLink Minikit	Ambion	12183018A
Superscript IV reverse transcriptase	Invitrogen	18090010
SYBR Select master mix	ThermoFisher	4472942

Mouse work

Mouse housing

Experimentation animals were housed in the specific pathogen-free (SPF) mouse facility of the Barcelona Science Park (PCB, Barcelona). Experiments were performed following the European Union, national and institutional guidelines, and experimentation protocols were approved by the PCB's Animal Care and Use Committee (CEEA-PCB).

Generation of mouse models

Generation of RingoA, RingoB and RingoA/RingoB constitutive and inducible knock-outs

The RingoA knock-out model (*RingoA KO*) was generated by flanking exon 3 of the *Spdya* gene encoding RingoA with loxP sequences (Mikolcevic et al. 2016). RingoA lox/+ animals were crossed with Sox2-Cre transgenic mice in order to delete exon 3 and obtain RingoA +/- mice. These animals were inter-crossed for the generation of RingoA -/- mice. In order to generate RingoA inducible KO mice, RingoA lox/lox animals were crossed with mice carrying UBC-Cre-ERT2 (Ruzankina et al. 2007).

The Ringo B knock-out model (*RingoB KO*) was generated by IRB Barcelona's Mouse Mutant Facility using the "knock-out first strategy" (Testa et al. 2004) in which a splice acceptor- β -galactosidase gene-trap cassette was inserted into intron 2-3 of the *Spdyb* gene encoding RingoB. This allele can be converted to a conditional allele by FlpO mediated removal of the cassette to leave only LoxP sites flanking exons 3 and 4. The gene-targeting vector was electroporated into C57B6/129S6 hybrid ES cells. Positive clones were used to generate chimeras that produce RingoB +/- mice, which were inter-crossed to generate the RingoB knock-out model (*RingoB KO*). In addition, the knock-out first allele was converted to a conditional allele by crossing with FlpO expressing transgenic mice. These RingoB lox/+ mice were interbred to generate RingoB lox/lox mice, which were then crossed with mice carrying UBC-Cre-ERT2 to generate the RingoB inducible knock-out model.

Materials & Methods

To generate RingoA and RingoB double knock-out (RingoA/RingoB KO) RingoA +/- RingoB -/- animals were interbred. To obtain RingoA/RingoB inducible KO, RingoA lox/lox and RingoB lox/lox animals were crossed and the animals obtained were then crossed with UBC-Cre-ERT2 mice.

Generation of RingoA Katushka- Luciferase reporter

RingoA Katushka-Luciferase reporter (RAKL) mice were generated by the IRB Barcelona's Mouse Mutant Facility. The targeting vector was prepared from an already existing H2B-venus-luciferase gene targeting cassette, by exchanging the H2B-Venus for TurboFP635 (Katushka), thereby creating a cassette with the Katushka cDNA, a 2A sequence and then the luciferase cDNA followed by an SV40 polyA sequence. The whole cassette was flanked by L1 and L2 gateway sites, which allowed it to be placed between the RingoA homologous arms in a 3-way gateway reaction. This created a gene-targeting vector that inserted a frame specific dual reporter cassette into intron 2-3 of the RingoA-encoding gene, immediately downstream of the first coding exon. The vector was transfected into ES cells to generate mice carrying the knock-in allele.

Generation of PyMT mice with RingoA/RingoB conditional KO or RAKL reporter.

RingoA/RingoB inducible KO PyMT animals, which develop mammary tumors, were obtained by crossing RingoA lox/lox, RingoB lox/lox, UBC-Cre-ERT2 mice with MMTV-PyMT mice (mouse mammary tumor virus -Polyoma Middle T Antigen) provided by William Muller (McGill University, Canada). PyMT RAKL mice were generated by crossing RAKL mice with MMTV-PyMT mice.

Animal treatments

4-hydroxytamoxifen (4-OHT) treatment: For RingoA and RingoB deletion, animals were injected intraperitoneally with 1 mg of 4-OHT each day for 5 consecutive days to induce the expression of Cre recombinase. 4-OHT was dissolved in 10% ethanol and 90% corn oil.

Mouse genotyping

Mouse tails were digested in 750 μ l of tail buffer with proteinase K (0.5 μ g/ μ l) at 56°C overnight. After that, 250 μ l of saturated NaCl was added, mixed for 5 min and centrifuged at 1600xg 10 min. The supernatant was mixed with 500 μ l of isopropanol and spun at full speed for 10 min. The supernatant was discarded and the pellet was washed with 70% EtOH, dried and finally resuspended in autoclaved ddH₂O. DNAs were analyzed by polymerase chain reaction (PCR). The mixture was prepared with 50 ng of DNA, 2 μ l of 10x Taq buffer, 0.6 μ l of MgCl₂ (50 mM), 1 μ l of each primer (10 μ M), 0.5 μ l of dNTP mix (10 μ M), 0.3 μ l Taq polymerase (BioTaq) and ddH₂O to a final volume of 20 μ l. Primers were purchased from Sigma. Sequences are shown in **Table M1**. The mix was incubated in a BioRad Thermal Cycler with the following PCR program: an initial step of 94°C for 5 min; 35 cycles of 94°C for 30 sec, 57°C for 30 sec, 72°C for 45 sec; and a final extension step of 72°C for 10 min. PCR products were resolved by electrophoresis in a 2% agarose gel.

Table M1. Primer sequences for mouse genotyping

RingoA KO			
Alleles	Primer A	Primer B	Size (bp)
RingoA WT	TGGGCCATTAGCATTTTGTGAGCT	TGCTTTGGGGCCAGTGAGATGA	298
RingoA lox	TGCTTTGGGGCCAGTGAGATGA	GGCTGCTAAAGCGCATGCTCCA	197
RingoA KO	GCCGCATAACTTCGTATAAT	CCACCACTCTGGGATAGATA	296
RingoB KO			
RingoB WT	CTCCCACTGTTTTTGTGTTGTTG	GCCCACAGAATGAACTAATCATGGC	315
RingoB lox	CTCCCACTGTTTTTGTGTTGTTG	GCCCACAGAATGAACTAATCATGGC	507
RingoB KO conditional	CTCCCACTGTTTTTGTGTTGTTG	CTGGCTCTGGGTCAGTTCTGAGG	465
RingoB KO	ACCCCCGGATCTAAGCTCTAGA	GCCCACAGAATGAACTAATCATGGC	502
RingoA Katushka Luciferase reporter			
RAKL	GCACCGGTGAAACAGACTTT	CCTCGGATGTGCACTTGAAG	172
Reference genes for the quantification of deletion of RingoA and RingoB by qPCR			
RingoA ex6	GGACCTAGTGCCACACCACACAGT	GGTATGAGGAGGGTACCTG	

Materials & Methods

RingoB ex2	CCAGCATCCAAAAGAGGAAG	GAGCAGCTTGGTGAAGACCT	
Others			
Cre	ACGAGTGATGAGGTTTCGCAAG	CCCACCGTCAGTACGTGAGAT	520
PyMT	AGGATCGGATCGAAATGAGCCC	CACAGATACACCCGCACATACTGC	300
Sexing	TGGATGGTGTGGCCAATG	CACCTGCACGTTGCCCTT	150X 200Y

Tumor growth analysis in mice

Tumor growth was monitored twice a week with a caliper until the tumors reached a minimum of 150-200 mm³ (calculated using the formula $V=(\pi \times length) \times wide^2$). Once this volume was acquired, the animals were injected with 4-OHT as previously described. Tumor size progression was followed for 8 or 15 days until the animals were sacrificed, and tumor samples collected. Genomic DNA was extracted from tumors using tail buffer as described for mouse genotyping, and gene deletion was confirmed by qPCR using RingoA lox and RingoB lox primers in combination with RingoA ex 6 and RingoB ex2, respectively, as reference genes (**Table M1**). *These experiments were done in collaboration with Dr. Marc Núñez.*

Immunohistochemistry

Tumors and organs with the exception of the brain and testis were fixed with formalin for 24 h at 4°C. Brains were fixed by intracardiac perfusion with PBS followed by 4% paraformaldehyde (PFA) for 20 min. They were then extracted and incubated with 4% PFA at 4°C overnight. Testes were fixed with Davidson's fixative at 4°C overnight.

Tissues were washed with PBS and dehydrated in a tissue processor (Sakura). Samples were then embedded in paraffin blocks using a paraffin embedding module (Leica) and cut with a microtome (Leica) in 4 µm sections. In order to proceed with sample staining, sections were de-waxed in xylene for 10 min and rehydrated following 3 min series of ethanol solutions at decreasing concentrations (100%, 95%, 75%, 50% and ddH₂O). Sections were then used for immunohistochemical (IHC) analysis, stained with Haematoxylin and Eosin (H&E) or stained with Nissl (0.1% Cresyl Violet) in the case of brain sections. For TUNEL staining, tissues were

processed following the manufacturer's instructions. For IHC, sections were treated with peroxidase blocking buffer for 15 min at RT to block endogenous peroxidase activity and then washed in water. Antigen retrieval was performed according to the primary antibody requirements (**Table M2**). Slides were incubated in blocking buffer (10% goat serum, 0.3% Triton X-100 in PBS) and then primary antibodies were added and incubated overnight at 4°C. After washing, secondary antibodies were added and incubated for 1 h at RT. Signal from HRP-conjugated secondary antibodies was visualized with 3,3-diaminobenzidine (DAB) and counterstained with hematoxylin. Tissue was again dehydrated and mounted using DPX mounting medium.

Table M2. Antibodies for Immunohistochemistry

Primary antibodies					
Antibody	Host	Antigen retrieval	Company	Reference	Dilution
Ki67	Rabbit	Citrate pH6	Abcam	Ab15580	1:1000
H3S10p	Rabbit	Citrate pH6	Merck	06-570	1:3000
γH2AX	Mouse	Citrate pH6	Millipore	05-636	1:600
F4/80	Rat	Citrate pH6	Bioscience	14-4801	1:50
CD3	Rabbit	Citrate pH9	Dako	IS50330	1:10
P27	Rabbit	Citrate pH6	Thermofisher	PA5-16717	1:500
Secondary antibodies					
Antibody			Company	Reference	Dilution
anti-mouse IgG-HRP			Dako	P0447	1:100
anti-rabbit IgG-HRP			Dako	DPVR110HRP	RTU
anti-rat IgG-HRP			Dako	P0450	1:100

Visualization of Katushka-Luciferase reporter

Bioluminescence and fluorescence imaging

Mice were anesthetized and injected retro-orbitally with D-luciferin (75 mg/kg). Immediately after injection, animals were placed in IVIS Spectrum CT chamber for bioluminescence imaging. Data were recorded using Living Image software (Xenogen). Katushka (TurboFP635)

Materials & Methods

fluorescent reporter expression *in vivo* was tested using the same equipment. *These experiments were done in collaboration with Dr. Marc Núñez and Dr Petra Mikolcevic.*

Fixation of testis for confocal microscopy

Testis were directly embedded in Optimal Cutting Temperature compound (OCT) and frozen, or alternatively they were fixed in 2% PFA at 4°C O/N, incubated in 30% sucrose until the tissue sank and finally embedded in OCT and frozen. Slices were cut by cryostat or with a microtome (Leica), respectively. They were then analyzed by confocal microscopy at an excitation/emission of 588/635 nm.

Isolation of testicular and brain cells for FACS

After tissue dissection, the tunica albuginea was removed from testes, which were cut into small pieces. In a petri dish, the seminiferous tubules were digested with 5 ml of collagenase/DNase solution (1 mg/ml collagenase, 300 mg/ml DNase I, DMEM) and incubated at 37 °C until the tubules were separated (approximately 20 min). Seminiferous tubule fragments were collected and centrifuged at 200xg for 5 min at RT. Tubule fragments were washed three times and subsequently incubated with a dispase/DNase solution (1.5U/ml dispase, 400 mg/ml DNase I, PBS) at 37°C for 15 min agitating every 3-5 min. Finally, the cells were dispersed by pipetting up and down and passed through a 70 µm cell strainer. Brain cells were isolated using the same protocol as for the isolation of neurosphere-producing cells. They were then pelleted by centrifugation at 300xg, resuspended in PBS at 4°C and analyzed by FACS.

Maintenance and subculture of adherent cells

Human osteosarcoma U2OS cells, embryonic kidney HEK293-T cells and breast cancer MCF-7 cells were purchased from ATCC and cultured in DMEM medium supplemented with 10% fetal bovine serum (FBS), 1% penicillin/streptomycin and 1% glutamine. Cells were cultured in humidified atmosphere in a 37°C incubator at 5% CO₂. For cell passaging, cells were washed with PBS and incubated in 1 ml of trypsin at 37°C until detached; cells were then diluted (1:6- 1:10) in culture medium and plated in a new dish.

Freezing and thawing of cells

For freezing, cell suspension was centrifuged at 150xg for 5 min at RT for pellet collection, resuspended in freezing medium (90%FBS, 10% DMSO) and transferred into cryo-tubes. Cryo-tubes were placed in Mr. Frosty Freezing Containers (ThermoFisher) at -80°C for 24h and then transferred to liquid nitrogen for long term storage.

For thawing, frozen cells were placed in a water bath at 37°C until thawed and then immediately transferred to a 15 ml tube with medium and centrifuged at 150xg (300xg for neurospheres) for 5 min. Cells were then resuspended in their required growth medium and plated.

Mycoplasma detection

In order to avoid mycoplasma contamination, cells were routinely tested using MycoAlert mycoplasma detection kit following the manufacturer's instructions. Briefly, 2 ml of 3 days old cell culture medium was centrifuged at 200xg for 5 min at RT. Next, 100 µl of the supernatant was collected and mixed with the detection reagent provided with the kit, incubated for 5 min and luminescence was measured. Then, 100 µl of substrate was added and incubated for 10 min. Luminescence was measured again and the ratio between the two measures was calculated. Ratios <0.9 indicated that cells were negative for mycoplasma.

Generation, maintenance and differentiation of adult brain-derived neurospheres

Generation of neurospheres derived from subventricular (SVZ) zones of adult mice

Brains were extracted immediately after mouse sacrifice and placed on ice in HBSS 1% glucose. SVZ were dissected as described previously (Fischer et al. 2011). For tissue dissociation, dissected tissue was washed twice with HBSS, minced using a blade, transferred into a 15 ml falcon tube and subsequently disrupted with a 21G needle. 300 µl of 0.05% Trypsin-EDTA was added and incubated for 5 min in a water bath set at 37 °C. The disrupted tissue was washed twice with medium and centrifuged at 300xg for 5 min at RT. 1 ml of

Materials & Methods

growth medium was added and the cells were dissociated by gently pipetting up and down approximately 7-10 times using a P1000 pipette. Growth medium was added to a total of 5 ml, and the cell suspension filtered through a 70 μm cell strainer. Live cells were counted with a Neubauer chamber using Trypan Blue and seeded at the density of 10 cells/ μl . Cells plated in non-treated low-attachment cell culture plates formed spherical colonies.

Maintenance and subculture of neurospheres

Cells were cultured in medium composed of Neural Basal Medium supplemented with 2% B27, 1x GlutaMAX, 2 $\mu\text{g/ml}$ heparin, 50 units/ml penicillin/streptomycin, 20 ng/ml recombinant bovine fibroblast growth factor (bFGF) and 20 ng/ml purified mouse receptor-grade epidermal growth factor (EGF). For passaging of neurospheres, medium with free-floating neurospheres was transferred to a 15 ml tube and centrifuged at 300xg for 5 min at RT. The supernatant was discarded, the neurospheres were resuspended in 500 μl of pre-warmed accutase and incubated 3 min at 37°C. In order to wash out the accutase, 5 ml of medium was added and the cell suspension was centrifuged at 300xg for 5 min at RT, this was repeated twice. After discarding the supernatant, 1 ml of medium was added and cells were dissociated by gently pipetting up and down 10 times. Cells were counted and seeded at 10 cells/ μl density. For sub-culturing, cells were passaged approximately twice per week and cultured for approximately 15-20 passages. Neurosphere imaging and cell harvesting for experiments was done on day 7 after cell passage. Phase contrast imaging was performed with ScanR (Olympus) equipment for scanning wells of 48 well plates. Image analysis was done using Fiji software Macros written by the Advanced Digital Microscopy Unit (IRB Barcelona). These macros detect individual neurospheres and determine the total number and size of neurospheres per well analyzed.

Differentiation of neurospheres

Before neurosphere differentiation, Poly-D-lysine /Laminin coated plates were prepared: PDL (10 $\mu\text{g/ml}$ in dH₂O) was added to cover the surface and incubated overnight (O/N) at RT protected from light. The following day, the surface was washed three times with ddH₂O and coated with 5 $\mu\text{g/ml}$ of laminin (dissolved in H₂O) for 3h. For differentiation, neurospheres were dissociated and plated at 1×10^4 cells/cm² density on the coated plate using the neurosphere growth medium already described. When cells reached approximately 80% confluency, medium was replaced with medium containing 5 ng/ml of

bFGF without EGF. After 2 days, medium was replaced with EFG/bFGF free growth medium and cultured for 3 days before harvesting.

Generation of epithelial cell lines from PyMT tumors

Mammary tumors from the PyMT mouse model were isolated once they reached 150mm³. Tumors were chopped with a blade and digested at 37°C for 1h rocking in DMEM containing Hyaluronidase (1.5 units/ml) and Collagenase A (1 mg/ml). Once digested, the tissue was filtered using a 70µm cell strainer and centrifuged at 300xg for 30 seconds at RT. The cell pellet was resuspended in DMEM and centrifuged briefly after which the supernatant was discarded. This procedure of resuspension and centrifugation was repeated for four consecutive times in order to favor the elimination of fibroblasts. The final pellet with the epithelial cells was resuspended and plated in full growth medium (DMEM/F12, 10% fetal bovine serum (FBS), 1% penicillin/streptomycin, 1% glutamine). Cells were cultured in humidified atmosphere in a 37°C incubator at 5% and passaged using trypsin until spontaneous immortalization was reached. Once immortalized, the cells were maintained in the same growth medium and conditions.

Cre recombinase induction with 4-hydroxytamoxifen (4-OHT)

When 4-OHT is used in a CreERT2/lox system, it binds to a modified fragment of the estrogen receptor, which is bound to the Cre recombinase. The addition of 4-OHT relocates Cre into the nucleus, where it recombines the loxP sites, resulting in deletion of floxed genes.

A 10mM stock of 4-OHT was prepared in ethanol and stored at -20°C. To induce RingoA and RingoB deletion, cells were treated with 100 nM 4-OHT for 48h. To confirm gene deletion, genomic DNA was extracted from treated and non-treated cells using NID buffer. Briefly, cells were trypsinized, collected and centrifuged for pellet collection; the pellet was then resuspended in 100 µl of NID buffer supplemented with 100 µg/ml proteinase K and incubated 2-12h at 56°C, followed by Proteinase K inactivation at 95°C for 10 min. Gene deletion was confirmed by qPCR as described above (see section: *Mouse genotyping*), using *RingoA lox* and *RingoB lox* primers in combination with *RingoA ex 6* and *RingoB ex2* primers respectively as reference genes (primers detailed in table M1).

Materials & Methods

Cell transfection

Transfection of HEK293-T cells with polyethylenimine (PEI)

Cells were plated in order to reach a 80% confluence at the moment of transfection. For transfection in a 100 mm dish, 5µg of DNA was mixed with 800 µl of sterile 150mM NaCl in an Eppendorf tube to which 80 µl of PEI was added without touching the walls and mixed. The mixture was incubated for 15 min at RT and then added to cells. Medium was replaced 10-16h later.

Transfection of HEK293-T using calcium chloride

HEK293-T cells were plated in order to reach 60-70% confluence at the moment of transfection. DNA was dissolved in 450 µl of water to which 50 µl of CaCl₂ was added. 500 µl of 2xHBS was added dropwise while bubbling the DNA mix and then incubated for 20 min at RT. The mix was added to the cells cultured in DMEM 10% FBS and antibiotics and incubated O/N. The following day, medium was replaced.

6-Myc-tagged plasmids (RingoA, CDK2, Cyclin A2 and Cyclin E2) used for transfection were provided by Dr. Michitaka Isoda. The sequences were cloned using the Gateway system.

Transfection of U2OS with lipofectamine 3000

U2OS cells were plated in order to reach 60% confluence and transfected following the manufacturer's instructions. Briefly, DNA (5µg for transfection in a 60mm dish) was mixed with 250 µl of Opti-MEM and 10 µl of p3000 reagent. In parallel, 10 µl of lipofectamine was mixed with 250 µl of Opti-MEM. Five min later, the mixture containing the DNA was transferred to the tube containing the lipofectamine and mixed thoroughly. After 10 min incubation at RT, the mixture was added to the cells cultured in medium without penicillin/streptomycin in a 60mm dish. Medium was replaced 10-16h later.

siRNA transfection

Cells were plated in order to reach a 60% confluence and transfected with siRNA (100 nM) using Lipofectamine RNAiMAX following the manufacturer's instructions. Briefly, 25 µl of lipofectamine was mixed with 700 µl of Opti-MEM. In parallel, siRNA was mixed with the same volume of Opti-MEM. The mixture containing the siRNA was then added to the mixture with lipofectamine and mixed thoroughly. The mixture was incubated for 10 min at RT. Cells

growth medium was replaced with 3.6 ml of DMEM 10% FBS without antibiotics and the transfection mixture was added. Cells were then incubated for 24 h in antibiotic-free media, split and analyzed 48 h later unless otherwise indicated.

Table M3. Small interfering RNAs

siRNA	Company	Reference
ON-TARGETplus Human SPDYA	Cultek	L-009141-01-0005
ON-TARGETplus Non-targeting	Cultek	D- 001810-10-05

Retroviral and lentiviral infection

Viruses were produced in HEK293-T cells through PEI transfection of packaging vector plasmids together with the desired retroviral or lentiviral vectors. For lentivirus generation, 4.5 µg of δ 89 plasmid (containing Gag, Pol, Rev, and Tat genes) and 0.5 µg of VSV-G plasmid (containing Env gene) were transfected together with 5 µg of shRNA vectors. For retrovirus generation, 4.5 µg of Gag-Pol and 0.5 µg of VSV-G were transfected together with the desired expression vectors. The following day cell medium was refreshed. After 48 h, the supernatant containing the viruses was passed through a 0.45 µm PVDF filter and used for cell infection at a 1:1 ratio with fresh medium plus 8 mg/ml polybrene. Two days later, cells were passaged and incubated in medium supplemented with puromycin (1µg/ml) for selection of cells that incorporated the plasmid. In experiments using RingoA shRNA, cells were directly plated for experiments two days after infection.

The shRNA vectors used for lentiviral infection were obtained from MISSION human shRNA library (Sigma) and were provided by IRB Barcelona's Functional Genomics Facility. The pbabe-H2B-GFP vector used for retroviral infection was obtained from Addgene (26790).

Cellular and molecular biology

Colony assay

Cells were trypsinized and, unless otherwise indicated, 2000 cells per well were plated in 6 well plates. Once the colonies were visible (after 7-10 days), cells were fixed in 4%PFA for 15 min at RT. Plates were then washed with dH₂O, stained for 10 min with crystal violet and then washed with dH₂O until clear colonies were visible. Colony area was quantified using Fiji software.

Time-lapse imaging

For time-lapse imaging, cells were seeded in 24 well plates and images were taken using ScanR microscope (Olympus). Cells were maintained at 37°C and 5% CO₂ during imaging and pictures were taken every 10 min using phase contrast and green fluorescence channel for the detection of H2B-GFP. Videos were analyzed using Fiji software.

Flow cytometry

Cell cycle analysis

Cells were harvested, fixed in 70% ice cold ethanol and stored at -20°C for at least 4h. Cells were then washed twice in PBS, resuspended in PBS supplemented with 25 µg/ml propidium iodide and 0.1mg/ml RNaseA and incubated for 20 min at RT. 10000 cells were acquired on Gallios Flow Cytometer (Beckman Coulter) and analyzed by FlowJo software.

Analysis of BrdU incorporation and cell cycle

Cells in S phase, which undergo DNA synthesis, were quantified on the basis of uptake of BrdU, a synthetic analog of thymidine. Growing cells were incubated with 10µM BrdU for 1.5h, harvested, fixed in 70% ice cold ethanol and incubated at -20°C for 24h. Fixed cells were then centrifuged at 200xg for 5 min at RT and washed once with 0.5% BSA/PBS. Pellets were then resuspended in denaturing solution (2M HCl) and incubated 20 min at RT. Afterwards, cells were washed and then incubated for 2 min in 0.5 ml of 0.1M sodium borate, pH 9.5, to neutralize any residual acid. Cells were then washed and resuspended in

100µl of PBS 0.5% Tween-20 containing 10µl of anti-BRDU-FITC. After 1h of incubation in the dark, cells were washed and then resuspended in a PI staining solution (PBS with 25µg/ml propidium iodide and 0.1mg/ml RNaseA). After incubation for 20 min in the dark at RT, 10000 cells were acquired on Gallios Flow Cytometer (Beckman Coulter) and cell cycle distribution was analyzed with the FlowJo software.

Phospho-S10 Histone H3 staining

Phospho-S10 Histone H3 is widely used as a mitotic cell marker. Cells were harvested, fixed in 70% ice cold ethanol and incubated at -20°C for 24h. Fixed cells were centrifuged at 200xg for 5 min at RT and washed twice with PBS containing 0.25% Triton X-100. After centrifugation, the pellet was resuspended in 100 µl of PBS with 1% BSA containing anti-H3 Phospho S10 antibody (Millipore, 06-570) diluted 1:200, and incubated for 1h at RT. Cells were then washed with PBS 1%BSA and incubated in 100 µl of the same buffer containing anti-rabbit Alexa-Fluor 488 antibody (Invitrogen, A21076) diluted 1:200. After 45 min of incubation in darkness, cells were washed again and resuspended in PI staining solution (PBS with 25µg/ml propidium iodide and 0.1mg/ml RNaseA). After 20 min of incubation, 10000 cells were acquired on Gallios Flow Cytometer (Beckman Coulter) and cell cycle distribution was analyzed with the FlowJo software.

Annexin V staining

Cells were stained using Annexin-V FITC Apoptosis detection kit following the manufacturer's instructions. Briefly, cells were harvested together with their media, and the cell pellet was washed with cold PBS and resuspended in 100 µl of 1X Annexin V binding buffer with 5 µl of Annexin-V-FITC antibody. Samples were then incubated for 20 min at RT in the dark. 400 µl of propidium iodide solution was added for DNA staining immediately before the acquisition and 10000 cells were recorded on Gallios Flow Cytometer (Beckman Coulter) and analyzed with the FlowJo software.

CFSE-based proliferation assays

Carboxyfluorescein succinimidyl ester (CFSE) was used to measure cell proliferation in neurospheres. Each time that a cell divides, CFSE is transferred equally to the daughter cells, reducing fluorescence in half. Neurospheres were dissociated as detailed for neurosphere subcultures. 10⁶ cells/ml were labelled with 1 µl CFSE following the manufacturer's

Materials & Methods

instructions. Cells were incubated in normal growth conditions and harvested at 24h, 48h, 72h, or 96h. For cell harvesting, neurospheres were pelleted, dissociated and resuspended in PBS at 4°C and then analyzed by FACS.

Table M4. FACS antibodies

Antibody	Company	Reference
H3 Phospho S10	Millipore	06-570
BRDU	BD Bioscience	556028
EPCAM-FITC	Santa Cruz	53532

Metaphase spreads

Cells were treated with colcemid (100ng/ml) for arresting cells in metaphase for 2h and harvested. Cell pellets were then incubated in hypotonic solution of 75mM of KCl at 37°C for 20 min. Swollen cells were then fixed with ice-cold fixing solution (75% methanol/ 25% acetic acid). After three washes in the fixing solution, cells were spread over a Superfrost glass slide, briefly dried and then steam treated for 10 sec. Finally, cells were dried, stained with GIEMSA and mounted with DPX. Images were taken using the ScanR microscope (Olympus).

Protein detection by immunofluorescence

Cells grown on coverslips were washed with PBS and fixed for 20 min in ice-cold methanol. After fixing, cells were washed with PBS, permeabilized and blocked for 1 h at RT in PBS-BT solution (PBS 3% BSA, 0.1% Triton X-100) and incubated O/N at 4°C with primary antibodies. The following day, coverslips were washed with PBS-BT buffer and incubated with secondary antibodies for 1h at RT protected from light. After washing in PBS-BT buffer, coverslips were mounted on Superfrost glass slides using ProLong Gold Antifade Mountant with Dapi. Primary and secondary antibodies were diluted with PBS-BT and are indicated in **(Table M5)**. Images were taken using a ScanR microscope (Olympus) for fluorescence microscopy and LSM780 (Zeiss), SP5 (Leica) or Airyscan LSM880 (Zeiss) for confocal microscopy. Quantification of co-localization was performed with JACoP plug-in using FIJI software.

Table M5. Immunofluorescence antibodies

Primary antibodies				
Antibody	Host	Company	Reference	Dilution
RingoA	Mouse	Custom made		1:100
SC35	Rabbit	abcam	ab28428	1:50
SMC1	Rabbit	Gift from Ana Losada		1:100
Fibrillarin	Goat	abcam	ab4566	1:500
H2AX Phospho S139	Mouse	Millipore	05-636	1:200
FLAG	Mouse	Sigma	F1804	1:200
ACA	Human	Antibodies incorporated	15-235	1:500
Secondary antibodies				
Antibody		Company	Reference	Dilution
Alexa-Fluor anti- rabbit	594	ThermoFisher	A-21442	1:400
Alexa-Fluor anti- mouse	488	ThermoFisher	A-11017	1:400
Alexa-Fluor anti- goat	594	ThermoFisher	A-21468	1:400
Alexa-Fluor anti- human	555	ThermoFisher	A-21433	1:400

Protein extraction and quantification

Adherent cells were washed once with PBS and placed on ice. RIPA buffer was added and cells were collected using a scraper. They were then incubated on ice for 10 min and sonicated using a water bath sonicator (Diagenode). Next, the lysate was spun at maximum speed for 15 min at 4°C, and the supernatant was collected and either kept at -80°C or used for protein quantification. If the lysate was subsequently used for co-immunoprecipitation (co-IP), the same procedure was done using IP buffer instead of RIPA buffer.

Protein concentration was estimated using the RC DC protein assay kit II. 2µl of protein sample was mixed with 25µl of working reagent A (a mixture of 10µl of Protein Assay Reagent S and 500µl of Reagent A). Then, 200µl of Protein Assay reagent C was added and the solution was incubated for 5 min at RT. Absorbance at 750nm was measured using a spectrophotometer (BioTek, FLx800) and concentrations were calculated using a BSA standard curve.

Protein detection by western blotting

Loading buffer was added to the quantified samples, which were boiled for 5 min at 95°C. Proteins (20-40µg) were then separated by SDS-PAGE using 8%, 10%, 12% or 14% Laemmli gels, depending on the molecular weight of the protein. After electrophoresis, proteins were

Materials & Methods

transferred from the polyacrylamide gel to a nitrocellulose membrane using a wet transfer system (Bio-Rad). Ponceau Red was used to reversibly stain proteins in order to check transfer quality and was then washed out with PBS. The membrane was blocked for 1h with 5% non-fat milk in PBS at RT and then primary antibody was diluted in 3% BSA in TBS-0.05% tween and incubated O/N at 4°C. Membranes were washed three times in TBS-0.05% Tween and incubated for 1h at RT with the secondary antibodies diluted in the same buffer with 3% BSA. Finally, membranes were washed three times with TBS-0.05% Tween and one time with TBS. Proteins were detected using the Odyssey Infrared Imaging System. The antibodies are indicated in **Table M6**.

Table M6. Antibodies for western blotting

Antibody	Host	Company	Reference	Dilution
ANKRD11	Mouse	Santa Cruz	sc-514916	1:500
ANP32A	Mouse	Santa Cruz	sc-100767	1:500
Cdc27	Mouse	Santa Cruz	sc-9972	1:500
CDK2	Mouse	Santa Cruz	sc-6248	1:1000
CENP-C	Mouse	Santa Cruz	sc-166099	1:500
cMyc	Goat	Santa Cruz	sc-789	1:2000
Cyclin- T1	Mouse	Santa Cruz	sc-271348	1:500
FLAG-HRP	Mouse	Sigma	a8592	1:2000
NMT1	Mouse	Santa Cruz	sc-393702	1:500
PCM1	Mouse	Santa Cruz	sc-398365	1:500
SCC1	Mouse	Merck	05-908	1:1000
SMC1	Rabbit	Gift from Ana Losada		1:200
SMC3	Rabbit	Gift from Ana Losada		1:500
WAPL	Mouse	Santa Cruz	sc-365189	1:1000
α Tubulin	Mouse	Sigma	T9026	1:10.000

Immunoprecipitation beads

Anti-c-Myc agarose conjugate	SIGMA	A7470
------------------------------	-------	-------

Protein co-immunoprecipitation

6-myc tagged proteins were transfected in HEK-293-T cells using the PEI transfection method described previously. The day after transfection, samples were lysed with IP buffer as detailed in the protein extraction section. A portion of the sample was mixed with loading buffer and kept as input sample for western blotting. The remaining sample was used for co-IP of myc-tagged proteins using myc beads following the manufacturer's instructions.

Briefly, 20 μ l of beads previously washed 5 times with PBS was added to 400 μ g of protein lysates and incubated at 4°C in rotation. The following day, beads were washed 4 times with PBS, resuspended in 2x protein loading buffer and boiled for 5 min at 95°C. Samples were subsequently used for western blotting.

BioID screening

Sample processing: Three 15cm plates of HEK-293-T cells at 60% were transfected with BirA*-RingoA (20 μ g) or BirA*-ev (2 μ g) using the calcium phosphate transfection method described earlier. The following day medium was replaced and 50 μ M of biotin was added. 24h later, cells were harvested and resuspended in 3 ml of lysis buffer. Lysates were incubated on a rotator at 4°C for 1h and then briefly sonicated to disrupt any visible aggregates. An aliquot was kept for immunoblotting. 100 μ l of streptavidin Dynabeads was added to the lysates and kept in rotation O/N at 4°C. The following day, beads were collected using a Magnet (DynaMag) and were washed once with 1 mL lysis buffer and twice with 1 mL of 50 mM ammonium bicarbonate (pH 8.3). Beads were transferred to a new tube and washed two more times with 1 mL ammonium bicarbonate buffer. Tryptic digestion was performed by incubating the beads with 1 μ g of sequencing grade modified trypsin dissolved in 200 μ l of 50 mM ammonium bicarbonate (pH 8.3) O/N at 37°C. The following morning, an additional 0.5 μ g trypsin was added, and the beads were incubated 2 hr at 37°C. They were then pelleted, and the supernatant was transferred to a new Eppendorf tube. Beads were washed twice with 150 μ l of 50 mM ammonium bicarbonate, and these washes were pooled with the first eluate. The sample was lyophilized and resuspended in buffer A (0.1% formic acid). 1/5th of the sample was analyzed per MS run.

Sample analysis: Analysis was performed by IRB Barcelona's Mass Spectrometry (MS) & Proteomics Facility. High-performance liquid chromatography was conducted using a 2cm pre-column (Acclaim PepMap 50 mm x 100 μ m inner diameter, and 50 cm analytical column (Acclaim PepMap, 500 mm x 75 μ m diameter; C18; 2 μ m; 100 Å, Thermo Fisher Scientific, Waltham, MA), running a 120 min reversed-phase buffer gradient at 225 nl/min on a Proxeon EASY-nLC 1000 pump in-line with a Thermo Q-Exactive HF quadrupole-Orbitrap mass spectrometer. A parent ion scan was performed using a resolving power of 60,000,

Materials & Methods

then up to the twenty most intense peaks were selected for MS/MS (minimum ion count of 1,000 for activation), using higher energy collision-induced dissociation fragmentation. Dynamic exclusion was activated such that MS/MS of the same m/z (within a range of 10 ppm; exclusion list size = 500) detected twice within 5 sec were excluded from analysis for 15 sec. Proteins identified with an iProphet cut-off of 0.9 (corresponding to $\leq 1\%$ FDR) and at least two unique peptides were analyzed with SAINT Express v.3.3. High confidence interactors were defined as those with $FDR \leq 0.02$.

Cloning of FLAG-RingoA-BirA plasmid*

RingoA was amplified from 6-myc-RingoA plasmid using the following primers:

Forward AAAAGGCGCGCCTATGAGGCACAATCAGATGT

Reverse AAAAGCGGCCGCTCATTCTTCACTTCCTGTAAACCAC

The sequence obtained was digested with *Ascl* and *NotI* restriction enzymes and sub-cloned into the vector pcDNA5 N-term-FLAG-BirA* (which was a kind gift from Dr. Travis Stracker's lab).

Gene expression analysis by RT-qPCR

RNA isolation: Cells were washed with PBS, resuspended in 500 μ l Trizol and placed in a 1.5 ml Eppendorf tube, whereas tissue samples were homogenized using a Percellys instrument. 100 μ l of chloroform was added and tubes were centrifuged 15000 $\times g$ at RT for 10 min. From the two liquid phases generated, the fraction with less density was transferred into new tubes. After adding 200 μ l of 70% ethanol, the RNA extraction was followed using the PureLink RNA mini kit. DNase treatment was performed using on-column DNase treatment following the manufacturer's instructions. RNA purity and concentration were determined by measuring absorbance at 260nm and 280nm using a NanoDrop 2000 spectrophotometer (Thermo Scientific).

Synthesis of cDNA: cDNA was obtained from 500 ng – 4 μ g of purified RNA using random primers and RNAsin following the instructions of the manufacturer of SuperScript IV reverse transcriptase.

RT-qPCR: 25-50ng of cDNA was mixed with 5 μ l of SYBR green, 0.25 μ l of each primer (primers in **Table M7**) and up to 10 μ l of ddH₂O. The mix was incubated in a BioRad C1000 Thermal Cycler with the following PCR program: an initial step of 50°C for 2 min and 95°C for 10 min; 40 cycles of 95°C for 30 sec, 60°C for 40 sec and 72°C for 60 sec; and a final step of 95°C for 15 sec, 60°C for 2 min and 95°C for 15 sec.

Samples were analyzed in triplicates and normalized to GAPDH, and/or beta-Actin reference genes. Analysis was done using the Δ Ct method.

Table M7. Primers for RT-qPCR

Gene	Forward	Reverse
mbeta-Actin	GGCACCACACCTTCTACAATG	GTGGTGGTGAAGCTGTAGCC
mDCX	AGCTGACTCAGGTAACGACCA	GCTTTGACTTAGGTGTTGAGAGC
mGAPDH	CTTCACCACCATGGAGGAGGC	GGCATGGACTGTGGTCATGAG
mGfap	ACAGACTTTCTCCAACCTCCAG	CCTTCTGACACGGATTTGGT
mNestin	CCCTGAAGTCGAGGAGCTG	CTGCTGCACCTCTAAGCGA
mNeuN	TGAATGGTCACACCGTGGAA	CTTGCCTTCTGCTGTTTCTG
mRingoA	TTCTTGTGGATGGACTGCTG	TTGCCAGATGTAATGGGTTG
mRingoB	GGCGACGTGTGTCTACAGTG	ACACCCAAAGGTCTGGATTG
mSox2	CACAACCTCGGAGATCAGCAA	CTCCGGGAAGCGTGTACTTA
mBmi1	TCTTTGATCAGAGCAGATTGGA	TTTCTCAAGTGCATCACAGTCA

Statistical analysis

All statistical analyses were performed using GraphPad Prism 6 software. Data are presented as mean \pm SEM unless otherwise indicated. Statistical significance was determined by the Student's test for comparison of two groups. P values were calculated and P<0.05 was considered to be statistically significant. P-values are expressed as *(P \leq 0.05), **(P \leq 0.01 and) ***(P \leq 0.001).

Results

SECTION 1- Elucidating the molecular function of RingoA in human cells

RingoA knock-down reduces cell proliferation and increases cell death

As detailed in the introduction, there is strong evidence implicating RingoA in mammalian meiotic regulation (Mikolcevic et al. 2016; Tu et al. 2017). Moreover, as a CDK1 and CDK2 activator, RingoA also has a potential function in mitotic cell cycle regulation, which has been partially explored *in vitro*, mostly in overexpression conditions. To further understand the role of RingoA in human cells, we assessed the effect of RingoA downregulation in proliferation and cell cycle progression. Two different shRNAs were used to knock-down (KD) RingoA in U2OS cells. First, we analyzed cell cycle distribution using propidium iodide (PI) staining and FACS. We found an increased percentage of RingoA KD cells arrested in G1 and a decrease in S and G2 phases (**Figure R1.A**). By BrdU incorporation assays we confirmed a reduction in DNA replication, i.e., cells in S phase, in RingoA KD cells (**Figure R1.B**).

Due to the low levels of endogenous RingoA expression, the shRNA efficiencies were tested in cells transfected with myc-RingoA. Both shRNAs were found to efficiently down-regulate the overexpressed RingoA protein (**Figure R1.C**)

Results

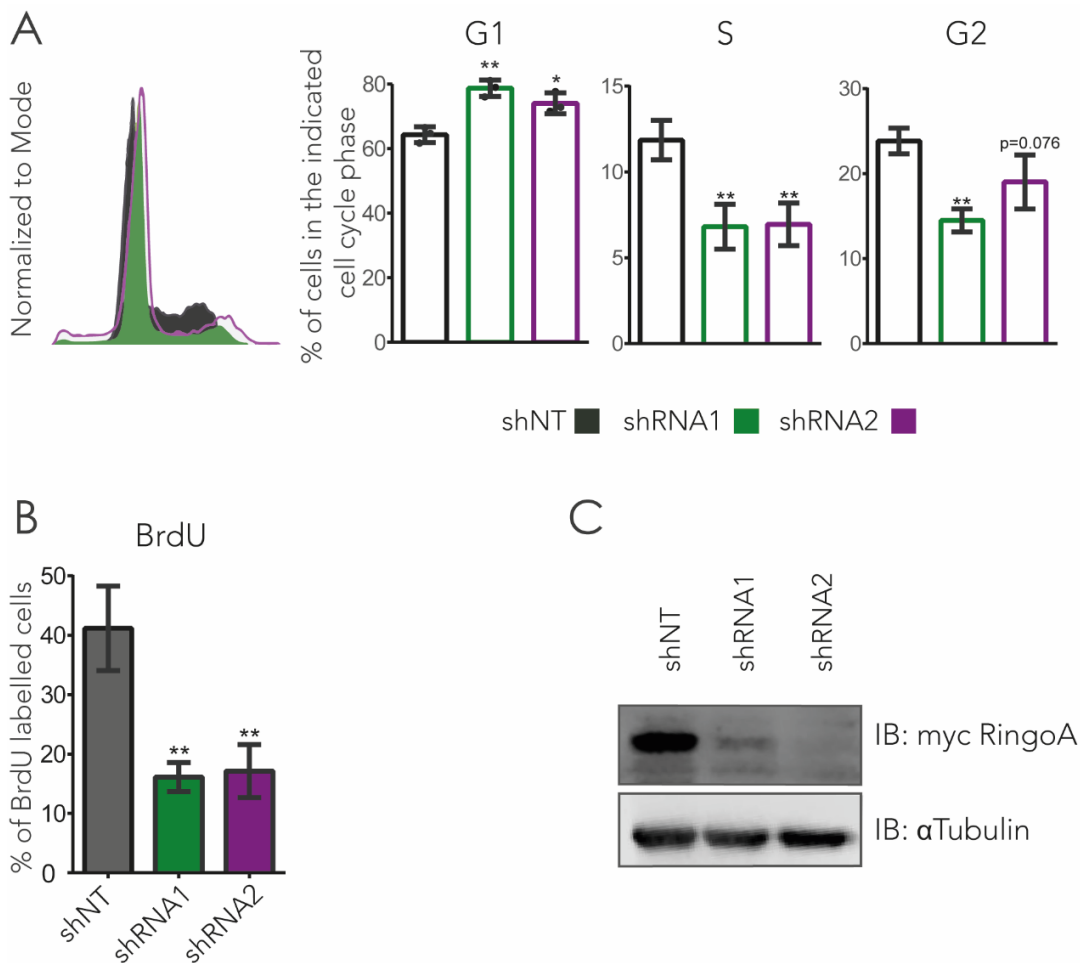
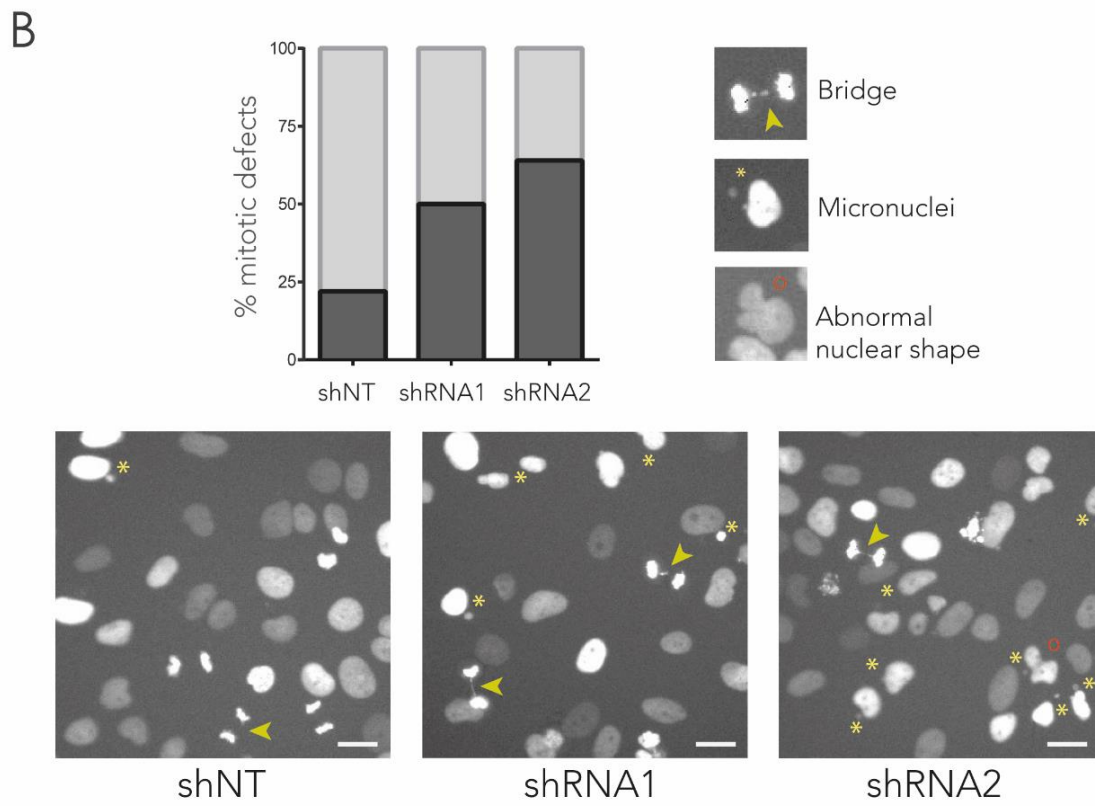
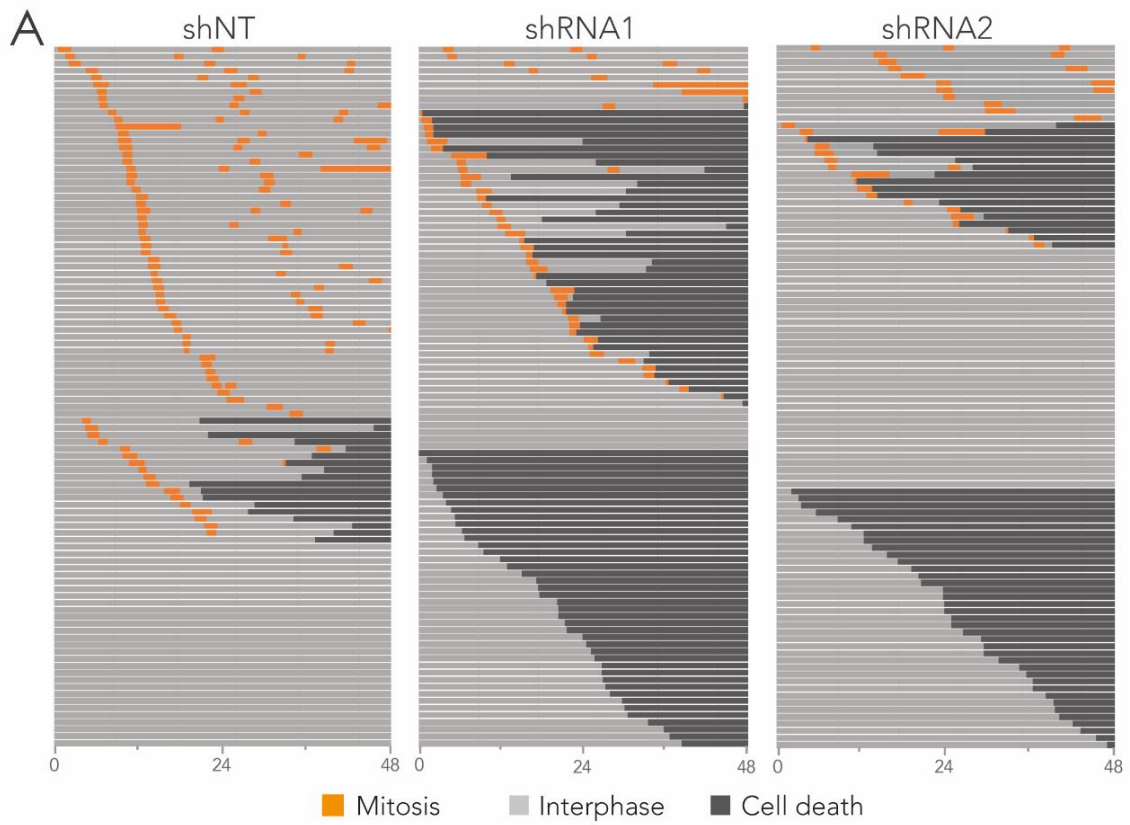


Figure R1. Cell cycle changes and reduced DNA replication in RingoA KD cells. **A.** Cell cycle analysis by FACS in U2OS cells labeled with propidium iodide (PI). Quantifications of each cell cycle phase are shown comparing cells expressing non-targeting (shNT) control shRNA or two shRNAs targeting RingoA. (Data are represented as average with SEM, n=3). **B.** Quantification of BrdU incorporation analyzed by FACS in the indicated cells. Graphs are representative of 3 independent experiments. (Data are represented as average with SEM, n=3). **C.** U2OS cells were infected with lentivirus carrying NT or two different RingoA-targeting shRNAs and then were transfected with myc-RingoA. 24h later cells were harvested and cell lysates were analyzed by western blot with a myc antibody. (*= p-value <0.05, **= p-value <0.01).

To better understand the phenotypes observed, time-lapse microscopy experiments were performed. U2OS cells expressing histone H2B-GFP and either non-targeting (NT) or RingoA shRNAs were used recording images every 10 min over a 48h period. A clear reduction in the number of cells undergoing mitosis was observed upon RingoA downregulation, this decrease being more severe in the case of RingoA shRNA2. Control cells underwent up to three rounds of mitosis during the course of the experiment, whereas most of RingoA KD cells remained in interphase or underwent a single round of mitosis and afterwards died, either during or after mitosis. In fact, the number of RingoA KD cells that died was dramatically increased in comparison with control cells (**Figure R2A**).



Results

Figure R2. Reduced number of mitoses and increased cell death in RingoA KD cells. U2OS cells expressing H2B-GFP and either non-targeting (shNT) or two different RingoA shRNAs were analyzed by time-lapse microscopy. **A.** Interphase is shown in grey, mitosis in orange, and dead cells in dark grey. Cells undergoing at least one mitotic division are shown at the top. Each lane represents one cell (n=100 cells per condition). Time lapse was performed for 48 h, x-axis represents time (h). **B.** Quantification of the percentage of mitosis that led to the formation of daughter cells with micronuclei or abnormal nuclear shape and/or anaphase bridges (at least 80 mitoses per condition were quantified). All these phenotypes are referred to as mitotic defects. Representative pictures of the different conditions are shown below the graph. Bridges are indicated with an arrowhead, micronuclei with an asterisk and cells with abnormal nuclear shape with a red circle.

The time-lapse videos allowed us to analyze mitoses in more detail. During the first 12h, we quantified mitoses with anaphase problems and/or that lead to the formation of micronuclei, as well as cells with abnormal nuclear shape were quantified (**Figure R2B**). All these features were increased in RingoA KD cells and are signs of mitotic chromosomal instability. (Fenech et al. 2011; Gisselsson et al. 2001; Neumann et al. 2010).

Unbiased proteomic approach for the identification of potential RingoA interactors

Time-lapse microscopy analysis and cell cycle characterization pointed to a reduction in the number of mitoses, changes in the cell cycle and increased cell death upon RingoA KD in U2OS cells. Moreover, RingoA has been proposed to be involved in cell cycle and the DDR (Dinarina et al. 2009; Lubanska et al. 2014; Mikolcevic et al. 2016; McGrath et al. 2017). However, little is known about how RingoA participates in these processes and the mechanisms behind them. Thus, we aimed to identify potential interactor proteins that would help us to understand the cellular functions of RingoA, as well as the organelles and pathways in which RingoA is implicated.

For this purpose, we decided to perform Proximity-Dependent Biotin Identification (BioID), a proteomic approach to identify stable and transient interactors. This technique consists of labeling proteins in close proximity through the use of a bait protein fused with a promiscuous biotin ligase (BirA*). BirA* is a modified promiscuous version of *Escherichia coli* BirA, a 35-kD DNA-binding protein that originally regulates the biotinylation of a subunit of acetyl-CoA carboxylase. After biotin labeling, proteins are pulled down with streptavidin and

peptides are identified by mass spectrometry (MS) (**Figure R3.A**). This procedure allows us to mark proteins in their cellular context in live cells. BioID is a very powerful technique that allows the identification of proteins that can be divided into three categories: a) stable or transient direct interactions with the bait protein; b) indirect interactions; c) vicinal proteins that are in close proximity but do not interact directly or indirectly with the bait protein (Roux et al. 2012).

Setting up the RingoA BioID screening: BirA**RingoA* expression and location

Human RingoA was cloned into a vector to generate a fusion protein with BirA*-FLAG in the N-terminus. BirA* alone (BirA*-ev) was used as a control to compare with the enzyme that is specifically directed to certain spots by the bait protein.

The BirA*-RingoA and BirA*-ev were transfected into HEK293-T cells and biotin was added the day after. After 24h, cells were harvested and the expression levels of BirA*-RingoA and BirA* proteins were found to be similar by western blot. In both cases, a smear like pattern of biotinylated protein was observed, indicating the presence of biotinylated proteins of different sizes. However, the patterns were different in the two conditions, indicating a likely change of targets biotinylated by BirA*-ev compared to BirA*-RingoA (**Figure R3.B**). Moreover, we tested whether the overexpressed protein was located in the nucleus. Cells were seeded in coverslips, transfected with either BirA*-RingoA or BirA*-ev and the following day were incubated with biotin for 24 h. After fixation, cells were labeled with either FLAG antibody for BirA*-RingoA and BirA*-ev, or streptavidin for the biotinylated target proteins. The results showed that BirA*-RingoA was expressed mainly in the nucleus with some more intense spots forming a puncta-like pattern; however, BirA*-ev was expressed in both the nucleus and cytoplasm. In the case of BirA*-RingoA, biotinylated proteins were restricted to the nucleus, with stronger signal in a rounded structure, probably corresponding to the nucleolus. In contrast, the biotinylation signal in BirA*-ev was present in both the nucleus and cytoplasm, also with slightly increased signal in the nucleolus-like organelle (**Figure R3.C**)

Results

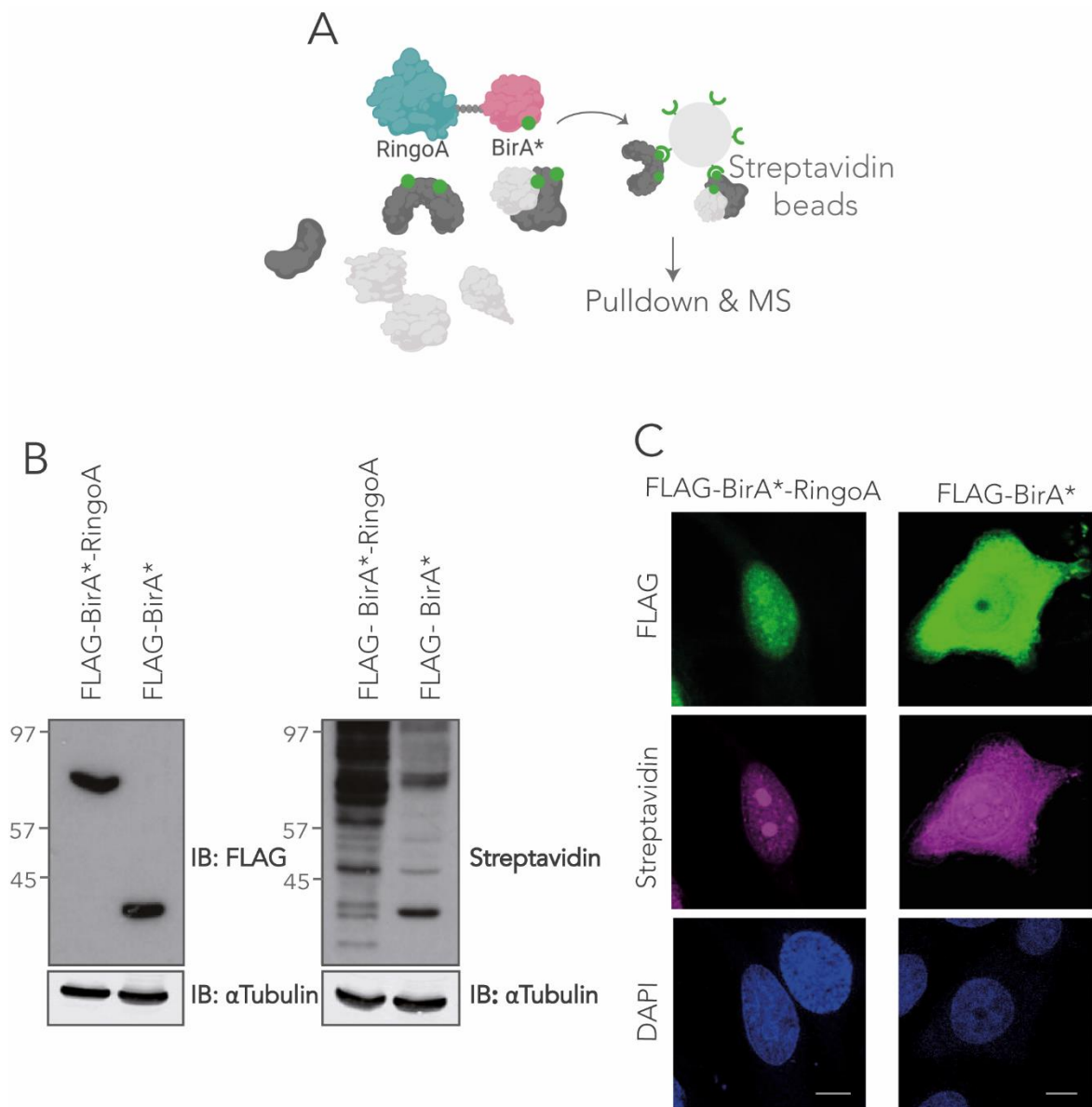


Figure R3. Setting-up the RingoA BioID screening. **A.** Schematic representation of the Bio-ID screening process. BirA*-RingoA fused protein is expressed in cells, which are incubated with biotin, so that proteins in close proximity to the bait will be labeled. Biotinylated proteins are then pulled down with Streptavidin beads and identified by MS. **B.** (Left panel): immunoblots showing FLAG-BirA*-RingoA and FLAG-BirA* expression in HEK-293 cells. (Right panel): cells transfected with the same constructs were incubated with biotin for 24h and then analyzed by western blot with Streptavidin-HRP to label biotinylated proteins. **C.** IF showing cells transfected with the indicated constructs and stained with FLAG antibody for BirA*-RingoA and BirA* or Streptavidin for biotinylated proteins.

BiOID analysis suggests three different clusters of potential RingoA interactors involved in cell cycle regulation and RNA processing

In order to proceed with the screening, HEK293T cells were transfected with the constructs and incubated with biotin, as described in Methods section. Briefly, the protein lysates were incubated with streptavidin beads to pulldown the biotinylated proteins, which were analyzed by MS. The procedure was performed twice. Four control runs representing four different experimental replicates, from cells expressing the Flag BirA* were compared to the two experimental replicates using Flag- BirA*-RingoA. High confidence interactors were defined as those with $FDR \leq 0.02$ (false discovery rate) and SAINT (Significance Analysis of INTeractome) score > 0.9 . In total, 92 proteins that fulfill these criteria were identified (**Supplementary Figure 1**). We analyzed the protein interactions of the 92 putative candidates using the STRING database, which provides a critical assessment and integration of protein-protein interactions (Szklarczyk et al. 2015). This analysis detected three main clusters of proteins. Two clusters contained a high percentage of proteins involved in RNA metabolism and processing, and the other cluster mainly proteins involved in cell cycle regulation (**Figure R4**).

RNA related clusters: Both clusters contained proteins involved in RNA metabolism and gene expression. The cluster labeled in light green contained proteins involved in mRNA processing, including processing of Capped intron-containing pre-mRNA, mRNA splicing and RNA polymerase II transcription. The other RNA related cluster, labeled in dark green, contained proteins related to ribosomal RNA (rRNA) processing.

Cell cycle related cluster: This cluster, labeled in yellow, contained proteins directly or indirectly related to the cell cycle. These included CDK1 and CDK2, two known interactors of RingoA *in vitro*, at the center of the network and other proteins involved in mitosis, cell cycle progression and checkpoints. Interestingly, Skp2 was also detected in the analysis, and it has been previously proposed to interact with and ubiquitinate RingoA, promoting its degradation (Dinarina et al. 2009).

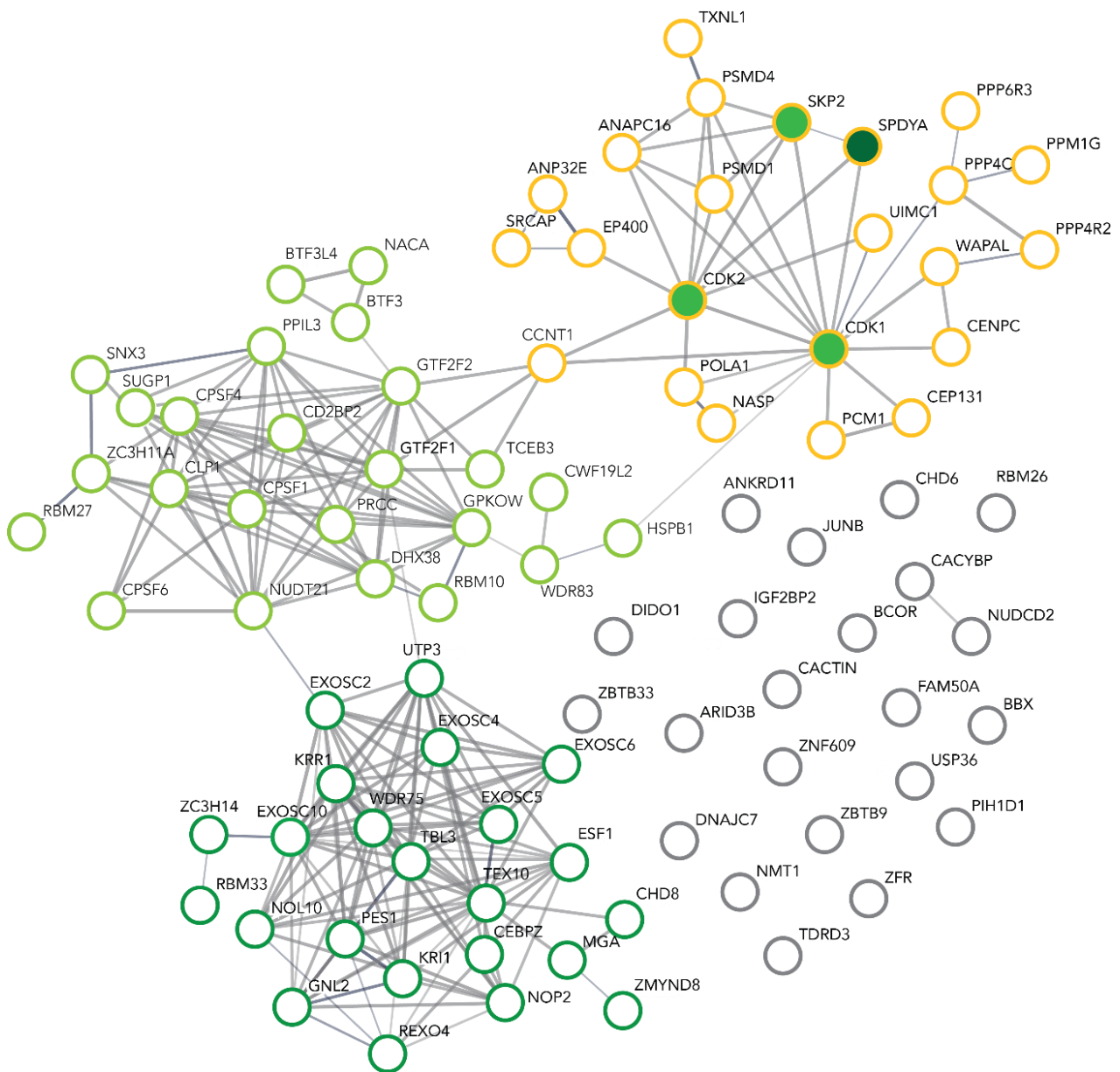


Figure R4. Interacting networks of the candidate RingoA interactors identified in the BioID screening.

The cell cycle cluster (yellow) contains CDK1 and CDK2 at the center. Previously reported RingoA interactors are filled green and Spdya (RingoA) in dark green. Two RNA processing related clusters were identified. The upper cluster (light green) contains mainly mRNA processing proteins, whereas lower cluster (dark green) contains rRNA related proteins. Several proteins that were not reported as part of any network are shown in grey. Analysis was done with the STRING tool and only associations with a minimum confidence of 0.5 are considered (being 0.15 the lowest and 0.9 the highest possible confidence values). Thickness of edges represents the strength of the data support, from medium (0.5) to highest (0.9).

In parallel, Reactome over-representation analysis was performed (**Supplementary Figure 2**). Highly enriched pathways were consistent with the RNA processing clusters identified and included RNA metabolism, mRNA splicing and rRNA processing proteins. There was also a representation of the pathways of mitosis, G2/M and G1/S transition checkpoints. Interestingly, 84 of the 92 candidate proteins identified have been described to locate or to have a function in the nucleus, agreeing with the expected RingoA location, and 34 candidate proteins have nucleic acid binding capacity.

Validation of RingoA potential interactors

As mentioned above, BioID can identify direct interactions (stable or transient), indirect interactions or proteins that are in close proximity but do not interact with the bait. As a first approach to identify new RingoA interactors, we used co-IP to validate the interaction with several candidate proteins, as this method probably detects the strongest interactions.

The candidates for validation were selected based on the following criteria: high score comparing reads of BirA*-RingoA versus BirA*-ev control, low score in CRAPome (Contaminant Repository for Affinity Purification) (**Supplementary Figure 1**), involvement in cell cycle regulation, potential connection with RingoA phenotypes described in the literature and, finally, availability of antibodies. Of the 92 candidate proteins identified in the BioID screening, 8 were tested for validation by co-IP: PCM-1, CENP-C, NMT-1, ANP32-A, Cyclin T, the APC/C component Cdc27, WAPL and ANKRD11. Lysates prepared from HEK293T cells expressing human myc-RingoA or the myc vector were immunoprecipitated with myc antibodies and then analyzed by western blot using specific antibodies for the endogenous candidate proteins. The technique had been previously validated by co-immunoprecipitating overexpressed RingoA with the overexpressed previous known interactors CDK2 and Skp2 (**Supplementary Figure 3**).

These experiments identified two proteins able to interact with overexpressed RingoA (**Figure R5.A**). One interactor was WAPL, which negatively regulates cohesin association with chromatin, allowing the unloading of the cohesin complex from the DNA. This process is crucial both for sister chromatid cohesion during interphase and also for sister-chromatid resolution during the early stages of mitosis (Kueng et al. 2006; Tedeschi et al. 2013). The other was ANKRD11, which has been proposed to be a chromatin regulator involved in

Results

neural development and in diseases such as autism and cancer (Gallagher et al. 2015; Neilsen et al. 2008). The rest of the proteins analyzed were not found to co-immunoprecipitate with RingoA (**Figure R5.B**). In all the co-IP experiments, endogenous CDK2 was used as a positive control for the interaction with RingoA.

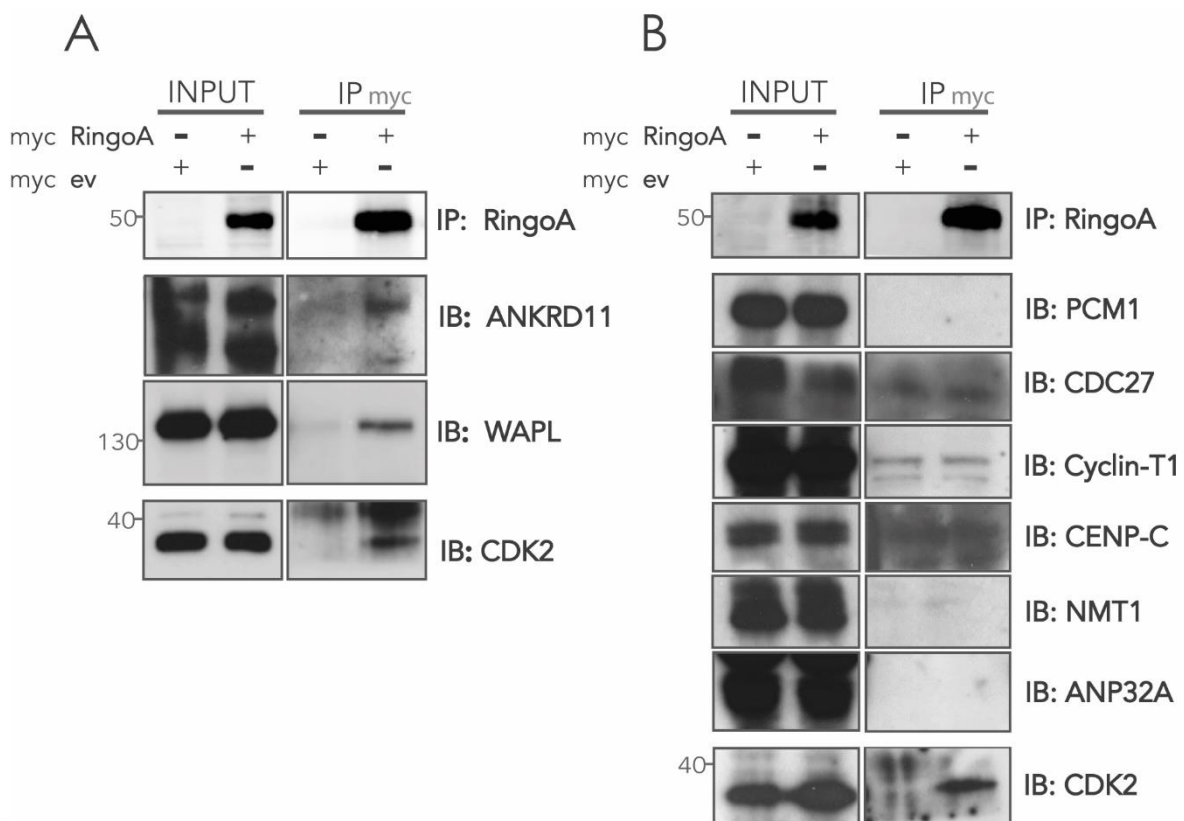


Figure R5. RingoA interacts with WAPL and ANKRD11. A,B. Lysates from HEK293-T cells expressing myc-RingoA or myc-ev were incubated with myc beads overnight and the resulting immunoprecipitates were analyzed by immunoblotting. Myc antibody was used for RingoA detection, and specific antibodies were used for detection of the endogenous proteins, as indicated. An aliquot of the cell lysates before co-IP was also analyzed by immunoblotting (INPUT).

RingoA interacts with the cohesin complex

Since RingoA interacted with the cohesin complex regulator WAPL, we evaluated whether it was able to interact with the components of the cohesin core complex. Endogenous SMC1, SMC3 and Scc1 were also found to co-immunoprecipitate with RingoA (**Figure R6**), thereby confirming that overexpressed RingoA is able to bind to the cohesin complex.

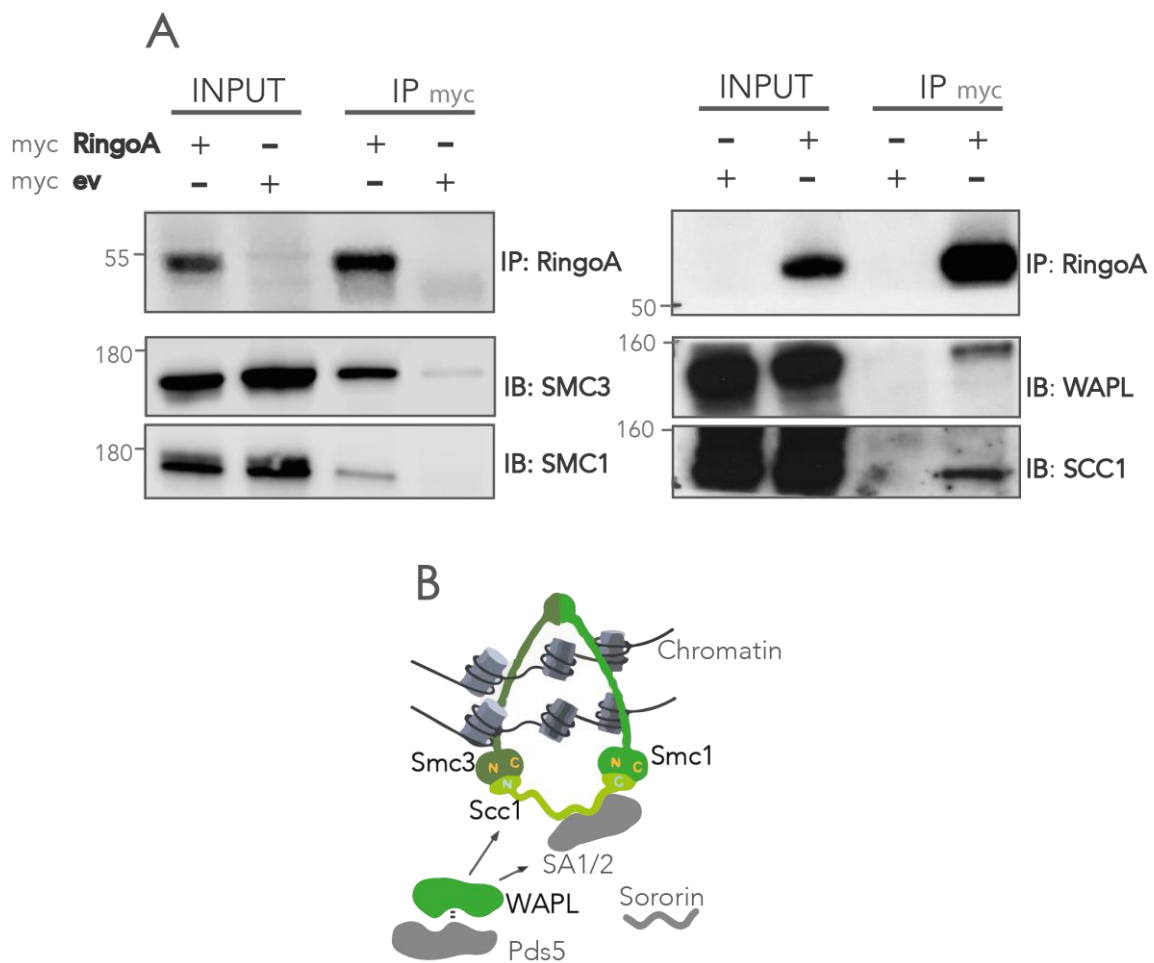


Figure R6. RingoA co-immunoprecipitates with different subunits of the cohesin complex. A. Lysates from MCF-7 cells expressing myc-RingoA or myc-ev were incubated with myc beads overnight and the resulting immunoprecipitates were analyzed by immunoblotting. Myc antibody was used for RingoA detection, and specific antibodies were used for detection of the endogenous proteins, as indicated. An aliquot of the cell lysates before co-IP was also analyzed by immunoblotting (INPUT). **B.** Schematic representation of the cohesin complex architecture in mammals. The cohesin core complex is composed of Scc1, Smc1, Smc3 and either SA1 or SA2. WAPL is associated with the core through Scc1 and SA1, and there is evidence of WAPL-Pds5 direct interaction (modified from Peters et al. 2008). Proteins found to co-IP with RingoA are highlighted in green.

Furthermore, in order to study whether the interaction with WAPL was exclusive of RingoA, we evaluated the capacity of CDK2, Cyclin E and Cyclin A to co-immunoprecipitate with WAPL. Despite being less expressed than the CDK2 and the cyclin proteins, RingoA was found to bind to WAPL much more efficiently than the other proteins analyzed (**Figure R7**).

Results

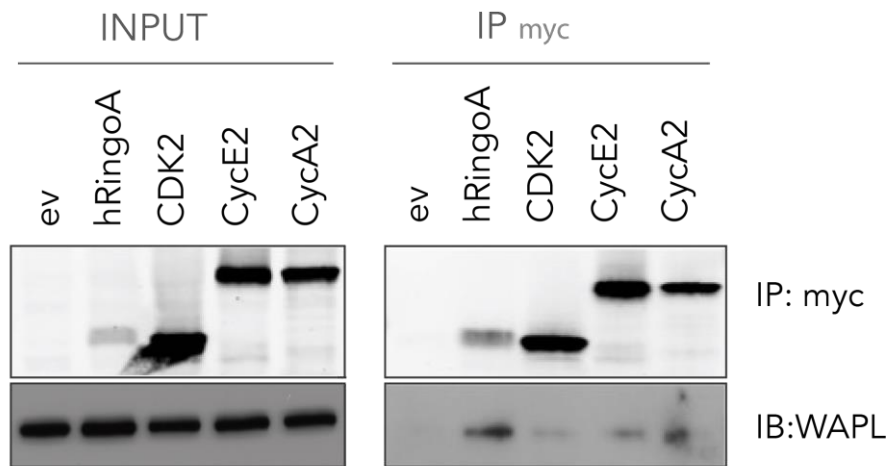


Figure R7. WAPL interacts with RingoA better than with CDK2, Cyclin E2 and Cyclin A2. Lysates from HEK293T cells expressing myc-RingoA, myc-ev, myc-CDK2, myc-cyclin E2 or myc-cyclin A2 were incubated with myc beads overnight and the resulting immunoprecipitates were analyzed by immunoblotting. A specific WAPL antibody was used to detect the endogenous WAPL, and myc antibody to detect the overexpressed proteins. An aliquot of the cell lysates before co-IP was also analyzed by immunoblotting (INPUT).

RingoA localizes to discrete nuclear sites in human cells and its expression depends on the cell cycle

In order to detect the endogenous RingoA human protein by IF, a homemade mouse monoclonal antibody was used. In U2OS cells, RingoA was found to be localized in discrete nuclear sites inside the nucleus; however, its expression and localization changed during the cell cycle. Interestingly, the expression was conserved during interphase and removed at the prophase of mitosis. The protein was then re-expressed in anaphase-telophase, forming dots that encircled the DNA, and it was subsequently surrounded by chromatin again in G1 (**Figure R8.A**). To validate the antibody specificity, it was confirmed that the signal of the endogenous protein was downregulated in cells treated with RingoA-targeting siRNA (**Figure R8.B**). The epitope recognized by the antibody was identified by screening a peptide array as amino acids 283-289 (NDHQS^{NK}) of human RingoA (**Figure R8.C**) (Mikolcevic et al. 2016).

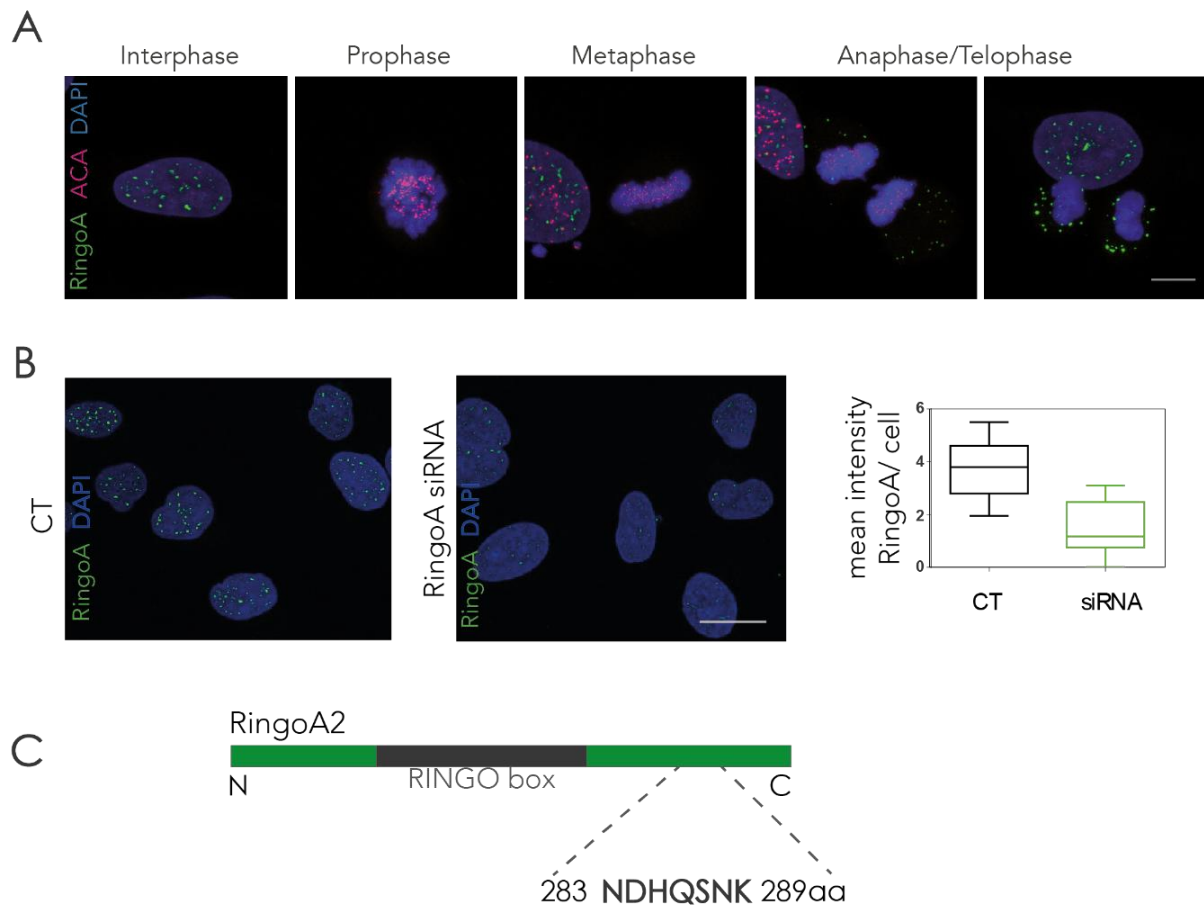


Figure R8. RingoA locates to discrete nuclear sites during interphase and its expression is lost in mitosis. A. U2OS cells were stained with DAPI (DNA) and with antibodies against RingoA (green) and centromeric protein (ACA, red). Representative examples of the RingoA expression pattern in interphase and in the indicated phases of mitosis are shown. Scale bar = 10 μ m. **B.** U2OS cells were treated with control (CT) or RingoA-targeting siRNA and then were stained with DAPI (DNA) and with the RingoA antibody. Signal intensity was quantified per cell and is represented as an average. Scale bar = 25 μ m. **C.** Scheme showing the sequence of the human RingoA2 protein recognized by the antibody.

Results

RingoA location in human cells

BioID screening gives information not only of interactors but also proteins in close proximity and therefore can inform on the location of the protein. We observed that most of the proteins identified using RingoA-BirA* as bait were nuclear. This is the same localization detected for the endogenous RingoA protein. The identified candidates included centromeric proteins, proteins involved in rRNA processing (most of them nucleolar), mRNA processing proteins and splicing factors.

RingoA partially localizes to nuclear speckles and accumulates upon transcription inhibition

Given the observed abundance of mRNA processing proteins, we wondered whether RingoA could be located in nuclear speckles. Endogenous RingoA protein was found to partially colocalize with the SC35 marker of nuclear speckles in human U2OS cells (**Figure R9.A**). Nuclear speckles are membrane-less compartments that are very rich in splicing factors and RNA modification proteins but also contain kinases, phosphatases and proteins involved in chromosome localization or chromatin modification (Galganski et al. 2017).

Nuclear speckle proteins, such as splicing factors, accumulate when transcription is inhibited for example, with Actinomycin D. In these conditions, nuclear speckles grow in size and become rounded (Lamond and Spector 2003). Interestingly, we found that treatment with Actinomycin D for 4 h induced RingoA protein accumulation, as determined by IF (**Figure R9.B**). RingoA showed a similar behavior to the protein SC35, a broadly used marker of nuclear speckles.

Membrane-less bodies are highly enriched in proteins that contain stretches of low sequence complexity, known as intrinsically disordered proteins or with intrinsically disordered regions (Shin and Brangwynne 2017). We analyzed the RingoA sequence using PONDR predictor software and confirmed different regions predicted to be disordered, the longest one at the C-terminus (**Figure R9.C**).

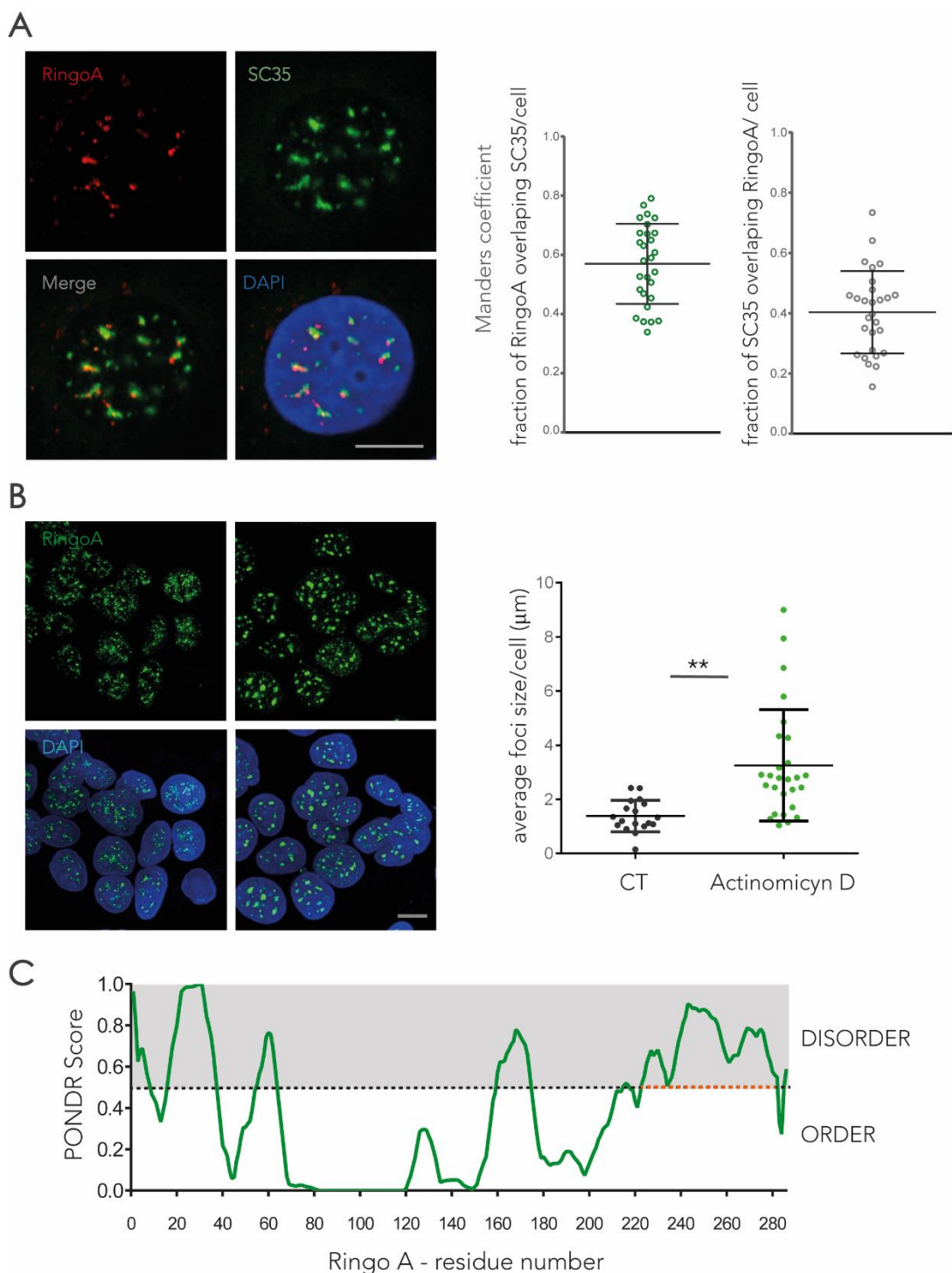


Figure R9. RingoA co-localizes with nuclear speckles and accumulates upon transcription inhibition. **A.** IF of U2OS cells stained with antibodies against RingoA (red) or the nuclear speckle marker SC35 (green). Graphs show the Mander's coefficient representing the fraction of RingoA overlapping with SC35 (left), and the fraction of SC35 overlapping with RingoA (right). Each dot represents an individual cell, data are representative of two independent experiments. Scalebar = 5 μ m **B.** IF comparing RingoA staining (green) in cells untreated or treated with Actinomycin D (1 μ g/ml). Graph shows the quantification of the average volume of foci per cell (n = 3 experiments). Scalebar = 10 μ m **C.** PONDR score showing the residues of human RingoA protein considered as disordered. Seven disordered regions are detected, including the long C-terminal region indicated with a red dashed line.

Results

Moreover, since RingoA was found to interact with the cohesin complex by co-IP, we compared the location of endogenous RingoA with that of cohesin, as determined by using a SMC1 antibody. Cohesins are extensively expressed across the nucleus and RingoA was found to overlap with SMC1 staining by almost 80%, whereas approximately 10% of total nuclear SMC1 overlapped with RingoA (**Figure R10.A**).

Finally, as several rRNA processing proteins were detected and RingoA-BirA* seemed enriched in the nucleolus, we also used fibrillarin as a marker of this organelle. However, we found no co-localization with RingoA. Furthermore, despite the identification of some centromeric candidates, we did not detect co-localization of RingoA with centromeres (**Figure R10.B**).

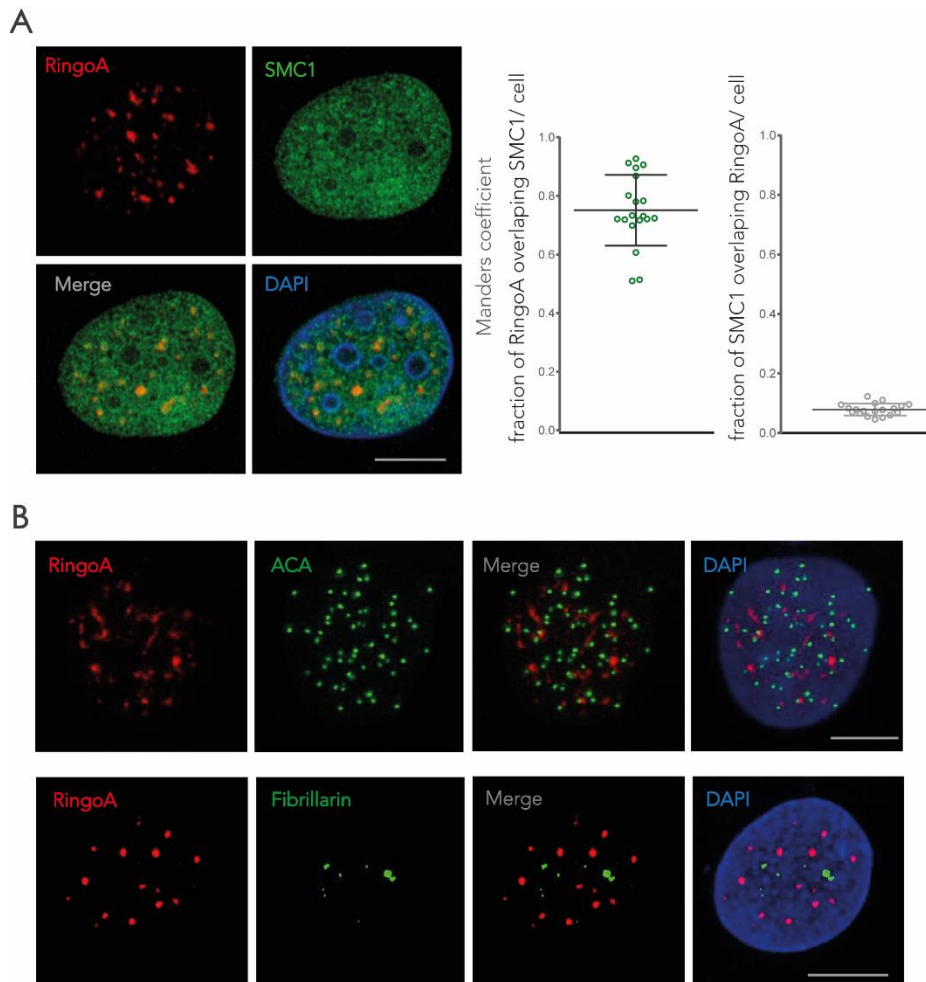


Figure R10. RingoA partially colocalizes with cohesins. A. IF of U2OS cells stained with antibodies against RingoA (red) and the cohesin subunit SMC1 (green). Graphs show Manders coefficient representing the fraction of overlapping of RingoA with SMC1 (left) and the fraction of overlapping of SMC1 with RingoA (right). Each dot represents an individual cell, data are representative of two independent experiments. Scalebar = 10 μm **B.** IF of RingoA and the centromeric protein ACA (upper panel) or the nucleolar protein fibrillarin (lower panel). RingoA is shown in red and ACA and fibrillarin in green.

SECTION 2 - Characterization of RingoA and RingoB KO mouse models

Expression of RingoA and RingoB mRNAs

Having determined the relevance of RingoA for cell cycle progression of human cell lines, we turned our attention to the role of RingoA at tissue level. To this end, experiments using mouse models were performed. We first used RT-qPCR to determine the level of expression of the RINGO family members RingoA and RingoB in different mouse tissues. RingoA mRNA was expressed mainly in testis, followed by brain and skin, and with lower levels other tissues like kidney, liver or lung (**Figure R11.A**). RingoB mRNA expression was only detected in testis (**Figure R11.B**).

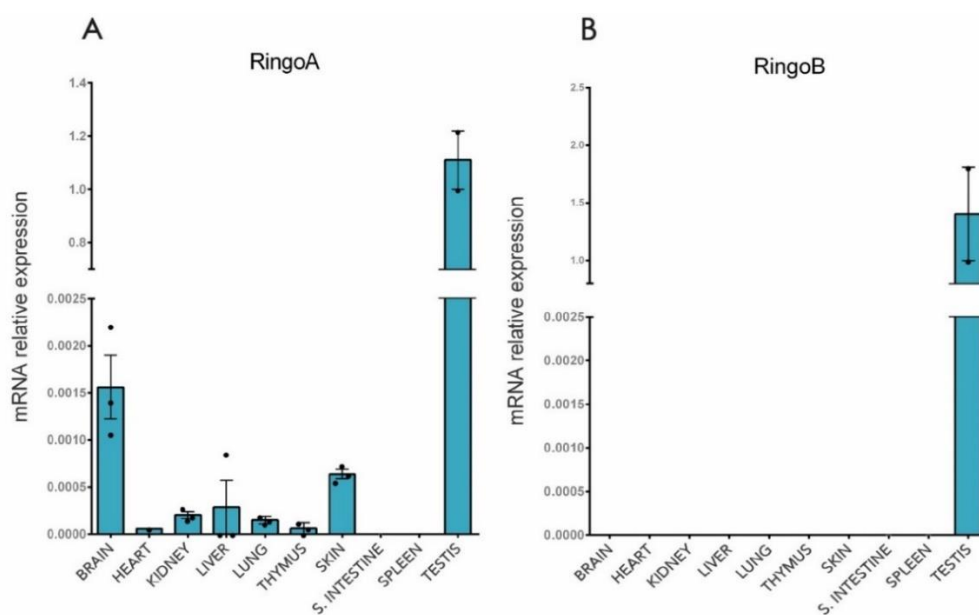


Figure R11. RingoA and RingoB mRNA expression in mouse. A,B. RT-qPCR analysis of RingoA (**A**) and RingoB (**B**) in different organs. Levels of mRNAs are relative to testis. GAPDH was used as a reference. The expression of each animal is represented as a dot, the bars indicate average and SEM (n= 3 animals).

Histological characterization of RingoA KO, RingoB KO and RingoA/RingoB double KO mice

As mentioned in the introduction, a RingoA KO mouse model was generated to study the role of RingoA in mammalian meiosis (Mikolcevic et al. 2016). Using the same model, we aimed to study the role of RingoA in somatic tissues. Moreover, given the high expression of RingoB in testis, which resembled that of RingoA, we also wanted to test its role in gonads and compare it with RingoA function. Therefore, a RingoB KO mouse model was used. Finally, we crossed RingoA and RingoB KO strains to obtain RingoA and RingoB double KO (RingoA/RingoB KO). This model was generated with the aim to elucidate the possible functional complementation between the two Ringo proteins, which could potentially mask their functions in mouse tissues. The results observed in the different models, both in gonads and in somatic tissues, are described in the following section.

Effects of RingoB or RingoA/RingoB depletion in gonads

RingoB KO: As shown above, RingoB was highly expressed in testis. We therefore questioned whether it could have a similar function to RingoA (Mikolcevic et al. 2016). Analysis of gonads of young animals showed that both testis and ovaries were histologically normal (**Figure R12**). Moreover, both males and females RingoB KO mice were fertile, further supporting the functionality of their gonads.

RingoA/RingoB KO: Gonads of RingoA/RingoB KO animals were also studied in order to compare them with the RingoA KO phenotypes. In testis, the epithelia of most of the seminiferous tubules were abnormal, with only a single layer of Sertoli cells and spermatogonial cells (**Figure R12**). The seminiferous tubules were narrower and degenerated. Ovaries were also atrophic and had no ovarian follicles. In both cases, as it could be expected the results observed in RingoA/RingoB KO animals resembled the RingoA KO phenotype.

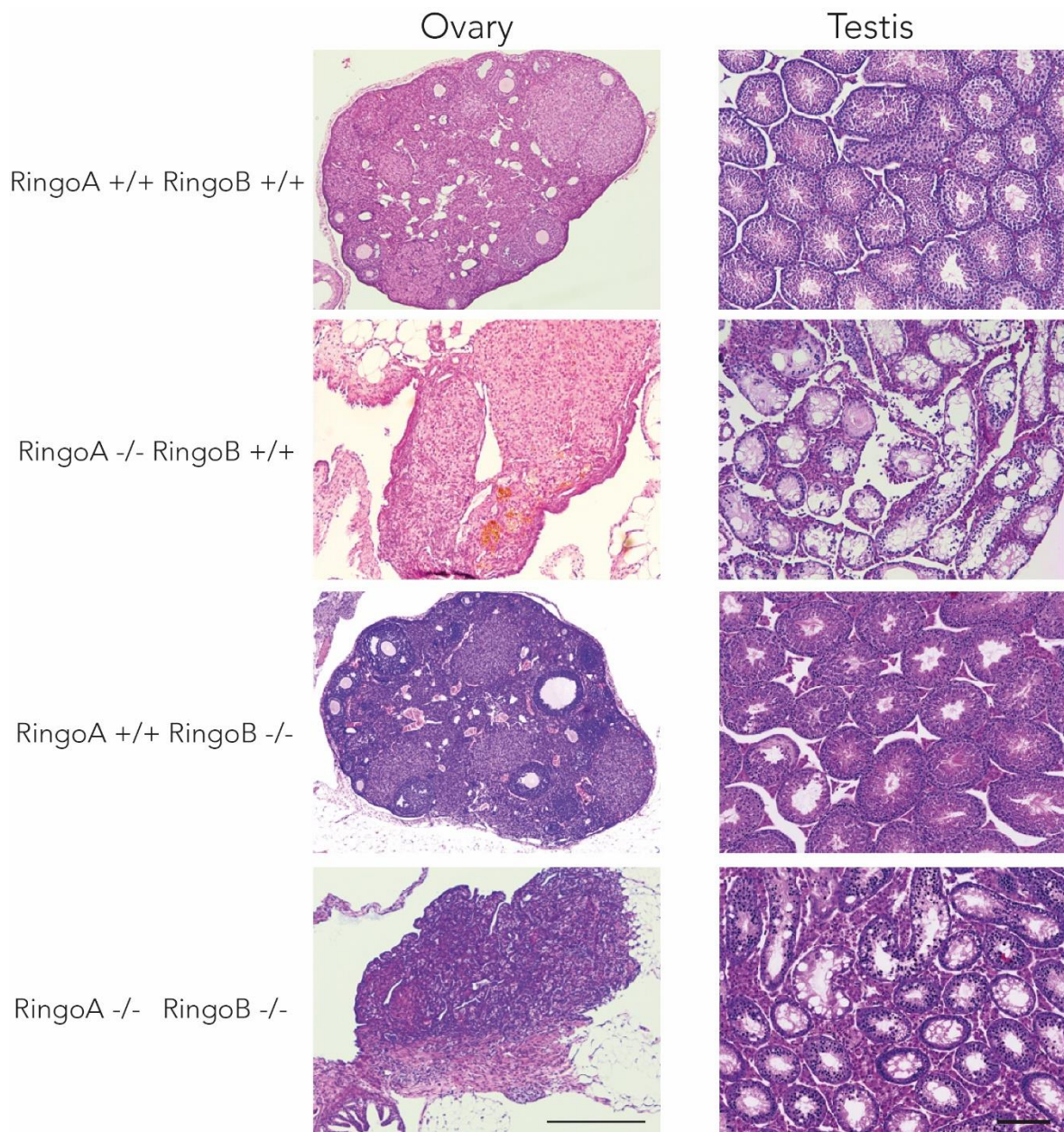


Figure R12. Histological analysis of ovaries and testes. Representative pictures from testes and ovaries of animals of the indicated genotypes. Sections are stained with H&E. Scale bar = 500 μ m in ovaries and 200 μ m in testes. Age: 3-4 months, ($n \geq 2$ per genotype). Phenotypes of RingoA $-/-$ gonads are reported in (Mikolcevic et al. 2016).

Effects of RingoA, RingoB or RingoA/RingoB downregulation in somatic tissues

RingoA and *RingoA/RingoB* KO, young: Besides the impaired meiosis and sterility, no other phenotypes were detected at the histological level in basal conditions in any of the mouse tissues analyzed at young ages.

Results

RingoB KO and RingoA/RingoB KO, aged: RingoB KO and RingoA/RingoB KO mice were sacrificed at 16 and 25 months of age, respectively, with the aim to identify potential phenotypes acquired during aging. Despite all the animals presenting similar age-related phenotypes, such as multisystem inflammatory lesions in several tissues or thalamus multifocal mineralization in the brain, no relevant differences were observed between WT and RingoB KO or RingoA/RingoB KO mice (**Table R1**).

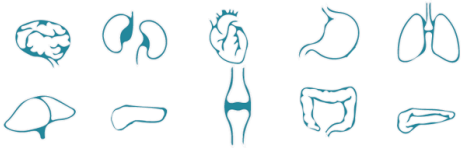
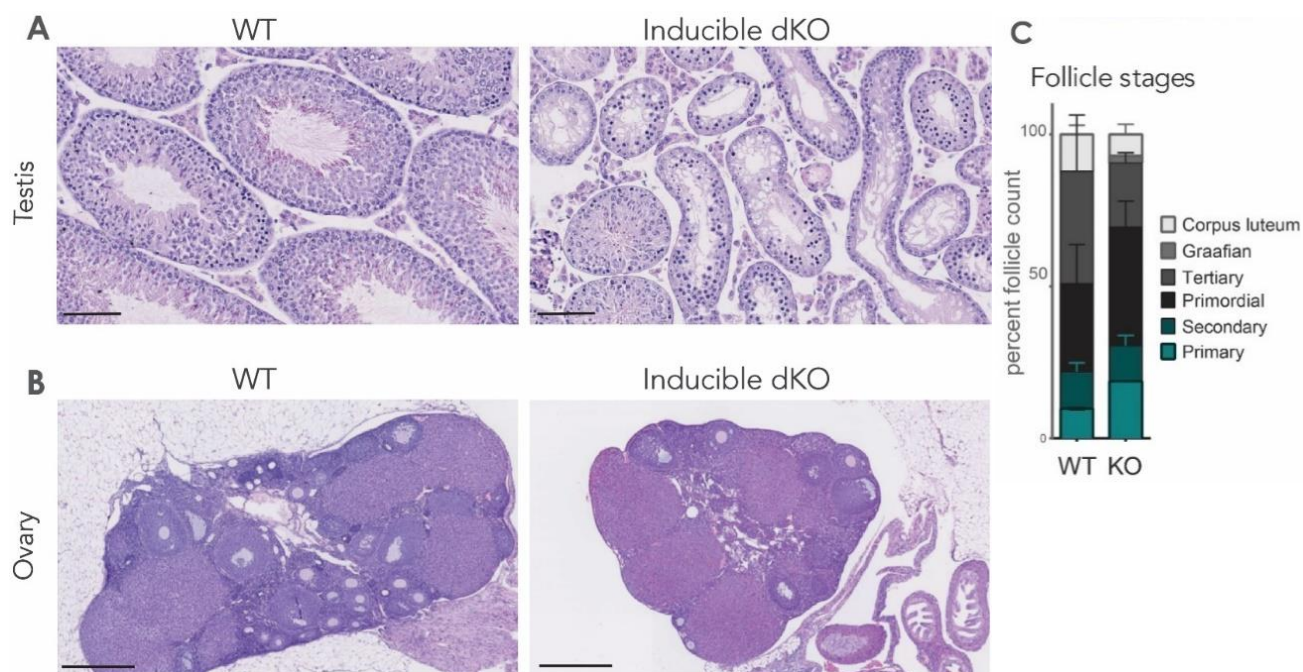
Histological characterization	
GENOTYPE	
RingoA <i>-/-</i> Ringo B <i>+/+</i> young	Normal
RingoA <i>+/+</i> Ringo B <i>-/-</i> aged	Normal
RingoA <i>-/-</i> Ringo B <i>-/-</i> young	Normal
RingoA <i>-/-</i> Ringo B <i>-/-</i> aged	Normal

Table R1. Histological analysis of somatic tissues. Brain, kidney, heart, stomach, lung, liver, spleen, bone marrow, muscle, intestine and pancreas were analyzed. $n \geq 2$ per group. Age: (RingoA $-/-$, RingoB $+/+$) 2-3 months; (RingoA $+/+$, RingoB $-/-$) 16 months; (RingoA $-/-$, RingoB $-/-$, young) 4 months, (RingoA $-/-$, RingoB $-/-$, aged) 25 months.

Histological characterization of RingoA/RingoB inducible KO: male testes but not female ovaries mimic phenotypes of constitutive RingoA KO

To study whether the acute deletion of RingoA and RingoB would produce additional phenotypes to those observed in the constitutive KO models, RingoA^{lox/lox}, Ringo B^{lox/lox}, UBC-Cre ERT2^{+TG} mice were injected with 4-OH tamoxifen (4-OHT) to induce gene deletion and were analyzed 2 months later. On the one hand, males had testicular atrophy and seminiferous tubule degeneration, indicating a similar testis phenotype as the constitutive RingoA KO (**Figure R13.A**). On the other hand, no significant alterations were observed in the females (**Figure R13.B**), and both follicle type and number were similar in KO and WT

mice (**Figure R13.C**), thereby indicating that the ovary phenotype observed in the constitutive RingoA KO was not mimicked upon inducible downregulation. Moreover, we found that females in which RingoA and RingoB downregulation was induced with 4-OHT were fertile when crossed with wild type males (n=2), thus proving the functionality of the female reproductive organs in the inducible RingoA/RingoB KO mice.



Some proteins, including cell cycle regulators, have been reported to have redundant functions, and thus their downregulation during development does not result in any detectable phenotype due to functional complementation. Therefore, we studied potential phenotypes arising after acute depletion of RingoA and RingoB in adult mice. We evaluated the same tissues as for the constitutive KO, but no consistent phenotypes were found in any of the non-reproductive tissues (**Table R.2**).

Histological characterization	
GENOTYPE	
(RingoA ^{lox/lox} , Ringo B ^{lox/lox} , UbiCRE ERT2 ^{TG/+})	
	<u>Testis</u> : Testicular atrophy and seminiferous tubule degeneration. <u>Ovaries</u> : normal
	
	Normal

Table R2. Histological analysis of the inducible RingoA/RingoB KO. RingoA^{lox/lox}, Ringo B^{lox/lox}, UBC-Cre ERT2^{TG/+} animals were analyzed. Gonads in the upper part, somatic tissues in the lower part (brain, kidneys, heart, stomach, lungs, liver, spleen, bone and muscle, intestine and pancreas.) Age: 3.5 months. Animals were treated with 4-OHT 2 months before sacrifice for the induction of Cre ERT2, (n ≥ 2 per group).

Katushka-Luciferase reporter of RingoA promoter activity

As mentioned before, RingoA mRNA is highly expressed in testis, where it plays an essential function in meiosis. RingoA protein is also detected in testis by western blot, although at very low levels (Mikolcevic et al. 2016). When other somatic tissues were analyzed, no signal was detected by western blot despite being detected in several tissues at mRNA level. In order to better analyse the expression of RingoA in particular tissues and cell populations, a Katushka-Luciferase (K/L) reporter was generated. This reporter consisted of a cassette with two genes encoding the far-red fluorescent protein Katushka (Turbo FP635) and the luciferase enzyme, respectively, both being expressed under control of the endogenous RingoA promoter. The cassette with the two genes was integrated (knock-in(KI)) between the exons 2 and 3 of the *RingoA* gene (**Figure R14.A**), so that RingoA promoter expression induced the transcription of both Katushka and Luciferase genes. It should be noted that the cassette disrupts the expression of the RingoA gene, therefore, the reporter KI allele mimics the KO allele of RingoA (**Figure R14.B**).

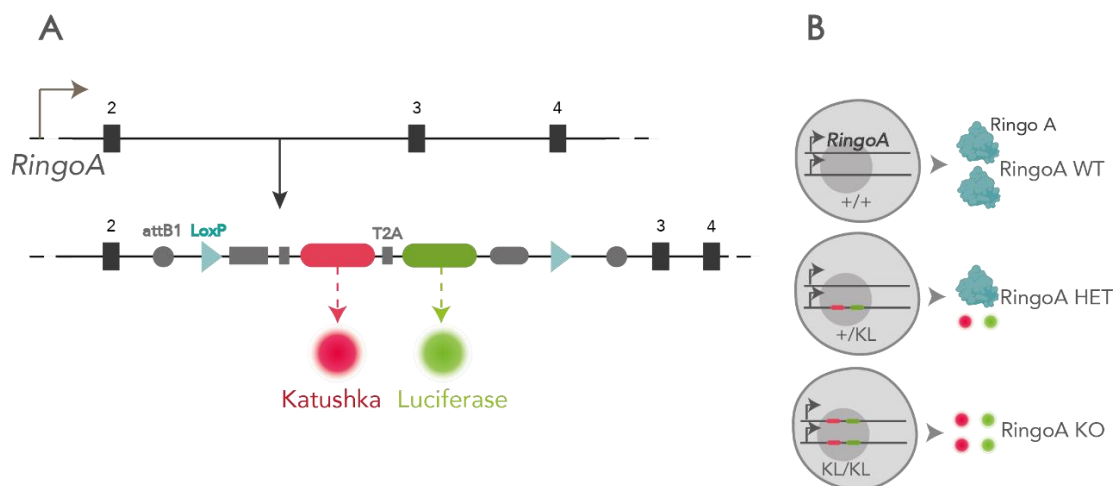


Figure R14. Schematic representation of the Katushka-Luciferase (K/L) reporter. **A.** Scheme of the Katushka-luciferase reporter mouse. The K/L cassette was inserted between exons 2 and 3 (represented as black boxes). Simplification of the construct where the red box represents Katushka gene, green box represents luciferase gene. T2A is used as a transcription terminator. LoxP sites (blue) and Attb1 recombination sequences (gray circles) were used for the cloning and insertion of the reporter genes. **B.** Representation of the possible genotypes and phenotypes in K/L reporter model, considering that the RingoA gene is truncated upon K/L insertion. +/+ animals have normal expression of RingoA (WT) whereas +/KL and KL/KL animals are functionally as HET and KO animals for RingoA respectively.

Analysis of RingoA promoter activity using the Katushka reporter

In vivo

In order to test the expression of the reporter Katushka (Turbo FP635) *in vivo*, two approaches were used. First, the whole body was analyzed by using the IVIS- Spectrum CT equipment system, but no signal was detected. As this was probably due to the inability of the signal to be transmitted through the different tissues, the animal was dissected and the expression in the tissues was analyzed *ex vivo* using a magnifying glass. In these conditions, a medium intensity signal was detected in testis of KI/+ animals compared with WT ones, and a very mild signal was detected in the (KI/+) brain compared to the WT brain (**Figure R15.A**). The other tissues did not show a consistent signal of the Katushka reporter *ex vivo*. To better analyze the reporter expression at the cellular level, tissues were fixed and analyzed by confocal microscopy. As a positive control, we first used testes, given its very high expression and that Katushka reporter was previously seen in this tissue *ex vivo*. However, no signal of the reporter was detected in testis analyzed at 588/635 nm excitation/emission (data not shown).

Results

Flow cytometry

We hypothesized that the expression of the Katushka reporter might not have been seen by confocal microscopy because of the fixation or freezing conditions used. With the aim of optimizing the use of the reporter at the cellular level, flow cytometry FACS analysis was attempted. Testes from WT mice, heterozygous for the reporter knock-in (+/KL) and homozygous for the reporter (KL/KL), were analyzed by FACS (**figure R15.B**). Using this technique, a cell population was found positive for Katushka expression in heterozygous compared to WT mice. Owing to the fact that the animals (KL/KL) are, from a functional point of view, like RingoA KO mice, we studied the effects of the RingoA depletion by FACS. Interestingly, the cell population that was positive for Katushka expression in the HET animals was absent in the KL/KL mice, consistent with the idea that RingoA KO cells are unable to undergo meiosis and finally die. The DNA content of the cells in testis was also analyzed (**Figure R15.B bottom**). In normal adult testis, we first found a big peak at 50K (formed of two peaks) corresponding to elongated spermatid and round spermatids, which are haploid (1C). Second, a smaller peak corresponding to spermatogonia and secondary spermatocytes, which are diploid (2C), was observed. Finally, we found a peak corresponding to primary spermatocytes, which were tetraploid (4C). However, in RingoA KO animals (KL/KL), the 1C peak was dramatically reduced and the 2C and 4C peaks were increased. Altogether, the RingoA KO mice showed a dramatic decrease of the cell population in which the RingoA promoter was expressed (1C) and a parallel increase of the cell populations with DNA content 2C and 4C. Brain cells of adult mice were also analyzed by FACS but in this case no cells were detected as positive for Katushka expression (**Figure R15.C**).

Analysis of RingoA promoter activity using the Luciferase reporter

The K/L reporter also allowed the expression of luciferase, which can be detected by its ability to metabolize luciferin resulting in the emission of light that marks cells where the RingoA promoter and the reporter are expressed.

After the injection of luciferin, animals were sacrificed and the signal of various tissues was compared. The highest luciferase activity was detected in testis, followed at a much lower level by lung, brain and intestine (**figure 16.A**).

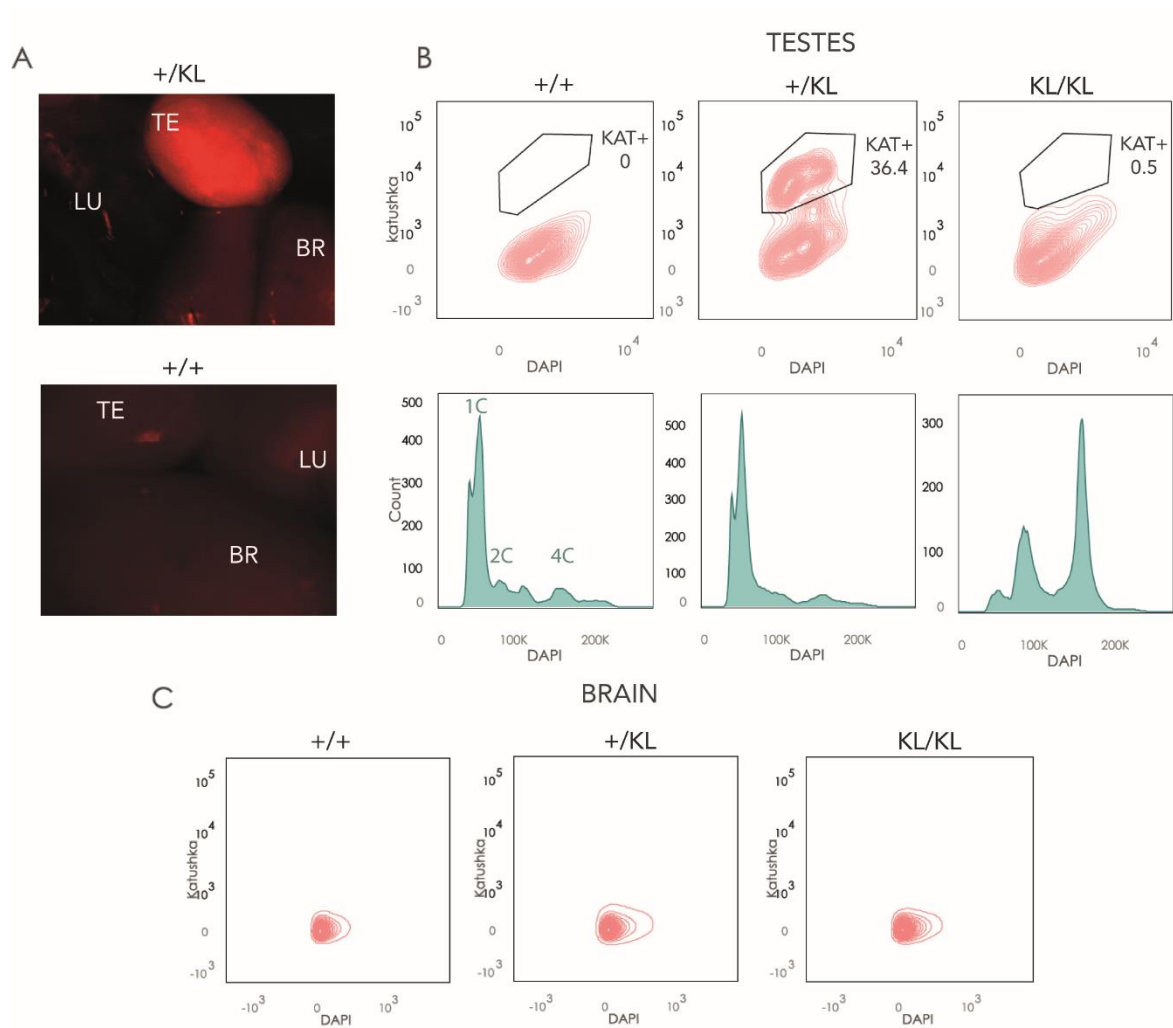


Figure R15. Katushka expression under control of the RingoA promoter. **A.** Representative images of testis (TE), lung (LU) and brain (BR) from (KL/+) and (+/+) mice were acquired with a magnifying glass. $n=2$ animals per genotype. **B.** Flow cytometry analysis of cells from testis of animals with the K/L reporter. WT animals (+/+) were used as a negative control. The upper figure shows Katushka expression with positive cells gated. The lower figure shows the relative amount (counts) of different cell populations with the indicated DNA content, as determined by DAPI staining. Graphs are representative of $n=2$ animals per genotype. **C.** Flow cytometry analysis of cells from adult brains of animals with the K/L reporter. Age: 2 months. $n = 2$ animals per genotype.

The luciferase reporter was also used to test the expression of RingoA during embryo development. Taking into account the potential expression of the RingoA promoter in developing reproductive tissues, the sex of the animals is indicated. The signal was found, both in males and females mainly in the upper body probably corresponding to the brain (Figure R16.B).

Results

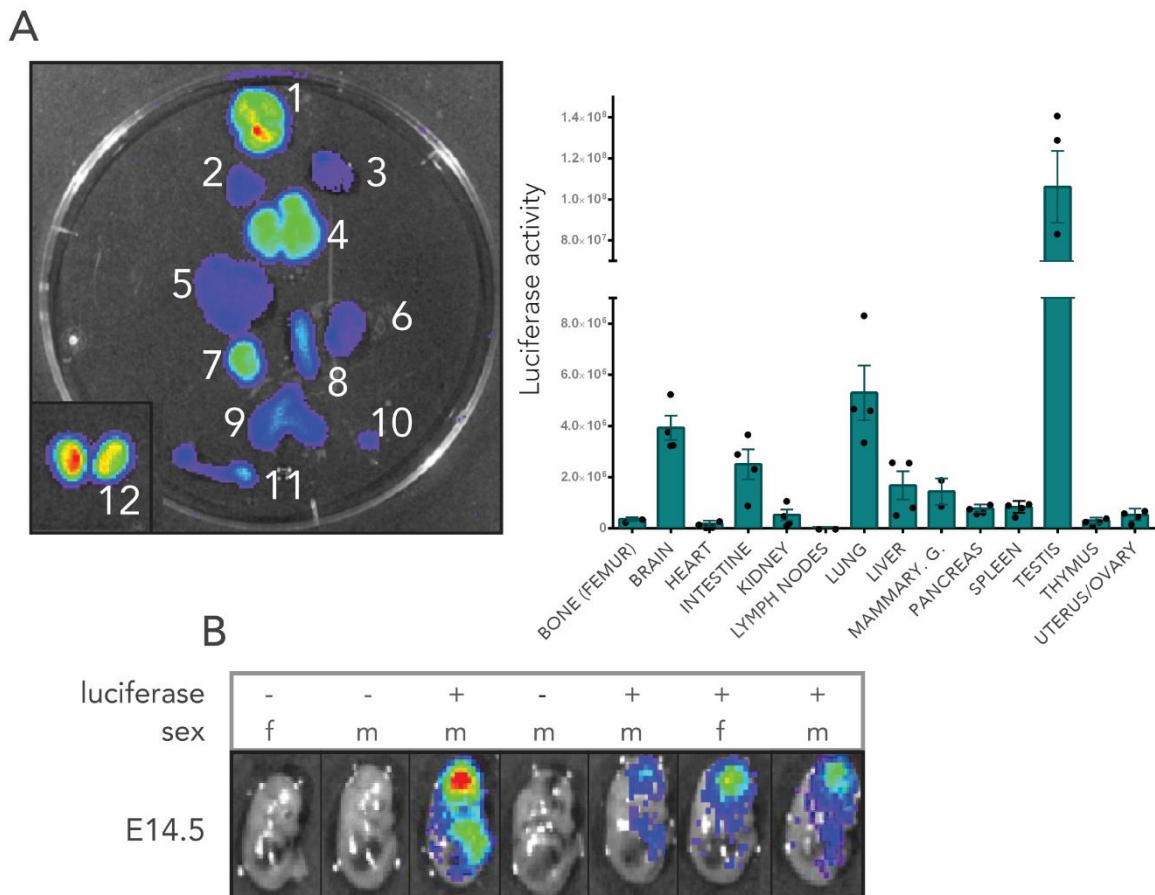


Figure R16. Luciferase expression under control of the RingoA promoter. A. IVIS image showing luciferase activity of different organs *ex vivo* from a representative (KL/+) animal that was injected with luciferin. Tissue numbers correspond to 1. Brain, 2. Thymus, 3. Heart, 4. Lung, 5. Liver, 6. Kidney, 7. Intestine, 8. Spleen, 9. Pancreas, 10. Lymph node, 11. Bone, 12. Testes. Light intensities are represented in chart. The expressions of the different animals are represented as dots, the bars indicate average and SEM. $n=4$ except testis ($n=3$) and mammary gland ($n=2$). **B.** IVIS image showing luciferase activity of different littermate embryos. Sex and genotype are indicated: m (male), f (female). The pregnant female was injected with luciferin before sacrifice.

Altogether, the luciferase reporter showed the highest expression of the RingoA promoter in adult mouse testis, coinciding with the process of gametogenesis. Remarkably, the reporter was extensively expressed in the upper body of the embryo concomitant with brain expression. Moreover, in adult mice, the brain was among the tissues showing more luciferase activity. This observation is also consistent with the RT-qPCR results, which indicated that RingoA expression in the brain was the highest among somatic tissues.

SECTION 3 - The role of RINGO proteins in the brain

The RingoA promoter is expressed in both the embryo and adult brain, as shown above (Figure R15). Following testis, the brain is the somatic tissue where RingoA mRNA is mostly expressed.

Considering the potential involvement of RingoA in the cell cycle, mainly supported by its ability to bind to and activate CDK1 and CDK2, we wondered whether RingoA has a role in the proliferative sub-populations of the brain, progenitor and stem cells.

Of interest, CDK2 has been reported to be important for the proliferation of brain stem cells in the subventricular zone (SVZ) (Jablonska et al. 2007). The study show a decrease in the self-renewal capacity of neurospheres derived from SVZ, and also a decrease in the number of progenitor cells. Interestingly, upon CDK2 KO in embryos, proliferation in the embryonic brain is normal due to functional redundancy with CDK4.

Given that CDK2 can be activated by RingoA and that CDK2 is important in stem and progenitor cells of the adult SVZ cells, we examined the potential role of RingoA in this niche of the adult brain.

RingoA mRNA is expressed in neural stem cells and proliferating progenitor cells

Llorens-Bobadilla and collaborators performed single-cell transcriptomics of NSCs isolated from their *in vivo* niche followed by hierarchical clustering, allowing the identification of a cluster named active NSCs (aNSCs) based on the expression of Egfr as well as cell cycle genes such as Ki67 and Mcm2. The aNSCs cluster comprised modules functionally related to the

Results

cell cycle (such as Cdk2) or protein synthesis (including Rpl family). Based on a module containing mitosis-associated genes (such as Aurkb), this cluster was finally separated in two groups: non-mitotic-aNCS1 and mitotic-aNCS2 (Llorens-Bobadilla et al. 2015).

From this publicly available data, we obtained information about the expression of RingoA in the different cell populations. Interestingly, RingoA expression was found mainly in cycling cells, both mitotic-active-NSC (aNCS2) and transit amplifying progenitors (TAPs) (**Figure R17**), thereby supporting a potential role of RingoA in cycling neuronal cells. In contrast, RingoB mRNA expression was not detected in any of the groups.

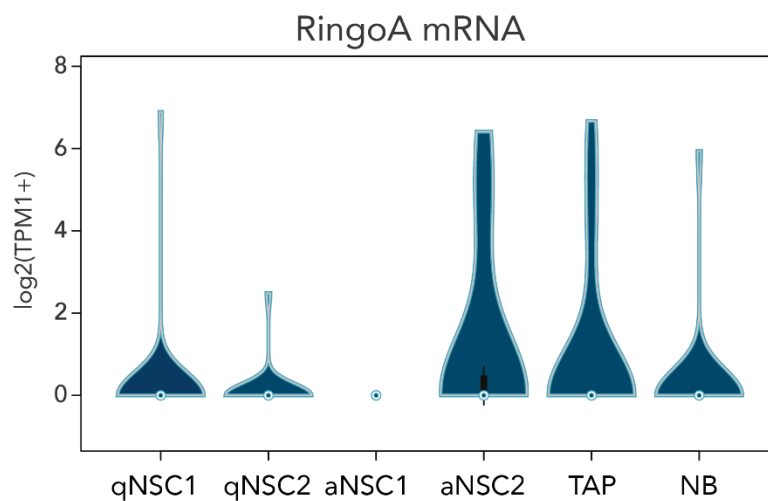


Figure R17. RingoA is expressed in actively dividing NSC. Violin plot showing the expression of RingoA mRNA in different clusters of NSC and progenitor populations from the SVZ. The populations evaluated are dormant-quiescent NSC (qNSC1), primed-quiescent NSC (qNSC2), non-mitotic active NSC (aNCS1), mitotic-active NSC (aNCS2), transit-amplifying progenitors (TAP), Neuroblasts (NB). Data obtained from (Llorens-Bobadilla et al. 2015).

Neuronal progenitors can be extracted and grown *in vitro* as neurospheres. Over the years, the formation of neurospheres has been used to determine whether a neuronal cell has stem-like properties. The evaluation of the number of growing neurospheres allows comparison of the stem cells from different regions, conditions or ages, and the diameter of a neurosphere can also indicate the mitogenic potency (Singec et al. 2006). Moreover, neurospheres can be desegregated, cultured in adherent conditions and induced to differentiate, resulting in the loss of their proliferation capacity (**Figure R18.A**). In order to validate the observations from single-cell sequencing data, we evaluated the expression of RingoA mRNA in proliferating NSCs grown *in vitro*. Cells were extracted from the SVZ of mice,

and RingoA mRNA expression was tested both in proliferating neurospheres and in differentiated cells. Interestingly, RingoA mRNA was detected in neurospheres, with cells proliferating, but this expression was lost in differentiated cells. Proliferation and differentiation markers were tested in parallel (**Figure R18.B**).

Altogether, the expression of RingoA mRNA in SVZ cells was restricted to proliferating cells. Therefore, we hypothesized that RingoA might have a role in neural cell proliferation.

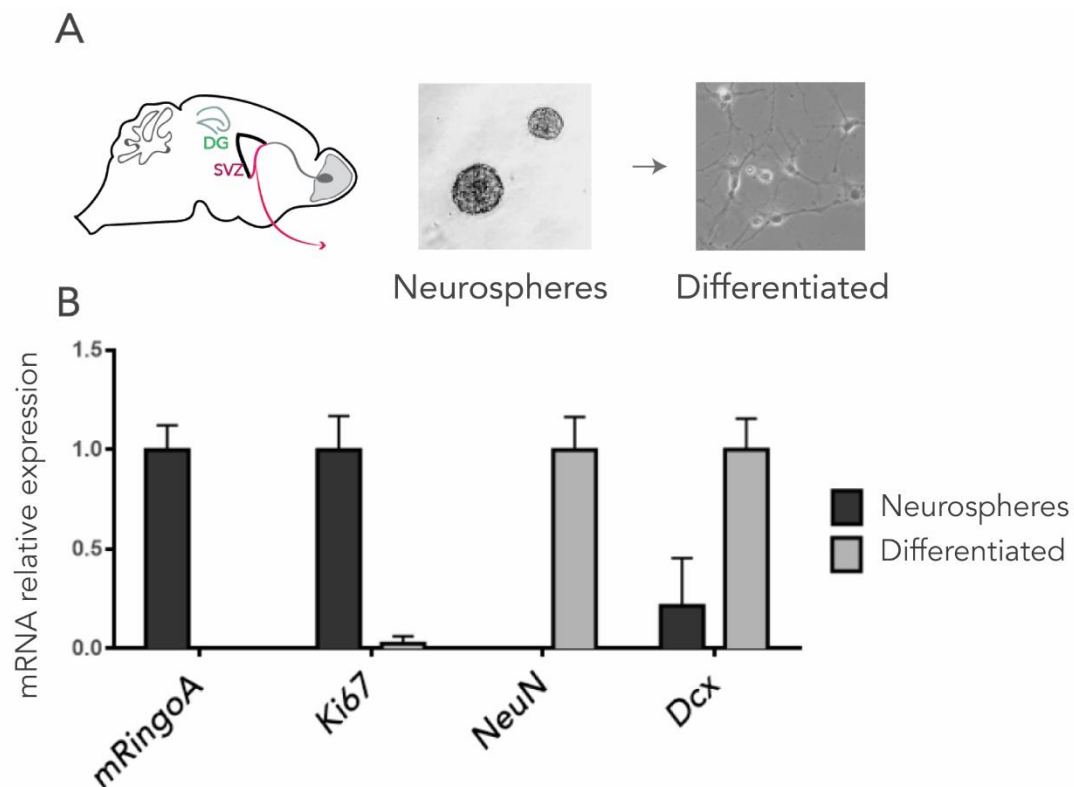


Figure R18. RingoA mRNA is expressed in proliferating NSCs but not in differentiated cells. A. Cells were dissected from the SVZ of male mice (3-month old), and were cultured as neurospheres (middle picture). Culturing neurospheres for 5 days in adherent conditions and in the absence of growth factors give rise to differentiated cells (right picture). **B.** mRNA levels of RingoA and of proliferation and differentiation markers in NSCs grown as proliferating neurospheres or in differentiated cells. All data are expressed as means with SEM, (n=2).

Results

Analysis of neural stem cells and progenitor self-renewal capacity in RingoA/RingoB KO

Impaired ability of RingoA/RingoB KO cells to form neurospheres

To understand whether RINGO expression was important for neural progenitor growth in culture, we took advantage of the RingoA/RingoB inducible KO system. Cells were extracted from the SVZ of RingoA^{lox/lox}, Ringo B^{lox/lox}, UBC-Cre ERT2^{+TG} mice and were either treated with 4-OHT, to induce RingoA and RingoB depletion, or left untreated as WT control, and then were grown as neurospheres. We found that RingoA and RingoB deleted neurospheres were consistently reduced in number and size when compared with WT cells (**Figure R19.A**). As a control, cells were also extracted from the SVZ of UBC-Cre ERT2^{+TG} mice with WT RingoA and Ringo B alleles. In this case no significant differences were observed in the number or size of neurospheres with or without 4-OH-Tamoxifen treatment (**Figure R19.B**).

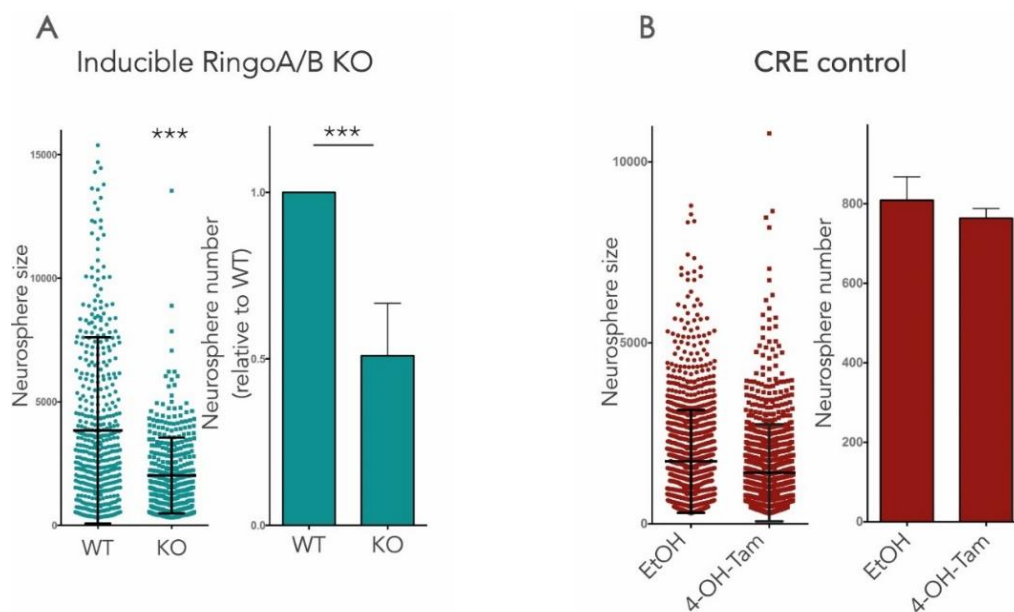


Figure R19. Reduction of neurosphere number and size upon RingoA and RingoB deletion. **A.** Cells from the SVZ of RingoA^{lox/lox}, Ringo B^{lox/lox}, UBC-Cre ERT2^{+TG} mice were disaggregated and were left untreated (WT) or were treated with 4-OH-T (KO) for 2 days to induce *RingoA* and *RingoB* gene deletion. Single cells were seeded in order to form neurospheres. After 7 days, pictures were taken and the size and number of neurospheres were quantified. **B.** The same procedure was performed using RingoA^{+/+} Ringo B^{+/+} UBC-Cre ERT2^{+TG} mice, as a control for Cre expression. Data are expressed as means with SEM and are representative of n=3 experiments from three different animals for inducible KO and n=2 experiments from one animal in UBC-Cre CT. Asterisks denote statistical significance (***)= p-value <0.001.)

To understand why the RingoA and RingoB deleted neurospheres were smaller, several experiments were performed. First, no differences were detected in cell proliferation evaluated by measuring 5-Bromo-2'-deoxyuridine (BrdU) incorporation by FACS (**Figure R20.A**). Moreover, neither were differences found in cell cycle phases or in the mitotic index, as determined by FACS using PI and Histone H3 phosphorylated at serine 10 (PS10-H3) staining, respectively (**Figure R20.B,C**). As an alternative method to assess cell proliferation, we used the fluorescent cell tracer CFSE, whose intensity per cell is diluted proportionally to the number of cell divisions. WT and RingoA/RingoB KO cells were stained with CFSE and their proliferation was followed over several days by FACS, however, no differences were observed (**Figure R20.D**). Finally, cell death was also analyzed by Annexin V staining, but no differences were detected between WT and KO cells (**Figure R.20.E**).

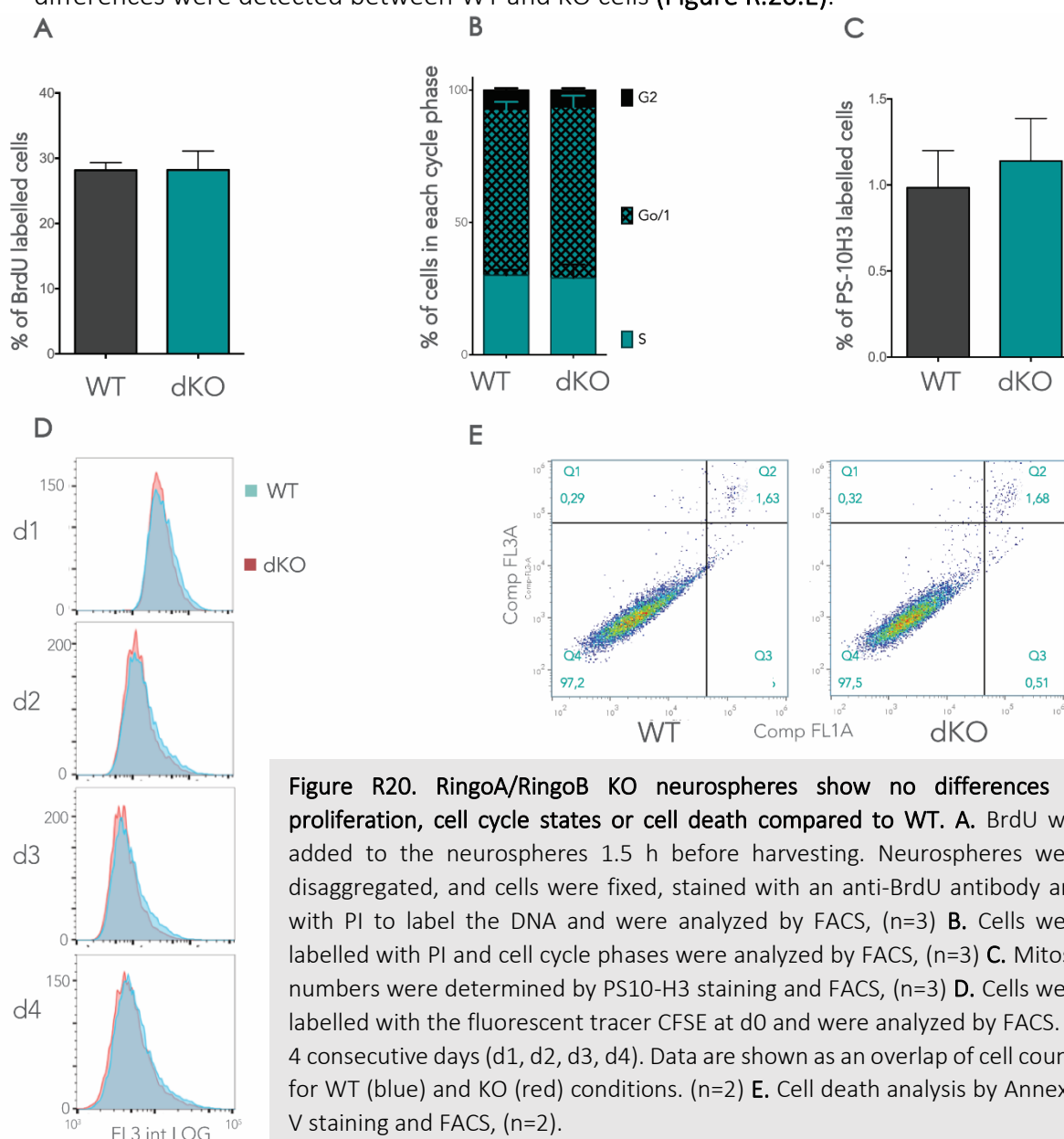


Figure R20. RingoA/RingoB KO neurospheres show no differences in proliferation, cell cycle states or cell death compared to WT. A. BrdU was added to the neurospheres 1.5 h before harvesting. Neurospheres were disaggregated, and cells were fixed, stained with an anti-BrdU antibody and with PI to label the DNA and were analyzed by FACS, (n=3) **B.** Cells were labelled with PI and cell cycle phases were analyzed by FACS, (n=3) **C.** Mitosis numbers were determined by PS10-H3 staining and FACS, (n=3) **D.** Cells were labelled with the fluorescent tracer CFSE at d0 and were analyzed by FACS. at 4 consecutive days (d1, d2, d3, d4). Data are shown as an overlap of cell counts for WT (blue) and KO (red) conditions. (n=2) **E.** Cell death analysis by Annexin V staining and FACS, (n=2).

Results

We next evaluated the expression of stemness and differentiation markers of NSC and neural progenitors in culture. We used RT-qPCR to study the expression of the following stemness markers in NSCs and progenitor cells: Sox2, Nestin, Bmi1 and GFAP (Bernal et al. 2015). Neurospheres were generated from neuronal cells previously treated with EtOH or 4-OHT to induce RingoA and RingoB downregulation. After 7 days, neurosphere cells were harvested, and mRNA was analyzed. No significant differences between WT and RingoA/RingoB KO neurospheres were observed in the genes tested (**Figure R21.A**).

As detailed in the introduction (Figure I12), progenitors from the SVZ undergo different steps of proliferation, differentiation and migration. Neuroblasts start expressing Dcx, and NeuN is expressed in the final stages of neural differentiation (Gusel'nikova and Korzhevskiy 2015; Walker et al. 2007). To study potential changes in the differentiation of neuronal progenitors, we analyzed these markers. mRNA was extracted from proliferating neurospheres and from differentiated cells and assessed by RT-qPCR. Interestingly, Dcx was found to be significantly downregulated in proliferating RingoA/RingoB KO cells compared with proliferating WT cells. However, the differences between WT and RingoA/RingoB KO were not conserved in differentiated cells. NeuN is a marker of neuronal differentiation and, as expected, was not detected in neurospheres but was up-regulated in differentiated cells. The expression of NeuN was significantly reduced in RingoA/RingoB KO differentiated cells compared with differentiated WT cells (**Figure R21.B**), suggesting a potential role for RingoA and RingoB in neural differentiation.

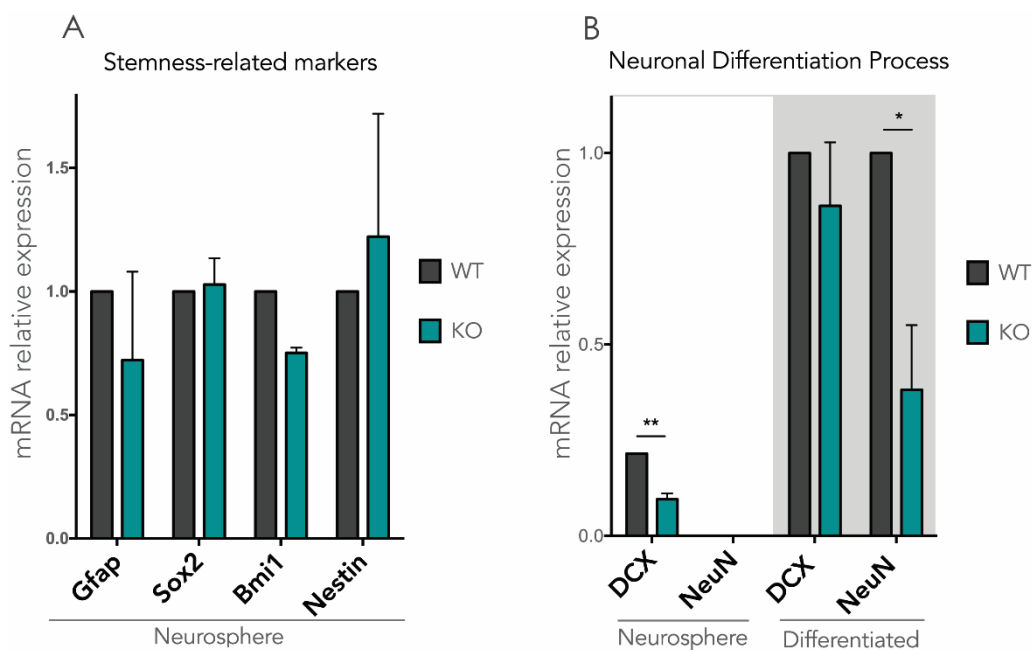


Figure R21. RingoA/RingoB downregulation affects the expression of neural differentiation markers. RT-qPCR analysis of mRNAs related with stemness (A) or neural differentiation (B). GAPDH was used as a reference. Values are shown relative to the WT condition, which was given the value of 1, (n=3 animals). Asterisks denote statistical significance (* = p-value <0.05, ** = p-value <0.01).

In summary, the downregulation of RingoA and RingoB in proliferative brain cells from adult mice decreased self-renewal capacity, generating fewer and smaller neurospheres. However, this was not reflected in a reduction in cell proliferation, cell cycle progression or increased cell death, at least under the experimental conditions tested. In addition, the analysis of neuronal lineage markers pointed to potential changes in neuronal lineage differentiation. Therefore, to further characterize the observations in primary cultures, we decided to study the NSCs and progenitors *in vivo*.

Brains of RingoA/RingoB KO mice show normal histology and unaltered proliferation and mitotic index in the SVZ

To determine whether RingoA/RingoB KO brains were normal, we first analyzed the brain and cortex size in coronal sections stained with Nissl. Brains had apparent normal histology, cellular density, cortex thickness and hemisphere size (**Figure R22.A,B**).

Finally, for the purpose of examining the proliferation capacity of neural progenitors and NSCs, the SVZ of 3 months-old mice was studied in basal conditions. In order to have a representative analysis, slices were obtained from the anterior, medial and posterior SVZ (**Figure R22.C**). Slides were labeled with antibodies against Ki67 to detect proliferation and against pS10- histone H3 as a mitotic marker. Nevertheless, we found no significant differences in cell proliferation (**Figure R22.D**) or in number of mitoses (**Figure R22.E**).

Results

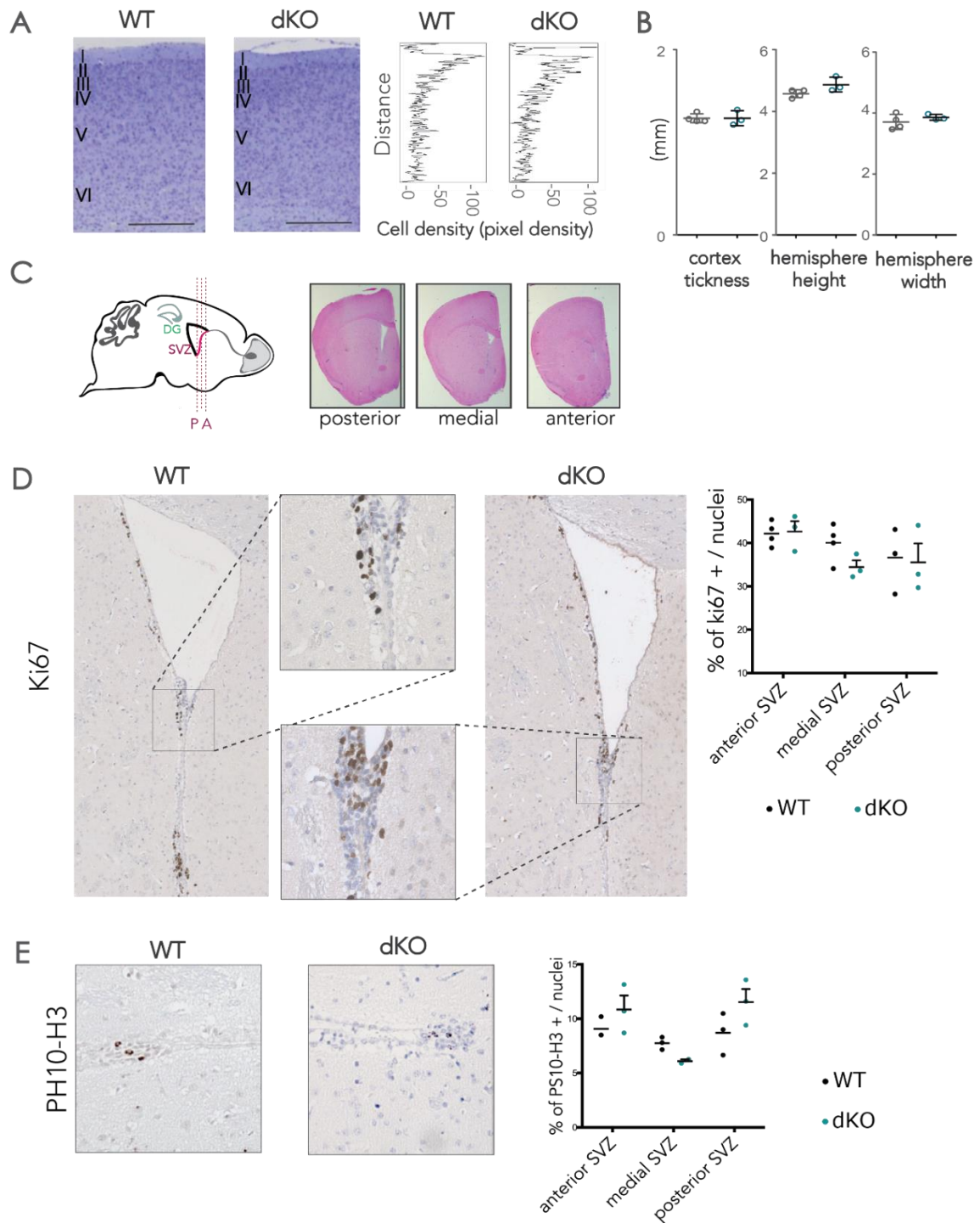


Figure R22. RingoA/RingoB KO brains have normal histology and cell proliferation in the SVZ. **A** Representative picture of Nissl staining with indicated cortex layers and quantification of cellular density of the cortex. **B.** Graph showing cortex and coronal brain hemisphere size of WT and KO mice. Cortex measures were taken from primary motor cortex (M1); approximately 0.98mm anterior to bregma. **C.** Scheme representing the SVZ regions taken for histological analysis of coronal sections. **D,E.** representative pictures and quantification of slides of WT and KO brains stained with Ki67 to detect cell proliferation (**D**), and PS10-H3 to detect mitosis (**E**). Graphs show the quantification of the stained cells/nuclei. Data are represented as average plus SEM. Each dot represents a different animal, $n \geq 3$ per group. Statistical analysis did not show significant differences between conditions.

SECTION 4- The role of RINGO proteins in breast cancer

RingoA is expressed in PyMT-induced mammary tumors

RingoA/RingoB were not found essential for the development of most mice tissues in homeostasis. However, tumor cells might have specific cell cycle requirements that differ from their cell of origin (Malumbres and Barbacid 2009). It has been proposed that RingoA is involved in different types of cancer, such as glioblastoma and breast cancer (Golipour et al. 2008; Lubanska et al. 2014; Al Sorkhy et al. 2012). However, the relevance of RingoA for *in vivo* tumor growth has not been studied. Therefore, we aimed to test the importance of this protein in tumor development using mammary tumor mouse models.

In order to assess RingoA expression in mammary tumors, the RingoA K/L reporter was used in combination with the MMTV-PyMT model of mammary tumorigenesis. In this model, the PyMT (middle T antigen of polyomavirus) is expressed in the mammary gland under the control of MMTV promoter, which results in the transformation of mammary epithelial cells (Guy et al. 1992).

Animals expressing MMTV-PyMT and the RingoA K/L reporter were generated by breeding and animals of three groups were analyzed. The first group was formed by females Luciferase TG/+, PyMT TG/+, which developed tumors and had the reporter. This group was compared with animals Luciferase +/+, PyMT TG/+, which developed tumors but did not have the reporter, and with animals Luciferase TG/+, PyMT +/+, which had the reporter but did not generate tumors. Luciferase expression was monitored weekly for 12 weeks using IVIS - Spectrum CT equipment. As shown in **Figure R23**, the expression of the luciferase

Results

reporter was found significantly increased in animals that developed mammary tumors (Luciferase TG/+, PyMT TG/+) compared to the control groups.

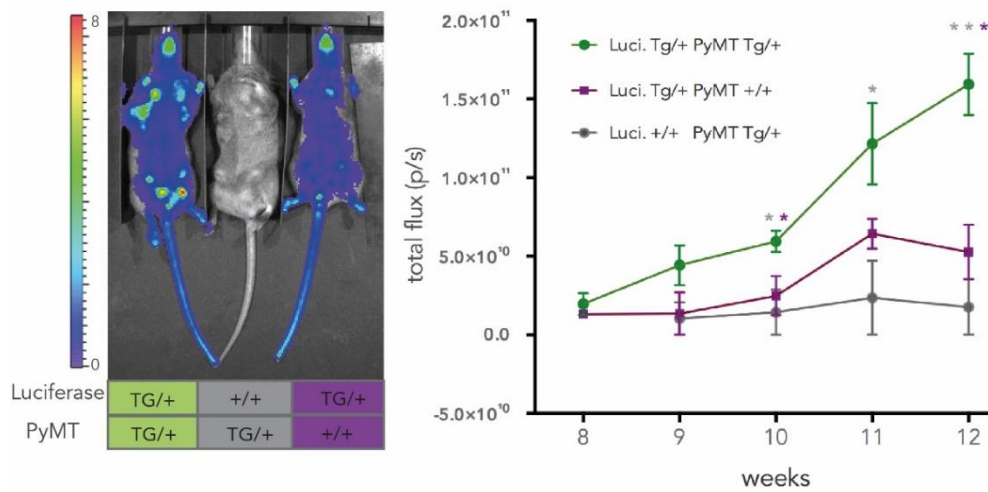


Figure R23. RingoA gene promoter is expressed in mammary tumors. Representative examples of animals of the three groups analyzed by IVIS equipment after D-luciferin retro-orbital injection. The graph shows the luciferase expression in the different groups at the time indicated. The dots indicate average expression plus SEM, ($n \geq 3$ per group). (* = p-value < 0.05 , ** = p-value < 0.01). The star colors denote comparison of the Luciferase TG/+ PyMT TG/+ mice with Luciferase TG/+ PyMT +/+ (purple) or with Luciferase +/+ PyMT TG/+ (gray) animals.

RingoA and RingoB are required for mammary tumor growth

To study the importance of RingoA and RingoB in mammary tumor progression *in vivo*, the MMTV-PyMT transgene was combined with floxed conditional alleles of *RingoA* and *RingoB*, and with inducible UBC-CreERT2. In these mice, RingoA and RingoB can be deleted at any time of the tumor development by 4-OHT administration. Initially, animals with floxed *RingoA* and *RingoB* genes and inducible Cre were compared with animals with floxed *RingoA* and *RingoB* without Cre as a control. Mammary tumors were allowed to grow until a size of 150-200 mm³, and then animals of both groups were treated with 4-OHT to induce Cre activation and RingoA/RingoB deletion. Tumors were measured during a 15-day period and then sacrificed (**Figure R24.A**). Tumor growth was found to be decreased upon RingoA/RingoB deletion compared to the control animals (**Figure R24.B**).

Moreover, to exclude a potential effect of the Cre recombinase, animals with WT *RingoA* and *RingoB* and inducible Cre (Cre+) were compared to animals with WT *RingoA* and *RingoB* but without Cre (Cre-). The analysis of both mice groups after treatment with 4-OHT showed that Cre recombinase activation alone did not affect mammary tumor growth. This observation therefore supports the notion that the effects observed upon inducible downregulation of *RingoA* and *RingoB* were specific (Figure R24.C).

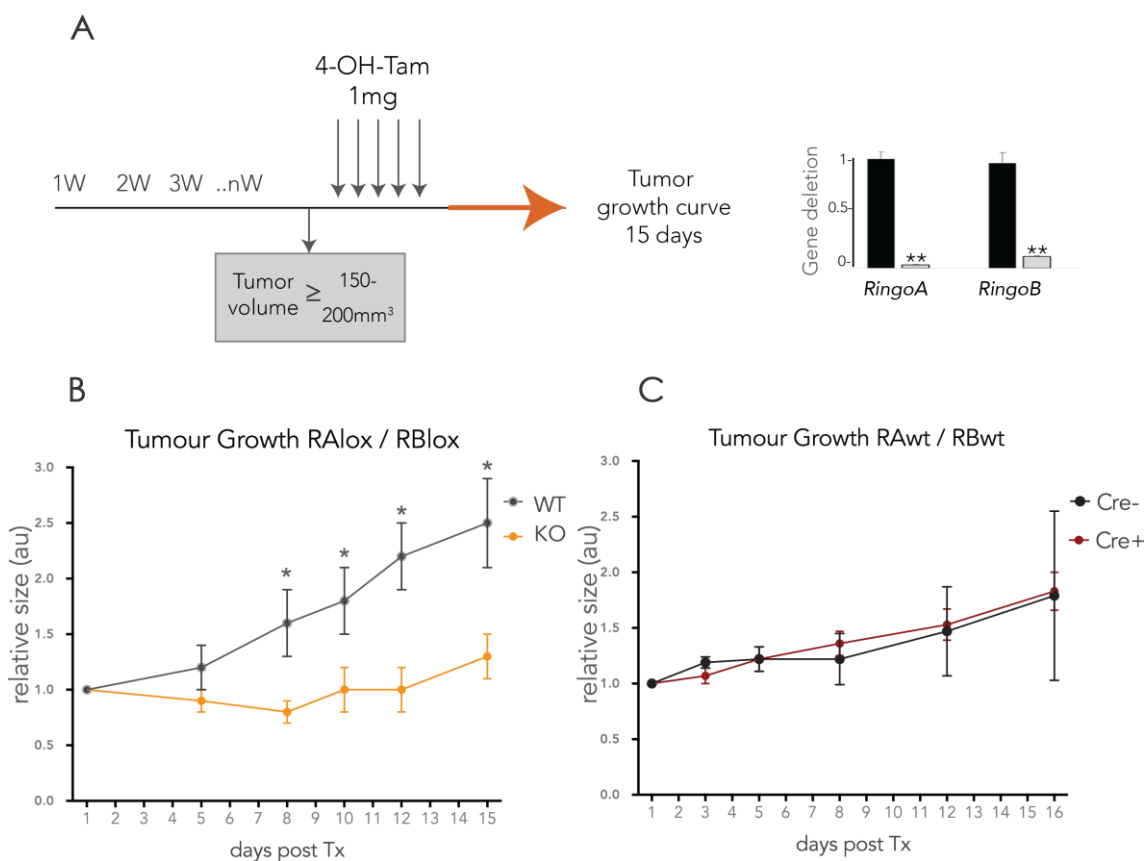


Figure R24. Mammary tumor growth decreases upon *RingoA*/*RingoB* downregulation. A. Scheme of the experimental design. When mammary tumors reached a size of 150-200 mm³, mice were injected with 1 mg of 4-OHT each day for 5 consecutive days and tumor growth was followed for 15 days. Histograms show the *RingoA* and *RingoB* deletion at day 15 in mice treated with 4-OHT. **B.** Tumor growth in mice *RingoA*^{lox/lox}, *RingoB*^{lox/lox}, *UBC-CreERT2*^{TG/+} (KO) compared to mice *RingoA*^{lox/lox}, *RingoB*^{lox/lox}, *UBC-CreERT2*^{+/+} (WT), both treated with 4-OHT. **C.** Tumor growth in mice *RingoA*^{+/+}, *RingoB*^{+/+}, *CreERT2*^{TG/+} (Cre+) compared to *RingoA*^{+/+}, *RingoB*^{+/+}, *CreERT2*^{+/+} (Cre-) both treated with 4-OHT. Measurements were normalized to the initial tumor size. The dots indicate average expression plus SEM, (n \geq 7). (* = p-value <0.05).

Results

Role of RingoA and RingoB in immortalized cancer cell lines derived from mammary tumors

With the aim to examine the underlying molecular mechanisms behind tumor reduction, epithelial cancer cell cultures were derived from mammary tumors.

We generated an immortalized cell line with *RingoA*^{lox/lox}, *RingoB*^{lox/lox} and *UBC-CreERT2*^{TG/+}, which allowed to delete *RingoA* and *RingoB* upon the addition of 4-OHT *ex vivo*. To exclude potential non-specific effects, two additional control cell lines were generated. One with *RingoA*^{lox/lox}, *RingoB*^{lox/lox} but without Cre to test the effects of 4OHT, and another one with WT *RingoA* and *RingoB* (*RingoA*^{+/+}, *RingoB*^{+/+}) and inducible Cre (*UBC-CreERT2*^{TG/+}) to test the potential off-target effects of Cre activation. All the cell lines were tested for expression of the EpCAM marker by FACS, and more than 95% of the cells were found positive for the epithelial marker (**Figure R25**).

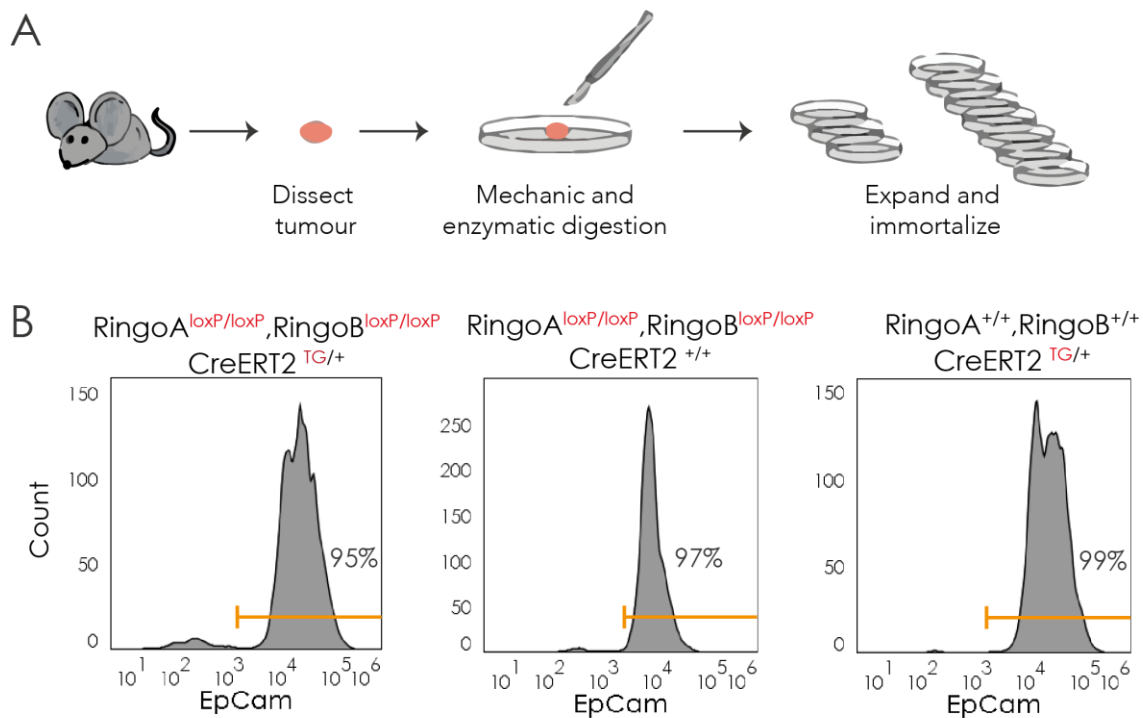


Figure R25. Generation of epithelial cell lines derived from PyMT mammary tumors. **A.** Schematic representation of the process of cancer cell isolation and immortalization. Tumors were dissected, digested and expanded until spontaneous immortalization. **B.** FACS profiles obtained by staining the cells with antibodies against the EpCAM epithelial marker. Genotypes are indicated on top of each panel.

Effect of RingoA and RingoB downregulation in mammary cancer cells

Several experiments were performed to see the effects of RingoA/RingoB deletion in epithelial cells derived from mammary tumors. *RingoA*^{lox/lox}, *RingoB*^{lox/lox}, *UBC-CreERT2*^{TG/+} cells were treated with 100nM 4-OHT and split after two days; experiments were performed 3 days after split unless otherwise indicated.

To evaluate the proliferation ability of RingoA/RingoB KO cells, we performed colony assays and BrdU incorporation assays. In both cases, RingoA/RingoB deficient cells were found to show reduced proliferation compared to WT cells (**Figure R26**).

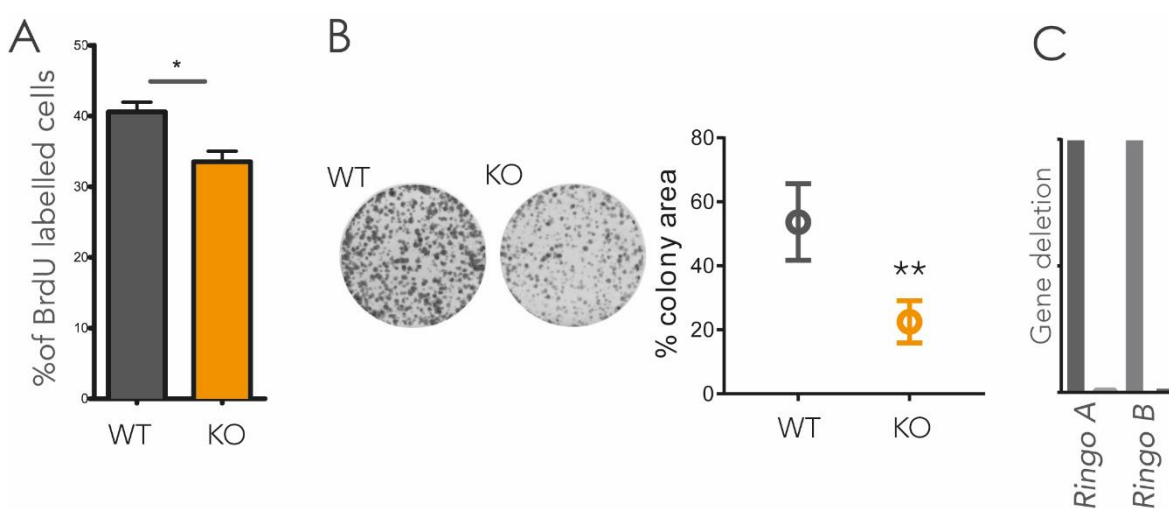


Figure R26. RingoA/RingoB double KO cells show reduced proliferation. Cells were treated with 100nM 4-OH-T for 48h and plated for experiment performing. **A** BrdU uptake in WT cells compared to KO cells. 3 days after split cells were treated with BrdU for 90 min, harvested and analyzed by FACS, (n=3). **B.** Colony assays using WT cells and KO cells. Left, representative picture of a clonogenic assay 10 days after seeding 2000 cells, (n=4). **C.** qPCR data showing *RingoA* and *RingoB* deletion in the immortalized mammary cancer cells treated with 4-OHT. (* = p-value <0.05, ** = p-value <0.01).

To study the nature of this reduction in proliferation, the cell cycle was analyzed by flow cytometry. A small but significant increase in G2 phase was found in RingoA/RingoB deficient cells (**Figure R27.A**). Time-lapse video analysis showed that binucleated cells and cells with micronuclei were more abundant in RingoA/RingoB KO cells (**Figure R27.B**), which correlated with a significantly reduced number of mitoses, as determined by Phospho-Ser10-H3 staining and flow cytometry analysis (**Figure R27.C**). Mitotic spreads were also performed,

Results

and the distances between chromatids were found to be significantly reduced in RingoA/RingoB KO cells (**Figure R27.D**). Finally, staining for γ H2AX revealed the presence of more DNA damage in RingoA/RingoB deficient cells compared with WT cells (**Figure R27.E**).

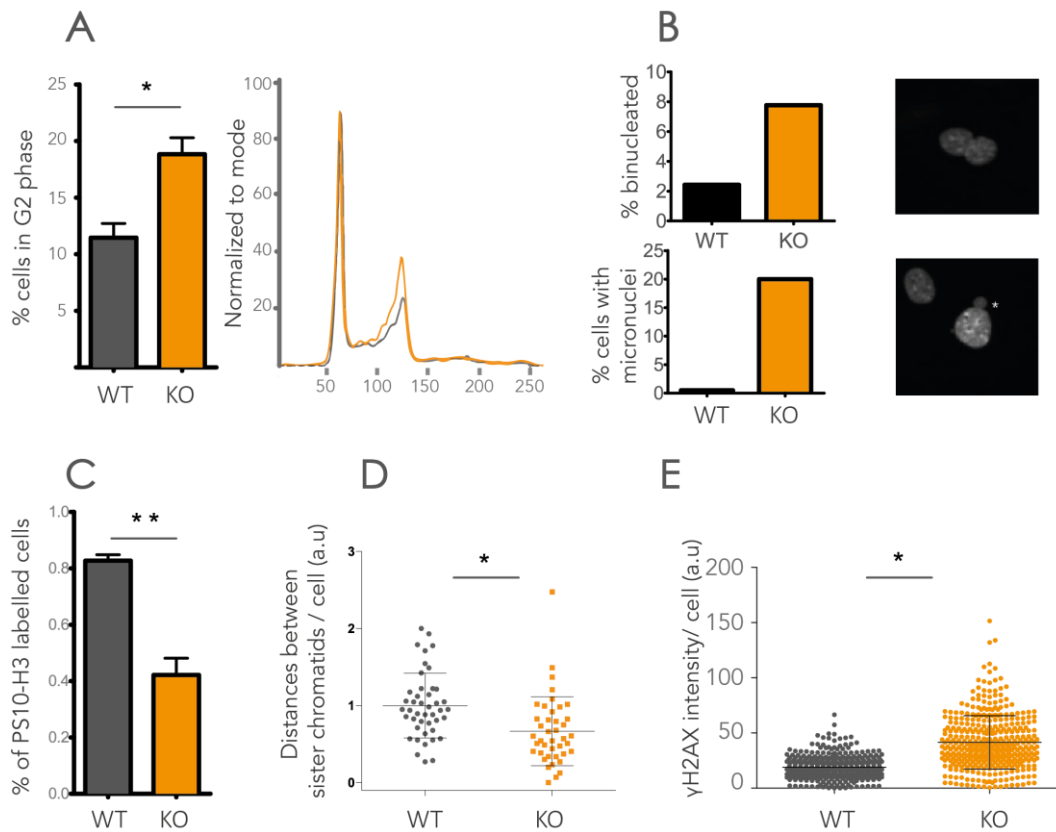


Figure R27. Analysis of the effects of RingoA and RingoB downregulation in mammary cancer cells. A. Cell cycle profiles in WT cells compared to KO cells, (n=3). **B.** Quantification of binucleated cells (upper graph) and cells with micronuclei (lower graph) in WT and KO cells from a 20 h time-lapse video. At least 250 cells were analyzed per condition **C.** FACS analysis of PS10-H3 stained WT and KO cells to evaluate the number of mitoses, (n=3). **D.** Quantification of the distance between chromatids in mitotic cells. Dots represents average distance per cell, (n=3). **E.** Quantification of the average intensity of γ H2AX foci per cell. Each dot indicates one cell. Data are represented as average with SEM, (n=3).

Effect of 4-OHT treatment and Cre activation in mammary cancer cells

As explained above, control cell lines were generated to exclude a potential effect of 4-OHT treatment or Cre activation. These cell lines were also treated with 4-OHT and used for experiments performed in the same conditions as described in the previous section to test the effect of RingoA/RingoB downregulation.

First, *RingoA*^{lox/lox}, *RingoB*^{lox/lox} *CreERT2*^{+/+} cells were used to test the effect of 4-OHT. We did not find any effect on BrdU incorporation, colony formation assays or cell cycle progression upon 4-OHT treatment (**Figure R28**). These results indicate that the doses of 4-OHT used do not affect mammary cancer cell proliferation.

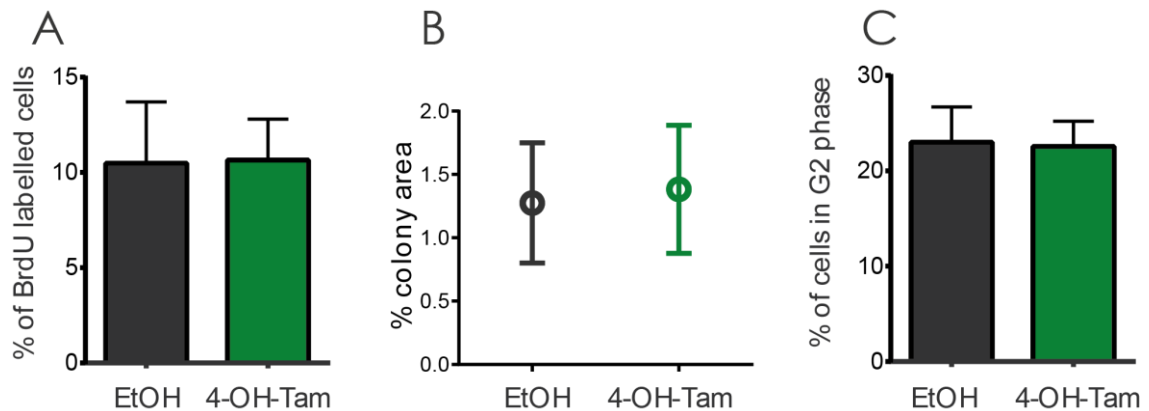
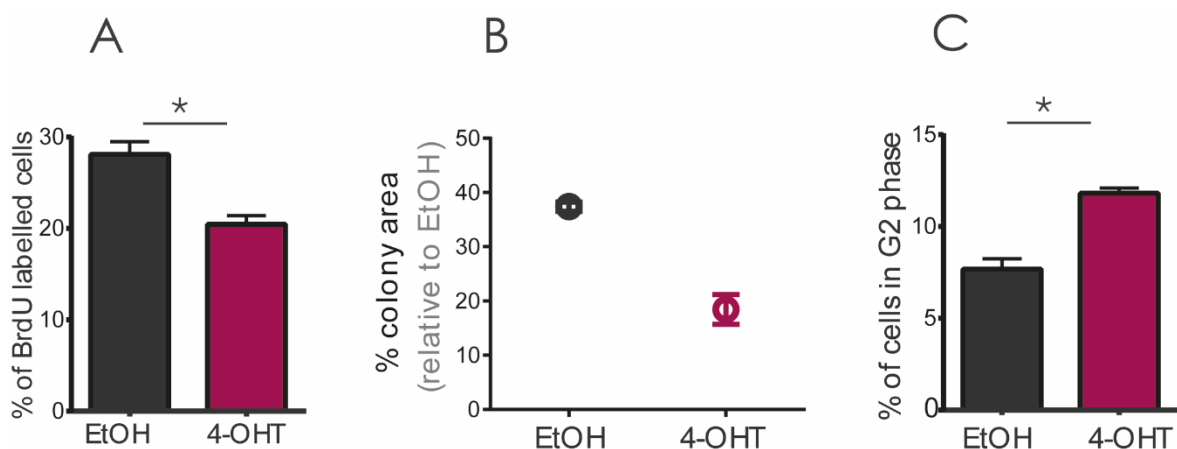


Figure R28. 100nM 4-OHT does not have an effect in mammary cancer cell proliferation. Cells were treated with 100nM 4-OH-T for 48h and plated for performing the experiments. **A.** BrdU uptake analyzed by FACS **B.** Quantification of colony assays 10 days after seeding 5000 cells **C.** Quantification of the percentage of cells in G2 phase analyzed by FACS. Data are representative of 2 independent experiments.

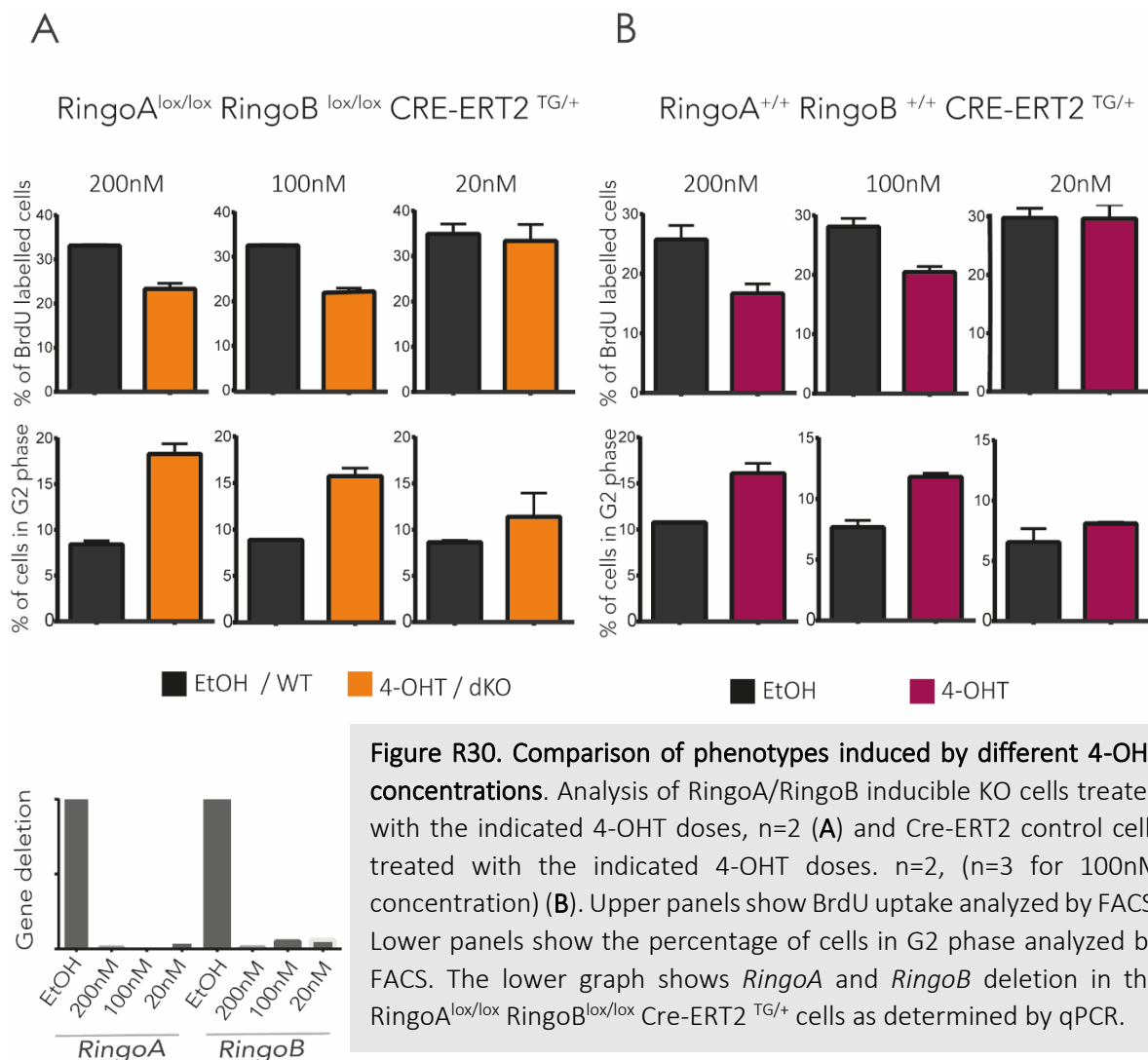
In addition, *RingoA*^{+/+}, *RingoB*^{+/+} *CreERT2*^{TG/+} cells were used in order to test the effect of Cre recombinase activation alone, in the absence of RingoA and RingoB downregulation. Surprisingly, the treatment of these cells with 4-OHT reduced both BrdU incorporation and colony formation efficiency, and also increased the percentage of cells in G2 phase to a similar extent as that observed in RingoA/RingoB KO cells (**Figure R29**). These results indicate that Cre induction suffices to impair the proliferation of immortalized mammary cancer cells.



Results

Figure R29. Activation of Cre recombinase impairs cell proliferation and cell cycle progression. Cells were treated with 100nM 4-OHT for 48h and plated for performing the experiments. **A.** BrdU uptake analyzed by FACS. **B.** Quantification of colony assays 10 days after seeding 5000 cells. **C.** Quantification of the percentage of cells in G2 phase analyzed by FACS. Data are representative of 3 independent experiments (*=p-value <0.05).

To find a concentration in which Cre recombinase was activated but produced no off-target effects, a range of concentrations of 4-OHT were tested. Cre-ERT2 activation as determined by the deletion of *RingoA* and *RingoB* was detected in all the conditions tested. However, at 20 nM 4-OHT, there was neither increased arrest in G2 phase nor reduced BrdU incorporation (**Figure R30**). Cre control cells showed similar effects in a dose dependent manner, thereby suggesting that the phenotypes observed are a consequence of the activation of Cre recombinase rather than depletion of *RingoA* and *RingoB*.



Histological characterization of RingoA/RingoB deficient mammary tumors

Our results indicated that RingoA and RingoB are required for the growth of PyMT-induced mammary tumors *in vivo*. Although we could not explain this effect by analyzing the immortalized cancer cell lines, we ruled out that differences in tumor growth observed *in vivo* were due to off-target effects of Cre expression. Therefore, we decided to evaluate the histological characteristics of the tumors. All the analyses correspond to tumors at 8 days after 4-OHT administration had started.

Cell proliferation and the number of mitotic cells were significantly decreased, as determined by Ki67 and PS10-H3 staining, whereas DNA damage was increased based on γ H2AX staining in RingoA/RingoB KO tumors. Moreover, in order to evaluate cell death TUNEL assay was performed and showed an increased number of dead cells in the KO tumors (**Figure R31.A**). Finally, the CKI p27^{Kip1} was also analyzed. RingoA/RingoB KO tumors had an increased number of positive cells. The intensity of the nuclear signal was quantified, showing a reduction of cells with lower intensity towards an increase of cells with higher p27^{Kip1} nuclear intensity in the RingoA/RingoB KO (**Figure R31.B**).

The differences found between the outcome of RingoA/RingoB depletion in tumors *in vivo* and in cancer cells *in vitro* raised the possibility that the interaction of tumor cells with the tumor microenvironment might contribute to the decreased tumoral growth observed. As a first approach to address this question, we analyzed immune cell infiltration in the tumors by immunohistochemistry. We found that F4/80 expressing macrophages and CD3 expressing lymphocytes were increased in the RingoA/RingoB KO tumors. (**Figure R31.C**).

Taken together, despite the absence of specific effects in mammary tumor immortalized cells upon RingoA/RingoB depletion, the knock-out of these proteins *in vivo* resulted in a reduction of tumoral growth. This growth reduction correlated with a reduced proportion of cycling tumor cells, as well as increased DNA damage and cell death. Moreover, tumors had enhanced immune cell infiltration which might also contribute to the reduction in tumor size.

Results

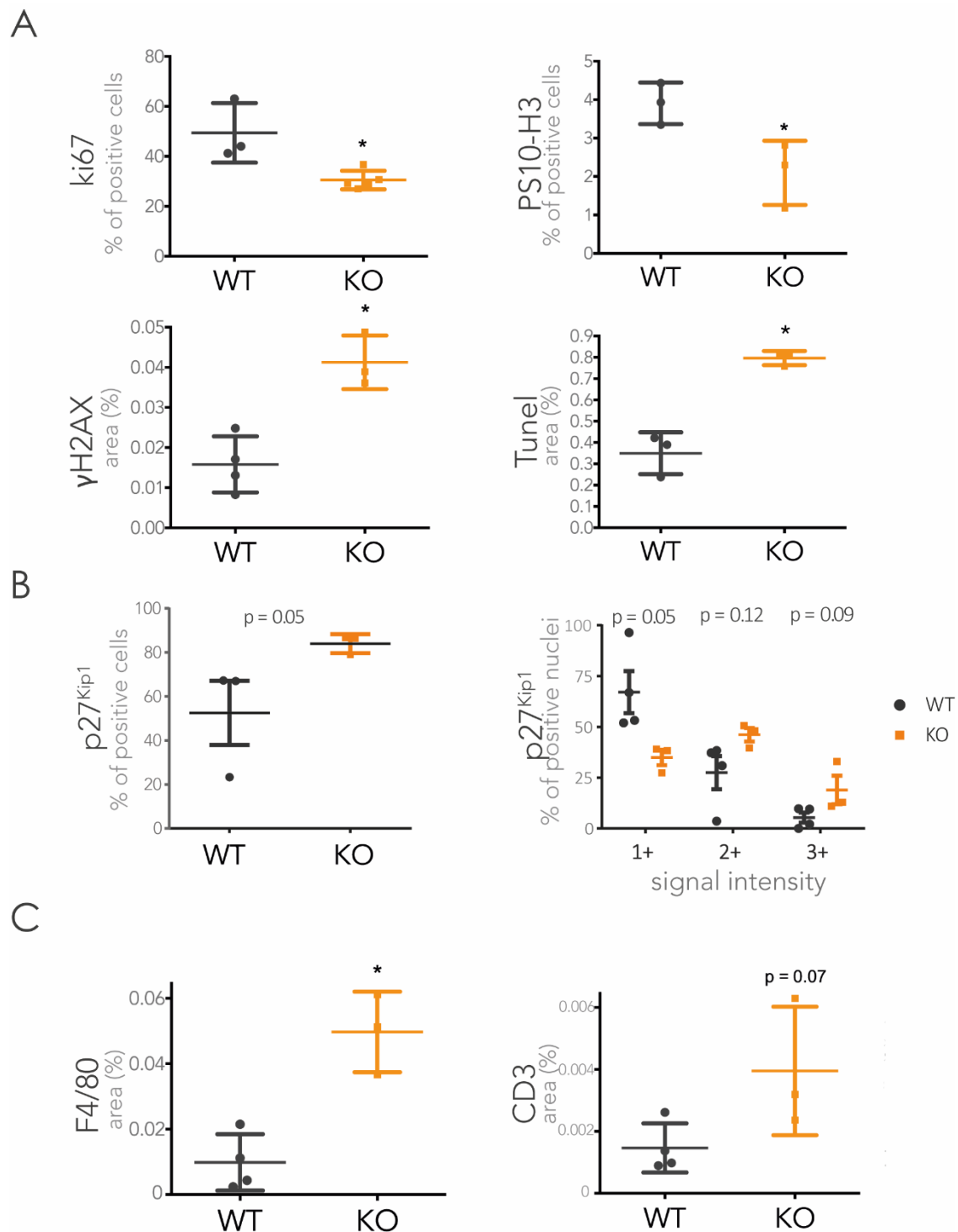


Figure R31. Histological analysis of RingoA and RingoB KO mammary tumors. RingoA^{lox/lox}, RingoB^{lox/lox} UBC-Cre-ERT2^{+TG} (KO) and RingoA^{lox/lox}, RingoB^{lox/lox} UBC-Cre-ERT2^{+/+} (WT) mice were injected with 4-OHT and 8 days later tumors were analyzed. **A.** Tumor sections were stained for Ki67 (cell proliferation), PS10-H3 (mitotic cells), γH2AX (DNA damage), TUNEL assay (cell death) **B.** Tumor sections were stained for p27^{Kip1} and the signal was quantified. The graph on the left shows the percentage of positive cells. The graph on the right shows the quantification of p27^{Kip1} signal classified according to the intensity per cell, from lower (+1) to the highest (+3) **C.** Tumor sections were stained for F4/80 as a marker of macrophages and CD3 as a marker of T cells. Data are shown as average with SEM, (n≥3).

Discussion

Cell cycle regulation by RingoA in mammalian cell lines

RingoA has a well-described role in meiosis; it regulates the G2/M progression in *Xenopus* oocytes (Ferby et al. 1999; Gutierrez et al. 2006; Ruiz et al. 2008) and is also essential for the meiotic prophase in mouse (Mikolcevic et al. 2016; Tu et al. 2017). Its ability to bind to and regulate CDKs suggests a potential role in regulating also the mitotic cell cycle. In this regard, it has been shown that RingoA mRNA is expressed during the whole cell cycle oscillating in a phase-dependent manner, similarly to Cyclin A. Furthermore, it has been demonstrated that RingoA can interact with p27^{Kip1} *in vitro*, that CDK2-RingoA complexes are less sensitive to p27^{Kip1} inhibition, and that RingoA overexpression leads to p27^{Kip1} degradation in cells. This degradation induction is likely due to the activation of CDK2 and the phosphorylation of p27^{Kip1} on T187 (Dinarina et al. 2009; McGrath et al. 2017; Porter et al. 2002), in a similar manner to that described for CDK2-Cyclin E complexes (Sheaff et al. 1997).

During the course of this project, we aimed to examine in greater detail the role of RingoA in mammalian cells. Loss of function studies in U2OS cells showed a dramatic reduction of the number of cells undergoing mitosis, as well as an increase in those in G1 phase, while those in S and M phases decreased, thereby pointing to a G1 arrest (**Figure R1.A**), which is further supported by the reduced BrdU incorporation (**Figure R1.B**).

The arrest of some of the cells in G1 may be due to the activation of the DNA damage checkpoint. Within the population of cells that underwent mitosis, the vast majority died before the next division, indicating that they carried problems that did not allow them to survive and progress to the next division round (**Figure R2A**). We also detected increased signs of chromosome segregation problems such as DNA bridges and micronuclei in the fraction of cells that divide (**Figure R2B**), which might lead to cell cycle arrest by the G1/S checkpoint (Sablina et al. 1998).

Replicative stress is a major cause of pre-mitotic errors leading to CIN (Burrell et al. 2013). Thus, the chromosome segregation errors observed in RingoA knockdown U2OS cells might result from pre-mitotic defects potentially derived from replication stress or unrepaired DNA damage. DNA replication stress results in phenotypes such as DNA damage in

Discussion

prometaphase, ultrafine DNA bridges and 53BP1 nuclear bodies in G1 (Burrell et al. 2013), and these indicators could be evaluated in our system. Moreover, DNA fiber assays could be done to assess whether cells have alterations in replication fork dynamics that could lead to replication stress (Quinet et al. 2017). Alternatively, the errors might originate directly from mitotic defects. It has been reported that if the problem precedes mitosis, dividing cells usually carry anaphase bridges and chromosome fragments without centromeres, but if the origin is a mitotic defect, cells are likely to have lagging chromosomes with centromeres (Burrell et al. 2013). Therefore, one way to elucidate the origin of the errors would be to analyze whether the lagging DNA observed in our experiments upon RingoA knockdown contains centromeres. The underlying reason could potentially be the regulation of some of the RingoA interactors identified, such as the proteins of the cohesin complex, which are discussed below. To understand the origin of cell death and further characterize cell arrest, cell cycle progression could be followed in living cells using systems such as FUCCI (Zielke and Edgar 2015) in combination with time-lapse fluorescence microscopy. Finally, to understand whether indeed the phenotypes and cell death are due to DNA damage, the potential implication of DNA damage in the observed phenotypes could be analyzed by evaluating more markers of the DDR and checkpoints such as pRPA, pChk1 or p53 (Kastan and Bartek 2004). Interestingly, a link between RingoA and the DDR has been already suggested, as RingoA overexpression was proposed to counteract the activation of DDR markers such as pChk1 or γ H2AX in U2OS cells treated with UV (Gastwirt et al. 2006). In addition, it has been reported that proteins involved in DSB repair are upregulated following RingoA depletion in mSOD cells with basal levels of DNA damage (Wang et al. 2019).

Besides DNA damage, alterations in the cell cycle might be explained by the lack of RingoA mediated p27^{Kip1} inhibition in the RingoA KD. Of note, it seems unlikely that RingoA could be an essential regulator of the G1/S transition in mammalian cells process where CDK-cyclin complexes have a well-defined role (Montagnoli et al. 1999). *In vitro* experiments suggest that CDK2 can be much more efficiently activated by Cyclin A (with the requirement of T160 phosphorylation) than by RingoA (McGrath et al. 2017). Moreover, the low abundance of RingoA would make CDK activation stoichiometrically difficult. Nevertheless, although CDK-RingoA complexes are less active than CDK-cyclin complexes, they are still active in conditions where CDK-cyclin are likely to be inhibited (Karaiskou et al. 2001; McGrath et al.

2017). Therefore, part of the cell cycle arrest could be explained by a lack of CDK-RingoA mediated degradation of p27^{Kip1} upon RingoA KD.

Uncovering the RingoA interactome network

RingoA can bind to and activate CDK1 and CDK2 *in vitro*, but very little is known about its interactome network. BioID is a powerful technique to identify proteins at close proximity. It has the advantage of marking not only strong interactors but also proteins transiently interacting, indirectly interacting or co-localizing but without direct interaction (Roux et al. 2012), which is especially interesting in the case of RingoA. The interactions with CDK-RINGO complexes could be expected to be transient and may be restricted to a particular phase of the cell cycle, which makes it challenging to track these interactions with classical methods such as co-IP followed by MS. BioID gave us information on both the subcellular location of RingoA and new RingoA interacting proteins, thereby indicating processes in which RingoA might be involved. Although overexpressed RingoA protein has been found mostly at the nucleus, it is still unknown where the endogenous protein is located. Our data indicate that most potential RingoA interactors are nuclear proteins, thus supporting the expected nuclear location. Interestingly, the proteins identified are involved mainly in RNA processing and the regulation of the cell cycle. The identified RingoA cell cycle related interactome cluster includes as high confidence hits CDK1 and Skp2, two known interactors of RingoA (Dinarina et al. 2005; Dinarina et al. 2009), thereby supporting the reliability of our screening. Of note, CDK2 was present in the list of hits but below the set threshold. Nevertheless, we included this protein in our analysis due to its known association with RingoA.

Identification of new RingoA interactors

Among the list of putative interactors, we have been able to validate WAPL and ANKRD11 as novel RingoA interacting proteins (**Figure R5.A**). WAPL is a regulatory factor that is essential for cohesin unloading from chromatin both in interphase and mitosis (Haarhuis et al. 2017; Tedeschi et al. 2013). Moreover, RingoA can also interact not only with WAPL but also with

Discussion

the cohesin core proteins SMC1, SMC3 and Scc1 (**Figure R6**). These observations further support the notion that RingoA interacts with the cohesin complex, and also show that RingoA interaction with this complex is not necessarily a direct interaction with WAPL, as RingoA might interact with one or several of the mentioned proteins. Our findings open the door to study a novel regulatory mechanism of the cohesin complex by RingoA. There are several examples of regulation of members of the cohesin complex by phosphorylation that lead to distinct cellular outcomes. CDK1 has been described to phosphorylate Sororin, and Sororin phosphorylation is known to mediate WAPL regulation and chromatin unloading (Ladurner et al. 2016; T. Nishiyama et al. 2013; T. Nishiyama et al. 2010). Moreover, the kinase Haspin, which is essential for mitosis, phosphorylates WAPL thereby preventing its binding to PDS5B and thus inhibiting the unloading of centromeric cohesin (Liang et al. 2018). On the other hand, Polo phosphorylates Scc1, enhancing its cleavage in yeast (Alexandru et al. 2001). SMC1 is phosphorylated by ATM in response to ionizing radiation (Kim et al. 2002; Yazdi et al. 2002) and SMC3 has also been proposed to be phosphorylated in irradiated cells (Luo et al. 2008). It will be interesting to analyze whether RingoA regulates the function of the cohesin complexes and if CDK-RingoA complexes phosphorylate WAPL or the cohesin core proteins. Given that CDK-RINGO substrates might be partly redundant with CDK-cyclins, the information obtained in our screening may also be relevant for the identification of CDK-cyclin substrates.

CDK-RINGO may interact with the cohesin complex through CDK. Alternatively, RingoA may bind to the substrates and localize CDK to their proximity, acting as a scaffold protein. For instance, RingoA has been shown to be essential for recruiting CDK2 to telomeres in meiotic cells (Mikolcevic et al. 2016; Tu et al. 2017). In this particular case, RingoA directly binds the telomere component TRF1, whereas CDK2 does not (Wang et al. 2018). Therefore, RingoA might be required for sequestering CDKs to particular cohesin complexes. To examine whether RingoA interaction with WAPL is mediated by CDK2, we compared myc-RingoA to myc-CDK2 and myc-Cyclin E2/A2 (**Figure R7**). Interestingly, RingoA had a higher capacity to interact with endogenous WAPL than CDK2 and cyclins, thereby suggesting that WAPL interaction is not through CDK2. It would be interesting to test whether a RingoA mutant deficient in CDK binding maintains its ability to interact with WAPL. Maintenance of such

interaction capacity would suggest that RingoA acts as a scaffold protein or that RingoA has CDK independent functions.

Altogether, the BioID screening has allowed us to identify novel RingoA interactors that might help to elucidate the molecular mechanism underlying RingoA function. Cohesin regulation would be a potential explanation for at least some of the phenotypes observed in RingoA-deficient human cells *in vitro*. In addition to their crucial role in mitosis, cohesin complexes, together with CTCF, participate in chromatin organization in interphase through the formation of chromatin loops (Haarhuis et al. 2017). They are also involved in the maintenance of replication fork speed (Terret et al. 2009), in chromosome integrity by mediating the start of DNA replication of stalled forks (Tittel-Elmer et al. 2012), and in DNA repair (Ström et al. 2004). In addition, SMC1 phosphorylation is important for the DDR in the intra-S checkpoint (Kitagawa et al. 2004). The KO of the cohesin regulatory factor WAPL have increased p27^{Kip1} and decreased Cyclin A, indicating that this cohesin regulator is important for the G1/S transition (Tedeschi et al. 2013), which would be in line with our observed arrest in G1.

Time-lapse videos of HeLa cells gathered in the Mitocheck mitotic cell atlas (Neumann et al. 2010) show that downregulation of SCC1, SMC3 or WAPL leads to abnormal nuclear shape, nuclei staying close together, chromatin bridges, lagging chromosomes, and an increase in micronuclei. SMC3 and SCC1 KD cells additionally show metaphase alignment problems, including no metaphase and in some cases chromatin condensation followed by decondensation (Neumann et al. 2010). Interestingly, in similar time-lapse videos in U2OS cells, we have observed increased signs of chromosome segregation problems following mitosis, such as DNA bridges, micronuclei or unusual nuclear shapes (**Figure R2.B**). Moreover, U2OS cells overexpressing a stable and non-degradable form of RingoA show abnormal chromatin condensation which appears to be CDK dependent (Dinarina et al. 2009). It would be interesting to address chromosome segregation and cohesion by analyzing mitotic metaphase spreads. Moreover, the cohesin levels loaded in mitosis and interphase should be examined in order to determine whether RingoA contributes to the regulation of cohesin dynamics. Of note, RingoA is not present on the whole chromosome arms or centromeres but is mainly located close to nuclear speckles (**Figure R9**). This distribution makes it unlikely that RingoA regulates cohesin complexes at the critical step of

Discussion

unloading from the whole chromosome arms during mitosis. Instead, RingoA might regulate a particular subset of cohesin complexes, which is a more plausible possibility given the low expression of RingoA.

In addition to cohesins, the list of potential interactors includes other proteins related to DNA replication and DDR that could account for some DNA damage issues, such as the DNA polymerase alpha 1 catalytic subunit (*POLA1*) (Taricani et al. 2009). Also, UIMC1/RAP80 is an essential protein for DNA repair as it mediates the ubiquitination of γ H2AX sites prior to BRCA1 binding (Foulkes et al. 2007) for DSB repair. Furthermore, PPP4C and PP4R2 participate in mediating the dephosphorylation of Ser-140 of H2AFX generated during DNA replication, and it is required for DSB repair (Chowdhury et al. 2008).

Altogether, our screening has allowed the identification of novel proteins that can interact with overexpressed RingoA. It would be interesting to validate these interactions with the endogenous RingoA protein using techniques such as proximity ligation assay (PLA) (Söderberg et al. 2008). Moreover, our results point to various possibilities that could potentially explain the phenotypes observed upon RingoA overexpression or downregulation in mammalian cell lines.

Molecular clues for the identification of RingoA sub-cellular location and dynamics

We have used a monoclonal antibody to identify endogenous RingoA in human cells, which was validated by its downregulation upon RingoA siRNA treatment (**Figure R8.C**). Interestingly, RingoA is distributed in discrete nuclear sites during interphase and removed during mitosis (**Figure R8.A**). It has been previously shown that cells expressing a stable form of GFP-RingoA, which is not degraded in mitosis, have problems in completing mitosis exit that are comparable to those observed after overexpression of a stable form of Cyclin B, a mechanism defined as “reversal of mitosis exit” (Dinarina et al. 2009; Potapova et al. 2006). This finding suggests that the degradation of RingoA in mitosis is required for proper cell cycle progression.

The eukaryotic nucleus has several compartments that are defined by the absence of surrounding membranes, which allows these compartments to rapidly form or dissolve in

response to signals. The nucleolus, nuclear speckles (NS), PML bodies, and Cajal bodies are among these membrane-less compartments, which frequently harbor proteins with intrinsically disordered domains. The disordered nature of these proteins may mediate the weak interaction with several target sites, facilitating the liquid phase separation (Boeynaems et al. 2018). Interestingly, RingoA contains several intrinsically disordered regions (**Figure R9.C**).

The main function of the nucleolus is the synthesis and processing of rRNA, and ribosome assembly. However, it is also involved in the regulation of other processes. For example, this compartment sequesters enzymes involved in the DDR and cell cycle progression (Iarovaia et al. 2019). From the elevated number of rRNA processing proteins found in the list of BioID hits, we first speculated that RingoA could be located in the nucleolus. However, endogenous RingoA did not overlap with this organelle, as shown by IF (**Figure R10.B**). In contrast, the IF experiments in RingoA-BirA* transfected cells, showed elevated BirA activity in the nucleolus. However, the signal in this organelle was also slightly enriched in the BirA* empty-vector control cells (**Figure R3.C**). These results suggest that the enrichment of RingoA in the nucleolus and the elevated presence of rRNA proteins might be due to an artifactual activity of the BirA*-tag to this organelle.

NS or SC35 domains are another example of membrane-less compartments. These compartments are enriched mostly in proteins involved in mRNA modification, such as splicing factors and 3' processing factors. However, several proteins involved in chromosome localization and chromatin modification are also assembled there, thereby suggesting that NS may act as hubs to coordinate the regulatory steps of gene expression (Galganski et al. 2017; Lamond and Spector 2003; Shah et al. 2018). BioID analysis showed a cluster highly enriched in mRNA processing proteins and splicing factors, which is consistent with the finding that RingoA is partially located to NS (**Figure R9.A**). In addition, NS are known to grow in size upon transcription inhibition (Galganski et al. 2017) and we show that RingoA also accumulates in this condition (**Figure 9.B**). Furthermore, NS are stable during interphase and disassembled during mitosis upon nuclear envelope disruption. Later in mitosis, they reassemble in small cytoplasmic granules, which become visible in telophase. During mid-late telophase, after the deposition of the nuclear envelope, these proteins enter daughter nuclei and relocate to chromatin (Lamond and Spector 2003). In fact, RingoA has a similar

Discussion

pattern of expression, as it disappears in prophase and is then re-expressed, forming dots at the end of mitosis (**Figure R8.A**). Thus, RingoA protein pattern during cell cycle and its accumulation upon transcription inhibition indicate that this protein has similar dynamics to NS. These observations raise the question as to whether RingoA somehow regulates NS functions.

In addition to RNA processing proteins, NS have proteins of diverse nature, such as chromatin processing proteins and protein kinases. For instance, Cyclin T, which was detected at the BioID screening, and Cyclin L1, CDK11, CDK9 have been all located at NS (Dow, Liu, and Rice 2010; Herrmann et al. 2007; Loyer et al. 2008). Although NS appear to be clearly separated from the nucleoplasm, they are highly dynamic and many of their components are in constant flux with the nucleoplasm (Phair and Misteli 2000). Most of the proteins present in NS are also found in other locations. However, while many have well-described roles out of the NS, it is unclear whether they also have functions in these membrane-less compartments. Therefore, the presence of RingoA in NS does not necessarily mean that this protein has a central function there, nor does it exclude functions in other nuclear sites. In addition, it has to be noted that the colocalization of RingoA with NS is partial (about 60%), meaning that RingoA also localizes in surrounding locations. This notion is supported by the observation that RingoA co-localizes with a portion of the cohesion component Smc1 in the regions close to NS, and Smc1 is expected to interact with DNA. As an example, FANCI, an ATM/ATR substrate required for DNA repair (Smogorzewska et al. 2007), localizes to chromatin in response to DNA damage and also associates with NS factors thereby promoting they release upon DNA damage (Moriel-Carretero et al. 2017). It would be interesting to study this distribution and co-localization within NS and surrounding chromatin domains in greater detail. This analysis could be done by super-resolution techniques, such as STORM, which have been useful to study chromatin domains and the distribution of its regulators, such as cohesins (Nozaki et al. 2017).

Role of RingoA *in vivo*

RingoA expression in mice

RingoA is expressed mainly in testis, as confirmed by RT-qPCR and the luciferase reporter data (**Figure R11 & R16**). Despite being poorly expressed in somatic tissues, the use of a luciferase reporter identified lung and brain as the somatic tissues with most activity of the RingoA promoter (**Figure R16.A**). In the RT-qPCR data, the brain was consistently the tissue with the highest overall expression (**Figure R11**). Regarding other somatic tissues, there was an apparent discrepancy between promoter activity and mRNA expression levels in organs such as lung and intestine. This observation could be attributed to a decreased stability of the mRNA, to differences in the penetration of light in some tissues compared to others, or to a higher background.

In contrast with the luciferase reporter and mRNA analysis, Katushka expression was only clearly detected in testis by FACS (**Figure R15.B**). Therefore, the Katushka reporter seems to be less sensitive than luciferase in our conditions, and we therefore preferentially used luciferase for *in vivo* experiments, such as those addressing mammary tumorigenesis (**Figure R23**). In embryos, the luciferase signal was located mainly in the upper part of the body, coincident with the brain (**Figure R16.B**).

In the framework of a role of RingoA in cell cycle regulation, we hypothesize that RingoA is expressed in proliferating NSC and progenitors, a notion that is supported by publicly available data (Llorens-Bobadilla et al. 2015). In particular, within the niche of stem cells of the adult SVZ, RingoA is expressed in mitotically-active neural stem cells (aNSC1) and transit amplifying progenitors (TAPs) (**Figure R17**). These observations are consistent with our data, as RingoA mRNA was detected in cells growing as neurospheres but not in differentiated cells (**Figure R18**). Of note, RingoA mRNA expression in neurospheres was low, which suggests that RingoA is either lowly expressed or restricted to a small proportion of cells.

RingoA is essential for meiosis

RingoA is essential for the progression of prophase of meiosis I in mice (Mikolcevic et al. 2016). Intriguingly, although RingoB expression is very high in testis, we have found that this protein does not play a major role in meiosis, as gonads of both males and females are normal and the animals are fertile. These findings suggest that RingoA and RingoB do not have conserved functions or that the function of RingoB in meiosis can be complemented by RingoA. Furthermore, as expected, RingoA and RingoB double KO mice have a similar gonadal phenotype as that of RingoA KO mice (**Figure R12**).

In males, the entire meiotic cycle occurs in adults. Conversely, in females this process begins in embryonic stages and is arrested in diplotene of prophase I until the moment of ovulation. Afterwards, the cycle is again arrested in metaphase of meiosis II until fertilization (Li and Albertini 2013; Phillips et al. 2010). We took advantage of this interruption in the meiotic process to study whether RingoA is relevant for stages following prophase I, during oocyte maturation. The inducible deletion of RingoA impaired meiosis in males but did not affect ovaries, which showed normal histology and follicle stages (**Figure R13**). In addition, adult females were fertile after RingoA depletion in adults, thereby further confirming ovary functionality. This finding is consistent with another study based on ovary-specific deletion of RingoA in postnatal mouse using Zp3-Cre, which confirmed normal oocyte maturation *in vitro* (Tu et al. 2017). Taken together, our data suggests that RingoA is not essential beyond diplotene of meiosis I or meiosis II in oogenesis.

RingoA is not essential for the homeostasis of somatic tissues

The classic regulators of the cell cycle, cyclins and CDKs, have undergone several functional specifications during evolution. Examples of molecular and functional complementation among cell cycle proteins in mammals can be found. The nature of the interactions between CDKs and cyclins has been, to a large extent, reported *in vitro*. However, the biochemical promiscuity of CDK-cyclin interactions, together with the frequent complementation among different members, makes it difficult to determine the physiological relevance of specific CDK-cyclin complexes *in vivo*. As an example, CDK1 was thought to be activated mainly by Cyclin A and Cyclin B; however, in the absence of CDK4/CDK6, it can also bind Cyclin D.

Moreover, when CDK2 is absent, CDK1 can bind to Cyclin E (Aleem et al. 2005; Malumbres et al. 2004; Santamaría et al. 2007).

This might also be true for atypical CDK activators. RingoA can interact with and activate CDK1 and CDK2, and in testes, the RingoA KO mouse has a phenotype that resembles that observed in CDK2 KO animals. However, RingoA KO mice are born at the expected Mendelian ratio, thereby indicating that embryo viability is not affected (Mikolcevic et al. 2016). Moreover, in spite of dedicated efforts, we have not observed any phenotype in the somatic tissues in young or aged mice (**Table R1**). Does this mean that RingoA does not play any major role in these tissues? Or, conversely, does it imply that normal RingoA function is complemented by other proteins? The observation that RingoA expression is much lower in somatic tissues than in meiotic tissues may explain the lack of phenotypes in most organs. However, RingoA mRNA is detected in some tissues and, although not very abundant, it could be important in particular cells or situations. Therefore, in some RingoA-expressing cells, the lack of phenotypes could be caused by functional redundancy. In an attempt to reduce the probability of complementation, we generated RingoA and RingoB double KO mice. We did not detect any phenotype. However, there is another poorly studied RINGO family member in mice, RingoD, which might be functionally redundant. In addition, RingoA might be complemented by classical CDK activators, for instance, Cyclin A and Cyclin B in the case of CDK1 dependent functions or Cyclin E or Cyclin A in CDK2 dependent ones. Finally, it is also plausible that RINGO does not have essential functions in basal conditions but becomes relevant in specific situations, for example in response to stress.

RingoA in the brain

Despite not being essential for the proliferation of most somatic cells, CDK2 has been shown to be important for the proliferation of cells in the SVZ of the adult brain. Interestingly, in developing embryonic brains, the absence of CDK2 seems to be complemented by the function of CDK4 (Jablonska et al. 2007). Since RingoA might be relevant for CDK2 activation, we also studied the fitness of NSCs and progenitors in adult brains rather than during development, where redundancy would be more likely. We found that RingoA-deficient neural progenitors were impaired in neurosphere formation (**Figure R19**), similarly to what have been reported for CDK2 deficient neural progenitors, which show a reduced size and

Discussion

number of neurospheres (Jablonska et al. 2007). However, cell proliferation was not reduced as reflected by BrdU incorporation analysis, and the cell cycle appeared normal (**Figure R20**). Thus, on the one hand, the reduced number of neurospheres could be explained by a decreased number of cells with the ability to form spheres. On the other hand, given that the experiments were done 7 days after neurosphere passage, the reduction in size might be explained by the progressive accumulation of small defects. For example, small changes in cell proliferation, cell death or cell cycle arrest might not be high enough to be detected by the techniques used at the “snapshot” of the time of harvesting. Alternatively, the smaller size might reflect a delay in the ability to start forming a new neurosphere, thereby resulting in retarded growth and a smaller size at the final timepoint. It would be interesting to analyze the initial cell divisions leading to neurosphere formation by live microscopy.

The size and histological characteristics of RingoA/RingoB double KO brains were normal (**Figure R22**). Therefore, our analysis of adult brains *in vivo* indicates that RingoA is not essential for embryonic brain development. Given the defects observed in the formation of neurospheres derived from neural progenitors and stem cells, we analyzed cell proliferation in the SVZ *in vivo*. We did not find differences between WT and RingoA/RingoB double KO animals (**Figure R22.D,E**). This finding suggests that, *in vivo*, RingoA KO does not resemble the CDK2 KO phenotypes in the brain. However, although we found no differences in the overall levels of cell proliferation in the SVZ, with the data available so far, we cannot conclude that the SVZ cells are fully functional upon RingoA deletion. Analysis of particular sub-populations, cell migration and behavior experiments would be required to further investigate the functionality of neurogenesis in the SVZ of RingoA KO mice.

The ventricles of the adult mammalian brain contain NSCs distributed along their walls. Progenitors from the SVZ undergo various steps of proliferation, differentiation and migration. Activated NSCs (aNSCs) can undergo asymmetric division for self-renewal and produce TAPs, which express markers of early neuronal differentiation. TAPs divide approximately three times and give rise to neuroblasts, which divide generally once and migrate to the olfactory bulb where they become primarily interneurons (Dulken et al. 2017; Ponti et al. 2013). Neuroblasts, which are at a more advanced stage of differentiation, start expressing Dcx, and only a low percentage of these Dcx+ cells express the Ki67 proliferation

marker. Later, NeuN is expressed during the final stages of neural differentiation, when cells exit the cell cycle (**Figure I12**) (Walker et al., 2007; Gusel'nikova & Korzhevskiy, 2015).

Adult NSCs regulate their self-renewal potential by maintaining low proliferation rates, remaining at G0 for long periods (Götz and Huttner 2005). The cell cycle regulator p21^{Cip1} has been reported to be important for NSC self-renewal, and p21^{Cip1} depletion increases neurosphere number and size at early passages but reduces BrdU incorporation in the following passages, thereby suggesting premature exhaustion. This also connects cell cycle control with NSC self-renewal. P21^{Cip1} has been shown to negatively regulate Sox2, which plays a crucial role in maintaining the stem cells in an undifferentiated state (Kippin et al. 2005; Marqués-Torrejón et al. 2013; Porlan et al. 2013). We tested whether RingoA depletion could lead to changes in the expression of Sox2 and other markers of NSCs. In this regard, the levels of expression remained unaltered (**Figure R21.A**). Several studies correlate the interphasic CDK activity and increased length of G1 in brain stem cells with higher rates of differentiation. For instance, CDK6 KO leads to increased differentiation (Beukelaers et al. 2011) and CDK4-CyclinD1 overexpression results in an expansion of progenitor cells (Lange et al. 2009). We did not detect changes in the G1 phase of RingoA depleted neurospheres (**Figure R20.B**). However, evaluation of the cell differentiation markers DCX and NeuN *in vitro*, showed that neurospheres had decreased DCX mRNA levels and differentiated cells showed a decrease in overall NeuN mRNA levels (**Figure R21.B**). The decreased DCX in neurospheres suggests a reduction in neuroblast-like cells in early stages, when cells are in “proliferation like” conditions, while the lack of changes in DCX once the cells reach differentiation indicates that differentiated RingoA depleted cells achieve full DCX expression. On the other hand, the decrease in NeuN in differentiated cells points to a potential impaired capacity to reach neuronal differentiation stages. It is important to emphasize that these experiments were done in primary cultures, which lack most of the signals present in the SVZ and rostral migratory stream of the brain. In the brain, blood vessels penetrate the SVZ and contain endothelial cells, pericytes and fibroblasts. Actively dividing cells are concentrated next to these vessels, since factors derived from this region are important for the SVZ niche, stimulating self-renewal and lineage progression of committed progenitors (Shen et al. 2004; Walton et al. 2006). It has also been shown that direct contact between NSCs and endothelial cells is important for their arrest in G0-G1 and

Discussion

for the promotion of stem cell identity (Ottone et al. 2014). Therefore, given the complexity described, our results suggest that it might be worth exploring the relative representation of neural lineages, as well as the migration and differentiation of these cells *in vivo*. This could be done by labeling proliferating cells with BrdU and then quantifying the migration and expression of specific markers.

It might be also interesting to explore the potential implication in such phenotypes of some of the proteins identified in our BioID screening. For instance, ANKRD11, which we validated to be able to bind overexpressed RingoA, is a chromatin regulator that has been shown to be important for neural precursors of both developing and adult brains. It has a role in the regulation of neural precursors acetylation and gene expression. Mice with deficient ANKRD11 show behavior changes. Moreover, neural precursors in these animals show reduced proliferation and alterations such as reduction of adult-born NeuN positive olfactory bulb neurons. (Gallagher et al. 2015).

In summary, we have shown a reduction of neurosphere growth *in vitro* without any effect on cell proliferation *in vivo*. This apparent discrepancy between *in vitro* and *in vivo* results could be due to a loss of “essentiality” of RingoA *in vivo*, perhaps due to functional redundancy with other CDK activators, or conversely, it could evidence the differences between the conditions of the progenitors *in vitro* and *in vivo*. NSCs *in vitro* are constantly exposed to the mitogens FGF and EGF and are maintained in elevated rates of proliferation. In contrast, *in vivo*, it is important to maintain stem cell capacity and therefore NSCs probably proliferate at lower rates (Pastrana et al. 2011; Urbán and Guillemot 2014). Thus, differences *in vitro* and *in vivo* might also be due to the different proliferation rates. It is known that in some situations, proliferation in the SVZ is boosted. For example, focal ischemia stimulates SVZ proliferation in rodents (Arvidsson et al. 2002; Jin et al. 2001; Thored et al. 2006), and is believed to enhance not only neurogenesis but also astrogenesis (Benner et al. 2013). We speculate that RingoA KO mice might show a phenotype *in vivo* in these conditions of higher proliferation requirements. For example, in basal conditions, the SVZ generates relatively low levels of oligodendrocytes compared to neurogenesis. After demyelinating injury, oligodendrocyte progenitor cells are recruited from surrounding intact tissue to the damaged areas, thereby contributing to remyelination; these remyelinating oligodendrocytes can come from the SVZ (Franklin and Ffrench-Constant 2008).

Interestingly, CDK2 has been proposed to participate in controlling self-renewal of oligodendrocyte progenitors, thus accelerating remyelination after damage (Caillava et al. 2011). These observations raise the question as to whether RingoA might be required in these specific situations.

RingoA in tumorigenesis

The cell cycle requirements of cancer cells might differ from their cells of origin. RingoA is expressed in testis, and it is known that tumors express some testis antigens, which are encoded by genes usually expressed in the germline but that are overexpressed in cancer cells (Simpson et al. 2005). Although some studies have proposed a role for RingoA in cancer, none of them have used genetic loss of function mouse models (Ferraiuolo et al. 2017; Lubanska et al. 2014; Al Sorkhy et al. 2012). This led us to study the role of this protein in mammary tumors using the PyMT model. The RingoA protein has been proposed to be up-regulated in human tumors such as glioma, ovarian cancer and colorectal cancer. However, the specificity of the antibodies used has not been demonstrated (Jin et al. 2018; Lu et al. 2016; Zhang et al. 2012). In our experience, immunohistochemistry studies with RingoA antibodies in mouse tumors and in the SVZ show a positive signal in some cases but this signal is also present in RingoA KO animals, thereby suggesting that it is unspecific. Thus, it is essential to use controls for immunohistochemistry analysis in order to avoid misassumptions, particularly when the protein is expected to have very low abundance.

To study RingoA promoter expression in tumors, we used a luciferase reporter. We found a continuous increase in luciferase activity concomitant with the growth of PyMT-induced tumors (**Figure R23**). This observation demonstrates that the RingoA promoter is active during mammary tumor development. However, this approach does not allow us to distinguish whether there is an increased expression of RingoA promoter per cell or whether it reflects an increased number of proliferating cells with active RingoA promoter.

Our study is the first to evaluate the requirement of RINGO proteins for tumor development *in vivo*. After confirming the expression of the RingoA promoter in mammary tumors, RingoA and RingoB were deleted from the tumors. We observed that tumor growth was reduced (**Figure R24**), thereby suggesting that these proteins are required for mammary tumor growth. By immunohistochemistry analysis, we observed increased DNA damage and p27^{Kip1}

Discussion

expression, as well as CD3 and F4/80 immune cell infiltration (**Figure R31**). These observations could be inter-related in several aspects.

In tumors, we observed increased p27^{Kip1} protein upon RingoA KO (**Figure R31.B**). This increase could be a result of its direct regulation by RingoA or may alternatively indicate an accumulation of cells arrested in G1/S phase (Aleem et al. 2005; Porter et al. 2003). We also observed γ H2AX upregulation, which indicates DNA damage, and might support the notion that some of the cells were arrested due to this damage. Moreover, the DNA damage could potentially lead to the observed increase in apoptosis (**Figure R31.A**).

In our BioID screening, we identified the Skp2 ubiquitin ligase among the putative interactors. Overexpressed RingoA had been shown to be able to interact with this ubiquitin ligase. We also validated this interaction (**Supplementary Figure 3**). Skp2 promotes the degradation of overexpressed RingoA and the inhibition of Skp2 leads to the accumulation of overexpressed RingoA in both interphase and mitosis (Dinarina et al. 2009). RingoA has been proposed to induce p27^{Kip1} degradation, and CDK-RINGO complexes have reduced susceptibility to p21^{Cip1} and p27^{Kip1} inhibition (Karaiskou et al. 2001; McGrath et al. 2017). At the same time, Skp2 is well known to trigger p27^{Kip1} and p21^{Cip1} degradation (Carrano et al. 1999). These observations point to a situation in which p21^{Cip1}, p27^{Kip1}, and potentially RingoA can be induced to degrade by Skp2. The overexpression of Skp2 has been correlated with poor prognosis, by inducing the downregulation of the tumor suppressor p27^{Kip1} (Gstaiger et al. 2001). In contrast, RingoA downregulation seems to reduce tumor progression and increase p27^{Kip1} expression. Therefore, the relationships between these proteins is intriguing. It would be interesting to study whether Skp2 regulates endogenous RingoA and, if so, how this relates to p27^{Kip1} stability.

Given that these hypotheses are difficult to test *in vivo*, we generated immortalized cancer cell lines from PyMT tumors. This should provide a tool to study these possibilities and to analyze the proteins identified in our BioID screening, such as WAPL or RAP80. We found that Cre-induced downregulation of RingoA in the mammary cancer cell lines, decreased proliferation and increased G2 phase, γ H2AX staining, DNA bridges and mitotic defects (**Figure R27**). These findings partially agreed with what we observed in the mouse tumors and the human cell lines. However, further experiments showed that Cre expression sufficed to induce cell cycle changes in the mouse immortalized cancer cell line (**Figure R29**). Cre is a

protein from P1 bacteriophages that catalyzes the recombination between two so-called loxP recognition sites (Nagy 2000), and it is a widely used tool to inactivate genes in mammalian systems in a time and tissue specific manner. However, Cre can have growth-inhibitory genotoxic effects, and Cre induction in MEFs can result in reduced cell proliferation, increased DNA damage with the presence of micronuclei, and G2 arrest, in a dose dependent manner. In particular, doses equal to or below 100 nM of 4-OHT have been shown to not have a significant effect in the proliferation of MEFs (Loonstra et al. 2001). However, in our study, this concentration affected proliferation, thereby indicating that PyMT mammary cancer cells have more sensitivity to the effect of Cre recombinase expression. When the concentration of 4-OHT was decreased five times (20 nM), we still observed *RingoA* gene deletion of more than 90%. However, we did not detect any effect on cell cycle (**Figure R30**). These observations indicate that the effects observed were dependent on the levels of Cre activity rather than on the depletion of RingoA/RingoB. Experiments using a mammary cancer cell control line, in which 4-OHT treatment did not lead to RingoA/RingoB downregulation, further supported the Cre activity-induced effects and ruled out an effect of 4-OHT per se (**Figure R28**). Therefore, the mentioned studies and our findings highlight the importance of careful titration of Cre activity and use of Cre control lines of the same cell type in order to avoid undesired off-target effects.

In summary, we observed a reduction in tumor growth when RingoA and RingoB were downregulated, which was specific for RingoA/RingoB deletion and not due to the off-target effect of Cre. However, we were not able to reproduce this effect using immortalized cancer cell lines derived from the same tumors. This could be due to the cancer cells having changed their molecular requirements for proliferation upon immortalization. Alternatively, the reduction of tumor growth might require some contribution from the tumor microenvironment, as might be suggested by the observed increase in immune cell infiltration (**Figure R31.C**).

Our inability to reproduce the *in vivo* observations *in vitro*, and the difficulties encountered to detect endogenous RingoA expression, makes it challenging to address essential questions such as which cells express RingoA, and when is this protein expressed or stabilized. Therefore, future experiments should be done to test whether the observed reduction in mammary tumor growth upon RingoA depletion is due to a cancer cell

Discussion

autonomous effect or whether it involves other compartments, such as the immune cells. To address this issue, experiments are underway in mice with mammary tumors that express Cre recombinase under control of the K14 promoter (K14-Cre), which is expressed in stratified epithelia including the mammary gland (Jonkers et al. 2001). Confirmation that RingoA depletion with K14-Cre reduces mammary tumor growth would indicate a requirement for RingoA in mammary cancer cells.

Altogether, we have shown that RingoA depletion reduces mammary tumor growth. Although the underlying molecular mechanism still needs to be determined, our results provide further evidence of a differential requirement of a cell cycle regulatory protein in cancer cells and somatic tissues. This might open future opportunities for cancer treatment reducing side effects on healthy cells. Moreover, we have identified novel RingoA interactors that might help to understand the tumor promoting functions of the RINGO proteins.

Conclusions

- RingoA is required for cell cycle progression of human cancer cell lines and its downregulation increases cell death.
- RingoA interacts with the cohesin complex.
- RingoA is partially localized at nuclear speckles.
- RingoB plays no major function in meiosis or in gonad development.
- RingoA and RingoB are not essential for mouse somatic tissues under homeostatic conditions.
- RingoA is expressed in actively dividing adult neural stem cells and is important for their fitness when grown as neurospheres.
- RingoA and RingoB are required for mammary tumor growth *in vivo*.

Appendix

Supplementary Figure 1

Accession num.	Name	Counts	CT.Counts	Saint	F.Change	FDR	CRAPOME
E9PAV3	NACA	122 48	1 8 2 4	1	22,67	0	
O00541	PES1	8 7	2 3 1 0	0,99	5	0	
O15355	PPM1G	19 8	0 2 0 0	1	27	0	
O60563	CCNT1	8 2	0 0 0 0	0,99	50	0	
O95639	CPSF4	5 2	0 0 0 0	0,99	35	0	
P17275	JUNB	3 3	0 0 0 0	1	30	0	
P20290	BTF3	70 33	2 9 0 4	1	13,73	0	
P30419	NMT1	94 41	1 13 4 4	1	12,27	0	
Q01780	EXOSC10	4 2	0 0 0 0	0,99	30	0	
Q03188	CENPC	20 11	1 2 0 0	1	20,67	0	
Q03701	CEBPZ	36 17	0 2 0 0	1	53	0	
Q15154	PCM1	6 8	1 1 0 0	1	14	0	
Q16630	CPSF6	43 16	1 6 0 5	0,99	9,83	0	
Q5MJ70	SPDYA	80 67	0 1 0 0	1	294	0	
Q5RKV6	EXOSC6	13 5	0 1 0 0	1	36	0	
Q6PJT7	ZC3H14	13 10	0 2 0 1	1	15,33	0	
Q6W2J9	BCOR	3 3	0 0 0 0	1	30	0	
Q6ZRS2	SRCAP	15 7	0 0 0 0	1	110	0	
Q8IWI9	MGA	5 3	0 0 0 0	1	40	0	
Q8IWZ8	SUGP1	4 2	0 0 0 0	0,99	30	0	
Q96C00	ZBTB9	3 3	0 0 0 0	1	30	0	
Q96EV2	RBM33	6 3	0 0 0 0	1	45	0	
Q96KR1	ZFR	14 10	0 3 0 0	0,99	16	0	
Q96RL1	UIMC1	4 4	0 1 0 0	0,99	16	0	
Q99460	PSMD1	4 4	0 0 0 0	1	40	0	
Q99615	DNAJC7	3 3	0 0 0 0	1	30	0	
Q9BRX9	WDR83	6 4	0 1 0 0	1	20	0	
Q9BTT0	ANP32E	4 2	0 0 0 0	0,99	30	0	
Q9H501	ESF1	31 14	0 1 0 1	1	45	0	
Q9HCK8	CHD8	7 4	0 1 0 0	1	22	0	
Q9NPD3	EXOSC4	6 2	0 0 0 0	0,99	40	0	
Q9NXF1	TEX10	11 2	0 0 0 0	0,99	65	0	
Q9NY27	PPP4R2	5 3	0 0 0 0	1	40	0	
Q9UPN4	CEP131	8 7	0 0 0 0	1	75	0	
O60493	SNX3	2 2	0 0 0 0	0,97	20	0,01	
O75152	ZC3H11A	22 18	2 9 0 3	0,97	5,71	0,01	
O95400	CD2BP2	2 2	0 0 0 0	0,97	20	0,01	
P04792	HSPB1	13 5	0 2 0 1	0,98	12	0,01	
P06493	CDK1	16 6	1 3 0 0	0,96	11	0,01	
P09884	POLA1	13 7	0 3 0 2	0,97	8	0,01	
P13984	GTF2F2	6 3	0 1 0 0	0,98	18	0,01	
P35269	GTF2F1	2 2	0 0 0 0	0,97	20	0,01	
P46087	NOP2	51 32	14 12 10 10	0,98	3,61	0,01	
P55036	PSMD4	2 2	0 0 0 0	0,97	20	0,01	
P60510	PPP4C	3 2	0 0 0 0	0,98	25	0,01	
P98175	RBM10	15 6	0 3 0 0	0,97	14	0,01	
Q13309	SKP2	3 2	0 0 0 0	0,98	25	0,01	
Q13601	KRR1	6 3	1 0 0 0	0,98	18	0,01	
Q14320	FAM50A	5 3	0 1 0 0	0,98	16	0,01	
Q5H9R7	PPP6R3	3 2	0 0 0 0	0,98	25	0,01	

Appendix

Q5T8P6	RBM26	14 12	0 5 0 2	0,97	7,43	0,01	
Q6UB99	ANKRD11	13 5	0 2 0 1	0,98	12	0,01	
Q7Z5K2	WAPL	5 3	0 1 0 0	0,98	16	0,01	
Q8IWW6	ARID3B	19 8	0 4 0 2	0,96	9	0,01	
Q8IWA0	WDR75	15 9	1 2 3 5	0,97	4,36	0,01	
Q8N9T8	KRI1	9 5	2 1 1 0	0,96	7	0,01	
Q8TD26	CHD6	3 2	0 0 0 0	0,98	25	0,01	
Q8WY36	BBX	10 3	0 1 0 0	0,98	26	0,01	
Q92917	GPKOW	8 6	1 3 0 1	0,97	5,6	0,01	
Q92989	CLP1	2 2	0 0 0 0	0,97	20	0,01	
Q96DE5	ANAPC16	9 3	0 1 0 0	0,98	24	0,01	
Q96K17	BTF3L4	14 9	0 4 0 0	0,97	11,5	0,01	
Q9BSC4	NOL10	9 5	2 0 0 0	0,98	14	0,01	
Q9H2H8	PPIL3	8 5	2 1 0 0	0,98	8,67	0,01	
Q9H7E2	TDRD3	6 3	1 0 0 0	0,98	18	0,01	
Q9HB71	CACYBP	77 22	0 13 3 4	0,96	9,9	0,01	
Q9NQT4	EXOSC5	5 3	0 1 0 0	0,98	16	0,01	
Q9NQZ2	UTP3	13 6	2 3 0 1	0,96	6,33	0,01	
Q9NWS0	PIH1D1	7 5	0 2 0 1	0,98	8	0,01	
Q9P275	USP36	21 13	0 7 1 2	0,96	6,8	0,01	
Q9ULU4	ZMYND8	6 5	1 2 0 0	0,98	7,33	0,01	
O15014	ZNF609	8 3	0 1 0 1	0,93	11	0,02	
O43396	TXNL1	158 74	0 47 0 23	0,95	6,63	0,02	
O43809	NUDT21	29 16	0 10 1 5	0,93	5,62	0,02	
P49321	NASP	4 6	0 2 0 0	0,95	10	0,02	
Q10570	CPSF1	19 7	0 4 0 1	0,95	10,4	0,02	
Q12788	TBL3	16 10	3 4 4 2	0,92	4	0,02	
Q13823	NGP1	22 12	9 2 0 0	0,92	6,18	0,02	
Q13868	EXOSC2	17 5	1 3 0 0	0,92	11	0,02	
Q14241	ELOA	18 8	0 5 2 1	0,92	6,5	0,02	
Q2TBE0	CWF19L2	13 4	0 2 0 1	0,95	11,33	0,02	
Q86T24	ZBTB33	4 6	0 1 0 2	0,94	6,67	0,02	
Q8WUQ7	CACTIN	21 8	4 3 0 1	0,95	7,25	0,02	
Q8WVJ2	NUDCD2	7 4	0 2 0 0	0,95	11	0,02	
Q92620	DHX38	19 2	0 1 0 0	0,92	42	0,02	
Q92733	PRCC	8 4	0 2 0 1	0,95	8	0,02	
Q96L91	EP400	11 5	0 3 0 0	0,94	10,67	0,02	
Q9BTC0	DIDO1	22 10	0 6 0 3	0,94	7,11	0,02	
Q9GZR2	REXO4	25 10	2 6 0 0	0,95	8,75	0,02	
Q9P2N5	RBM27	5 4	0 2 0 0	0,94	9	0,02	
Q9Y6M1	IGF2BP2	10 5	1 3 0 0	0,92	7,5	0,02	

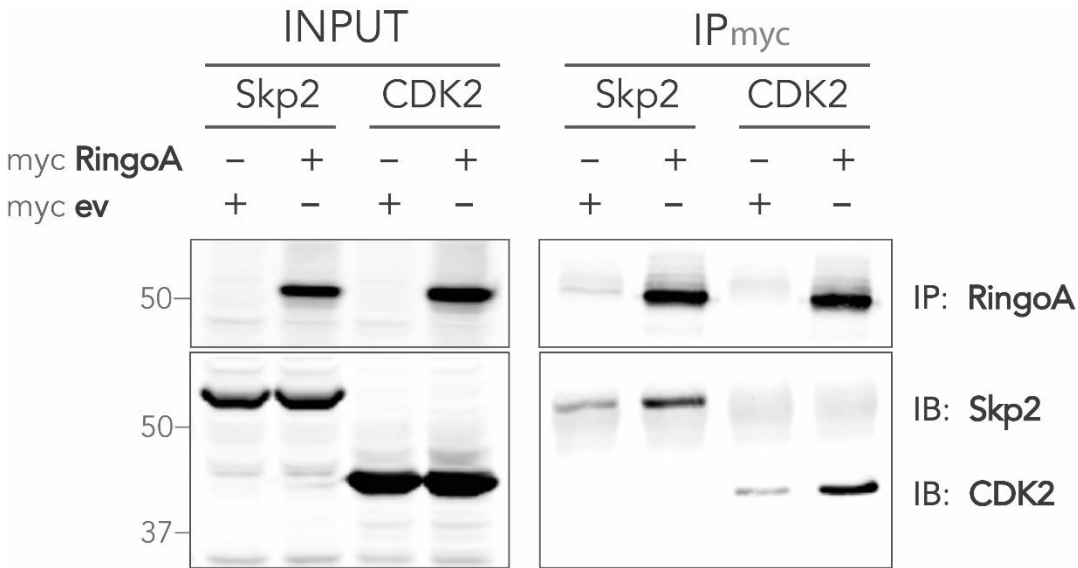
Supplementary figure 1. Proteins identified in BiOID screening. Proteins considered as potential candidate interactors with SAINT>0,9 and FDR ≤0,02 are listed. Spectral counts of BirA*RingoA (third column) and BirA*ev controls (fourth column) are shown. Fold change of BirA*RingoA condition compared to BirA*ev controls are indicated. CRAPOME contaminant repository help to identify proteins that have a greater propensity to be a contaminant by comparing with available experimental data obtained in similar conditions. In the last column candidates are marked in blue when were detected in less than 10% of experiments in the database and therefore are less likely to be contaminants.

Supplementary Figure 2

Pathway name	ratio	p-value	FDR*
Metabolism of RNA	0.055	5.22e-15	2.08e-12
mRNA Splicing - Major Pathway	0.013	1.12e-10	2.23e-08
mRNA Splicing	0.014	2.36e-10	3.13e-08
Processing of Capped Intron-Containing Pre-mRNA	0.018	7.58e-10	7.50e-08
rRNA processing in the nucleus and cytosol	0.015	4.76e-08	3.76e-06
Major pathway of rRNA processing in the nucleolus and cytosol	0.013	1.71e-07	1.13e-05
rRNA processing	0.017	2.86e-07	1.43e-05
mRNA 3'-end processing	0.004	2.91e-07	1.43e-05
Processing of Intronless Pre-mRNAs	0.001	3.59e-07	1.58e-05
RNA Polymerase II Transcription Termination	0.005	7.57e-07	2.95e-05
Processing of Capped Intronless Pre-mRNA	0.002	2.37e-06	8.52e-05
Regulation of mRNA stability by proteins that bind AU-rich elements	0.007	6.43e-06	2.12e-04
Tristetraprolin (TTP, ZFP36) binds and destabilizes mRNA	0.001	1.34e-05	3.75e-04
Butyrate Response Factor 1 (BRF1) binds and destabilizes mRNA	0.001	1.34e-05	3.75e-04
KSRP (KHSRP) binds and destabilizes mRNA	0.001	1.64e-05	3.98e-04
G1/S Transition	0.011	1.66e-05	3.98e-04
mRNA decay by 3' to 5' exoribonuclease	0.002	3.32e-05	7.63e-04
Mitotic G1-G1/S phases	0.012	4.53e-05	9.96e-04
APC/C-mediated degradation of cell cycle proteins	0.006	5.89e-05	0.001
Regulation of mitotic cell cycle	0.006	5.89e-05	0.001
ATF4 activates genes in response to endoplasmic reticulum stress	0.002	1.00e-04	0.002
Cell Cycle	0.048	1.42e-04	0.003
rRNA modification in the nucleus and cytosol	0.005	1.93e-04	0.003

Supplementary figure 2. Results of Reactome analysis of the Bio-ID derived data. The ratio between the relative representation in the screening and the expected representation of the different categories is shown, (FDR: false discovery rate).

Supplementary Figure 3



Supplementary figure 3. RingoA co-immunoprecipitates with CDK2 and Skp2. myc-RingoA and flag-Skp2 or flag-CDK2 were transfected in HEK293-T cells. Myc-RingoA was immunoprecipitated and total lysates were immunoblotted using myc antibody for RingoA detection and Flag antibody for Skp2 and Cdk2 detection.

References

- Alberts, B., Johnson, A., Lewis, J., Raff, M., Roberts, K., & Walter, P. (2002). *Molecular biology of the cell*. 6th ed. New York: Garland Science.
- Aleem, Eiman, Hiroaki Kiyokawa, and Philipp Kaldis. 2005. "Cdc2-Cyclin E Complexes Regulate the G1/S Phase Transition." *Nature Cell Biology* 7(8):831–36.
- Alexandru, Gabriela, Frank Uhlmann, Karl Mechtler, Marc-André Poupart, and Kim Nasmyth. 2001. "Phosphorylation of the Cohesin Subunit Scc1 by Polo/Cdc5 Kinase Regulates Sister Chromatid Separation in Yeast from Their Genesis during DNA Replication until Their Part-Ing at the Onset of Anaphase (Reviewed by Nasmyth et Al., 2000). Sister Chromatid Coh." *Cell* 105:459–72.
- Arvidsson, Andreas, Tove Collin, Deniz Kirik, Zaal Kokaia, and Olle Lindvall. 2002. "Neuronal Replacement from Endogenous Precursors in the Adult Brain after Stroke." *Nature Medicine* 8(9):963–70.
- Asghar, Uzma, Agnieszka K. Witkiewicz, Nicholas C. Turner, and Erik S. Knudsen. 2015. "The History and Future of Targeting Cyclin-Dependent Kinases in Cancer Therapy." *Nature Reviews Drug Discovery* 14:130.
- Barazzuol, Lara, Nicole Rickett, Limei Ju, and Penny A. Jeggo. 2015. "Low Levels of Endogenous or X-Ray-Induced DNA Double-Strand Breaks Activate Apoptosis in Adult Neural Stem Cells." *Journal of Cell Science* 128(19):3597–3606.
- Barnes, Elizabeth A., Lisa A. Porter, Jean Luc Lenormand, Ryan W. Dellinger, and Daniel J. Donoghue. 2003. "Human Spy1 Promotes Survival of Mammalian Cells Following DNA Damage." *Cancer Research* 63(13):3701–7.
- Barrière, Cédric, David Santamaría, Antonio Cerqueira, Javier Galán, Alberto Martín, Sagrario Ortega, Marcos Malumbres, Pierre Dubus, and Mariano Barbacid. 2007. "Mice Thrive without Cdk4 and Cdk2." *Molecular Oncology* 1(1):72–83.
- Bell, Stephen P. and Anindya Dutta. 2002. "DNA Replication in Eukaryotic Cells." *Annual Review of Biochemistry* 71(1):333–74.
- Benner, Eric J., Dominic Luciano, Rebecca Jo, Khadar Abdi, Patricia Paez-Gonzalez, Huaxin Sheng, David S. Warner, Chunlei Liu, Cagla Eroglu, and Chay T. Kuo. 2013. "Protective Astrogenesis from the SVZ Niche after Injury Is Controlled by Notch Modulator Thbs4." *Nature* 497(7449):369–73.
- Bernal, Carolina, Claudia Araya, Verónica Palma, and Miguel Bronfman. 2015. "PPAR β/δ and PPAR γ Maintain Undifferentiated Phenotypes of Mouse Adult Neural Precursor Cells from the Subventricular Zone." *Frontiers in Cellular Neuroscience* 9(March).
- Berthet, Cyril, Kimberly D. Klarmann, Mary Beth Hilton, Hyung Chan Suh, Jonathan R. Keller, Hiroaki Kiyokawa, and Philipp Kaldis. 2006. "Combined Loss of Cdk2 and Cdk4 Results in Embryonic Lethality and Rb Hypophosphorylation." *Developmental Cell* 10(5):563–73.
- Bertoli, Cosetta, Jan M. Skotheim, and Robertus A. M. De Bruin. 2013. "Control of Cell Cycle Transcription during G1 and S Phases." *Nature Reviews Molecular Cell Biology* 14(8):518–28.

References

- Beukelaers, Pierre, Renaud Vandenbosch, Nicolas Caron, Laurent Nguyen, Shibeshih Belachew, Gustave Moonen, Hiroaki Kiyokawa, Mariano Barbacid, David Santamaria, and Brigitte Malgrange. 2011. "Cdk6-Dependent Regulation of G1 Length Controls Adult Neurogenesis." *Stem Cells* 29(4):713–24.
- Blackford, Andrew N. and Stephen P. Jackson. 2017. "ATM, ATR, and DNA-PK: The Trinity at the Heart of the DNA Damage Response." *Molecular Cell* 66(6):801–17.
- Blagosklonny, Mikhail V. and Arthur B. Pardee. 2002. "The Restriction Point of the Cell Cycle." *Cell Cycle (Georgetown, Tex.)* 1(2):103–10.
- Boeynaems, Steven, Simon Alberti, Nicolas L. Fawzi, Tanja Mittag, Magdalini Polymenidou, Frederic Rousseau, Joost Schymkowitz, James Shorter, Benjamin Wolozin, Ludo Van Den Bosch, Peter Tompa, and Monika Fuxreiter. 2018. "Protein Phase Separation: A New Phase in Cell Biology." *Trends in Cell Biology* 28(6):420–35.
- De Bondt, Hendrik L., Jody Rosenblatt, Jarmila Jancarik, Heather D. Jones, David O. Morgant, and Sung Hou Kim. 1993. "Crystal Structure of Cyclin-Dependent Kinase 2." *Nature* 363(6430):595–602.
- Bortner, D. M. and M. P. Rosenberg. 1997. "Induction of Mammary Gland Hyperplasia and Carcinomas in Transgenic Mice Expressing Human Cyclin E." *Molecular and Cellular Biology* 17(1):453 LP – 459.
- Bracken, Adrian P., Marco Ciro, Andrea Cocito, and Kristian Helin. 2004. "E2F Target Genes: Unraveling the Biology." *Trends in Biochemical Sciences* 29(8):409–17.
- Brandeis, Michael, Ian Rosewell, Mark Carrington, Tessa Crompton, Mary Ann Jacobs, Jane Kirk, Julian Gannon, and Tim Hunt. 1998. "Cyclin B2-Null Mice Develop Normally and Are Fertile Whereas Cyclin B1-Null Mice Die in Utero." *Proceedings of the National Academy of Sciences of the United States of America* 95(8):4344–49.
- Brieño-Enríquez, Miguel A., Stefannie L. Moak, Melissa Toledo, Joshua J. Filter, Stephen Gray, José L. Barbero, Paula E. Cohen, and J. Kim Holloway. 2016. "Cohesin Removal along the Chromosome Arms during the First Meiotic Division Depends on a NEK1-PP1 γ -WAPL Axis in the Mouse." *Cell Reports* 17(4):977–86.
- Bulavin, Dmitry V, Yuichiro Higashimoto, Zoya N. Demidenko, Sarah Meek, Paul Graves, Crissy Phillips, Hui Zhao, Sally A. Moody, Ettore Appella, Helen Piwnica-Worms, and Albert J. Fornace. 2003. "Dual Phosphorylation Controls Cdc25 Phosphatases and Mitotic Entry." *Nature Cell Biology* 5(6):545–51.
- Burrell, Rebecca A., Sarah E. McClelland, David Endesfelder, Petra Groth, Marie Christine Weller, Nadeem Shaikh, Enric Domingo, Nnennaya Kanu, Sally M. Dewhurst, Eva Gronroos, Su Kit Chew, Charles Swanton. 2013 et al. "Replication Stress Links Structural and Numerical Cancer Chromosomal Instability." *Nature* 494(7438):492–96.
- Busslinger, Georg A., Roman R. Stocsits, Petra Van Der Lelij, Elin Axelsson, Antonio Tedeschi, Niels Galjart, and Jan Michael Peters. 2017. "Cohesin Is Positioned in Mammalian Genomes by Transcription, CTCF and Wapl." *Nature* 544(7651):503–7.

- Caillava, Céline, Renaud Vandenbosch, Beata Jablonska, Cyrille Deboux, Giulia Spigoni, Vittorio Gallo, Brigitte Malgrange, and Anne Baron Van Evercooren. 2011. "Cdk2 Loss Accelerates Precursor Differentiation and Remyelination in the Adult Central Nervous System." *Journal of Cell Biology* 193(2):397–407.
- Carrano, Andrea C., Esther Eytan, Avram Hershko, and Michele Pagano. 1999. "SKP2 Is Required for Ubiquitin-Mediated Degradation of the CDK Inhibitor P27." *Nature Cell Biology* 1(4):193–99.
- Chen, Daniel S. and Ira Mellman. 2017. "Elements of Cancer Immunity and the Cancer-Immune Set Point." *Nature* 541(7637):321–30.
- Cheng, Aiyang, Shannon Gerry, Philipp Kaldis, and Mark J. Solomon. 2005. "Biochemical Characterization of Cdk2-Speedy/Ringo A2." *BMC Biochemistry* 6:1–17.
- Cheng, Aiyang, Wen Xiong, James E. Ferrell, and Mark J. Solomon. 2005. "Identification and Comparative Analysis of Multiple Mammalian Speedy/Ringo Proteins." *Cell Cycle* 4(1):155–65.
- Cheng, Li Chun, Erika Pastrana, Masoud Tavazoie, and Fiona Doetsch. 2009. "MiR-124 Regulates Adult Neurogenesis in the Subventricular Zone Stem Cell Niche." *Nature Neuroscience* 12(4):399–408.
- Cho, Hyun Jung, Yun Jung Oh, Seung Hun Han, Hee Jin Chung, Chang Hee Kim, Nam Soo Lee, Won Ju Kim, Je Min Choi, and Hongtae Kim. 2013. "Cdk1 Protein-Mediated Phosphorylation of Receptor-Associated Protein 80 (RAP80) Serine 677 Modulates DNA Damage-Induced G2/M Checkpoint and Cell Survival." *Journal of Biological Chemistry* 288(6):3768–76.
- Chotiner, Jessica Y., Debra J. Wolgemuth, and P. Jeremy Wang. 2019. "Functions of Cyclins and CDKs in Mammalian Gametogenesis†." *Biology of Reproduction* 0(April):1–11.
- Chowdhury, Dipanjan, Xingzhi Xu, Xueyan Zhong, Fariyal Ahmed, Jianing Zhong, Ji Liao, Derek M. Dykxhoorn, David M. Weinstock, Gerd P. Pfeifer, and Judy Lieberman. 2008. "A PP4-Phosphatase Complex Dephosphorylates γ -H2AX Generated during DNA Replication." *Molecular Cell* 31(1):33–46.
- Chu, Isabel M., Ludger Hengst, and Joyce M. Slingerland. 2008. "The Cdk Inhibitor P27 in Human Cancer: Prognostic Potential and Relevance to Anticancer Therapy." *Nature Reviews Cancer* 8:253.
- Ciccia, Alberto and Stephen J. Elledge. 2010. "The DNA Damage Response: Making It Safe to Play with Knives." *Molecular Cell* 40(2):179–204.
- Cooper, Tim J., Kayleigh Wardell, Valerie Garcia, and Matthew J. Neale. 2014. "Homeostatic Regulation of Meiotic DSB Formation by ATM/ATR." *Experimental Cell Research* 329(1):124–31.
- Coverley, Dawn, Heike Laman, and Ronald A. Laskey. 2002. "Distinct Roles for Cyclins E and A during DNA Replication Complex Assembly and Activation." *Nature Cell Biology* 4(7):523–28.

References

- D'Adda Di Fagagna, Fabrizio. 2008. "Living on a Break: Cellular Senescence as a DNA-Damage Response." *Nature Reviews Cancer* 8(7):512–22.
- Davidson, Gary and Christof Niehrs. 2010. "Emerging Links between CDK Cell Cycle Regulators and Wnt Signaling." *Trends in Cell Biology* 20(8):453–60.
- Dinarina, Ana, Laurent H. Perez, Amparo Davila, Markus Schwab, Tim Hunt, and Angel R. Nebreda. 2005. "Characterization of a New Family of Cyclin-Dependent Kinase Activators." *Biochemical Journal* 386(2):349–55.
- Dinarina, Ana, Patricia G. Santamaria, and Angel R. Nebreda. 2009. "Cell Cycle Regulation of the Mammalian CDK Activator RINGO/Speedy A." *FEBS Letters* 583(17):2772–78.
- Dobbelstein, Matthias and Claus Storgaard Sørensen. 2015. "Exploiting Replicative Stress to Treat Cancer." *Nature Reviews Drug Discovery* 14(6):405–23.
- Doetsch, Fiona, José Manuel-Garcia Verdugo, Isabelle Caille, Arturo Alvarez-Buylla, Moses V. Chao, and Patrizia Casaccia-Bonnel. 2002. "Lack of the Cell-Cycle Inhibitor P27Kip1 Results in Selective Increase of Transit-Amplifying Cells for Adult Neurogenesis." *Journal of Neuroscience* 22(6):2255–64.
- Dow, Eugene C., Hongbing Liu, and Andrew P. Rice. 2010. "T-Loop Phosphorylated Cdk9 Localizes to Nuclear Speckle Domains Which May Serve as Sites of Active P-TEFb Function and Exchange Between the Brd4 and 7SK / HEXIM1 Regulatory Complexes." (March):84–93.
- Dulken, Ben W., Dena S. Leeman, Stéphane C. Boutet, Katja Hebestreit, and Anne Brunet. 2017. "Single-Cell Transcriptomic Analysis Defines Heterogeneity and Transcriptional Dynamics in the Adult Neural Stem Cell Lineage." *Cell Reports* 18(3):777–90.
- Dunphy, William G. and Akiko Kumagai. 1991. "The Cdc25 Protein Contains an Intrinsic Phosphatase Activity." *Cell* 67(1):189–96.
- El-Deiry, Wafik S. 2016. "P21(WAF1) Mediates Cell-Cycle Inhibition, Relevant to Cancer Suppression and Therapy." *Cancer Research* 76(18):5189 LP – 5191.
- Esashi, Fumiko, Nicole Christ, Julian Cannon, Yilun Liu, Tim Hunt, Maria Jasin, and Stephen C. West. 2005. "CDK-Dependent Phosphorylation of BRCA2 as a Regulatory Mechanism for Recombinational Repair." *Nature* 434(7033):598–604.
- Evans, Tom, Eric T. Rosenthal, Jim Youngblom, Dan Distel, and Tim Hunt. 1983. "Cyclin: A Protein Specified by Maternal mRNA in Sea Urchin Eggs That Is Destroyed at Each Cleavage Division." *Cell* 33(2):389–96.
- Fenech, M., M. Kirsch-Volders, A. T. Natarajan, J. Surralles, J. W. Crott, J. Parry, H. Norppa, D. A. Eastmond, J. D. Tucker, and P. Thomas. 2011. "Molecular Mechanisms of Micronucleus, Nucleoplasmic Bridge and Nuclear Bud Formation in Mammalian and Human Cells." *Mutagenesis* 26(1):125–32.
- Ferby, Ingvar, Montserrat Blazquez, Amparo Palmer, Ramon Eritja, and Angel R. Nebreda. 1999. "A Novel P34(Cdc2)-Binding and Activating Protein That Is Necessary and Sufficient to Trigger G2/M Progression in *Xenopus* Oocytes." *Genes and Development* 13(16):2177–89.

- Fernandez-Capetillo, Oscar, Alicia Lee, Michel Nussenzweig, and André Nussenzweig. 2004. "H2AX: The Histone Guardian of the Genome." *DNA Repair* 3(8–9):959–67.
- Ferraiuolo, Rosa Maria, Janice Tubman, Indrajit Sinha, Caroline Hamm, and Lisa Ann Porter. 2017. "The Cyclin-like Protein, SPY1, Regulates the ERα and ERK1/2 Pathways Promoting Tamoxifen Resistance." *Oncotarget* 8(14):23337–52.
- Fischer, Judith, Ruth Beckervordersandforth, Pratibha Tripathi, Andrea Steiner-Mezzadri, Jovica Ninkovic, and Magdalena Götz. 2011. "Prospective Isolation of Adult Neural Stem Cells from the Mouse Subependymal Zone." *Nature Protocols* 6(12):1981–89.
- Fiskus, Warren and Nicholas Mitsiades. 2016. "B-Raf Inhibition in the Clinic: Present and Future." *Annual Review of Medicine* 67(1):29–43.
- Foulkes, W. D., Y. Wang, J. Qin, S. J. Elledge, D. M. Lowery, A. Nguyen, M. B. Yaffe, X. Yu, J. Chen, Z. Songyang, C. C. Chini, M. He, G. Mer, J. Chen, T. Ludwig, C. A. Joazeiro, D. Hemmati, T. Hunter, I. M. Verma, M. Jasin et al. 2007. "References and Notes 1." (May):1198–1203.
- Fragkos, Michalis, Olivier Ganier, Philippe Coulombe, and Marcel Méchali. 2015. "DNA Replication Origin Activation in Space and Time." *Nature Reviews Molecular Cell Biology* 16(6):360–74.
- Franklin, Robin J. M. and Charles Ffrench-Constant. 2008. "Remyelination in the CNS: From Biology to Therapy." *Nature Reviews Neuroscience* 9(11):839–55.
- Gajewski, Thomas F., Hans Schreiber, and Yang-Xin Fu. 2013. "Innate and Adaptive Immune Cells in the Tumor Microenvironment." *Nature Immunology* 14:1014.
- Galganski, Lukasz, Martyna O. Urbanek, and Wlodzimierz J. Krzyzosiak. 2017. "Nuclear Speckles: Molecular Organization, Biological Function and Role in Disease." *Nucleic Acids Research* 45(18):10350–68.
- Gallagher, Denis, Anastassia Voronova, Mark A. Zander, Gonzalo I. Cancino, Alexa Bramall, Matthew P. Krause, Clemer Abad, Mustafa Tekin, Paul M. Neilsen, David F. Callen, Freda D. Miller. et al. 2015. "Ankrd11 Is a Chromatin Regulator Involved in Autism That Is Essential for Neural Development." *Developmental Cell* 32(1):31–42.
- Gastwirt, Randy F., Daniela A. Slavin, Christopher W. McAndrew, and Daniel J. Donoghue. 2006. "Spy1 Expression Prevents Normal Cellular Responses to DNA Damage: Inhibition of Apoptosis and Checkpoint Activation." *Journal of Biological Chemistry* 281(46):35425–35.
- Gisselsson, David, Jonas Björk, Mattias Höglund, Fredrik Mertens, Paola Dal Cin, Måns Åkerman, and Nils Mandahl. 2001. "Abnormal Nuclear Shape in Solid Tumors Reflects Mitotic Instability." *American Journal of Pathology* 158(1):199–206.
- Golipour, Azadeh, Dorothy Myers, Tiffany Seagroves, Daniel Murphy, Gerard I. Evan, Daniel J. Donoghue, Roger A. Moorehead, and Lisa A. Porter. 2008. "The Spy1/RINGO Family Represents a Novel Mechanism Regulating Mammary Growth and Tumorigenesis." *Cancer Research* 68(10):3591–3600.

References

- Götz, Magdalena and Wieland B. Huttner. 2005. "The Cell Biology of Neurogenesis." *Nature Reviews Molecular Cell Biology* 6(10):777–88.
- Gstaiger, Matthias, Richard Jordan, Megan Lim, Charles Catzavelos, Jürgen Mestan, Joyce Slingerland, and Wilhelm Krek. 2001. "Skp2 Is Oncogenic and Overexpressed in Human Cancers." *Proceedings of the National Academy of Sciences of the United States of America* 98(9):5043–48.
- Gu, Y., J. Rosenblatt, and D. O. Morgan. 1992. "Cell Cycle Regulation of CDK2 Activity by Phosphorylation of Thr160 and Tyr15." *The EMBO Journal* 11(11):3995–4005.
- Gusel'nikova, V. V. and D. E. Korzhevskiy. 2015. "NeuN as a Neuronal Nuclear Antigen and Neuron Differentiation Marker." *Acta Naturae* 7(2):42–47.
- Gutierrez, Gustavo J., Andrea Vöggtlin, Ana Castro, Ingvar Ferby, Giorgia Salvagiotto, Ze'ev Ronai, Thierry Lorca, and Angel R. Nebreda. 2006. "Meiotic Regulation of the CDK Activator RINGO/Speedy by Ubiquitin-Proteasome-Mediated Processing and Degradation." *Nature Cell Biology* 8(10):1084–94.
- Guy, C. T., R. D. Cardiff, and W. J. Muller. 2015. "Induction of Mammary Tumors by Expression of Polyomavirus Middle T Oncogene: A Transgenic Mouse Model for Metastatic Disease." *Molecular and Cellular Biology* 12(3):954–61.
- Haarhuis, Judith H. I., Robin H. van der Weide, Vincent A. Blomen, J. Omar Yáñez-Cuna, Mario Amendola, Marjon S. van Ruiten, Peter H. L. Krijger, Hans Teunissen, René H. Medema, Bas van Steensel, Benjamin D. Rowland et al. 2017. "The Cohesin Release Factor WAPL Restricts Chromatin Loop Extension." *Cell* 169(4):693-707.e14.
- Hanahan, Douglas and Robert A. Weinberg. 2011. "Hallmarks of Cancer: The next Generation." *Cell*.144: 646-674.
- Hartwell, L. H., J. Culotti, and B. Reid. 1970. "Genetic Control of the Cell-Division Cycle in Yeast. I. Detection of Mutants." *Proceedings of the National Academy of Sciences of the United States of America* 66(2):352–59.
- Heldin, Carl Henrik. 2012. "Autocrine PDGF Stimulation in Malignancies." *Upsala Journal of Medical Sciences* 117(2):83–91.
- Helleday, Thomas, Eva Petermann, Cecilia Lundin, Ben Hodgson, and Ricky A. Sharma. 2008. "DNA Repair Pathways as Targets for Cancer Therapy." *Nature Reviews Cancer* 8(3):193–204.
- Herrmann, Andreas, Katrin Fleischer, Hanna Czajkowska, Gerhard Müller-Newen, and Walter Becker. 2007. "Characterization of Cyclin L1 as an Immobile Component of the Splicing Factor Compartment." *The FASEB Journal* 21(12):3142–52.
- Hershko, Dan D. 2008. "Oncogenic Properties and Prognostic Implications of the Ubiquitin Ligase Skp2 in Cancer." *Cancer* 112(7):1415–24.
- Hirasawa, Motoyuki, Toshio Ohshima, Satoru Takahashi, Glenn Longenecker, Yasuyuki Honjo, Veeranna, Roscoe O. Brady, and Ashok B. Kulkarni. 2004. "Perinatal Abrogation of Cdk5 Expression in Brain Results in Neuronal Migration Defects." *Proceedings of the National Academy of Sciences of the United States of America* 101(16):6249–54.

- Huertas, Pablo, Felipe Cortés-Ledesma, Alessandro A. Sartori, Andrés Aguilera, and Stephen P. Jackson. 2008. "CDK Targets Sae2 to Control DNA-End Resection and Homologous Recombination." *Nature* 455(7213):689–92.
- Iarovaia, Olga V., Elizaveta P. Minina, Eugene V. Sheval, D. Onichtchouk, Svetlana Dokudovskaya, Sergey V. Razin, and Yegor S. Vassetzky. 2019. "Nucleolus: A Central Hub for Nuclear Functions." *Trends in Cell Biology* 29(8):647–59.
- Jablonska, Beata, Adan Aguirre, Renaud Vandenbosch, Shibeshih Belachew, Cyril Berthet, Philipp Kaldis, and Vittorio Gallo. 2007. "Cdk2 Is Critical for Proliferation and Self-Renewal of Neural Progenitor Cells in the Adult Subventricular Zone." *Journal of Cell Biology* 179(6):1231–45.
- Jeffrey, Philip D., Alicia A. Russo, Kornelia Polyak, Emma Gibbs, Jerard Hurwitz, Joan Massagué, and Nikola P. Pavletich. 1995. "Mechanism of CDK Activation Revealed by the Structure of a CyclinA-CDK2 Complex." *Nature* 376(6538):313–20.
- Jin, Kunlin, Manabu Minami, Jing Q. Lan, Xiao Ou Mao, Sophie Batteur, Roger P. Simon, and David A. Greenberg. 2001. "Neurogenesis in Dentate Subgranular Zone and Rostral Subventricular Zone after Focal Cerebral Ischemia in the Rat." *Proceedings of the National Academy of Sciences of the United States of America* 98(8):4710–15.
- Jin, Qin, Gang Liu, Luri Bao, Yuzhen Ma, Huidong Qi, Zhizhong Yun, Yanfeng Dai, and Shu Zhang. 2018. "High Spy1 Expression Predicts Poor Prognosis in Colorectal Cancer." *Cancer Management and Research* 10:2757–65.
- Jonkers, Jos, Ralph Meuwissen, Hanneke van der Gulden, Hans Peterse, Martin van der Valk, and Anton Berns. 2001. "Synergistic Tumor Suppressor Activity of BRCA2 and P53 in a Conditional Mouse Model for Breast Cancer." *Nature Genetics* 29(4):418–25.
- Karaiskou, Anthi, Laurent H. Perez, Ingvar Ferby, René Ozon, Catherine Jesus, and Angel R. Nebreda. 2001. "Differential Regulation of Cdc2 and Cdk2 by RINGO and Cyclins." *Journal of Biological Chemistry* 276(38):36028–34.
- Kastan, Michael B. and Jiri Bartek. 2004. "Cell-Cycle Checkpoints and Cancer." *Nature* 432(7015):316–23.
- Kastenhuber, Edward R. and Scott W. Lowe. 2017. "Putting P53 in Context." *Cell* 170(6):1062–78.
- Kim, Seong Tae, Bo Xu, and Michael B. Kastan. 2002. "Involvement of the Cohesin Protein, Smc1, in Atm-Dependent and Independent Responses to DNA Damage." *Genes and Development* 16(5):560–70.
- Kippin, Tod E., David J. Martens, and Derek Van Der Kooy. 2005. "P21 Loss Compromises the Relative Quiescence of Forebrain Stem Cell Proliferation Leading To Exhaustion of Their Proliferation Capacity." *Genes and Development* 19(6):756–67.
- Kitagawa, Risa, Christopher J. Bakkenist, Peter J. McKinnon, and Michael B. Kastan. 2004. "Phosphorylation of SMC1 Is a Critical Downstream Event in the ATM-NBS1-BRCA1 Pathway." *Genes and Development* 18(12):1423–38.

References

- Ko, Jane, Sandrine Humbert, Roderick T. Bronson, Satoru Takahashi, Ashok B. Kulkarni, En Li, and Li Huei Tsai. 2001. "P35 and P39 Are Essential for Cyclin-Dependent Kinase 5 Function During Neurodevelopment." *Journal of Neuroscience* 21(17):6758–71.
- Koepp, Deanna M., Laura K. Schaefer, Xin Ye, Khandan Keyomarsi, Claire Chu, J. Wade Harper, and Stephen J. Elledge. 2001. "Phosphorylation-Dependent Ubiquitination of Cyclin E by the SCF^{ɪ}Fbw7^{ɪ} Ubiquitin Ligase." *Science* 294(5540):173 LP – 177.
- Kowalczyk, Anna, Robert K. Filipkowski, Marcin Rylski, Grzegorz M. Wilczynski, Filip A. Konopacki, Jacek Jaworski, Maria A. Ciemerych, Piotr Sicinski, and Leszek Kaczmarek. 2004. "The Critical Role of Cyclin D2 in Adult Neurogenesis." *Journal of Cell Biology* 167(2):209–13.
- Kriegstein, Arnold and Arturo Alvarez-Buylla. 2009. "The Glial Nature of Embryonic and Adult Neural Stem Cells." *Annual Review of Neuroscience* 32(1):149–84.
- Kueng, Stephanie, Björn Hegemann, Beate H. Peters, Jesse J. Lipp, Alexander Schleiffer, Karl Mechtler, and Jan Michael Peters. 2006. "Wapl Controls the Dynamic Association of Cohesin with Chromatin." *Cell* 127(5):955–67.
- Ladurner, Rene, Emanuel Kreidl, Miroslav P. Ivanov, Heinz Ekker, Maria Helena Idarraga-Amado, Georg A. Busslinger, Gordana Wutz, David A. Cisneros, and Jan-Michael Peters. 2016. "Sororin Actively Maintains Sister Chromatid Cohesion." *The EMBO Journal* 35(6):635–53.
- Lagace, Diane C., David R. Benavides, Janice W. Kansy, Marina Mapelli, Paul Greengard, James A. Bibb, and Amelia J. Eisch. 2008. "Cdk5 Is Essential for Adult Hippocampal Neurogenesis." *Proceedings of the National Academy of Sciences of the United States of America* 105(47):18567–71.
- Lamond, Angus I. and David L. Spector. 2003. "Nuclear Speckles: A Model for Nuclear Organelles." *Nature Reviews Molecular Cell Biology* 4(8):605–12.
- Lange, Christian, Wieland B. Huttner, and Federico Calegari. 2009. "Cdk4/CyclinD1 Overexpression in Neural Stem Cells Shortens G1, Delays Neurogenesis, and Promotes the Generation and Expansion of Basal Progenitors." *Cell Stem Cell* 5(3):320–31.
- Lecona, Emilio and Oscar Fernandez-Capetillo. 2018. "Targeting ATR in Cancer." *Nature Reviews Cancer* 18(9):586–95.
- Lenormand, J. L. 1999. "Speedy: A Novel Cell Cycle Regulator of the G2/M Transition." *The EMBO Journal* 18(7):1869–77.
- Li, Rong and David F. Albertini. 2013. "The Road to Maturation: Somatic Cell Interaction and Self-Organization of the Mammalian Oocyte." *Nature Reviews Molecular Cell Biology* 14(3):141–52.
- Liang, Cai, Qinfu Chen, Qi Yi, Miao Zhang, Haiyan Yan, Bo Zhang, Linli Zhou, Zhenlei Zhang, Feifei Qi, Sheng Ye, and Fangwei Wang. 2018. "A Kinase-dependent Role for Haspin in Antagonizing Wapl and Protecting Mitotic Centromere Cohesion." *EMBO Reports* 19(1):43–56.

- Lim, Shuhui and Philipp Kaldis. 2012. "Loss of Cdk2 and Cdk4 Induces a Switch from Proliferation to Differentiation in Neural Stem Cells." *Stem Cells* 30(7):1509–20.
- Liu, F., J. J. Stanton, Z. Wu, and H. Piwnica-Worms. 1997. "The Human Myt1 Kinase Preferentially Phosphorylates Cdc2 on Threonine 14 and Localizes to the Endoplasmic Reticulum and Golgi Complex." *Molecular and Cellular Biology* 17(2):571 LP – 583.
- Llorens-Bobadilla, Enric, Sheng Zhao, Avni Baser, Gonzalo Saiz-Castro, Klara Zwadlo, and Ana Martin-Villalba. 2015. "Single-Cell Transcriptomics Reveals a Population of Dormant Neural Stem Cells That Become Activated upon Brain Injury." *Cell Stem Cell* 17(3):329–40.
- Loonstra, Ate, Marc Vooijs, H. Berna Beverloo, Bushra Al Allak, Ellen Van Drunen, Roland Kanaar, Anton Berns, and Jos Jonkers. 2001. "Growth Inhibition and DNA Damage Induced by Cre Recombinase in Mammalian Cells." *Proceedings of the National Academy of Sciences of the United States of America* 98(16):9209–14.
- Lord, Christopher J. and Alan Ashworth. 2017. "In the Clinic." 1158(March):1152–58.
- Losada, Ana. 2014. "Cohesin in Cancer: Chromosome Segregation and Beyond." *Nature Reviews Cancer* 14(6):389–93.
- Loyer, Pascal, Janeen H. Trembley, Jose A. Grenet, Adeline Busson, Anne Corlu, Wei Zhao, Mehmet Kocak, Vincent J. Kidd, and Jill M. Lahti. 2008. "Characterization of Cyclin L1 and L2 Interactions with CDK11 and Splicing Factors: Influence of Cyclin I Isoforms on Splice Site Selection." *Journal of Biological Chemistry* 283(12):7721–32.
- Lu, Shumin, Rong Liu, Min Su, Yingze Wei, Shuyun Yang, Song He, Xia Wang, Fulin Qiang, Chen Chen, Shuyang Zhao, Weiwei Zhang, Pan Xu, and Guoxin Mao. 2016. "Spy1 Participates in the Proliferation and Apoptosis of Epithelial Ovarian Cancer." *Journal of Molecular Histology* 47(1):47–57.
- Lubanska, Dorota, Brenna A. Market-Velker, Ana C. deCarvalho, Tom Mikkelsen, Elizabeth FidalgoSilva, and Lisa A. Porter. 2014. "The Cyclin-like Protein Spy1 Regulates Growth and Division Characteristics of the CD133+ Population in Human Glioma." *Cancer Cell* 25(1):64–76.
- Lukas, Claudia, Claus Storgaard Sørensen, Edgar Kramer, Eric Santoni-Rugiu, Claes Lindeneg, Jan-Michael Peters, Jiri Bartek, and Jiri Lukas. 1999. "Accumulation of Cyclin B1 Requires E2F and Cyclin-A-Dependent Rearrangement of the Anaphase-Promoting Complex." *Nature* 401(6755):815–18.
- Lukas, Jiri, Claudia Lukas, and Jiri Bartek. 2004. "Mammalian Cell Cycle Checkpoints: Signalling Pathways and Their Organization in Space and Time." *DNA Repair* 3(8–9):997–1007.
- Luo, Hao, Yehua Li, Jung Jung Mu, Jinglan Zhang, Toru Tonaka, Yasuo Hamamori, Yun Jung Sung, Yi Wang, and Jun Qin. 2008. "Regulation of Intra-S Phase Checkpoint by Ionizing Radiation (IR)-Dependent and IR-Independent Phosphorylation of SMC3." *Journal of Biological Chemistry* 283(28):19176–83.
- Luo, Ji, Nicole L. Solimini, and Stephen J. Elledge. 2009. "Principles of Cancer Therapy: Oncogene and Non-Oncogene Addiction." *Cell* 136(5):823–37.

References

- Malumbres, Marcos. 2014. "Cyclin-Dependent Kinases." *Genome Biology* 15(6):122.
- Malumbres, Marcos and Mariano Barbacid. 2009. "Cell Cycle, CDKs and Cancer: A Changing Paradigm." *Nature Reviews Cancer* 9(3):153–66.
- Malumbres, Marcos, Rocío Sotillo, David Santamaría, Javier Galán, Ana Cerezo, Sagrario Ortega, Pierre Dubus, and Mariano Barbacid. 2004. "Mammalian Cells Cycle without the D-Type Cyclin-Dependent Kinases Cdk4 and Cdk6." *Cell* 118(4):493–504.
- Marqués-Torrejón, M. Ángeles, Eva Porlan, Ana Banito, Esther Gómez-Ibarlucea, Andrés J. Lopez-Contreras, Óscar Fernández-Capetillo, Anxo Vidal, Jesús Gil, Josema Torres, and Isabel Fariñas. 2013. "Cyclin-Dependent Kinase Inhibitor P21 Controls Adult Neural Stem Cell Expansion by Regulating Sox2 Gene Expression." *Cell Stem Cell* 12(1):88–100.
- Marston, Adèle L., Angelika Amon, and Howard Hughes Medical. 2004. "Meiosis : Cell-Cycle controls shuffle and deal." 5-10.
- Mazouzi, Abdelghani, Georgia Velimezi, and Joanna I. Loizou. 2014. "DNA Replication Stress: Causes, Resolution and Disease." *Experimental Cell Research* 329(1):85–93.
- McAndrew, Christopher W., Randy F. Gastwirt, April N. Meyer, Lisa A. Porter, and Daniel J. Donoghue. 2007. "Spy1 Enhances Phosphorylation and Degradation of the Cell Cycle Inhibitor P27." *Cell Cycle* 6(15):1937–45.
- McGrath, Denise A., Bre-Anne Fifield, Aimee H. Marceau, Sarvind Tripathi, Lisa A. Porter, and Seth M. Rubin. 2017. "Structural Basis of Divergent Cyclin-dependent Kinase Activation by Spy1/RINGO Proteins." *The EMBO Journal* 36(15):2251–62.
- Mehta, Anuja and James E. Haber. 2014. "Sources of DNA Double-Strand Breaks and Models of Recombinational DNA Repair." *Cold Spring Harbor Perspectives in Biology* 6(9):1–19.
- Michael, W. Matthew and John Newport. 1998. "Coupling of Mitosis to the Completion of S Phase Through Cdc34-Mediated Degradation of Wee1." *Science* 282(5395):1886 LP – 1889.
- Mikolcevic, Petra, Michitaka Isoda, Hiroki Shibuya, Ivan Del Barco Barrantes, Ana Igea, José A. Suja, Sue Shackleton, Yoshinori Watanabe, and Angel R. Nebreda. 2016. "Essential Role of the Cdk2 Activator RingoA in Meiotic Telomere Tethering to the Nuclear Envelope." *Nature Communications* 7:11084.
- Ming, Guo li and Hongjun Song. 2011. "Adult Neurogenesis in the Mammalian Brain: Significant Answers and Significant Questions." *Neuron* 70(4):687–702.
- Mitchison, T. J. and E. D. Salmon. 2001. "Mitosis: A History of Division." *Nature Cell Biology* 3(1):17–21.
- Montagnoli, Alessia, Francesca Fiore, Esther Eytan, Andrea C. Carrano, Giulio F. Draetta, Avram Hershko, and Michele Pagano. 1999. "Ubiquitination of P27 Is Regulated by Cdk-Dependent Phosphorylation and Trimeric Complex Formation." *Genes and Development* 13(9):1181–89.
- Moriel-Carretero, María, Sara Ovejero, Marie Gêrus-Durand, Dimos Vryzas, and Angelos Constantinou. 2017. "Fanconi Anemia FAN CD2 and FAN CI Proteins Regulate the Nuclear Dynamics of Splicing Factors." *Journal of Cell Biology* 216(12):4007–26.

- Mueller, Paul R., Thomas R. Coleman, Akiko Kumagai, and William G. Dunphy. 1995. "Myt1: A Membrane-Associated Inhibitory Kinase That Phosphorylates Cdc2 on Both Threonine-14 and Tyrosine-15." *Science* 270(5233):86 LP – 90.
- Murphy, Martin, Marie Georges Stinnakre, Catherine Senamaud-Beaufort, Nicola J. Winston, Claire Sweeney, Michal Kubelka, Mark Carrington, Christian Bréchet, and Joëlle Sobczak-Thépot. 1997. "Delayed Early Embryonic Lethality Following Disruption of the Murine Cyclin A2 Gene." *Nature Genetics* 15(1):83–86.
- Nagano, Takashi, Yaniv Lubling, Csilla Várnai, Carmel Dudley, Wing Leung, Yael Baran, Netta Mendelson Cohen, Steven Wingett, Peter Fraser, and Amos Tanay. 2017. "Cell-Cycle Dynamics of Chromosomal Organization at Single-Cell Resolution." *Nature* 547(7661):61–67.
- Nagy, Andras. 2000. "Cre Recombinase: The Universal Reagent for Genome Tailoring." *Genesis* 26(2):99–109.
- Nam, Edward.A. and David Cortez. 2011. "ATR Signalling: More than Meeting at the Fork." *Biochemical Journal* 436(3):527–36.
- Nebreda, Angel R. 2006. "CDK Activation by Non-Cyclin Proteins." *Current Opinion in Cell Biology* 18(2):192–98.
- Nebreda, Angel R. and Ingvar Ferby. 2000. "Regulation of the Meiotic Cell Cycle in Oocytes." *Current Opinion in Cell Biology* 12(6):666–75.
- Negrini, Simona, Vassilis G. Gorgoulis, and Thanos D. Halazonetis. 2010. "Genomic Instability an Evolving Hallmark of Cancer." *Nature Reviews Molecular Cell Biology* 11(3):220–28.
- Neilsen, P. M., K. M. Cheney, C. W. Li, J. D. Chen, J. E. Cawrse, R. B. Schulz, J. A. Powell, R. Kumar, and D. F. Callen. 2008. "Identification of ANKRD11 as a P53 Coactivator." *Journal of Cell Science* 121(21):3541–52.
- Neumann, Beate, Thomas Walter, Jean-Karim Hériché, Jutta Bulkescher, Holger Erfle, Christian Conrad, Phill Rogers, Ina Poser, Wolfgang Huber, Jan-Michael Peters, Anthony A. Hyman, Richard Durbin, Rainer Pepperkok, and Jan Ellenberg, et al. 2010. "Phenotypic Profiling of the Human Genome by Time-Lapse Microscopy Reveals Cell Division Genes." *Nature* 464(7289):721–27.
- Nishiyama, T., M. M. Sykora, P. J. Huis in 't Veld, K. Mechtler, and J. M. Peters. 2013. "Aurora B and Cdk1 Mediate Wapl Activation and Release of Acetylated Cohesin from Chromosomes by Phosphorylating Sororin." *Proceedings of the National Academy of Sciences* 110(33):13404–9.
- Nishiyama, Tomoko, Rene Ladurner, Julia Schmitz, Emanuel Kreidl, Alexander Schleiffer, Venugopal Bhaskara, Masashige Bando, Katsuhiko Shirahige, Anthony A. Hyman, Karl Mechtler, and Jan Michael Peters. 2010. "Sororin Mediates Sister Chromatid Cohesion by Antagonizing Wapl." *Cell* 143(5):737–49.
- Nozaki, Tadasu, Ryosuke Imai, Mai Tanbo, Ryosuke Nagashima, Sachiko Tamura, Tomomi Tani, Yasumasa Joti, Masaru Tomita, Kayo Hibino, Masato T. Kanemaki, Kerstin S. Wendt, Kazuhiro Maeshima, et al. 2017. "Dynamic Organization of Chromatin Domains Revealed by Super-Resolution Live-Cell Imaging." *Molecular Cell* 67(2):282-293.e7.

References

- Nurse, Paul. 1975. "Genetic Control of Cell Size at Cell Division in Yeast." *Nature* 256(5518):547–51.
- Ohshima, T., J. M. Ward, C. G. Huh, G. Longenecker, Veeranna, H. C. Pant, R. O. Brady, L. J. Martin, and A. B. Kulkarni. 1996. "Targeted Disruption of the Cyclin-Dependent Kinase 5 Gene Results in Abnormal Corticogenesis, Neuronal Pathology and Perinatal Death." *Proceedings of the National Academy of Sciences* 93(20):11173 LP – 11178.
- Ortega, Sagrario, Ignacio Prieto, Junko Odajima, Alberto Martín, Pierre Dubus, Rocio Sotillo, Jose Luis Barbero, Marcos Malumbres, and Mariano Barbacid. 2003. "Cyclin-Dependent Kinase 2 Is Essential for Meiosis but Not for Mitotic Cell Division in Mice." *Nature Genetics* 35(1):25–31.
- Otto, Tobias and Piotr Sicinski. 2017. "Cell Cycle Proteins as Promising Targets in Cancer Therapy." *Nature Reviews Cancer* 17(2):93–115.
- Ottone, Cristina, Benjamin Krusche, Ariadne Whitby, Melanie Clements, Giorgia Quadrato, Mara E. Pitulescu, Ralf H. Adams, and Simona Parrinello. 2014. "Direct Cell–Cell Contact with the Vascular Niche Maintains Quiescent Neural Stem Cells." *Nature Cell Biology* 16:1045.
- Pagano, M., R. Pepperkok, F. Verde, W. Ansorge, and G. Draetta. 1992. "Cyclin A Is Required at Two Points in the Human Cell Cycle." *The EMBO Journal* 11(3):961–71.
- Pastrana, Erika, Violeta Silva-Vargas, and Fiona Doetsch. 2011. "Eyes Wide Open: A Critical Review of Sphere-Formation as an Assay for Stem Cells." *Cell Stem Cell* 8(5):486–98.
- Pérez de Castro, Ignacio, Guillermo de Cárcer, and Marcos Malumbres. 2007. "A Census of Mitotic Cancer Genes: New Insights into Tumor Cell Biology and Cancer Therapy." *Carcinogenesis* 28(5):899–912.
- Peters, Jan Michael and Tomoko Nishiyama. 2012. "Sister Chromatid Cohesion." *Cold Spring Harbor Perspectives in Biology* 4(11).
- Peters, Jan Michael, Antonio Tedeschi, and Julia Schmitz. 2008. "The Cohesin Complex and Its Roles in Chromosome Biology." *Genes and Development* 22(22):3089–3114.
- Phair, Robert D. and Tom Misteli. 2000. "High Mobility of Proteins in the Mammalian Cell Nucleus." *Nature* 404(6778):604–9.
- Phillips, Bart T., Kathrin Gassei, and Kyle E. Orwig. 2010. "Spermatogonial Stem Cell Regulation and Spermatogenesis." *Philosophical Transactions of the Royal Society B: Biological Sciences* 365(1546):1663–78.
- Pietras, Kristian and Arne Östman. 2010. "Hallmarks of Cancer: Interactions with the Tumor Stroma." *Experimental Cell Research* 316(8):1324–31.
- Ponti, Giovanna Ponti, Kirsten Obernier, and Arturo Alvarez-Buylla. 2013. "Lineage Progression from Stem Cells to New Neurons in the Adult Brain Ventricularsubventricular Zone." *Cell Cycle* 12(11):1649–50.

- Porlan, Eva, José Manuel Morante-Redolat, María Ángeles Marqués-Torrejón, Celia Andreu-Agulló, Carmen Carneiro, Esther Gómez-Ibarlucea, Atenea Soto, Anxo Vidal, Sacri R. Ferrón, and Isabel Fariñas. 2013. "Transcriptional Repression of Bmp2 by P21 Waf1/Cip1 Links Quiescence to Neural Stem Cell Maintenance." *Nature Neuroscience* 16(11):1567–75.
- Porter, Lisa A., Ryan W. Dellinger, John A. Tynan, Elizabeth A. Barnes, Monica Kong, Jean Luc Lenormand, and Daniel J. Donoghue. 2002. "Human Speedy: A Novel Cell Cycle Regulator That Enhances Proliferation through Activation of Cdk2." *Journal of Cell Biology* 157(3):357–66.
- Porter, Lisa A., Monica Kong-Beltran, and Daniel J. Donoghue. 2003. "Spy1 Interacts with P27Kip1 to Allow G1/S Progression." *Molecular Biology of the Cell* 14(9):3664–74.
- Potapova, Tamara A., John R. Daum, Bradley D. Pittman, Joanna R. Hudson, Tara N. Jones, David L. Satinover, P. Todd Stukenberg, and Gary J. Gorbsky. 2006. "The Reversibility of Mitotic Exit in Vertebrate Cells." *Nature* 440(7086):954–58.
- Qiu, Jianhua, Yasushi Takagi, Jun Harada, Kamil Topalkara, Yumei Wang, John R. Sims, Guoguang Zheng, Paulina Huang, Yun Ling, David T. Scadden, Michael A. Moskowitz, and Tao Cheng. 2009. "P27Kip1 Constrains Proliferation of Neural Progenitor Cells in Adult Brain under Homeostatic and Ischemic Conditions." *Stem Cells* 27(4):920–27.
- Quandt, Eva, Mariana P. C. Ribeiro, and Josep Clotet. 2019. "Atypical Cyclins: The Extended Family Portrait." *Cellular and Molecular Life Sciences* (0123456789).
- Quinet, Annabel, Denisse Carvajal-Maldonado, Delphine Lemacon, and Alessandro Vindigni. 2017. *DNA Fiber Analysis: Mind the Gap!* Vol. 591. 1st ed. Elsevier Inc.
- Quinodoz, Sofia A., Noah Ollikainen, Barbara Tabak, Ali Palla, Jan Marten Schmidt, Elizabeth Detmar, Mason M. Lai, Alexander A. Shishkin, Prashant Bhat, Yodai Takei, Vickie Trinh, Mitchell Guttman, et al. 2018. "Higher-Order Inter-Chromosomal Hubs Shape 3D Genome Organization in the Nucleus." *Cell* 174(3):744-757.e24.
- Reig-viader, Rita and Aurora Ruiz-herrera. 2016. "Telomere Homeostasis in Mammalian Germ Cells : A Review." *Chromosoma* 337–51.
- Roux, Kyle J., Dae In Kim, Manfred Raida, and Brian Burke. 2012. "A Promiscuous Biotin Ligase Fusion Protein Identifies Proximal and Interacting Proteins in Mammalian Cells." *Journal of Cell Biology* 196(6):801–10.
- Ruiz, E. Josué, Tim Hunt, and Angel R. Nebreda. 2008. "Meiotic Inactivation of Xenopus Myt1 by CDK/XRINGO, but Not CDK/Cyclin, via Site-Specific Phosphorylation." *Molecular Cell* 32(2):210–20.
- Ruzankina, Yaroslava, Carolina Pinzon-Guzman, Amma Asare, Tony Ong, Laura Pontano, George Cotsarelis, Valerie P. Zediak, Marielena Velez, Avinash Bhandoola, and Eric J. Brown. 2007. "Deletion of the Developmentally Essential Gene ATR in Adult Mice Leads to Age-Related Phenotypes and Stem Cell Loss." *Cell Stem Cell* 1(1):113–26.

References

- Sablina, Anna A., Galina V. Ilyinskaya, Svetlana N. Rubtsova, Larissa S. Agapova, Peter M. Chumakov, and Boris P. Kopnin. 1998. "Activation of P53-Mediated Cell Cycle Checkpoint in Response to Micronuclei Formation." *Journal of Cell Science* 111(7):977--84.
- Santamaría, David, Cédric Barrière, Antonio Cerqueira, Sarah Hunt, Claudine Tardy, Kathryn Newton, Javier F. Cáceres, Pierre Dubus, Marcos Malumbres, and Mariano Barbacid. 2007. "Cdk1 Is Sufficient to Drive the Mammalian Cell Cycle." *Nature* 448(7155):811--15.
- Sebastian, B., A. Kakizuka, and T. Hunter. 1993. "Cdc25M2 Activation of Cyclin-Dependent Kinases by Dephosphorylation of Threonine-14 and Tyrosine-15." *Proceedings of the National Academy of Sciences* 90(8):3521 LP – 3524.
- Shah, Fouziya R., Younus A. Bhat, and Ajazul H. Wani. 2018. "Subnuclear Distribution of Proteins: Links with Genome Architecture." *Nucleus* 9(1):42–55.
- Sheaff, Robert J., Mark Groudine, and James M. Roberts. 1997. "Cyclin E-CDK2 Is a Regulator of P27 Kip1." 1464–78.
- Shen, Qin, Susan K. Goderie, Li Jin, Nithin Karanth, Yu Sun, Natalia Abramova, Peter Vincent, Kevin Pumiglia, and Sally Temple. 2004. "Endothelial Cells Stimulate Self-Renewal and Expand Neurogenesis of Neural Stem Cells." *Science* 304(5675):1338 LP – 1340.
- Sherr, Charles J. and James M. Roberts. 1999. "CDK Inhibitors: Positive and Negative Regulators of G1-Phase Progression." *Genes and Development* 13(12):1501–12.
- Shin, Yongdae and Clifford P. Brangwynne. 2017. "Liquid Phase Condensation in Cell Physiology and Disease." *Science* 357(6357).
- Shupp, Alison, Mathew C. Casimiro, and Richard G. Pestell. 2017. "Biological Functions of CDK5 and Potential CDK5 Targeted Clinical Treatments." *Oncotarget* 8(10):17373–82.
- Simpson, Andrew J. G., Otavia L. Caballero, Achim Jungbluth, Yao-Tseng Chen, and Lloyd J. Old. 2005. "Cancer/Testis Antigens, Gametogenesis and Cancer." *Nature Reviews Cancer* 5(8):615–25.
- Singec, Ilyas, Rolf Knoth, Ralf P. Meyer, Jaroslaw Maciaczyk, Benedikt Volk, Guido Nikkhah, Michael Frotscher, and Evan Y. Snyder. 2006. "Defining the Actual Sensitivity and Specificity of the Neurosphere Assay in Stem Cell Biology" *Nature Methods* 3(10):801--6.
- Smogorzewska, Agata, Shuhei Matsuoka, Patrizia Vinciguerra, E. Robert McDonald, Kristen E. Hurov, Ji Luo, Bryan A. Ballif, Steven P. Gygi, Kay Hofmann, Alan D. D'Andrea, and Stephen J. Elledge. 2007. "Identification of the FANCI Protein, a Monoubiquitinated FANCD2 Paralog Required for DNA Repair." *Cell* 129(2):289–301.
- Söderberg, Ola, Karl Johan Leuchowius, Mats Gullberg, Malin Jarvius, Irene Weibrecht, Lars Gunnar Larsson, and Ulf Landegren. 2008. "Characterizing Proteins and Their Interactions in Cells and Tissues Using the in Situ Proximity Ligation Assay." *Methods* 45(3):227–32.

- Al Sorkhy, Mohammad, Ryan Craig, Brenna Market, Ryan Ard, and Lisa A. Porter. 2009. "The Cyclin-Dependent Kinase Activator, Spy1A, Is Targeted for Degradation by the Ubiquitin Ligase NEDD4." *Journal of Biological Chemistry* 284(5):2617–27.
- Al Sorkhy, Mohammad, Rosa Maria Ferraiuolo, Espanta Jalili, Agnes Malysa, Andreea R. Fratiloiu, Bonnie F. Sloane, and Lisa A. Porter. 2012. "The Cyclin-like Protein Spy1/RINGO Promotes Mammary Transformation and Is Elevated in Human Breast Cancer." *BMC Cancer* 12(1):1–14.
- Al Sorkhy, Mohammad Al, Bre-anne Fifield, Dorothy Myers, Lisa A. Porter, Mohammad Al, Bre-anne Fifield, Dorothy Myers, and Lisa A. Porter. 2016. "Direct Interactions with Both P27 and Cdk2 Regulate Spy1-Mediated Proliferation in Vivo and in Vitro." *Cell Cycle* 15(1):128–36.
- Ström, Lena, Hanna Betts Lindroos, Katsuhiko Shirahige, and Camilla Sjögren. 2004. "Postreplicative Recruitment of Cohesin to Double-Strand Breaks Is Required for DNA Repair." *Molecular Cell* 16(6):1003–15.
- Subramanian, Vijayalakshmi V. and Andreas Hochwagen. 2014. "The Meiotic Checkpoint Network: Step-by-Step through Meiotic Prophase." *Cold Spring Harbor Perspectives in Biology* 6(10).
- Sun, Min, Qingqing Yuan, Minghui Niu, Hong Wang, Liping Wen, Chencheng Yao, Jingmei Hou, Zheng Chen, Hongyong Fu, Fan Zhou, Chong Li, Shaorong Gao, Wei-Qiang Gao, Zheng Li, and Zuping He. 2018. "Efficient Generation of Functional Haploid Spermatids from Human Germline Stem Cells by Three-Dimensional-Induced System." *Cell Death & Differentiation* 25(4):749–66.
- Szklarczyk, Damian, Andrea Franceschini, Stefan Wyder, Kristoffer Forslund, Davide Heller, Jaime Huerta-Cepas, Milan Simonovic, Alexander Roth, Alberto Santos, Kalliopi P. Tsafou, Christian Von Mering, et al. 2015. "STRING V10: Protein-Protein Interaction Networks, Integrated over the Tree of Life." *Nucleic Acids Research* 43(D1):D447–52.
- Tang, D., J. Yeung, K. Y. Lee, M. Matsushita, H. Matsui, K. Tomizawa, O. Hatase, and J. H. Wang. 1995. "An Isoform of the Neuronal Cyclin-Dependent Kinase 5 (Cdk5) Activator." *Journal of Biological Chemistry* 270(45):26897–903.
- Taricani, Lorena, Frances Shanahan, and David Parry. 2009. "Replication Stress Activates DNA Polymerase Alpha-Associated Chk1." *Cell Cycle* 8(3):482–89.
- Tedeschi, Antonio, Gordana Wutz, Sébastien Huet, Markus Jaritz, Annelie Wuensche, Erika Schirghuber, Iain Finley Davidson, Wen Tang, David A. Cisneros, Venugopal Bhaskara, Tomoko Nishiyama, Jan Michael Peters, et al. 2013. "Wapl Is an Essential Regulator of Chromatin Structure and Chromosome Segregation." *Nature* 501(7468):564–68.
- Terret, Marie Emilie, Rebecca Sherwood, Sadia Rahman, Jun Qin, and Prasad V. Jallepalli. 2009. "Cohesin Acetylation Speeds the Replication Fork." *Nature* 462(7270):231–34.
- Testa, Giuseppe, Julia Schaft, Frank Van Der Hoeven, Stefan Glaser, Konstantinos Anastassiadis, Youming Zhang, Thomas Hermann, Wolfgang Stremmel, and A. Francis Stewart. 2004. "A Reliable LacZ Expression Reporter Cassette for Multipurpose, Knockout-First Alleles." *Genesis* 38(3):151–58.

References

- Theis-Febvre, Nathalie, Odile Filhol, Carine Froment, Martine Cazales, Claude Cochet, Bernard Monsarrat, Bernard Ducommun, and Véronique Baldin. 2003. "Protein Kinase CK2 Regulates CDC25B Phosphatase Activity." *Oncogene* 22(2):220–32.
- Thored, Pär, Andreas Arvidsson, Emanuele Cacci, Henrik Ahlenius, Therése Kallur, Vladimer Darsalia, Christine T. Ekdahl, Zaal Kokaia, and Olle Lindvall. 2006. "Persistent Production of Neurons from Adult Brain Stem Cells During Recovery after Stroke." *Stem Cells* 24(3):739–47.
- Tittel-Elmer, Mireille, Armelle Lengronne, Marta B. Davidson, Julien Bacal, Philippe François, Marcel Hohl, John H. J. Petrini, Philippe Pasero, and Jennifer A. Cobb. 2012. "Cohesin Association to Replication Sites Depends on Rad50 and Promotes Fork Restart." *Molecular Cell* 48(1):98–108.
- Tsai, Li-Huei, Ivana Delalle, Verne S. Caviness, Teresa Chae, and Ed Harlow. 1994. "P35 Is a Neural-Specific Regulatory Subunit of Cyclin-Dependent Kinase 5." *Nature* 371(6496):419–23.
- Tu, Zhaowei, Mustafa Bilal Bayazit, Hongbin Liu, Jingjing Zhang, Kiran Busayavalasa, Sanjiv Risal, Jingchen Shao, Ande Satyanarayana, Vincenzo Coppola, Lino Tessarollo, Meenakshi Singh, Chunwei Zheng, Kui Liu, et al. 2017. "Speedy A–Cdk2 Binding Mediates Initial Telomere–Nuclear Envelope Attachment during Meiotic Prophase I Independent of Cdk2 Activation." *Proceedings of the National Academy of Sciences* 114(3):592–97.
- Urbán, Noelia and François Guillemot. 2014. "Neurogenesis in the Embryonic and Adult Brain: Same Regulators, Different Roles." *Frontiers in Cellular Neuroscience* 8:1–19.
- Uversky, Vladimir N. 2017. "Intrinsically Disordered Proteins in Overcrowded Milieu: Membrane-Less Organelles, Phase Separation, and Intrinsic Disorder." *Current Opinion in Structural Biology* 44:18–30.
- Viera, Alberto, Manfred Alsheimer, Rocío Gómez, Inés Berenguer, Sagrario Ortega, Catherine E. Symonds, David Santamaría, Ricardo Benavente, and José A. Suja. 2015. "CDK2 Regulates Nuclear Envelope Protein Dynamics and Telomere Attachment in Mouse Meiotic Prophase." *Journal of Cell Science* 128(1):88–99.
- Walker, T. L., T. Yasuda, D. J. Adams, and P. F. Bartlett. 2007. "The Doublecortin-Expressing Population in the Developing and Adult Brain Contains Multipotential Precursors in Addition to Neuronal-Lineage Cells." *Journal of Neuroscience* 27(14):3734–42.
- Walton, Noah M., Benjamin M. Sutter, Eric D. Laywell, Lindsay H. Levkoff, Sean M. Kearns, Gregory P. Marshall II, Bjorn Scheffler, and Dennis A. Steindler. 2006. "Microglia Instruct Subventricular Zone Neurogenesis." *Glia* 54(8):815–25.
- Wang, Lina, Zhaowei Tu, Chao Liu, Hongbin Liu, Philipp Kaldis, Zijiang Chen, and Wei Li. 2018. "Dual Roles of TRF1 in Tethering Telomeres to the Nuclear Envelope and Protecting Them from Fusion during Meiosis." *Cell Death and Differentiation* 25(6):1174–88.

- Wang, Xu Dong, Min Wei Zhu, Dan Shan, Shu Yu Wang, Xiang Yin, Yue Qing Yang, Tian Hang Wang, Chun Ting Zhang, Ying Wang, Wei Wei Liang, Jun Zhang, Hong Lin Feng, et al. 2019. "Spy1, a Unique Cell Cycle Regulator, Alters Viability in ALS Motor Neurons and Cell Lines in Response to Mutant SOD1-Induced DNA Damage." *DNA Repair* 74:51--62.
- Wood, Daniel J. and Jane A. Endicott. 2018. "Structural Insights into the Functional Diversity of the CDK–Cyclin Family." *Open Biology* 8(9).
- Yazdi, Parvin T., Yi Wang, Song Zhao, Nimitt Patel, Eva Y. H. P. Lee, and Jun Qin. 2002. "SMC1 Is a Downstream Effector in the ATM/NBS1 Branch of the Human S-Phase Checkpoint." *Genes and Development* 16(5):571–82.
- Zhang, Li, Aiguo Shen, Qing Ke, Wei Zhao, Meijuan Yan, and Chun Cheng. 2012. "Spy1 Is Frequently Overexpressed in Malignant Gliomas and Critically Regulates the Proliferation of Glioma Cells." *Journal of Molecular Neuroscience* 47(3):485–94.
- Zheng, Hui and Wei Xie. 2019. "The Role of 3D Genome Organization in Development and Cell Differentiation." *Nature Reviews Molecular Cell Biology* 20:535–50.
- Zielke, N. and B. A. Edgar. 2015. "FUCCI Sensors: Powerful New Tools for Analysis of Cell Proliferation." *Wiley Interdisciplinary Reviews: Developmental Biology* 4(5):469–87.